

AD-776 000

EXTINGUISHMENT OF COMPOSITE PRO-
PELLANTS AT LOW PRESSURES

Chung Poo Park, et al

Utah University

Prepared for:

Air Force Office of Scientific Research

10 December 1973

DISTRIBUTED BY:

NTIS

National Technical Information Service
U. S. DEPARTMENT OF COMMERCE
5285 Port Royal Road, Springfield Va. 22151

AD776 000

University of Utah

Department of Chemical Engineering

Scientific Report

EXTINGUISHMENT OF COMPOSITE PROPELLANTS
AT LOW PRESSURES

to Combustion Energetics Division, AFOSR

December 10, 1973

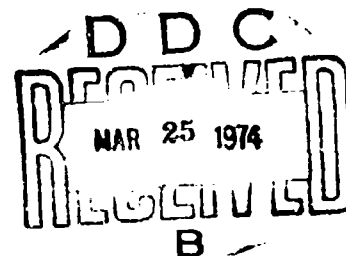
Work performed under sponsorship of the Combustion
Energetics Division of the Air Force Office of
Scientific Research
Grant AF-AFOSR 69-1656

Report prepared by C. P. Park

Report approved by Norman W. Ryan and Alva D. Baer

Norman W. Ryan
Alva D. Baer

NATIONAL TECHNICAL
INFORMATION SERVICE
Cameron Station
Springfield, VA 22151



REPORT DOCUMENTATION PAGE		READ INSTRUCTIONS BEFORE COMPLETING FORM
1. REPORT NUMBER AFOSR - TR - 74 - 0361	2. GOVT ACCESSION NO.	3. RECIPIENT'S CATALOG NUMBER
4. TITLE (and Subtitle) EXTINGUISHMENT OF COMPOSITE PROPELLANTS AT LOW PRESSURES		5. TYPE OF REPORT & PERIOD COVERED INTERIM
7. AUTHOR(s) CHUNG POO PARK NORMAN W RYAN ALVA D BAER		6. CONTRACT OR GRANT NUMBER(s) AFOSR 69-1656
9. PERFORMING ORGANIZATION NAME AND ADDRESS UNIVERSITY OF UTAH DEPARTMENT OF CHEMICAL ENGINEERING SALT LAKE CITY, UTAH 84112		10. PROGRAM ELEMENT, PROJECT, TASK AREA & WORK UNIT NUMBERS 681308 9711-01 61102F
11. CONTROLLING OFFICE NAME AND ADDRESS AIR FORCE OFFICE OF SCIENTIFIC RESEARCH/NA 1400 WILSON BOULEVARD ARLINGTON, VIRGINIA 22209		12. REPORT DATE Dec 1973
14. MONITORING AGENCY NAME & ADDRESS (if different from Controlling Office)		13. NUMBER OF PAGES 343
		15. SECURITY CLASS. (of this report) UNCLASSIFIED
		15a. DECLASSIFICATION/DOWNGRADING SCHEDULE
16. DISTRIBUTION STATEMENT (of this Report) Approved for public release; distribution unlimited.		
17. DISTRIBUTION STATEMENT (of the abstract entered in Block 20, if different from Report)		
18. SUPPLEMENTARY NOTES		
19. KEY WORDS (Continue on reverse side if necessary and identify by block number) COMBUSTION SOLID PROPELLANT COMBUSTION COMBUSTION INSTABILITY LOW-PRESSURE COMBUSTION COMBUSTION EXTINGUISHMENT		
20. ABSTRACT (Continue on reverse side if necessary and identify by block number) Propellants containing ammonium perchlorate and several commonly used polymer fuels were extinguished at low pressures. The extinguishment pressures were found to be strongly affected by the thermal environment, being lower when external flux compensated for heat loss. With a fixed thermal environment and extinguishment during depressurization, it was found that (1) at very low depressurization rates, the extinguishment pressure depends on the rate in a manner suggesting energy starvation at the zone of first reactions. At the very low pressures, extinguishment appears to be caused by an intrinsic combustion		

•instability featuring out-of-phase oscillations in the gasification rates of oxidant and polymer.

TABLE OF CONTENTS

	<u>Page</u>
TABLE OF CONTENTS	ii
LIST OF FIGURES	viii
LIST OF TABLES	xv
ABSTRACT	xvi
I. INTRODUCTION	1
II. REVIEW OF RELATED WORK	5
A. FLAMMABILITY LIMIT OF COMBUSTIBLE GASEOUS MIXTURES	5
B. PRESSURE DEFLAGRATION LIMIT OF AMMONIUM PERCHLORATE	6
C. PRESSURE DEFLAGRATION LIMIT OF COMPOSITE SOLID PROPELLANTS	9
D. EXTINGUISHMENT DURING DEPRESSURIZATION AT LOW PRESSURES	12
E. SUMMARY OF LITERATURE REVIEW	14
III. GENERAL FEATURES OF EXPERIMENTAL APPARATUS	16
A. COMBUSTION CHAMBER AND ACCESSORIES	16
B. FORCE TRANSDUCER	18
C. QUICK HEATING FURNACE AND COOLING COIL	19
D. SMALL-L* BLOW-DOWN CHAMBER AND ACCESSORIES	21
IV. STEADY BURNING BEHAVIOR OF COMPOSITE PROPELLANT STRANDS NEAR THEIR LOW-PRESSURE DEFLAGRATION LIMITS	23
A. BACKGROUND	23
B. EXPERIMENTAL PROCEDURE	24
1. Burning Rate Measurement	24
2. Go/no-go Test for P_{dl} Measurement	24

3. Flame Temperature Measurement	27
C. EXPERIMENTAL RESULTS	28
1. Burning Rate	28
2. Pressure Deflagration Limit	30
3. Flame Temperature	31
4. Supplementary Observations	33
a. Binder Melting	33
b. Surface Layer on PU Propellants	33
c. AP Ejection	34
d. Burning Surface Temperature	36
e. Oscillatory Burning	36
D. DISCUSSION OF RESULTS	37
1. General Features of Low Pressure Burning	37
2. High P_{d1} Propellants	38
3. Highly-Oxidized PU Propellants	40
4. PBAA Propellants	43
5. HTPB Propellants	46
V. INTRINSIC INSTABILITY	48
A. BACKGROUND	48
B. DATA ACQUISITION AND REDUCTION	54
C. EXPERIMENTAL RESULTS	56
D. DISCUSSION OF RESULTS	60
1. Stability Analysis by Denison-Baum Theory	60
2. Criticism of the Denison-Baum Type of One-Dimensional Theory	61
3. Advancement of an Alternative Theory	62
VI. EFFECT OF SUPPLEMENTAL ENERGY ON BURNING AND EXTINGUISH- MENT OF SOLID PROPELLANT AT LOW PRESSURES	68
A. BACKGROUND	68
B. EXPERIMENTAL PROCEDURE	71
1. Burning Rates and Flame Temperatures	71
2. Extinguishment Pressure with External Energy Supply	73
C. RESULTS AND DISCUSSION	77

1.	Transient Response of Low Pressure Burning to External Heat Flux	77
2.	Augmented Burning Rates and Flame Temperatures by External Heat Flux	79
3.	Further Interpretation of Burning Rate and Flame Temperature Data under Furnace Heating	80
	a. Activation Energy for Gas Phase Reaction	81
	b. Net Heat of Gasification	83
4.	Extinguishment under Furnace Heat Flux	85
VII.	EXTINGUISHMENT DURING DEPRESSURIZATION	91
A.	BACKGROUND	91
B.	EXPERIMENTAL PROCEDURE	101
	1. Extinguishment During Depressurization	101
	2. Measurement of Transient Burning Rate During Depressurization	106
C.	EXPERIMENTAL RESULTS	107
	1. Extinguishment During Depressurization	107
	2. Transient Burning Rates	111
	3. Comparison of Limiting Extinguishment Pressures Measured by Depressurization Tests and the Pressure Deflagration Limit Determined by Go/No-Go Tests	113
D.	DISCUSSION OF RESULTS	114
	1. Extinguishment in the High-Rate Regime	114
	2. Extinguishment in the Low-Rate Regime	115
VIII.	RAPID DEPRESSURIZATION EXTINGUISHMENT AND REIGNITION	
A.	BACKGROUND	118
B.	EXPERIMENTAL PROCEDURE	122
C.	EXPERIMENTAL RESULTS AND DISCUSSIONS	124
	1. The Effect of Initial Pressure on Extinguishment Requirements	125
	2. The Effect of Grain Shape on Extinguishment Requirements	128
	3. Temporary and Permanent Extinguishment Requirement of Various Propellants	128
	4. The Effect of Final Dump Tank Pressure on Reignition Time	130

5. The Unusual Reignition Tendency of a Catalyzed PBAA Propellant	130
6. The Representation of Extinguishment Data by the Critical Ratio of Characteristic Times	131
7. Summary of Results	132
IX. SUMMARY AND CONCLUSIONS	134
A. MECHANISMS OF EXTINGUISHMENT	134
B. EFFECT OF HEAT LOSSES ON THE COMBUSTION AND EXTINGUISHMENT	136
C. INFLUENCE OF BINDER CHEMISTRY ON LOW-PRESSURE COMBUSTION	137
D. STATUS OF UNSTEADY COMBUSTION THEORY	139
NOMENCLATURE	141
REFERENCES	146
FIGURES III.1 to VIII.10	158
TABLES VI.1 to VIII.1	221
APPENDIX	
A. EFFECT OF EXPERIMENTAL CONDITIONS ON THE PRESSURE DEFLAGRATION LIMIT	225
1. Effect of Strand Size on the Pressure Deflagration Limit	225
2. Effect of Strand Size Inhibitor and Environment Gas on Pressure Deflagration Limit	226
3. Effect of the Purging Rate of Cooling Nitrogen on Pressure Deflagration Limit	227
4. Effect of Initial Strand Temperature on Extinguishment Pressure	228
Figures A.1 to A.5	230
B. PROPELLANT PREPARATION, COMPOSITIONS, AND PROPERTIES	235
1. Propellant Preparation	235
2. Propellant Compositions and Properties	237
Tables B.1 to B.111	240
C. EXPERIMENTAL APPARATUS AND CALIBRATION DATA	244

1. Flow and Pressure Control Components for the Combustion Chamber	244
2. Electric Circuit for the Combustion Chamber	245
3. Circuits and Components of Measuring Units	248
4. Calibration of the Quick Heating Furnace	250
5. Pressure History During Depressurization Extinguishment Tests	253
Figures C.1 to C.7	256
Tables C.I to C.III	261
D. INTERMITTENT BURNING OF A HIGHLY-FUELED PU PROPELLANT UNDER FURNACE HEATING	264
1. Background	264
2. Experiment Results	265
3. Discussion of Results	269
a. Computation of the Net Heat of Gasification	269
b. The Mechanism of Intermittent Burning	270
Figures D.1 to D.3	272
Table D.I	275
E. MEASUREMENT OF THE SURFACE TEMPERATURES OF BURNING STRANDS	276
Figures E.1 to E.3	279
Table E.I	280
F. ELECTRICAL PROPERTIES OF COMPOSITE PROPELLANT COMBUSTION	281
1. Background	281
2. Experimental Procedure	283
a. Conductivity Near the Burning Surface	283
b. Burning Rate Augmentation by High Voltage Power	284
3. Results and Discussion	285
a. Ohmic Nature of the Conductivity Across the Burning Surface	285
b. Non-Ohmic Nature of the Conductivity Across the Burning Surface	285
c. Separation of Conductivity Between Gas and Solid Phase Contributions	287
d. Effect of Pressure on the Conductivity Across the Burning Surface	287
e. An Interpretation of the Maximum in the Conductivity Curves	290

f. Burning Rate Augmentation by High Voltage Power	291
g. Transient Conductivity During Depressurization	291
h. Conclusion	293
Figures F.1 to F.14	295
Table F.1	307
G. REDUCED DATA OF EXTINGUISHMENT TESTS	308
Tables G.I to G.II	309

LIST OF FIGURES

<u>Figure</u>	<u>Caption</u>	<u>Page</u>
III.1	A Schematic Diagram of the Combustion Chamber	158
III.2	A Schematic Diagram of the Force Measurement Assembly	159
III.3	An Overview Photograph of the Combustion Chamber and Accessories	160
III.4	A View of the Remote Control Panel and the Data Acquisition and Processing Equipment	160
III.5	A Schematic Diagram of the Quick Heating Furnace and Its Electrical Circuit	161
III.6	A Photograph of the Quick Heating Furnace	162
III.7	A Photograph of the Cooling Coil	162
III.8	A Sectioned View of the Small-L* Blow-down Chamber Showing Sample Mounting	163
IV.1	Burning Rate Behavior of Bimodal (60/40)-AP, Pu-fueled Propellants at Low Pressures	164
IV.2	Burning Rate Behavior of Bimodal (60/40)-AP, PBAA-fueled Propellants at Low Pressures	165
IV.3	Burning Rate Behavior of Bimodal (60/40)-AP, HTPB-fueled Propellants at Low Pressures	166
IV.4	Burning Rate Behavior of Many Bimodal-AP Propellants Below 0.2 atms	167
IV.5	Effect of the AP Particle Size on the Low Pressure Deflagration Limit	168
IV.6	Effect of AP Level on the Low Pressure Deflagration Limit for Series of Bimodal AP Propellants Fueled with Various Polymers	169
IV.7	Flame Temperatures of a PBAA Propellant at Subatmospheric Pressures	170
IV.8	Flame Temperatures of a PU Propellant at Subatmospheric Pressures	171

IV.9	Flame Temperatures of Many Propellants near Their Low Pressure Deflagration Limits	172
IV.10	Scanning Electron Microscope Micrograph of the Extinguished Surface of a Unimodal-AP (400 μ) PU Propellant (UDV) Burned near Its P_{dl} (55X)	173
IV.11	Scanning Electron Microscope Micrograph of the Extinguished Surface of a Bimodal-AP (200 μ /15 μ) PU Propellant Burned near Its P_{dl} (70X)	173
IV.12	Scanning Electron Microscope Micrograph of the Extinguished Surface of a Bimodal-AP (200 μ /15 μ) PBAA Propellant (UDL) Burned near Its P_{dl} (20X)	174
IV.13	Scanning Electron Microscope Micrograph of the Extinguished Surface of a Unimodal-AP (15 μ) PBAA Propellant (UDX) Burned near Its P_{dl} (600X)	174
IV.14	Burning Rates and Flame Temperatures of a Series of Unimodal PBAA Propellants near Their Low Pressure Deflagration Limits	175
IV.15	Comparison of Thermal Wave Thickness near the P_{dl} and the AP Particle Size for a Series of Unimodal PU Propellants	176
V.1	Force Transducer Signals for Bimodal PU, HTPB, and PBAA Propellants Burned and Extinguished near Their P_{dl} Showing Oscillatory Burning Behavior	177
V.2	Force and Light Signals Recorded Simultaneously During Low-Pressure (near P_{dl}) Oscillatory Burning of a Catalyzed Bimodal PU Propellant	178
V.3	Comparison Between the Measured Period of Oscillations and the Period Calculated by Boggs and Beckstead's Theory for a Series of Unimodal PBAA Propellants	179
V.4	Low-Pressure (near P_{dl}) Oscillatory Burning Data for PU Propellants Containing Bimodal AP (60/40, 200 μ /15 μ)	180
V.5	Low-Pressure (near P_{dl}) Oscillatory Burning Data for PBAA Propellants Containing Bimodal AP (60/40, 200 μ /15 μ)	181

V.6	Low-Pressure (near P_{dl}) Oscillatory Burning Data for HTPB Propellants Containing Bimodal AP (60/40, 200 μ /15 μ)	182
V.7	Summary of Long-Period Data Being Representative of Each Binder System	183
V.8	Parametric Study on the Denison and Baum-Type Stability Diagram to Fit the Observed Periods of Oscillations	184
V.9	This Figure Shows How the Averaged Burning Rate, Period and Amplitude of Oscillation, and the Phase Lag of Light Signal to Force Signal Changed During an Oscillatory Burning of a Catalyzed PU Propellant (UFA) Which Burned Just Below the P_{dl} and Eventually Self-Extinguished.	185
VI.1	Transient Responses of the Burning Rate and the Flame Temperature of a Catalyzed PU Propellant (UFA) to Furnace Heating	186
VI.2	Transient Responses of the Burning Rate and the Flame Temperature of an Uncatalyzed PU Propellant (UED) to Furnace Heating	187
VI.3	Effect of the External Heat Flux on the Burning Rate of a Catalyzed PU Propellant (UFA)	188
VI.4	Effect of the External Heat Flux on the Burning Rate of an Uncatalyzed PU Propellant (UED)	189
VI.5	Effect of the External Heat Flux on the Flame Temperature of a Catalyzed PU Propellant (UFA)	190
VI.6	Effect of the External Heat Flux on the Flame Temperature of an Uncatalyzed PU Propellant (UED)	191
VI.7	Determination of the Activation Energy of Gas Phase Reaction Using Denison and Baum's Model for a Catalyzed (UFA) and an Uncatalyzed (UED) PU Propellant	192
VI.8	Effect of the External Heat Flux on the Limiting Extinguishment Pressure of a Catalyzed PU Propellant (UFA)	193
VI.9	Effect of the External Heat Flux on the Limiting Extinguishment Pressure of an Uncatalyzed PU Propellant (UED)	194

VI.10	Heat Flux-Augmented Burning Rate Data of a Catalyzed PU Propellant (UFA) near the Limiting Extinguishment Pressures	195
VI.11	Heat Flux-Augmented Burning Rate Data of an Uncatalyzed PU Propellant (UED) near the Limiting Extinguishment Pressures	196
VI.12	Effect of the External Heat Flux on the Limiting Extinguishment Pressure of an Uncatalyzed PBAA Propellant (UEK)	197
VI.13	Effect of the External Heat Flux on the Extinguishment Pressure of a Fluorocarbon Propellant (TPF 1006)	198
VII.1	Oscilloscope Traces of Typical Depressurization Extinguishment Tests Using the Combustion Chamber	199
VII.2	Effect of the Initial Pressure on the Extinguishment Pressure for a Catalyzed PU Propellant (UFA) During Depressurization	200
VII.3	Effect of the Depressurization Rate on the Extinguishment Pressure of PU Propellants	201
VII.4	Effect of the Depressurization Rate on the Extinguishment Pressure of HTPB Propellants	202
VII.5	Effect of the Depressurization Rate on the Extinguishment Pressure of PBAA Propellants	203
VII.6	The Critical Ratio of Characteristic Times as a Function of the Extinguishment Pressure for Two PU Propellants of Higher Fuel Loading	204
VII.7	The Critical Ratio of Characteristic Times as a Function of the Extinguishment Pressure for Two PU Propellants of Lower Fuel Loading	205
VII.8	Transient Burning Rates During Depressurization at Low Pressures for a PBAA Propellant	206
VII.9	Transient Burning Rates During Depressurization at Low Pressures for a FC Propellant	207
VII.10	Comparison of Near-Limiting Extinguishment Pressures Measured by Depressurization Tests (P_E) and the Pressure Deflagration Limit Determined by Go/No-Go Tests (P_{dl}) for PU Propellants	208

VII.11	Comparison of Near-Limiting Extinguishment Pressures Measured by Depressurization Tests (P_E) and the Pressure Deflagration Limit Determined by Go/No-Go Tests (P_{dl}) for HTPB Propellants	209
VII.12	Comparison of Near-Limiting Extinguishment Pressures Measured by Depressurization Tests (P_E) and the Pressure Deflagration Limit Determined by Go/No-Go Tests (P_{dl}) for PBAA Propellants	210
VIII.1	Oscilloscope Traces of a Typical Rapid-Depressurization Extinguishment Test Followed by Reignition	211
VIII.2	Effect of the Initial Pressure on the Critical Dump-Tank Pressure for the Extinguishment of a Catalyzed Propellant (UFA) During Rapid Depressurization When the 0.450-cm Orifice was Used	212
VIII.3	Effect of the Initial Pressure on the Critical Dump-Tank Pressure for the Extinguishment of a Catalyzed PU Propellant (UFA) During Rapid Depressurization When the 0.953 cm Orifice Was Used	213
VIII.4	Influence of the Initial Chamber Pressure on the Pressure Histories During Rapid-Depressurization Extinguishment Tests	214
VIII.5	Influence of the Sample Shapes on the Pressure Histories During Rapid-Depressurization Extinguishment Tests	215
VIII.6	Temporary and Permanent Extinguishment Requirements for a Catalyzed PBAA Propellant (UEZ)	216
VIII.7	Reignition Time as a Function of Final Dump-Tank Pressure for a Catalyzed PBAA Propellant (UEZ)	217
VIII.8	Comparison of von Elbe-Type Theories and Extinguishment Data for a Catalyzed PU Propellant (UFA)	218
VIII.9	Comparison of von Elbe-Type Theories and Extinguishment Data for an Uncatalyzed PBAA Propellant (UEM)	219
VIII.10	Comparison of von Elbe-Type Theories and Extinguishment Data for a Catalyzed PBAA Propellant (UEZ)	220
9.1	Effect of Strand Size on the Pressure Deflagration Limit	230

A.2	Dependence of the Pressure Deflagration Limit on Strand Hydraulic Radius	231
A.3	Effect of Strand Side Inhibitors and Environmental Gases on the Pressure Deflagration Limit	232
A.4	Effect of the Flow Rate of Cooling Nitrogen on the Pressure Deflagration Limit	233
A.5	Effect of the Initial Strand Temperature on the Extinguishment Pressure	234
C.1	Flow Diagram for the Combustion Chamber	256
C.2	Electric Circuit Diagram for the Combustion Chamber	257
C.3	Circuit Schematic Diagram for Force Transducer	258
C.4	Circuit Schematic Diagram for Pressure Transducer	258
C.5	Circuit Schematic Diagram for Photocells	258
C.6	Calibration Data of Furnace Heat Flux with Respect to Furnace Wall Temperature	259
C.7	Actual Pressure Histories During Depressurization Extinguishment Runs for the Combustion Chamber in Comparison with Theoretical Isothermal and Adiabatic Blow-down Curves	260
D.1	Force Transducer Signals During Intermittent Burning of a Highly-fueled PU Propellant in Furnace Heated to 900°C	272
D.2	Effect of Pressure on the Averaged Burning Rates and Frequency Parameters of UDF Propellant During Intermittent Burning in Furnace Heated to 900°C	273
D.3	Effect of Furnace Heat Flux on the Ignition Period of UDF Propellant During Intermittent Burning in Furnace	274
E.1	Diagram Showing How the Thermocouple Junction Was Positioned in Propellant Sample	279
E.2	Circuit Schematic Diagram for the Measurement of Burning Surface Temperatures	279
E.3	Typical Oscilloscope Traces for a Run Measuring Burning Surface Temperature	280

F.1	Schematic Diagram of a Sample Prepared for the Measurement of Electrical Conductivity Across the Burning Surface	295
F.2	Circuit Schematic Diagram of a Resistor Box for the Measurement of Electrical Conductivity	295
F.3	The Ohmic Nature of Conductivity Across the Burning Surface	296
F.4	Effect of Distance Between Electrodes on the Resistance Across the Burning Surface for Two Pressures	297
F.5	Effect of Distance Between Electrodes on the Solid and and Gas Conductances Across the Burning Surfaces	298
F.6	Effect of Pressure on the Electrical Conductivities of Various Propellants	299
F.7	Effect of Electrode Materials on the Electrical Conductance Across the Burning Surface	300
F.8	Effect of Pressure on the Electrical Conductivities Through Gas and Solid Phase	301
F.9	Comparison of Low- and High-Voltage Conductivities for a PU Propellant	302
F.10	Augmentation of Regression Rate of a PU Propellant by Dissipating Electric Energy on the Burning Surface	303
F.11	Oscilloscope Traces Showing Light, Conductivity Signals Near Extinguishment During Depressurization	304
F.12	Typical Oscilloscope Traces of Pressure and Conductivity Signals During Slow Depressurization Using Combustion Chamber	305
F.13	Typical Oscilloscope Traces of Pressure and Conductivity Signals During Rapid Depressurization Using Small-L* Blow-down Chamber	306
F.14	Transient Conductivities During Depressurization	307

LIST OF TABLES

<u>Table</u>	<u>Caption</u>	<u>Page</u>
VI.I	Net Heat of Gasification Calculated Using Heat-Flux-Augmented Burning Rate Data	221
VII.I	Summary of Blow-down-Type Extinguishment Data Using a Rarefaction Tube Taken from the Previous Works at the University of Utah	222
VII.II	Comparison of Others' Data Concerning Compositional Effect on Depressurization Extinguishment	223
VIII.I	Summary of the Data of Rapid-Depressurization Extinguishment Tests	224
B.I	Propellant Formulations and Their Pressure Deflagration Limits	240
B.II	Thermophysical Properties of Propellants	242
B.III	Thermophysical Properties of Propellant Ingredients	243
C.I	Calibration Data of Temperature Controller for Quick Heating Furnace and Furnace Heating Times	261
C.II	Heating Rates of Samples in Furnace	262
C.III	Calculated Fractional Rates of Depressurization for Combustion Chamber and Small-L* Blow-down Chamber for Various Orifice Sizes	263
D.I	Summary of Data for Intermittent Burning of UDF Propellant Under Furnace Heating	275
E.I	Summary of Measured Burning Surface Temperatures	280
F.I	References for Appendix F	
G.I	Effect of the External Heat Flux on the Limiting Extinguishment Pressures of Various Propellants	309
G.II	Data of Depressurization Extinguishment Tests Using Combustion Chamber	314

ABSTRACT

A study was made of the extinguishment of composite solid propellant strands at low pressures. Both the extinguishment at a constant pressure near the low pressure deflagration limit (P_{dl}) and the extinguishment during depressurization were considered. The effects of the depressurization rate, the supplemental heat flux, and the propellant chemistry on the extinguishment were investigated.

Controlled thermal environments were produced inside a large-volume combustion chamber by a quick-heating nichrome-ribbon furnace or by a cooling coil. The steady-state and transient burning rates were determined by continuously measuring the weight of the strands.

Several catalyzed and uncatalyzed propellant formulations containing ammonium perchlorate and polyurethane (PU), polybutadiene-acrylic acid (PBAA), hydroxyl-terminated polybutadiene (HTPB), poly(lauryl methacrylate) (PLMA), and fluorocarbon (FC) binder-fuels have been used.

Two distinct extinguishment regimes were observed for the extinguishment during depressurization, signifying two different extinguishment mechanisms. In the high-rate regime, the starvation of energy in the zone of initial reactions is inferred to be the mechanism of extinguishment. In the low-rate regime, the extinguishment pressure took a limiting minimum value independent of the rate of depressurization, provided the rate was low enough. Extinguish-

ment in the low-rate regime appears to have the same mechanism as extinguishment observed in constant pressure experiments at or below the low-pressure deflagration limit (P_{dl}). That mechanism involves a self-excited, intrinsic instability, manifested as oscillations in burning rate, which develops in the combustion zone and eventually leads to extinguishment.

A large augmentation of the burning rate and flame temperature near the P_{dl} and a significant lowering of the P_{dl} was made by a moderate external heat flux, indicating that low-pressure burning behavior of propellants is strongly influenced by the thermal environment of the combustion chamber. If the near-linear relationship between the extinguishment pressure and the external heat flux is extrapolated to zero pressure, one obtains an intercept heat-flux value of about $1.0 \text{ cal/cm}^2 \text{ sec}$, which is inferred to be the minimum feedback heat flux required for combustion. The corresponding effective furnace temperature, about 650°C , is interpreted as the least effective surface temperature at which combustion can occur.

The very low rate of the low-pressure burning permit, the details of the polymer chemistry to emerge as important variables, because, when heated slowly, the polymers may undergo characteristic low-temperature, combustion-modifying changes. Polymer melting accompanying depolymerization is responsible for the high P_{dl} of fuel-rich propellants containing PU and PLMA polymers.

All the propellants considered exhibited oscillatory burning at a constant pressure near their P_{dl} , which leads to extinguishment below

the P_{dl} . Unimodal-AP propellants showed a single mode of oscillations. Bimodal-AP propellants showed two modes of oscillations, whose periods were proportional to the thermal wave time. The Denison-Baum model, one of the so-called "one dimensional" theories of combustion stability, fails to predict the observed periods of oscillation with reasonable values of kinetic and thermochemical parameters. It is proposed that a successful theory start with the proposition that oscillating gasification rates of the two main propellant ingredients are out of phase.

CHAPTER I

INTRODUCTION

Difficulty in combustion termination is one of the major disadvantages of solid propulsion systems, especially if restart capability is desired. Several methods of combustion termination have been developed to help design a controllable motor. Rapid depressurization and exploitation of L^* instability are two approaches. However, as the modern rocket technology advances, these methods become inadequate for an extremely fast-burning propellant system or a large rocket booster because of severe requirements in nozzle design. There is another mode of extinguishment; reduction of pressure below the so-called low pressure deflagration limit. The lowest pressure at which a solid propellant sustains combustion is termed the "low pressure deflagration limit (P_{dl}).". Although such a limit is inferred from practical experience and the concept has oriented some research groups to develop propellants with a high (even above atmospheric) apparent P_{dl} , there are some fundamental questions yet to be answered. Is there, in fact, a P_{dl} which is an intrinsic property of the propellant? The negative answer is generally given because it is found that the P_{dl} values observed are very much influenced by the experimental arrangements. Nevertheless, the concept of the P_{dl} may be useful as a measure of the extinguishability of solid propellants at low pressures just as the flammability limit of gaseous mixtures,

being determined by standardized experimental procedures, has proven to be a reliable safety guide.

If the steady operating pressure of a rocket chamber is dropped below the low pressure deflagration limit of the propellant, combustion ceases. The rate of depressurization is not critical if small enough, but if it is large, it may result in extinguishment before P_{dl} is reached. Since depressurization rate can thus affect results, a true P_{dl} must be determined in a burner in which pressure is controlled independent of the mass rate of burning. A large volume strand burner is adequate for this purpose but the inherent limitation of nonadiabatic conditions plagues any direct application of the strand bomb data to the motor design. In this study the simulation of rocket motor conditions in a strand burner was attempted by a quick-heating furnace inside the burner chamber. This apparatus allows us to perceive also the intrinsic instability of the combustion wave of solid propellants.

Besides the practical purpose of helping design of the controllable motors, this investigation takes the advantages of the extended thermal wave to study the fundamental processes governing composite propellant combustion in general.

From the literature survey, it is noted that closely standardized experimental procedures should be employed to obtain reproducible P_{dl} data. Also noted is that heat losses may affect the low-pressure burning and extinguishment. During the course of this study, it has been observed that the burning of solid propellants near their P_{dl} is oscillatory and very susceptible to pressure disturbances. Thus,

in this study, P_{dl} is regarded from various points of view: as a steady-combustion limit, as an intrinsic instability, as a feature of non-adiabatic burning, and as a limiting extinguishment pressure during depressurization.

The program of this project proceeds with the study of steady burning behavior at low pressures and P_{dl} measurement in Chapter IV. The intrinsic instability is discussed in Chapter V. In Chapter VI, the effect of external heat flux on the burning and extinguishment at low pressures is explored. An investigation on the transient burning during depressurization at low pressures is described in Chapter VII. In Chapter VIII, an effort is made to extend the study on depressurization extinguishment to higher pressures, and the reignition phenomenon after depressurization extinguishment is considered.

Reliable experimental data are the first requirement. Development of theory is deferred until after accumulation of a body of reliable data, and then has more a rationalizing than an innovative character. In Chapter II, a thorough literature survey on the low pressure limit is made. More extensive discussions of the relevant literature are found in the background section of the several chapters.

To avoid complexity, the general apparatus common to various phases of this study are described in Chapter III. Only the necessary part of the experimental procedures for the explanation of the results is presented in each chapter and the details of each procedure and the calibration data are found in Appendix C.

Because of the large volume of data to be presented, figures and summarized tables are placed at the end of the main text. The supplementary numerical data for the figures and tables are shown in Appendix G. The composition of all the propellants adopted in this study and the thermophysical properties of the propellants used extensively are found in Table B.I and B.II of Appendix B respectively. Supplementary studies on intermittent burning behavior of a PU propellant in a furnace, measurement of burning-surface temperatures, and the electrical properties of burning propellants appear in Appendices D, E and F, respectively.

CHAPTER II

REVIEW OF RELATED WORK

Little work has been done on the pressure deflagration limit of composite propellants. The investigation on ammonium perchlorate (AP) has generated some useful information on the general features of the phenomenon. Further fundamental aspects of the problem are found from the works on flammability limits of gaseous mixtures.

A. FLAMMABILITY LIMIT OF COMBUSTIBLE GASEOUS MIXTURES

The pressure or concentration limits of gaseous mixtures have been determined experimentally by standardized experimental procedures [39, 46, 79]. Although these limits are useful for a safety guide, it has been argued that the limits may not be fundamental properties of the mixture by the fact that the measured values are too much dependent upon experimental conditions [43, 79]. Early investigators [78, 110] have tried to explain the flammability limit in terms of flame-front instability to small disturbances from steady state within the adiabatic plane wave model. Spalding [119], however, clearly presented that even a large disturbance cannot extinguish a flame in an unlimited one-dimensional system without heat losses and developed a radiation-heat loss theory. The heat-loss theory still remains the only successful approach to the problem within the framework of one-dimensional flame propagation [79, 132]. However, the radiation-heat-loss theory fails to explain many of the fundamental

features of the phenomenon [43, 79]. After an in-depth analysis of the problem, Lewis and von Elbe [79] suggest a mechanism of flame quenching due to convective heat release to the unburned gas.

B. PRESSURE DEFLAGRATION LIMIT OF AMMONIUM PERCHLORATE

There are numerous studies on the deflagration of ammonium perchlorate (AP) and some experimental data on the limiting pressures are available [1, 2, 5], 66, 77]. Friedman, et al. [52] studied the pressure deflagration limit of pressed AP strands. Go/no-go ignition tests with ignition by a heated nichrome wire was used to determine the P_{dl} of AP strands with the cross-section of 4 mm by 4 mm. The lower deflagration limit was found to be very sensitive to AP particle size and the initial strand temperatures; the P_{dl} increases as the particle size is decreased and as the initial strand temperature is decreased. The P_{dl} of AP strands with a wide distribution of particle sizes was 45 atms at the ambient initial temperature. In a subsequent study, using a much more efficient ignition technique, Levy and Friedman [77] were able to reduce the P_{dl} of AP from 45 atms to 22 atms. They also found that a small amount of copper chromite powder catalyst increases the P_{dl} markedly; so does a small amount of platinum black. An external radiation flux about $10 \text{ cal/cm}^2\text{sec}$ was needed to reduce the P_{dl} of AP from 22 atms to atmospheric pressure. In summing up their results, Levy and Friedman proposed that the radiation heat loss from the burning surface could account for the P_{dl} . Arden, et al. [2] has found AP can deflagrate at atmospheric pressure if the sample is preheated to about 280°C or a small amount of fuel is added to give a final flame temperature of about 930°C . Jacobs and

Whitehead [66] summarized experimental data on pressure limits of AP in their recent review on decomposition and combustion of ammonium perchlorate, including many Soviet works:

1. The lower limit is predictably dependent on strand size, being lower for strands of large diameter;
2. The lower limit is also decreased by increasing the strand density or by increasing the particle size of AP used to form the strand;
3. The lower limit can be reduced to 1 atm or lower by heating of AP or by the incorporation of catalysts.

A theoretical explanation of the P_{dl} of ammonium perchlorate was attempted by Johnson and Nachbar [70] on the basis of the experimental findings of Friedman, et al. described above. The radiation-heat-loss theory first applied to solid-propellant systems by Spalding [120] was advanced with the assumption of a rate-controlled surface condition. Their calculation shows that the theory predicts P_{dl} due to heat loss only when a large amount of unaccountable heat loss is added to the radiation-heat loss from the burning surface. This result casts some doubt on the validity of the radiation-heat loss theory. The same doubt was evoked by the experimental results of Horton and Price [61] who found that the more nearly adiabatic condition with the burning inside hollow grains did not lower the P_{dl} of AP.

Recent observations of the burning surface using a scanning electronmicroscope have helped the combustion modelling and the interpretation of experimental results on P_{dl} of AP [16, 18, 61]. A

molten layer entrapping gas bubbles was observed to exist on the surface of burning AP at 20 - 50 atms. Boggs [16] deduced that this frothy liquid layer would provide an excellent site for energy transfer and pseudo-condensed phase reactions. Watt and Petersen [131] developed a technique measuring the P_{dl} dependency on the initial sample temperature and found the limiting pressure was the same for AP single crystals and pressed pellets in both nitrogen and helium. They explain that the limiting condition is a unique property of AP and it could possibly be related to the molten surface zone. Recent theories on AP deflagration [11, 54, 82] all emphasize the importance of condensed phase reactions. Guirao and Williams [54] have developed a model of AP deflagration considering exothermic condensed-phase reactions in the liquid layer, coupled with the exothermic gas-phase reactions. They conclude that 70 percent of heat release occurs in the liquid layer, and further, that the P_{dl} is due to the drop of surface temperature below the melting point of AP, approximately 560°C [38, 59]. Beckstead, et al. [11] also adopt this melting temperature-limiting view in applying their three-dimensional flame model to the AP deflagration. Their model calls for a heat loss of more than 200 cal/cm²sec to account for extinguishment at the observed P_{dl} .

C. PRESSURE DEFLAGRATION LIMIT OF COMPOSITE SOLID PROPELLANTS

On the deflagration limit of composite propellants only a few investigations have been reported. A slow depressurization method has been adopted to measure the limiting pressures by most investigators.

During the effort of developing high P_{dl} propellants for the controllable motor application, Peterson, et al. [100] have made an extensive study to find the effective way of increasing the P_{dl} of composite propellants. Since their main goal was to formulate propellants which have the P_{dl} higher than the atmospheric pressure at sea level, mostly aluminized polyurethane systems have been considered. The P_{dl} dependency on the ingredient kind, level, size and shape has been explored. Their results indicate that increased P_{dl} is obtained by: 1) increasing binder level 2) replacing hydrocarbon binders with oxygenated binders 3) increasing aluminum content 4) using small particle size oxidizer 5) coating AP with fluorocarbon polymer. Further studies for high P_{dl} propellants have been carried out by Peterson, et al. [99] and Reed, et al. [108, 109] and some mechanistic explanations on the effect of each ingredient on P_{dl} have been attempted. Because too many compositional factors were considered simultaneously, definite conclusions are hardly to be drawn. Most of their explanations on the contributory effects of ingredients on P_{dl} appear to be reasonable, but some are dubious, or at best vague. For instance, the abnormally high P_{dl} (several atms) of PU propellants compared with polybutadiene propellants was explained in terms of the higher heat of combustion and the greater reactivity of polybutadiene binders [109, 110]. The significant effect of

fine AP on increasing P_{dl} in PU systems was inferred to a shallow deflagration region due to light scattering [108].

Woolridge, et al. [134] reported some experimental results on the P_{dl} of propellants fueled with polybutadiene-acrylic acid-acrylonitrile (PBAA-AN) and polyurethane. They concluded that variation in AP level, aluminum content, and ferric oxide did not change the P_{dl} from the range 0.06 atms to 0.11 atms for PBAA-AN propellants. The use of potassium perchlorate in place of AP was shown to increase P_{dl} of a PBAA-AN propellant to 1.6 atms. A PU propellant of 80 percent AP is listed to have P_{dl} of 0.11 atms. Generally, the burning rate catalysts tend to decrease the P_{dl} of PBAA-AN and PU systems.

Some interesting observations on the low pressure deflagration limit have been made by Steinz, et al. [123] during their study on the steady burning mechanism of composite propellants. It is emphasized that the binder meltability plays an important role on both the steady state burning behavior and the extinction of composite propellants. They considered that the binder melting behavior is responsible for the high P_{dl} of PU propellants and the P_{dl} around 0.05 atms of normally burning propellants with non melting binders is mainly caused by convective cooling by entrained ambient gases together with a decrease in combustion efficiency at reduced pressures. Not much data to support their views have been reported. Inclusion of the radiative heat loss to their theory predicts P_{dl} of an order of lower values than 0.05 atms.

Still there have been some attempts to explain P_{dl} of composite propellants on the heat loss argument. Chaiken [24] tried to explain the extinction pressure of composite propellants by the extension of

his thermal-layer theory with the inclusion of heat losses. His development merely emphasizes that any combustion model can predict the existence of a pressure deflagration limit if heat loss term is introduced. Cookson and Fenn [37] measured the effect of sample cross-sectional area on the P_{dl} of polysulfide propellants in a strand burner, using the slow depressurization method. The P_{dl} is sharply increased as the sample cross-sectional area is decreased, indicating that the contribution of conductive and convective heat losses is significant in determining P_{dl} . However, comparing the extrapolation of P_{dl} values to infinite strand size and the extrapolation of Silla's burning rate data [118] to zero burning rate, they inferred that heat losses might not be the only cause of P_{dl} .

Thus far, the works on the pressure deflagration limit have been reviewed on the basis of compositional effects and the heat loss argument. There has been advanced another explanation of the pressure deflagration limit. It is suggested that a self-excited mode of instability can lead to the extinguishment of a steady deflagration at a constant pressure. The combustion instability theory developed by Denison and Baum [42] has shown a criterion under which a solid propellant combustion becomes unstable without stimulus by pressure perturbation. Soviet investigators [133] have long been interested in the stability of solid propellant combustion itself without any coupling of external pressure disturbances. The physical and chemical parameters of the propellant determine the stability criteria. Although the parameters appearing in their model such as the burning surface temperature are difficult to measure within a desired accuracy, their concept deserves consideration.

A comment is necessary on the methods of determining the P_{dl} of solid propellants. Most investigators have used the slow depressurization method because of the extreme difficulty of ignition at low pressures near the deflagration limit. Some investigators [37, 69, 123] observed that the combustion of propellants near their P_{dl} was very susceptible to the rate of depressurization. Investigators adopted a different rate of depressurization which was satisfactory to their experimental purpose in determining the low pressure limit. As it is certain that the rate of depressurization does often affect the measured value of the deflagration limit, a thorough study is needed on this subject. Moreover an extension of this study to the higher rates of depressurization may reveal some important aspects of the response of low-pressure combustion to pressure transients.

D. EXTINGUISHMENT DURING DEPRESSURIZATION AT LOW PRESSURES

A large volume of work is available on the extinguishment of solid propellants via rapid pressure excursion. After Ciepluch's earlier experimental works [27, 28, 29] and von Elbe's theoretical explanation [128] on the subject, numerous investigators have attacked this problem. Some of the major arguments have been centered on the usefulness of von Elbe's form of the extinguishment criterion. It expresses that there is a critical ratio of the characteristic times (for depressurization and for the relaxation of the thermal wave) which is proportional to the exponent in the steady-burning law, or

$$\frac{r^2/a}{-(dn/p)/dt} = \frac{n}{\Lambda} \quad (II-1)$$

In this equation r is the steady regression rate at pressure p ; α , the thermal diffusivity; p , pressure at time t ; and n , the burning rate exponent. Depending upon the author of the treatment [94, 96, 127], Λ takes the value of $1/2$, 1 or 2 . Criticism of this expression comes from the fact that this equation does not have a sound physical basis [86, 135] and moreover it fails to predict the extinction behavior of the catalyzed propellants [44, 83]. Von Elbe and McHale [129] by modified strand burner tests, and Jensen [67, 68] by motor tests, respectively, have shown that Eq. (II-1) predicts the extinction behavior of some propellants quite well and emphasize the merits of the simplicity of that expression.

More rigorous theoretical treatments of this problem have been undertaken by Horton, et al. [60], Woolridge, et al. [135], Merkle, et al. [86], and Coates and Horton [32, 33]. All of the authors have solved the transient heat conduction equation in the solid with different laws for transient heat feedback from the gas phase to the burning surface, claiming that their theories predict the extinction behavior of solid propellants very well. Since the uncertainty in the physicochemical parameters is not easily resolved, these theories need further examination. The evaluation of these theories is not in the scope of this work. What is concerned in this program is the findings of others that the extinction is most sensitive to the last part of the depressurization history or the final system pressure itself. Ciepluch's results [27, 28] with rapid depressurization indicate that the effect of initial pressure is mild on the extinction requirement, and the final pressure attained is important in determining whether extinguishment is permanent or is

followed by spontaneous reignition. A series of workers at the University of Utah have found the initial pressure produces little effect on the extinction requirement of a strand in a rarefaction tube during depressurization [4, 44, 83, 112]. Instead the final dump-tank pressure decides the extinguishment-no-extinguishment criterion within 0.01 atms [4, 112]. Woolridge, et al. [135] also reported that a motor extinguishment during depressurization was very sensitive to the final dump tank pressures.

What all these experimental results suggest is that the extinction during depressurization occurs at the final stage of the pressure history near the final dump tank pressure, when the nozzle is dechoked. The vital importance of low pressure processes near atmospheric or subatmospheric pressures is conceivable.

E. SUMMARY OF LITERATURE REVIEW

1. On the deflagration limit of composite propellants there have been accumulated too few reliable data to support a theory of extinguishment. Moreover, the data taken by different investigators are not compatible with each other due to non-standardized experimental procedures.
2. Analytical approaches for P_{dl} based on heat losses have not been successful in predicting the measured value of P_{dl} . The instability model appears to be promising, but may require heat loss considerations if Spalding's argument is accepted.

3. Certainly heat losses impose a significant influence on the extinguishability of a strand burning at low pressures, although they may not explain the pressure deflagration limit.
4. The extinguishment of solid propellants by rapid depressurization appears to be dominated by the low pressure combustion processes. Hence, the information on the response of the low pressure burning to pressure transients is necessary to understand the extinguishment during rapid depressurization.

CHAPTER III

GENERAL FEATURES OF EXPERIMENTAL APPARATUS

A. COMBUSTION CHAMBER AND ACCESSORIES

A combustion chamber, schematically shown in Figure III.1, was specially designed for low-pressure combustion studies and used throughout this investigation, except for the tests on the rapid depressurization and reignition study. The chamber consisted of a dome and a base which fitted together by flanges. The base, 25 cm i.d. and 13 cm height, had eleven threaded holes on the wall for the gas and electrical connections, including a 1-1/2-inch fitting for the exhaust line. The dome, 25 cm i.d. and 31 cm height, was equipped with three 5 cm diameter windows, two on the side wall and one on the top. An overhead pulley system with a counter-weight was utilized to facilitate handling the dome. The chamber was made of mild steel, plated by nickel to minimize corrosion. The chamber embraced 20 liters of free volume which gave enough room to put the necessary apparatus inside. Moreover, the large chamber volume was necessary to eliminate any possibility of dynamic coupling between chamber gases and combustion or the discharge of gas at low pressures. Inside the chamber a stand made of micarta plate was installed to support the electric terminals and the sample holder. There was also contained a fixture for a fast heating furnace or a cooling coil (described later in this chapter).

The flow diagram for the combustion chamber is shown in Figure C.1. There were two exhaust systems, main and auxiliary. The 1-1/2-inch diameter main exhaust line included a main orifice, a quick-opening ball valve of one inch port, and a large dump tank, 1,300 liters in volume. The auxiliary exhaust line depressurized the combustion chamber through an auxiliary orifice and a 3/8-inch needle valve operated by a quick acting pneumatic cylinder. The auxiliary line had a half inch diameter and the auxiliary dump tank had a volume of 120 liters. To draw the necessary vacuum in dump tanks, a Nash Hytor Vacuum Pump was utilized in series with a No. 2-26-6 Nash Air Ejector. Without gas generation inside the system, the vacuum could be drawn to as low as 0.016 atms. However, during experiments with a propellant sample burning inside, 0.02 atms was about the minimum attainable.

Compressed air admitted through solenoid valves was used to drive the pneumatic actuators. Nitrogen was introduced to purge the force transducer and the sample, when necessary. A pressure transducer was mounted on the inner wall of the combustion chamber.

The electric circuit diagram for the combustion chamber is shown in Figure C.2. The circuit had two control panels, local and remote. The remote control panel was located outside of the tunnel in the control room, and was used when tests were carried out with the chamber pressures more than 10 atms. Relays, timers, and a pressure switch were arranged so that a test by the predetermined cycle could be carried out. Hand operation was also possible by continuously monitoring the relevant switches, if necessary. A variac was utilized to supply the appropriate voltage to the ignition wire.

A pyrofuse wire or a nichrome wire was used for ignition. For detailed information on the flow control system and the operation of the control circuit, refer to Appendix C.

B. FORCE TRANSDUCER

A Stathan Model UC3 force transducer was adopted to measure the burning rate continuously. Figure III.2 shows the schematic diagram of the sample mounting on the force transducer. To prevent any damage by the corrosive combustion gas, the head and the chamber of the transducer were continuously purged by flow-controlled nitrogen which acted as a cooling gas around the sample edge. A mica sheet was inserted between the aluminum sample holder and the transducer head to prevent it from being heated by the flame and the furnace.

A recoil-force compensator was used when the transient burning rates were measured. It had the shape of a flat umbrella. The top plate, an aluminum disc of 5 cm diameter and 0.16 cm thick, was connected to the sample holder by four thin stainless steel rods. The distance between the plate and the sample holder is 6.5 cm. The fast moving combustion products struck the top plate and were deflected horizontally, exerting an upward force which compensated for the downward force resulting from the initial acceleration of the burned gases. The transducer thus detected only the weight of the sample. When the compensator was not attached, the transducer detected the recoil force in addition to the weight.

The electric circuit schematic diagram for the force transducer is shown in Figure C.3. The circuit was specially designed to

signal a zero output for the preload of the sample holder. A low pass filter was also designed to filter out the noise signal due to the natural frequency of the transducer and weight system which was around 100 Hz.

C. QUICK HEATING FURNACE AND COOLING COIL

To simulate the thermal conditions of a rocket motor in a strand burner, a quick heating furnace was needed. In Figure III.5 a schematic and wiring diagram of the quick heating furnace is shown. It was a cage of nichrome strip wound on a frame made of alumina tubes and transite plate. The heating element, nichrome strip, was so thin that it was possible to raise the temperature to 700°C within 20 seconds. The highest temperature to be obtained was about 900°C. The desired temperature level of the nichrome strip was maintained by a Leeds and Northrup three-mode temperature controller along with a SCR electronic switch. A few degree offset was noticed between the set temperature of the controller and the actual temperature but generally the performance of the controller was excellent. The bead of 0.01 inch diameter chromel and alumel thermocouple was directly welded on the nichrome strip at the position approximately 7 cm from the top plate.

A hinged fixture of aluminum which held the furnace made it easy to remove and relocate the cage over the propellant strand. The distance the sample protruded inside the cage was approximately 2 cm. The nichrome strip did not cover all of the hemi-spherical enclosure surface a burning surface would see. Moreover, the temperature distribution over the nichrome surface was not uniform

due to the natural convection, so that the calibration of the furnace was necessary. Later, a radiation reflector made of polished aluminum sheet (0.16 cm thick) was utilized to increase the furnace efficiency. The radiative heat flux reaching the position where a propellant surface would be located was calibrated by a Hy-Cal Engineering Calorimeter (Model C-1301-A-120-072) in terms of the actual furnace wall temperature. Figure C.6 shows the calibration data along with the black-body emissive power. By means of this figure it was possible to assign an effective black-body wall temperature corresponding to the measured furnace wall temperature. The variation of flux intensity at different distances from the bottom plate was rather small so that it was assumed to remain constant during the regression of the burning surface.

For experiments not using the furnace, the thermal surroundings were maintained at a fixed temperature by replacing the furnace with a cooling coil shown in Figure III.7. The coil consisted of tightly wound quarter-inch stainless steel tubing, the side wall being a helix of 7 cm diameter and 19 cm height and the top being a spiral of 10 cm diameter. The temperature of the coil was maintained at a constant level about 15°C by a continuous flow of cooling water. Thus, the burning surface, located near the bottom of the coil, saw nothing but the wall of the temperature-regulated stainless steel tube.

D. SMALL-L* BLOW-DOWN CHAMBER AND ACCESSORIES

For the rapid-depressurization extinguishment and reignition study, a small test chamber as shown in Figure III.8 was used in conjunction with a short (30 cm long) rarefaction tube and an orifice. The chamber and tube were originally designed and used by Schulz [112]. The combined chamber, in 5.3 cm i.d. and 44 cm long, was conveniently termed a small-L* blow-down chamber because it was not used as a rarefaction tube but as a blow-down chamber, in which at high pressure a series of small rarefactions approximates a continuous depressurization history. If there is sonic flow in the throat, the pressure-time curve can usually be adequately represented as a decaying exponential. If the nozzle flow is subsonic, the ambient (in this case, dump tank) pressure also affects the pressure history. The fractional rates of depressurization for sonic nozzle conditions were calculated for all the orifices employed with the assumptions of isothermal blow-down conditions and ideal nozzle and are given in Table C.III. This small-L* chamber, approximately one liter in volume, could produce a fractional rate of depressurization as high as 350 sec^{-1} when incorporated with orifices as large as 4.82 cm in diameter.

The sudden pressure drop was achieved by bursting a cellulose acetate diaphragm, mounted at the end of a connecting tube of 30 cm length, by an electrically operated plunger. The cellulose acetate diaphragm of an appropriate thickness was chosen for a given initial pressure. The exhaust line consisted of 2-inch pipe and a 2-inch port gate valve. The length of the exhaust line from the diaphragm

to the main tank was approximately 60 cm. A cooling coil was wound around the rerefaction tube to restore the tube quickly to original room temperature after each run. Cooling water at 15°C flowed continuously. Between tests, the small-L* chamber was purged with compressed air to quicken its cooling. The electric control circuit for combustion chamber was also used for the small-L* chamber operation after a slight modification was made.

CHAPTER IV

STEADY BURNING BEHAVIOR OF COMPOSITION PROPELLANT
STRANDS NEAR THEIR LOW-PRESSURE DEFLAGRATION LIMITS

A. BACKGROUND

Since the pressure deflagration limit is a boundary between the stable and the unstable combustion regimes, it is meaningful to see how the stable burning at higher pressures degenerates to the unstable regime at low pressures.

The burning rates of composite propellants at subatmospheric pressures have been measured by several investigators [49, 101, 118, 123]. Not much information can be obtained from others' burning rate data. Generally, burning rates are reasonably well represented by Vieille's Law, $r = a P^n$. The burning rate exponent is much dependent upon the type of the binder, ranging up to very close to unity. Ohlemiller and Summerfield [92] observed that a large amount of AP was ejected from the burning surface of PBAA-fueled propellants at low, subatmospheric pressures. The amount of AP ejected was, in some experiments, nearly 50% of the original content in the catalyzed propellants. Steinz, et al. [123] remarked that the combustion of composite propellants at subatmospheric pressures is very inefficient due to the evolution of white fumes containing 25% ammonium perchlorate and 55% ammonium chloride, as well as the ejected AP particles.

The burning surface temperatures at low subatmospheric pressures were measured by Powling [102] and Most [referred to in 123]. At about 0.05 atms the burning surface temperatures of AP-paraformaldehyde composites were around 400°C according to Powling and those of polysulfide propellants were reported in the range of 250-300°C by Most.

In this work, burning rates and flame temperatures were measured for several propellant systems at low pressures. A preliminary study on burning-surface temperature measurement was made. Standardization of P_{dl} measurement and the effect of composition on P_{dl} were sought.

B. EXPERIMENTAL PROCEDURE

1. Burning Rate Measurement

Burning rates were measured from the weight vs. time record of the combustion carried out at constant low pressure. Samples 1.25 cm X 1.25 cm in cross-section and approximately 2.4 cm long were inhibited on the sides by Krylon acrylic solution, or later by Kel-F #90 grease. Ignition was achieved by pyrofuse of nichrome wires. The transducer and the sample edges were continuously purged by nitrogen at a low flow rate during a test. A cooling coil was inserted inside the combustion chamber to maintain constant thermal surroundings. The pressure was measured by a pressure transducer. At least two runs were made for each of the experimental conditions employed.

2. Go/no-go Test for P_{dl} Measurement

During the preliminary study, the slow depressurization method was adopted, as by most other investigators. A propellant strand was ignited at a pressure where ignition was easily achieved, and

the system pressure was slowly decreased until extinguishment occurred. The extinguishment pressure was found to be very much dependent upon the rate of depressurization. To obtain a minimum asymptotic value of extinction pressure for slow-burning propellants, extremely small rates of depressurization were required. Moreover, for irregularly burning, high P_{dl} propellants, this method failed to give reproducible extinguishment pressures, values sometimes being even lower than the steady pressure at which the sample would sustain burning. Thus, a go/no-go test at a fixed pressure had to be devised.

In further preliminary experiments (described in Appendix A), it was established that heat losses from edges of the burning surfaces were not significant in quiescent ambient gas if the surface was 1.2 cm square or larger. It was observed that inhibitor material on the sides of the strands had a detectable influence on the extinguishment pressure. A thin film of Krylon was selected as standard. It was also observed that extinguishment pressures were different if air rather than nitrogen was used as ambient gas. Nitrogen was used thereafter. At first no effort was made to control the thermal surroundings, ambient gas and the chamber wall. Later, a cooling coil was inserted inside the chamber and the effect of thermal surroundings was noted. With these standardized experimental conditions, the P_{dl} of a propellant was measured in the following way.

The pressure was adjusted to the desired level in the combustion chamber and the connected large vacuum tank. The ignition was achieved by a nichrome resistance-heater filament one mm from the exposed

propellant surface. Even at pressures below P_{dl} , ignition could be achieved because of the thick heated zone developed in the solid by the slow ignition process. Ignition voltage was adjusted during the course of the ignition transient by a variac. During the slow heating stage, approximately 5V was applied for 20 to 30 seconds. If ignition did not occur after 30 seconds, the voltage was increased to about 8V. After ignition, the ignition power was reduced to about 4V, and maintained there until the flame spread all over the surface and a steady deflagration was established. Then the power was slowly reduced to zero. Initial burning was promoted by the stored energy and by the radiation heat feedback from the heated nichrome wire. The transient burning ordinarily ceased after the surface regressed about 6 mm, the estimated thickness of the preheated zone, if the pressure was far below the pressure deflagration limit. At pressure close to but slightly below the deflagration limit, the surface continued to regress beyond 6 mm, aided by the weak radiation from the heated wire, but deflagration stopped at a position of 10 mm to 18 mm, depending on the pressure level and the propellant kind. A slower-burning propellant deflagrated a little farther before it quit burning, verifying the effect of radiative heat flux on the secondary stabilization of combustion. Introduction of the electric power in the ignition wire detectably increased the distance burned. However, the pressure difference between the burn-out and the pressure at which a propellant deflagrated about 12 mm was negligible for most propellants, indicating that the radiation effect diminished quickly as the surface regressed from the igniter

wire. Thus the extinguishment pressure and the burn-out pressure could be identified with the burn-out pressure corresponding to 10 to 18 mm of surface regression.

3. Flame Temperature Measurement

Pt and Pt-10 percent Rh thermocouples were used. A 0.005-inch Pt wire and a 0.010-inch Pt-10 percent Rh wire were welded together with an oxygen-acetylene mini-torch. The bead portion of the thermojunction was coated by silica to minimize combustion catalysis. The size of the coated bead was about 0.6 mm. A radiation correction was necessary to get the true flame temperature. If the bead is assumed to be a sphere, the following relationships can be derived [107]:

$$\Delta T = \frac{1.36 \epsilon D}{kNu} \left[\left(\frac{T_c}{1000} \right)^4 - \left(\frac{T_a}{1000} \right)^4 \right] \quad (IV-1)$$

$$Nu = 2.0 + 0.6(Re)^{1/2}(Pr)^{1/3} \quad (IV-2)$$

where ΔT is the difference between the real flame temperature and the thermocouple temperature °C; ϵ , D , and k are emissivity, bead diameter in cm, and thermal conductivity in cal/cm sec °K of the thermocouple, respectively; Nu , Nusselt number; T_c , the thermocouple temperature, °K; T_a , the temperature of the surrounding, °K; Re , Reynolds number; Pr , Prandtl number. The emissivity of silica coated thermocouple can be taken to be 0.22 following Kaskan [71].

The thermocouple was vertically mounted above the burning surface, with the bead initially touching the surface. The signal was recorded by a Speedomax two-pen recorder along with pressure signal.

The flame temperature was observed to decrease as the burning surface moved away from the bead. The initial value near the burning surface was taken as the flame temperature. When the flame temperature was above about 1400°C, the failure of the silica coating was observed. Thus, less confidence is given to the flame temperature data higher than about 1400°C.

C. EXPERIMENTAL RESULTS

1. Burning Rate

Burning rates were measurable within three percent error. Burning rates below two atms to the P_{dl} of each propellant were measured for several PU, PBAA, and HTPB propellants and are shown in Figures IV.1, IV.2 and IV.3, respectively. The lines were drawn through the averaged values of at least two runs. Comparison can be made on the effects of oxidizer loading, aluminum content, and catalyst on the burning rates. Vieille's Law for burning rate as a function of pressure does not hold well for most propellants in this low pressure range except catalyzed propellants at pressures above 0.2 atms. For all propellants, the burning rate curves tend to bend downward as the pressure approaches the limiting pressure. This trend is most significant for slow-burning PU propellants. The slope of the curves, the burning rate exponent, increases at lower pressures to almost unity for most PBAA and HTPB propellants as the limiting pressure is approached. The maximum exponent is generally greater for slower burning propellants, being larger than unity for some PU propellants. The slowest burning propellant, UED, has the maximum value of 1.3. The burning-rate exponent greater than unity

is not likely in the context of an adiabatic flame model like Denison and Baum's because it implies a gas-phase reaction of order greater than two to be rate controlling. An alternative, and sufficient, explanation is that heat losses become significant at these low burning rates.

The prominent effect of fuel type is magnified at pressures below 0.1 atms. In order of decreasing burning rate are PBAA, HTPB, and PU propellants. The promotion of burning rate by copper chromite catalyst is also remarkable. Replacing AP by 5% aluminum powder (compare UFB with UEK, for example) produces a mild increase in burning rate of all types propellants.

Probably the most striking aspect of burning rate behavior of composite propellants at low pressure is the influence of oxidizer loading. One might expect that the more highly oxidized propellant would have a higher flame temperature due to a composition closer to stoichiometric and would, therefore, exhibit a higher burning rate, as is the case at higher pressures. In fact, the more fuel-rich propellant gives a higher burning rate at low pressures in the case of all those propellants. This trend is most conspicuous at the lowest pressures and tends to diminish as the pressure is increased. For PBAA and PU propellants (compare UEM and UEK, for example), this trend holds at pressures as high as 2 atms.

This anomalous burning behavior below 0.2 atms is best seen in Figure IV.4, where the results for some more propellants are also included. The curves for PBAA propellants of low AP loading, 70% and 72.5% AP, cross over those for the other more highly oxidized propellants at very low pressures. However, near their low-pressure

limits, they exhibit higher burning rates. The very fuel rich propellant, 70% AP, could not be extinguished in the experimental system used. In general, a propellant with a higher burning rate at low pressure exhibits a lower deflagration limit. This is only true for the same binder system. The extinguishment pressures for highly oxidized PBAA propellants are in the same range, around 0.05 atms, as those of PU propellants, although the burning rates of PBAA propellants are almost three times as fast as those of PU propellants. Certainly some other factors are affecting on the extinguishment pressures.

2. Pressure Deflagration Limit

The measured values of the deflagration limit with a cooling coil were a little higher than those without a cooling coil inside the chamber. The results are summarized in Table B-I. In Figures IV.5 and IV.6, the results without cooling coil are plotted since the P_{dl} data for most propellants were taken in this manner. The P_{dl} data with cooling coil for some propellants have already been shown in Figure IV.4.

In Figure IV.5, the deflagration limit is shown as a function of AP particle size (monomodal) for two propellant fuel binders. The deflagration limits of PBAA-fueled propellants are all very low and only slightly affected by the particle size of AP. The propellant of the finest AP size and the largest AP size have somewhat higher P_{dl} than that of intermediate particle size. The limits of PU propellants are markedly higher than those of PBAA ones and decrease sharply as the AP particle size is increased, up to about 400 μm .

The result is attributed to the melting of PU. Molten polymer coated the crystals as verified by scanning electron microscopy (shown in the following section) and prevented their participation in the surface reactions. Larger crystals project beyond the molten layer and can react.

Similar information is given in Figure IV.6 where the deflagration limit is plotted against AP loading for several binder types. Here AP is 60/40 bimodal mixture customarily used for high loadings. The reaction-inhibiting effect of molten PU polymer is again apparent. Above a loading of 80%, however, there is not enough melt to produce the effect; the deflagration limit is little affected by AP loading. Propellants fueled with poly(lauryl methacrylate) (PLMA) behaved similarly. This polymer seemed more prone to melting, as judged by inspection of the extinguished surface. More than 85% AP loading is needed to prevent the melting effect of this binder. The deflagration limit for a fluoro-carbon-fueled propellant (FC), supplied by the Thiokol Chemical Corporation, is found to be above 5 atms. Propellants containing PBAA or HTPB unexpectedly showed a higher P_{dl} for more highly oxidized propellants. This observation appears to be compatible with the previous observation that more fuel-rich propellants burn faster, and a common explanation will be offered.

3. Flame Temperature

The degree of combustion inefficiency is indicated by the difference between the flame temperature measured and the adiabatic, equilibrium flame temperature. The adiabatic, equilibrium flame temperature was calculated by the computer program obtained from the

U. S. Air Force Rocket Propulsion Laboratory, Edwards Air Force Base. In Figure IV.7, a comparison is made between the adiabatic flame temperatures and the measured thermocouple temperatures of a PBAA propellant as a function of pressure. Those measured thermocouple temperatures are direct readings from the thermocouple outputs, not being corrected for radiation to the surroundings. Even though the measured thermocouple temperature is not the real flame temperature, the difference between the theoretical value and the measured value is an indication how the combustion efficiency drops as the pressure is lowered. The difference clearly increases as the pressure is dropped. The effect would be more pronounced if the radiation correction were made because the magnitude of correction increases when the thermocouple temperature is higher. The radiation correction near the extinction pressure is about 100°C. Even so, the corrected flame temperature is on the order of one half of the adiabatic flame temperature at low pressure. It appears that the combustion of this propellant is very inefficient at all subatmospheric pressures, becoming more inefficient as the pressure drops.

Similar information is given in Figure IV.8 for a catalyzed PU propellant. Differing from Figure IV.7, the curve starts to drop sharply below about 0.3 atms and changes little above 0.3 atms. Again, a loss in efficiency is indicated at very low pressures.

The flame temperature data for many propellants near their low pressure deflagration limit are summarized in Figure IV.9. The uncorrected flame temperatures at P_{dl} range between 900°C and 1150°C. The temperature correction is calculated to be in the range 50 to

100°C, which makes the corrected flame temperature 950 - 1250°C. It is noted that 950°C, the minimum flame temperature found in this work, compares well with the results of other investigators for pure AP [2, 52].

4. Supplementary Observations

a. Binder Melting

The melting behavior of PU and HTPB polymers was confirmed by microscopic study of the burned surfaces. Figure IV.10 depicts the burned surface of a PU propellant photographed by a scanning electron microscope. This propellant, UDV, contains only 400 micron AP particles. The individual pancakes have the linear dimension of about 400µm across, and are polymer caps covering AP crystals. A similar photomicrograph (not presented) of extinguished surface of a PU propellant with fine AP particles indicates that most of the particles were covered by molten binder.

The burning of high P_{dl} propellants, having P_{dl} greater than 0.2 atms was very irregular, as revealed by the fluctuation of the weight transducer signal, by visual observation, and by the highly non-uniform extinguished surface. Such propellants burned rapidly on one portion of the propellant surface, then the flame shifted to another area and the burning occurred fast in that region. This erratic burning phenomenon appeared to be largely due to the melting characteristics of binders.

b. Surface Layer on PU propellants

A thick, brown colored surface layer was observed on the extinguished surface of bimodal PU propellants with oxidizer loading

higher than 80%. The thickness of the surface layer was greater for burning at lower pressures. Near the limiting pressure, the layer was as thick as 1.5 mm. A distinct boundary existed between the surface layer and the virgin propellant, so that the layer was easily separable from the rest of the strand. It was brittle and a little porous. A photomicrograph of this layer is shown in Figure IV.11. The upper part of the picture represents the interface of the virgin propellant surface, where the surface layer was removed. The lower part shows the surface layer and its burned surface. The structures of the two surfaces are similar. The large AP particles, being covered partly with the binder and showing no sign of decomposition, are seen on the burned surface. Several small pores are also seen in the binder matrix. The partially decomposed, molten polyurethane polymer appeared to hold AP particles on the surface, preventing ejection of the kind noted with PBAA, and to a lesser extent, HTPB propellants.

c. AP Ejection

After a low pressure burning, of bimodal PBAA propellants in particular, large AP particles were observed inside the combustion chamber, and also some white powder was deposited on the inner surface of the chamber dome. The solid combustion products, both the large solid particles and the white powder, were collected together on a glass disc under a downward-burning strand and analyzed by an X-ray crystal analyzer. The solid products were shown to be a mixture of ammonium perchlorate and ammonium chloride. Certainly large AP particles were ejected from the burning surface, while

ammonium chloride was likely to be formed in the after-burning zone.

Other evidence of AP ejection is from the examinations of the extinguished surface by scanning electron microscopy. Photomicrographs of the burned surface of a bimodal PBAA propellant, extinguished near its limiting pressure, are shown in Figure IV.12. The many holes are comparable in size to the larger AP particles, and it is believed that the particles were ejected from them. Other large AP particles are seen still in place.

Figure IV.13 shows the extinguished surface of a unimodal PBAA propellant containing 15-micron AP particles. AP particles are rarely seen on the surface. In the matrix of fuel residue, there are voids approximately the size of the particles. Some AP particles may have been ejected from these holes, but it is suggested that most of the fine AP particles were decomposed on the surface at a much faster rate than the fuel binder regressed. Supporting evidence is that the shape of the holes are not as smooth as those in Figure V.12. Furthermore, the flame temperature of this propellant near its P_{dl} still remains relatively high, as shown in Figure IV.14. Moreover, AP ejection was seldom observed from unimodal PBAA propellants of larger AP particles. It is probable that fine AP particles in a bimodal propellant promote the ejection of the larger particles. An explanation is given later.

Less but detectable amounts of AP were ejected from HTPB propellants and catalyzed PU propellants burned at very low pressure. No AP ejection was observed from uncatalyzed PU propellants. Copper chromite catalyst appeared to prevent the coverage of AP by the

molten binder. For a given binder system, the amount of AP ejection increases as the AP loading is increased and as the pressure is lowered.

d. Burning Surface Temperature

It was attempted to measure the surface temperature by thermocouples (for details, see Appendix E). A chromel-alumel thermocouple with a bead thickness of 25 μ m was imbedded in the propellant so that the flat surface was parallel to the regressing surface. The measured values of burning surface temperature for a PBAA propellant (G propellant) at 0.067 atms were in the range of 240 to 270°C. This temperature is taken to be a minimum possible value because corrections were not made for either conduction through the leads or radiation to the surroundings. The true temperature of the polymer at the burning surface was probably at least 350°C.

e. Oscillatory Burning

Most normally burning propellants exhibited oscillatory behavior in the vicinity of the P_{d1} , as detected both by the force transducer and by photocell signals. The nature of the oscillation was much dependent on fuel type, AP particle size, and the pressure level. For many bimodal propellants, two modes of oscillation at widely separated and not-harmonically related frequencies were observed. The oscillatory burning was very regular in PU and HTPB propellants and less regular in PBAA propellants. In general, the faster mode of oscillation was very distinct and regular, while the slower mode was less regular.

When the propellant combustion was initially stabilized by preignition heating, the oscillatory burning was most conspicuous, oscillation amplitude increasing as extinguishment was approached.

This oscillatory burning near the limiting pressure provides strong support to the view ascribing the low pressure extinguishment to the intrinsic instability of low pressure combustion. An extensive study on this subject and data analysis will be made in the next chapter.

D. DISCUSSION OF RESULTS

1. General Features of Low-Pressure Burning

The pronounced effect of fuel type on the burning and extinguishment of composite propellants at low pressure is not likely to be explained solely on the basis of the energetics and kinetics of the binder decomposition. While the magnitude of the heat of combustion and the ease of thermal and oxidative degradation of the binder are the primary factors differentiating the low-pressure burning behavior among different fuel systems, the physical characteristics of the binder as they determine melting and AP ejection are also important factors.

When the burning occurs at high pressures, the rates and, accordingly, the surface temperatures are high. Furthermore, the maximum rate of heating as the surface reaches any designated particles of polymer is also great so that polymer can attain high temperatures without degradation. Thus, the oxidative pyrolysis of polymer become prominent before depolymerization and other degradation reactions modify the polymer. The details of polymer chemistry are not

important. Near the P_{dl} , however, rates are slow enough that easily depolymerized polymers undergo combustion-modifying changes before the oxidant enters the act. The details of polymer chemistry become important. The PU binder exhibits a molten film; the PBAA binder, remaining dry during burning, provides a decomposition surface on which both polymer and AP particles are exposed directly to energy feedback; and HTPB exhibits an intermediate behavior.

2. High P_{dl} Propellants

The high P_{dl} (more than 0.2 atms) of PU and PLMA-fueled propellants (Figures IV.5 and IV.6) is due to melting of those polymer fuels. The inertness of fluorocarbon is thought to be the cause of the high P_{dl} of the FC propellant.

Melting can inhibit burning of a propellant by physically covering AP particles and by cooling the binder surface. The molten polymer can protect AP particles in several ways; the already-formed film is at low temperature and may consist of less-reactive decomposition intermediates; the hot molecules undergoing decomposition on the surface can be mixed with the others in the bulk; the melt can wet or flow over the surface of burning AP particles, and the burning AP particles may be drowned in the melt. Thus, the burning inhibition due to polymer melt is determined by the chemical nature and viscosity of the melt, by the thickness of the melt zone compared to the AP particle size, and by the amount of melt to cover AP particles.

The melting of PU binder is likely to be more than a simple physical melting which is probably accompanied by some depolymerization and perhaps other kinds of decomposition. Dyer and Wright [45]

report that the dissociation into isocyanate and alcohol is one of the reactions of urethane decomposition. Law [75], heating PU polymer with diol in stoichiometric excess of diisocyanate, noted spectrometrically the appearance of free isocyanate groups at about 350°C. He heated the sample at the rate of about 70°C/sec. At least some depolymerization should be noted at lower temperatures for PU propellant burning near its P_{dl} , where the maximum rate of heating of the burning surface is estimated to be about 5°C/sec. The endothermic effect of the depolymerization and other reactions cools the burning surface.

The melting temperature of PU polymer has been measured by several investigators. Varney [127], by DSC tests with a slow heating rate (5 - 80°C/min), observed that an Estane-type PU binder melts at 222°C and at 342°C, the liquid binder becomes very fluid, followed by a boiling-like activity. A similar melting temperature (215°C) is recorded by Shannon and Erickson [116]. They also adopted the DSC technique with the heating rate of 10°C/min. Bouck, et al. [20] report that rupture of a PU film occurs at 317°C when it is heated at the rate of 300°C/sec. However, their thermogram shows that the onset of endothermic effect occurs at a further lower temperature about 200°C. As is inferred from those works, the PU binder melts at temperatures far lower than the active AP decomposition temperature [14, 15].

A significant effect of depolymerization on the P_{dl} is found in PLMA propellants (Figure IV.6). More than 85 percent of the solid loading is required for those propellants to minimize the melting

effect compared with 80 percent for PU-fueled propellants. The depolymerization of polymethacrylates is well known [51, 81].

The influence of melt-zone thickness on ease of burning is perceived from the experimental results with the unimodal PU propellants. The propellant containing the finer oxidizer particles has the higher P_{dl} . A relation may exist between the size of oxidizer particles contained in a propellant and the melt-zone thickness near its P_{dl} . With this idea, the computed thermal wave thickness near the P_{dl} and the particle size of AP contained are compared in Figure IV.15 for several unimodal PU propellants. The thermal wave thickness, a measure of melt-zone thickness, is seen to be roughly proportional to the oxidizer particle size.

The high P_{dl} (more than 5 atms) of the propellant fueled with fluorocarbon binder appears mainly due to the inertness of the polymer as Peterson, et al. [99] suggested. The results of high-heating-rate thermal analysis by Bouck, et al. support this view. They observed that the film of a fluorocarbon polymer did not rupture at temperature more than 500°C and its degradation was little affected by an oxygen environment. The fluorocarbon-fueled propellant burns very slowly, compared with the propellants fueled with the other kind of binder, and the burning is erratic near the P_{dl} , suggesting that this polymer also may experience melting to some degree.

3. Highly-Oxidized PU Propellants

The burning of the bimodal PU propellants with AP loading more than 80 percent is normal in the sense that it is not erratic and is steady to very low pressures (Figure IV.1). However, these

propellants exhibit a very strange burning behavior, observed also for the PBAA and HTPB propellants; a more highly-oxidized propellant burns more slowly and has a higher P_{dl} (Figure IV.4). An explanation is necessary for this unexpected behavior.

In order to explain this contradiction, we introduce some postulates applicable to all three binder systems. The basic idea to work in is that with bimodal AP we have a very rich unimodal propellant (with fine AP) in which large AP particles are dispersed. Let us postulate that the regression rate of a propellant is determined by the regression of continuous phase (polymer with fine AP). We again postulate that the decomposition rate of large AP particles is so low that it contributes little to the oxidative pyrolysis of binder. The other postulates, as already inferred and applied previously, are that much of the polymer goes to gas via oxidative pyrolysis and that the burning rate is primarily determined by the surface temperature and thus likewise by the heating rate.

Most of those postulates are based on experimental observations. Now we are seeking their justification by closely examining their applicability to various experimental results. Although all three binder systems may have the common origin of abnormality in their burning behavior, the detailed processes are different depending upon the binder. Thus, the explanation is separately given for each binder system.

With more than 80 percent AP in bimodal PU propellants, the amount of melt is not enough to cover effectively the AP particles to produce erratic burning and then give a high P_{dl} . However, the melt can laterally cover the AP particles to reduce the AP

decomposition surface. Still, the heat of melting has the effect of cooling the burning surface. By these effects, the burning rates of those propellants are very small near their P_{dl} . The residence time of a polymer particle inside the thermal wave is so long that it is subjected to further combustion-modifying processes after melting in the depth of the propellant. The PU polymer by further changes, probably by cross-linking processes, may actually become a drier solid matrix as it approaches the burning surface. The AP particles are relieved from the melt coverage and can react.

The large AP particles do not decompose as fast as the fine AP. The decomposition products of fine AP particles promote the oxidative pyrolysis of the binder in their vicinity. Thus, the decomposition front of the polymer matrix including fine AP, proceeds faster leaving the large AP particles and associated polymer decomposition intermediate behind. The rich gases from the decomposition front of the continuous phase (the polymer and fine AP) flow through the porous bed containing large AP particles and enter into the gas phase, where they react with the oxidizer-rich decomposition products of the surface layer. In this manner the observed surface layer is inferred to be formed.

We further infer that the existence of this surface layer is responsible for the strange burning rate behavior of highly-oxidized bimodal PU propellants. The overall regression rate of those propellants seems to be governed by the rate of decomposition reaction of the continuous phase. The energy necessary for this endothermic reaction comes mainly from the gas phase reaction and also from the exothermic oxidative pyrolysis. Apparently, the large AP particles

act as an inert energy-absorbing medium, so that the more highly-oxidized propellant actually has a lower effective temperature at the controlling reaction zone. Moreover, the thicker surface layer as observed for the more highly-oxidized propellant lessens the effective energy feedback from the gas phase. Thus, the burning rate is less for a more highly-oxidized propellant.

The role of copper chromite catalyst increasing burning rate is not well known. From the tendency that a catalyzed PU propellant ejects AP, it appears that copper chromite promotes the decomposition of AP, of finer particles more effectively. With the help of the oxidizer decomposition products, the oxidative pyrolysis of binder could be still prominent for catalyzed propellant even at low pressures. The resultant faster burning rate gives a higher surface temperature and the heating rate of the polymer is so high that little time is available for the polymer to melt.

When some of the AP is replaced by the same amount of aluminum powder, the burning rate is probably increased by the hotter flame.

4. PBAA Propellants

The PBAA propellants do not exhibit a significant effect of AP particle size on the P_{dl} (Figure IV.5). They were the fastest-burning propellants among the binder systems considered (Figure IV.4) and eject a large amount of AP particles at low pressures when made with bimodal AP. Again, the chemical nature of this binder, as producing little melt during decomposition and giving high reactivity, largely dominates the observed burning phenomena.

The PBAA polymer does not readily melt during the course of degradation as inferred previously from the photos of the extinguished

surface of the PBAA-fueled propellants. Supporting evidence comes from the results of DSC tests by other investigators [116, 127]. One can also perceive its limited-melting behavior from its chemical structure. The PBAA binder, obtained by reacting the carboxyl groups in prepolymer with the epoxy groups in Epon, is cross-linked by ester-linkages. The ester-linkages are not expected to be so reversible as urethane-linkages [51]. Hence, melting by depolymerization is less likely to occur for PBAA polymer. The physical melting also seems more difficult for this polymer than for PU.

A high decomposition temperature of PBAA binder is predicted by its thermally stable structure. Varney reports that the decomposition of this polymer starts at 337°C and reaches a peak at 407°C. High-heating-rate tests by Bouck, et al. show the film rupture temperature of this polymer to be 464°C. Another chemical nature of the PBAA binder is that this polymer is more vulnerable to oxidative degradation than PU, due to the double bonds and reactive allylic hydrogen atoms on its backbone.

These properties of PBAA binder are the suggested fundamental explanation for the burning behavior of PBAA propellants. High temperature can be obtained by this polymer without degradation to liquid. Furthermore, as inferred from burning rates higher than for PU and HTPB propellants, the burning surface temperature is also greater. Likewise, the maximum rate of heating is greater, estimated for PBAA propellants burning near P_{dl} to be 50 - 100°C/sec. Thus, the combustion-modifying changes PBAA polymer may undergo in very slow heating conditions cannot occur.

Although the non-melting and the reactivity of the PBAA binder may explain the observed insensitivity of the P_{dl} of propellants fueled with this polymer to the oxidizer particles size and loading, there are many more questions to be answered. Note from Figure IV.14 that the limiting burning rate and flame temperature are much higher for a unimodal propellant containing the finer AP than one with a larger AP but the pressure deflagration limits of all propellants are nearly the same. Those extinguishment phenomena cannot be explained by the burning rate alone. The relative decomposition rates of AP and binder appear to be important. As mentioned previously, if AP particles are too fine, they decompose too fast on the burning surface leaving momentarily a fuel-rich burning surface. By stoichiometry, a moment later, the flame becomes rich in fuel with the rich surface decomposition. At a low pressure, a propellant may stop burning at this rich stage. The kind of instability inferred above appears to be the cause of the observed extinguishment behavior of unimodal PBAA propellants.

One of the prominent characteristics of PBAA propellants containing bimodal AP is the ejection of AP particles. In order to explain this phenomenon, we employ the postulate applied for the burning behavior of bimodal PU propellants. The continuous phase containing fine AP particles regresses faster than the large AP particles. Differing from PU propellants, PBAA has no molten layer to cement the large AP particles to the surface. The large AP particles may also decompose slowly and produce some oxidizer gases to help the decomposition of the continuous phase. When the regression front of the continuous phase passes, the exposed large AP particle is simply released and

driven away by the decomposition gases of the continuous phase. Before an oxidizer particle is fully exposed, it is also pushed out by some mechanism as indicated by the holes shown on the extinguished surface. One proposed mechanism is that reaction with gas generation occurs at the polymer-AP interface and the particle is flipped out. This is possible for the PBAA propellants which have supposedly a higher burning surface temperature than PU propellants. An alternative mechanism is that thermal expansion of rubbery material puts the surface under compression and the AP particles are squeezed out. If the surface were molten, the compressive stress would be relieved by flow.

The burning-rate behavior of bimodal PBAA propellants, the more rich propellant burning faster, can be explained by the premise postulated for PU propellants, namely, that the large AP particles are somewhat inert with respect to surface reactions. Large particles are simply flipped out of the surface with their sensible heat. As a result, the burning surface becomes cooler with fewer AP particles participating in reaction. Accordingly, the regression rate of the continuous phase becomes slower.

5. HTPB Propellants

The HTPB binder shows a behavior intermediate between those of PU and PBAA binders (Figure IV.4). It melts to some degree, and ejects some AP particles.

With regard to depolymerization the HTPB polymer should be regarded as a polyurethane. The HTPB prepolymer functions as a high-molecular weight diol, and the curing agent used was a diisocyanate.

Thus, the cross-linking bonds of HTPB polymer are similar to Estane-based PU while its backbone is polybutadiene. It shares the depolymerization melting with PU but its physical melting and reactivity of the backbone are similar to PBAA. The melting temperature of HTPB polymer is expected to be higher than PU. Bouck, et al. report the rupture temperature of HTPB film is 494°C. The fundamental differences of HTPB melt from the PU melt lie in the reactivity and the temperature of melting.

The HTPB polymer, supposedly having a higher melting temperature than PU, can attain higher temperature without melting. Moreover, the burning rate of the HTPB propellants are greater than the PU propellants so that the maximum heating rate of the polymer in the propellant burning near its P_{dl} is greater, estimated to be 10 - 15°C/sec and also the surface temperature is higher. With those factors and the higher reactivity of HTPB polymer, the effect of polymer melt is less pronounced for HTPB polymer than for PU. The polymer melt is observed to exist even on the burning surface of HTPB propellants loaded with high percent of oxidizer burning near its P_{dl} . The small amount of melt existing on the burning surface help retain the large AP particles from ejection. The best low pressure stability of HTPB propellants of high-oxidizer loading among the three binder systems considered appears to be obtained by the better combustion efficiency than for PBAA propellants and the faster burning rate than for the PU propellants.

CHAPTER V

INTRINSIC INSTABILITY

A. BACKGROUND

The oscillatory burning behavior of solid propellants when burned near their low pressure deflagration limit is very interesting in relation to the combustion instability problem of rocket motors. The oscillatory burning most frequently observed in a solid propellant motor is excited and sustained by a coupling between the combustion and the oscillating acoustic pressure. Strand combustion in a large strand bomb is very nearly an open process, not likely to couple with dynamic processes in the chamber. Therefore, if any oscillation is observed in strand burning, it could well be a property of the propellant and its combustion. It is conveniently called "intrinsic instability" or "intrinsic oscillatory combustion."

The solid propellant burning process consists of solid preheat, gasification, combustion and energy feedback to the surface. If the propellant is homogeneous and uniform, combustion being one-dimensional and adiabatic, then the process is monovariant in the steady state; it becomes uniquely determined if one process parameter is specified. Given a suitable model for the process, one can investigate the stability of the combustion process by the usual methods of perturbation analysis, checking under what conditions a transient or periodic

perturbation introduced in the process increases or decreases with time. If the disturbance decreases with time, the process is assumed to be stable, otherwise, unstable.

The stability analysis of a combustion zone has been performed by numerous investigators in connection with the motor stability. The resultant expression for the combustion stability has been conveniently expressed as the pressure response function, the ratio of mass flux perturbation to the perturbation in chamber pressure. Denison and Baum [42] were among early investigators concerned with the intrinsic instability of solid propellant combustion as a special case of the general instability problem in rocket motors. Applying the perturbation method to their version of the governing equations, they were able to express the instability criterion of the combustion zone itself in terms of steady state parameters. The same form of final result was deduced by Culick [40] in his review of unsteady burning of a solid propellant. Culick cast the results of several theoretical investigations of unsteady burning into a pressure response function of general form:

$$\frac{\dot{m}'/\dot{m}}{p'/p} = \frac{nAB}{\lambda + A/\lambda - (1 + A) + AB} \quad (V-1)$$

where \dot{m} is steady mass burning rate; p is pressure, the prime indicates the perturbed value; n is the pressure exponent in the burning rate law, $\dot{r} = ap^n$; A and B are dimensionless parameters differing for different combustion models; λ is a complex function of the complex dimensionless frequency, $\lambda = i\omega/r^2$,

$$\lambda(\lambda - 1) = i\omega; \quad (V-2)$$

α is the thermal diffusivity of the solid; ω is the complex angular frequency; and r is the linear regression rate.

Culick presents the intrinsic mode of instability will occur at the condition giving an infinite value of the real part of the response function; i.e., m'/m finite as p'/p vanishes. The response function will become infinite when the denominator of Eq. (V-1) vanishes;

$$\lambda(\lambda - 1) + \lambda A(B - 1) + A = 0 \quad (V-3)$$

Eq. (V-3) gives a formular for λ which, when substituted into Eq. (V-2), gives for the real and imaginary parts of ω

$$\omega_r = \pm \frac{1}{2} A(B - 1) [4A - (A - AB + 1)^2]^{1/2} \quad (V-4)$$

$$\omega_i = A + \frac{1}{2} A(B - 1)(A - AB + 1) \quad (V-5)$$

Since λ originally appeared as $i\omega$ in harmonic time variations, $-\omega_i$ is the perturbation growth factor. For stable transient motions $\omega_i \geq 0$ and then Eq. (V-5) leads to

$$B + 1 \geq A(B - 1)^2 \quad (V-6)$$

The real frequency at the stable and unstable boundary is obtained by putting Eq. (V-6) into Eq. (V-4):

$$\omega_o = AB^{1/2} \quad (V-7)$$

Those results are the same as Denison and Baum originally derived with their own expressions for A and B , both positive, real quantities.

Eq. (V-6) predicts the stability criterion and Eq. (V-7) gives the frequency of oscillations of the self-excited, intrinsic mode of instability.

In the Denison and Baum model, the parameters A and B are expressed in terms of more familiar physical and chemical parameters;

$$A = \frac{E_s}{RT_s} \left(1 - \frac{T_o}{T_s} \right)$$

$$B = \left(\frac{c_p}{c} \right) \left(\frac{T_f}{T_s} \right) / \left[\left(1 - \frac{T_o}{T_s} \right) \left(n + 1 + \frac{E_f}{2RT_f} \right) \right] \quad (V-8)$$

where E_s is the activation energy for surface reaction; T_s , burning surface temperature; R , universal gas constant; c_p and c , specific heat of gas and solid, respectively; T_f , flame temperature; n , burning rate exponent; E_f , activation energy for gas phase reaction.

For normal solid propellants, the intrinsic mode of oscillation as suggested above has not been observed experimentally in a strand burner before. Contrary to the prediction made by one-dimensional theory as above, there have been some observations which rather support the three-dimensional aspects of the oscillatory combustion. Price [48, 105] proposed the concept of preferred frequency explaining the burning behavior of aluminized propellants in a motor test. The propellant-like material, pellets of AP and aluminum, was observed to exhibit the phase-correlated oscillatory burning behavior even in a strand burner [105]. The explanation offered for these phenomena is that aluminum alternately accumulates on and sheds from the burning surface.

Boggs and Beckstead [17] developed the layer-frequency concept noting the failure of one-dimensional theory to correlate experimental

nonacoustic combustion instability data for some propellants. They found the discrepancy between theory and experimental data was more serious in PU propellants than in CTPB propellants, and at higher burning rates more than at lower burning rates. For propellants containing AP with a bimodal particle size distribution, two frequencies were observed. Boggs and Beckstead viewed the one-dimensional model as not valid when the thermal wave thickness is approximately the same as the mean particle size of AP and proposed the layer-frequency concept stating that there is a characteristic time related to the size of AP particle. The characteristic time (τ_i) of the burning of an oxidizer particle is obtained by dividing the characteristic distance associated with an oxidizer particle (D'_i) by the averaged regression rate (r) of the burning surface:

$$\tau_i = \frac{D'_i}{r} \quad (V-9)$$

The characteristic distance, D'_i , is calculated as the edge of a cube of propellant containing one oxidizer particle of D_i diameter, assuming uniform, cubic spatial distribution of particles. The ratio of the oxidizer volume to the total volume of the cube is expressed by the composition and the densities of the fuel and oxidizer:

$$\frac{\frac{\pi}{6} D_i^3}{D_i'^3} = \frac{X_i}{X_T + (\rho_{ox}/\rho_b)(1 - X_T)} \quad (V-10)$$

where D_i is the particle size; D'_i , the characteristic distance defined above; X_i , the weight fraction in the oxidizer of particles with D_i ; X_T , the total oxidizer loading; ρ_{ox} , the density of oxidizer;

ρ_b , the density of fuel. The rearrangement of the above equation gives the ratio of an oxidizer particle size to the characteristic distance

($K_i = D_i/D'_i$):

$$K_i = \left\{ \frac{X_i}{(\pi/6)[X_T + (\rho_{ox}/\rho_b)(1 - X_T)]} \right\}^{1/3} . \quad (V-11)$$

Thus, the frequency associated with D_i is

$$F_i = \frac{1}{\tau_i} = \frac{r}{D'_i} = K_i \frac{r}{D_i} . \quad (V-12)$$

Boggs and Beckstead reported that Eq. (V-12) better predicted the frequency trend at higher burning rates.

Eisel [47] also observed two-frequency behavior in bimodal PU propellants during his spectroscopic study of nonacoustic instability in a low- L^* burner. He found that the frequency predicted by Eq. (V-12) was close to the measured value for the large AP particle but was off by an almost constant factor for the smaller particles. The frequency of bulk-mode instability was noted to be controlled by the fine AP particles. Also, he found a mode of oscillation in composition and temperature which was not coupled to the pressure excursions and termed it local intrinsic instability. He was not able to identify the origin of the local instability, which had the frequency about 60 to 80 Hz regardless of AP particle size.

B. DATA ACQUISITION AND REDUCTION

The frequency data on the oscillatory burning were gathered during experiments intended to measure the steady burning rate and the P_{dl} . The fluctuation of the force transducer signal was the main source of information, while the photocell and thermocouple output provided supplementary data. As briefly stated in the previous chapter, the regularity and the distinctness of oscillatory burning were very much dependent on binder type, oxidizer level and pressure.

Figure V.1 shows force transducer signals for bimodal PU, HTPB, and PBAA propellants extinguished after initial forced deflagration at a pressure just below their P_{dl} values. As the recoil force compensator was not employed during the tests, those force transducer signals contain both the contribution of the weight and that of the combustion recoil. In the signal for the PU propellant, small fluctuations are seen riding on the large-period (on the order of 25 sec.) mode of oscillation. Similar signals were exhibited by most PU propellants except an aluminized one in which the small fluctuations were absent. Unimodal propellant gave an oscillation of only one frequency. In the case of the HTPB propellant, the amplitude of the small fluctuations is itself periodic, the period being interpreted as the same as that of the slow oscillation seen for the PU propellant. The cessation of deflagration occurs around the maximum amplitude of small oscillations, suggesting the oscillation growth is responsible. Overall mass burning rate indicated by the mean slope of the curve is also fluctuating with the total growth and decay time of the small

fluctuations, and with the same period as that of the large-period oscillations. In contrast to PU propellants in which the extinguishment occurred at the point where the derivative of the oscillating force takes minimum value, interpreted for this case as minimum burning rate, HTPB propellant extinguished at the maximum amplitude of the small oscillation. The data on the period of oscillation for PU and HTPB propellants were obtained relatively easily compared with those for PBAA propellants.

The force signal for PBAA propellants was very erratic in detail as shown in Figure V.1. In UEK, the second oscillation mode was hardly noticeable. The regularity of oscillation was a little better in more fuel-rich PBAA propellants which also exhibited the two frequencies more definitely. The catalyzed PBAA showed extremely erratic burning. Thus the data on PBAA propellants are less accurate than those on PU and HTPB propellants. The regularity and distinctness of oscillations were better in the order of catalyzed PU, aluminized PU, uncatalyzed PU, uncatalyzed HTPB, and the other propellants.

In Figure V.2, the force signal and the light signal are presented together for a catalyzed PU propellant. The light signal was detected by a photocell (1N2175) mounted inside the combustion chamber. The regularity of the oscillations is apparent. The signals are from the last portion of an unstable burning which eventually resulted in extinguishment. The amplitude of the low-frequency oscillation increases continuously to the extinguishment point. It is also noted that the light signal tends to lag the force signal more as the extinguishment point is approached.

C. EXPERIMENTAL RESULTS

Comparison between the measured period of oscillation and the period predicted by Boggs and Beckstead's theory, Eq. (V-12), is made for unimodal PBAA propellants in Figure V.3. The agreement is excellent except for UDX, one with 15-micron AP. Since the deviating UDX had the greatest ratio of thermal wave thickness to particle diameter, it is the one Boggs and Beckstead would least expect to conform to their prediction. For the other propellant as well, however, that ratio is larger than the range in which Boggs and Beckstead would assert that their prediction is valid.

It is also noteworthy that such good agreement with prediction is obtained with propellants containing PBAA, because when this polymer is mixed with bimodal AP, frequency prediction is very unsatisfactory. The PBAA-bimodal AP propellants burn (at low pressure) with ejection of a considerable quantity of unburned AP, which fact probably accounts in part for poor frequency prediction. The PBAA-unimodal AP propellants, on the other hand, burn with very little AP ejection.

On Figure V.4, the low-pressure (near P_{dl}) oscillatory burning data for PU propellants containing bimodal AP are plotted as period vs. burning rate. Two distinct periods are found, the ratio being approximately the same as that of two particle sizes. The influence of AP particle size in determining the oscillatory period appears to be firmly established. However, the predictions of the layer-frequency theory for those bimodal propellants are not so good as they are for the unimodal PBAA propellants discussed previously. Although the

propellants considered in this oscillatory burning study are not the same in details of their compositions, it is reasonable to consider them together because they contain the same mixture of coarse and fine AP particles. The constant K , appearing in the layer-frequency theory does not vary appreciably among different propellants. The values of oscillation periods predicted by the layer-frequency theory do not fit the data except for a catalyzed propellant, UFA, for which the shorter-period oscillations were perceived but could not be analyzed. It is interesting to notice that the slope of the points for the short-period oscillations of the uncatalyzed propellants are close to unity and the periods are off by a constant factor (approximately 1.5) from the layer-frequency predictions. This discrepancy is the same as that arising from Eisel's observations, referred to previously.

It is apparent that the long-period data for uncatalyzed PU propellants do not fit layer-frequency predictions. The applicability of the one-dimensional model of Denison and Baum [42] was examined for a fixed value of N . The reference line with N of 25 (arbitrarily assumed for best fit of data) is shown to correlate the long-period data for both catalyzed and uncatalyzed propellants. Even for a single propellant UFA, the slope of the line correlating the data points is close to -2. Now some promise for the one-dimensional theory is in view. A closer analysis of the UFA data, which are the most accurate, gives a N value slightly higher than 25.

We are in the position of having results for uncatalyzed propellants supporting, if not necessarily confirming, the layer-frequency

predictions. Certainly it is apparent that bimodal AP leads to two oscillation modes; yet, the catalyzed bimodal AP propellants show only one pronounced oscillation mode, with an indication that the frequency is predictable by a theory having no reference to AP particle size or other physical dimensions. Results with other propellants do not help in clarifying this dilemma.

Similar information on oscillatory burning for PBAA and HTPB propellants is presented in Figures V.5 and V.6, respectively. The layer-frequency theory fails to predict the period of oscillation for most PBAA and HTPB propellants except for the catalyzed PBAA propellant, UEZ. Even there, only one oscillation mode is seen. The burning of PBAA propellants was so erratic that two frequencies were hardly identified from the force transducer signals of more oxidizer-rich propellants. The long-period oscillations, being erratic and irregular, were observed for some very fuel-rich propellants (UEO, UEP) but the layer-frequency theory does not predict the observed frequencies. The long-period data for uncatalyzed fuel-rich propellants and data for catalyzed propellants are scattered around the $n = 5$ line. The short-period modes of several propellants cluster around a line for $n = 25$. Although two frequencies were observed for all the uncatalyzed HTPB propellants considered, none of the observed frequencies were predicted by the layer-frequency theory. Again, the one-dimensional theory with $n = 15$ correlates the long-period oscillations. For the short-period mode, a line with $n = 100$ approximately represents the data.

In Figure V.7, the long-period data, being relatively distinct and representative of each binder system, are summarized. The one-dimensional theory with N equal to 20 correlates all the data quite well.

At this point, a comparison with related studies is relevant. Muhlfeith, et al. [87] were able to locate the critical frequency corresponding to a maximum in the flux response function by a newly developed experimental technique. The critical frequency found by them should be comparable with the intrinsic frequency observed in this study if the one-dimensional theory is valid. Muhlfeith's blackened and catalyzed PU propellant (UCX), which has a very similar composition to UFA in this study, showed the critical dimensionless frequency a little bigger than 30 which compares well with the intrinsic frequency of UFA. Also, it is marked that UCX showed the sharpest resonance point as UFA exhibited most distinct and regular oscillatory burning in this work. The results for translucent PU propellants in their study are also in fair agreement with those blackened ones of this work. The weak maximum response shown by PBAA propellants in their study is also consistent to the observations in this program; the oscillatory burning behavior was least regular in PBAA propellants as repeatedly emphasized. Nevertheless, the response of UCW and UCV in their study are in moderate agreement with that of UEM and UEZ respectively, in this work. In addition, the frequency of intrinsic instability observed by Eisel can also be reduced to the dimensionless frequency around 20.

D. DISCUSSION OF RESULTS

1. Stability Analysis by Denison-Baum Theory

The experimental results as described above indicate that the frequencies of the oscillatory burning are of a contradictory nature, being in part, related to the particle size of the oxidizer and in the other part, having nothing to do with the particle size and being proportional to the square root of the regression rate. In order to resolve the contradiction, we are forced to infer that the composite propellant combustion inherently contains two types of instability; one due to the heterogeneity of the composition and another related to the overall combustion processes. Depending on the burning conditions, one of them becomes prominent and is observed. As Boggs and Beckstead suggested, one-dimensional theories of the unstable combustion need a modification so that the instability produced by the heterogeneity of the formulation can be included.

Since the modes of oscillations whose periods are proportional to the thermal wave times in the solid seem to be predominant for most bimodal propellants near their low pressure limit, the instability unrelated to the oxidizer particle size appears to account for the extinguishment of those propellants at low pressures. The applicability of one-dimensional theory is examined by the Denison-Baum model. A Denison-Baum type instability diagram is drawn in Figure V.8 in terms of A and B instead of the reciprocal of B . The boundary between the stable regime and the unstable regime is determined by Eq. (V-6). The unstable regime is also divided by two regions, oscillatory and nonoscillatory, by the equation $g^2 = 4A$, where

$g = 1 + A(1 - B)$. The frequency of oscillation in the unbounded oscillatory burning regime is in dimensionless form,

$$\Omega = \frac{g - 1}{2} \sqrt{4A - g^2} \quad (V-13)$$

To predict the intrinsic instability of solid propellant burning by Denison and Baum model, four parameters, E_f , E_s , T_f and T_s , must be known. The measured value of flame temperature in this study is in the 1200 - 1500°K range. The surface temperature can be estimated at about 600°K from this study and other investigations. One more constraint for the application of one-dimensional model is that the dimensionless frequency for an intrinsic oscillatory burning should be around 20. The results of a parametric study are shown in Figure V.8. With the values of T_s , T_f and Ω_0 observed in this study, $E_f = 20$ kcal/mole and $E_s = 60$ kcal/mole appear to establish the stability criterion within the framework of the Denison-Baum model.

2. Criticism of the Denison-Baum Type of One-Dimensional Theory

Before one claims the success of Denison-Baum model for predicting the oscillatory burning behavior of composite solid propellants at low pressures, other matters should be considered. One of the criticisms is that acceptance of the theory requires belief that the activation energy for the surface reaction is equal to or larger than 60 kcal/mole, a physically unrealistic value. As Muhlfeith, et al. [87] showed, the incorporation of the condensed-phase heat release does not permit one to take a more realistic value of the activation energy.

The activation energy for gas phase reaction, 20 kcal/mole, as needed for the interpretation of the observed periods of oscillations, might be regarded as supported by the experimental data of the furnace-augmented burning rates and flame temperatures as described in Chapter VI. However, E_f of 20 kcal is inferred there for relatively stable burning, and the value of E_f approaches zero as the stability limit is approached. The calculated zero activation energy for the gas-phase reaction indicates that the condensed-phase processes are rate controlling near the limiting pressure, a view also supported by the intermittent burning data of a fuel-rich PU propellant inside the heated furnace (refer to Appendix D).

Those observed modes of oscillation whose frequencies are predicted by the oxidizer particle size either contradict the one-dimensional theories or, at least, deny their general applicability. Another contradictory observation was made by Eisel [47], who observed gas-phase composition fluctuations during unstable burning. The necessary inference is that there are also fluctuations in the composition of the surface material, and further that the rates of decomposition of the oxidizer and the fuel fluctuate out of phase during unstable burning. A more rigorous theory concerning the unsteady composite propellant combustion should take composition fluctuations into account.

3. Advancement of an Alternative Theory

The failure of the conventional one-dimensional theories is noted in explaining the observed oscillatory burning behavior of composite propellants at very low pressures. The failure appears

to be attributable, at least in part, to neglect of the compositional fluctuations during oscillations. Most conventional one-dimensional theories assume the condensed phase to be homogeneous and are based on the simplified laminar flame theory for the gas phase flame. By the usual simplifying assumptions, the gas phase molecular species conservation equations are dissolved into the energy equation. Thus, the oscillatory feature is embodied in the temperature oscillation. Those theories have been successfully applied to the pressure-coupled oscillatory burning. Those theories, however, are not adequate to describe the oscillatory burning of solid propellant at constant pressure: only a unique frequency can be exhibited by the unstable burning of the composite propellants near their low pressure limit by conventional theories.

A more versatile and rigorous theory should allow the fluctuation of the composition as was observed experimentally. In order to allow the variation of compositions during oscillatory burning, we need at least one unique gas-phase-species continuity equation. The fluctuations in the gas compositions are due to the disproportionation of the oxidizer and binder decomposition rates. Not only the linear decomposition rate of each ingredient but the decomposition surface as well can affect the mass evolution rate of each ingredient. For simplicity, the linear decomposition rate of each ingredient can be expressed in an Arrhenius equation.

Then, the mass gasification rates of the binder and the oxidizer are expressed as follows:

$$\dot{m}_b = S_b \rho_b A_b \exp(-E_b/RT_{s,b}) \quad (V-14)$$

$$m_{ox} = S_{ox} \rho_{ox} A_{ox} \exp(-E_{ox}/RT_{s,ox}) \quad (V-15)$$

where m is the mass burning rate; S , the burning surface area; ρ , the density; A , the pre-exponential factor; E , the activation energy; R , the universal gas constant; T_s , the burning surface temperature; and the subscripts b and ox denote the properties of the binder and oxidizer, respectively. At steady burning conditions, the mass ratio of the decomposition products of the oxidizer to that of the binder (ϕ) is the same as the mass ratio of the oxidizer to the binder in the virgin propellant.

$$\phi = \left(\frac{S_{ox}}{S_b} \right) \left(\frac{\rho_{ox} A_{ox}}{\rho_b A_b} \right) \exp \left(\frac{E_b}{RT_{s,b}} - \frac{E_{ox}}{RT_{s,ox}} \right). \quad (V-16)$$

If the regression surface of the propellant were flat, the surface ratio, S_{ox}/S_b , would be simply the volumetric ratio of the oxidizer to the binder in the propellant. Since, because of the heterogeneity, the surface exhibits irregularities on the scale of the oxidizer particles, the actual ratio of the burning surface area should take the fact into account. Following the procedure of Beckstead, et al. [10], we find the corrected ratio of surface areas, ψ :

$$\psi = \frac{S_{ox}}{S_b} = \zeta \left[6 \left(\frac{h}{D_o} \right)^2 + 1 \right] \quad (V-17)$$

where ζ is the volumetric ratio of the oxidizer to the binder in the propellant; h , the height of the protruded part of the oxidizer; and D_o , the diameter of the oxidizer particles. The geometric factor h/D_o can be written [10]:

$$\frac{h}{D_o} = \frac{1}{2} \left(1 + \frac{1}{\sqrt{3}} \right) \left(1 - \frac{r_{ox}}{r_b} \right) + r_{ox} \frac{t_{ign}}{D_o}, \quad (V-18)$$

where r_{ox} and r_b are the regression rates of the oxidizer and binder, respectively, and t_{ign} is the ignition delay time.

Under perturbed burning conditions, Eq. (V-16) gives

$$\frac{\phi'}{\phi} = \frac{\psi'}{\psi} - \frac{E_b}{RT_{s,b}} \frac{T'_{s,b}}{T_{s,b}} + \frac{E_{ox}}{RT_{s,ox}} \frac{T'_{s,ox}}{T_{s,ox}} \quad (V-19)$$

Equation (V-19) enables the description of fluctuations during unstable burning.

From Eq. (V-19), it is seen that the fluctuation in the concentration is affected by the surface areas and the surface temperatures of the oxidizer and the binder. In an actual burning situation, the surface temperature fluctuation of the oxidizer is assumed to be much less than that of the binder on the grounds that the oxidizer particle protrudes above the binder surface so that it makes close contact with the flame. If the surface temperature fluctuation of the oxidizer is small enough compared to that of the binder, Eq. (V-19) is reduced to

$$\frac{\phi'}{\phi} = \frac{\psi'}{\psi} - \frac{E_b}{RT_{s,b}} \frac{T'_{s,b}}{T_{s,b}} \quad (V-20)$$

It is noted that the oxidizer/binder ratio in actual propellant is usually less than the stoichiometric ratio so that any positive increment in ϕ' should produce a hotter flame. In addition, from Eq. (V-17) and Eq. (V-18), it is seen that a positive increment in the binder surface temperature, producing an increase in its regression rate, results in an increase in the oxidizer/fuel surface area ratio.

Thus, the oscillatory burning at low pressures may happen in the following way. Consider a small increment in the flame temperature. The increased flame temperature produces an increase in feedback heat flux, which increases the binder surface temperature. With a lag, the oxidizer/fuel ratio decreases to give a more fuel-rich decomposition gas which decreases the flame temperature. However, after a short time later, the fuel-depleted surface, being oxidizer-rich, increases the oxidizer/fuel ratio to increase the flame temperature. In this way, the interaction between the rate of decomposition and the surface area ratio could be a possible forcing mechanism for the low-pressure oscillatory burning, even extinguishing the flame under certain conditions. In an unimodal propellant, a single mode of interaction is expected, while a bimodal propellant can generate two modes of interactions; one is between the fine AP particles and the binder and the other is between the coarse AP particles and the binder containing small AP particles.

It is shown above how, from the heterogeneity of composite propellants, one can rationalize the composition-driven oscillatory burning behavior at low pressures. Of course, the complete description of the model needs the conservation equations of energy and species in the solid and gas phase. Here, we are just suggesting another possibility of the unsteady burning model at low pressures.

Other information about the oscillatory burning near the limiting pressures can be obtained from some of the records of force and light intensity signals. On Figure V.9 are presented the analyzed results of a typical oscillatory burning test of UFA propellant such

as one shown on Figure V.2. The mean (over one period) burning rate decreases as the extinguishment point is approached, but both the amplitude and the period of the oscillation increase. Above all it is interesting to see that the phase lag of the light signal to the force signal seems to approach $\pi/4$ as the extinguishment point is reached. These observations pertain to all records obtained, but the local period-to-period excursions are random. Any successful unsteady burning theory should be able to explain these experimental observations. We suggest that these observations should be valuable guides in establishing a satisfactory theory.

CHAPTER VI

EFFECT OF SUPPLEMENTAL ENERGY ON BURNING AND EXTINGUISHMENT OF SOLID PROPELLANT AT LOW PRESSURES

A. BACKGROUND

Low pressure extinguishment has been explained in terms of combustion inefficiency and intrinsic instability in previous chapters. As discussed briefly in Chapter IV and more thoroughly in Appendix A, the extinguishment at low pressures was observed to be strongly influenced by experimental conditions, by the conditions at the edge of the flame zone in particular. The boundary conditions at the edge of the burning surface is an inevitable inherent limitation in a strand burner technique. With an experimentally tractable strand size, the transverse heat losses from the combustion zone could not be eliminated completely, although the losses were less significant when a larger strand size was used. Even then there remains the radiative heat loss from the burning surface to the cold surroundings, which is increasingly more important as the pressure approaches the limiting pressure. At those low pressures, a considerable portion of the energy feedback from the gaseous combustion zone to the burning surface is lost by the thermal radiation from the burning surface. It is one of our major concerns to see how the stability of combustion is improved when the compensation for the heat losses is made by an external heat flux.

The heat loss and the combustion inefficiency were not introduced in the phenomenological argument of intrinsic instability since the mechanism of instability can be described without reference to them. However, in any complete theory they must appear at least in the parameters because they determine the range of burning conditions in which instability is manifested. For example, heat loss and combustion inefficiency appear in the A and the B parameters of Denison and Baum's theory.

No extensive work has been done on the effect of external flux on the low pressure extinguishment of the composite solid propellant. Ohlemiller and Summerfield [92] have studied the radiation-augmented burning of a PBAA propellant, with an arc-image furnace as the radiation source. They were able to make the propellant sustain combustion at a pressure as low as 0.007 atms by a radiation flux $9 \text{ cal/cm}^2 \text{ sec}$; without the augmenting flux it would quit burning at 0.05 atms.

On the subject of the burning rate augmentation by external heat flux, there have been several experimental and theoretical studies [3, 34, 58, 62, 73, 74, 77, 87, 98, 126]. Some investigators [3, 98, 73, 74, 126] were concerned with the burning rate augmentation in translucent propellants by external radiant heat flux, ascribing the increased burning rate to the preheating of the propellant sample by the penetrating heat flux. In this case, the effect of thermal radiation was shown to be equivalent to an increase in initial temperature [3, 73, 74].

Horton and Youngberg [62] were able to predict the burning surface temperature and the heat of decomposition of a composite propellant by comparing the burning rates of externally burning strands inside

a temperature-regulated furnace with those of internally burning grains. Thomson and Suh [126] have reported that thermal radiation has an insignificant effect upon the burning rate of a double base propellant. Their experiments were carried out at extremely low pressure of 0.07 atms for a range of fluxes from 0 to $1.5 \text{ cal/cm}^2 \text{ sec}$. The absence of significant effect may be due to the relatively high burning rate of 0.08 cm/sec at the pressure. Hertzberg [58] made an investigation on the laser-induced combustion of ammonium perchlorate at atmospheric pressure. Muhlfeith, et al. [87] measured the effect of radiation heat flux on the steady burning rate of several composite propellants at atmospheric pressure. A burning rate increase up to 30 percent was indicated in their study with the maximum heat flux $14.85 \text{ cal/cm}^2 \text{ sec}$. They also computed the heat of decomposition for the propellants tested using their data. Coates and Kwak [34] used a stainless steel tube heated up to 950°C to measure the burning rate dependency on the incident external heat flux at low pressures. They found the burning rate of fluoro-carbon propellants at 0.68 atms could be enhanced as much as 100 percent by a heat flux of $2.64 \text{ cal/cm}^2 \text{ sec}$.

In this work, regression rates and flame temperatures were measured in a furnace for two composite propellants burning at very low pressures. Also, the effect of external heating on extinguishment pressure was investigated.

B. EXPERIMENTAL PROCEDURE

1. Burning Rates and Flame Temperatures

The quick-heating furnace described in Chapter III was used as a source of the external flux. The experimental methods for burning rate and for flame temperature measurement are, in most parts, the same as those described earlier except for the introduction of external heat flux. The sample of 1.25 cm X 1.25 cm cross-section and 2.4 cm long was ignited in the unheated furnace in the pressure-adjusted combustion chamber and permitted to regress to about 1 cm before the furnace power was turned on. Cooling nitrogen was continuously introduced during a test at a rate of 4 liters per minute. The weight of the sample was continuously monitored by a force transducer and the flame temperature was simultaneously measured by a thermocouple in the gas phase. The variation of the furnace wall temperature was also recorded during a test along with the force transducer signal on a Speedomax two-pen recorder. The thermocouple signal for the flame temperature was separately recorded on an Electronic 19 recorder.

A question inevitably arising for this sort of experimental arrangement is whether a steady state is attained during a test since the unburned part of the sample could be continuously heated by thermal radiation incident on its sides. The best answer to this question can be furnished by tracing the burning rate continuously during a test. This was done for a catalyzed PU propellant, UFA, burning at a pressure just above its low-pressure deflagration limit. The results are shown in Figure VI-1, where histories of burning rate, flame temperature, and furnace wall temperatures are shown.

Different symbols indicate two different runs. Almost immediate response of the burning rate and the flame temperature to the furnace wall temperature is noted. The burning rate rises to a new level and remains there, strongly suggesting the relative insignificance of sample side heating during a testing period. Supporting evidence is that the burning surface remained flat at least for the period concerned. When the furnace temperature used was over 750°C , however, a conical burning surface at the edge of the flat burning surface appeared less than a minute after the power was turned on. The slight effect on temperature and rate of cooling nitrogen used to protect the sample sides is revealed by comparing the results of two runs. Even without nitrogen cooling, the flame-induced convective flow around the sample was likely to protect sample sides from quick heating. The reproducibility of burning rate measurement is also found to be excellent.

The data reduction of burning rate tests was straightforward. The burning rate before and after the furnace was powered was obtained by taking an average slope of the force transducer signal over an appropriate time interval. The interpretation of flame temperature data was complicated by the spatial distribution of temperature in the flame. As shown in Figure VI.1, the flame temperature steadily decreases as the burning surface regresses away from the thermocouple bead, initially at a rate of about $-3^{\circ}\text{C}/\text{sec}$ or $-240^{\circ}\text{C}/\text{cm}$. The maximum thermocouple temperature shown when the furnace reaches the set temperature is not what it would be if the thermocouple bead were still located near the burning surface. Therefore, the

thermocouple temperature of the flame was deduced by adding the increment of thermocouple temperature due to furnace heating to the initial thermocouple temperature which was taken from the early part of the thermocouple signal. The increment of thermocouple temperature in the furnace was taken as the difference between the maximum furnace-augmented thermocouple temperature and a temperature the thermocouple would have at the time of the maximum thermocouple temperature if the furnace had not been turned on. The latter temperature was determined by linear extrapolation of the first part of the flame temperature history. The reproducibility of the flame temperature measurement appears to be good on Figure VI.1, but it was not so good in general. The poor spatial positioning of the thermocouple bead inside the flame cross-section is presumed to be the main reason, evidenced by an almost fixed temperature rise regardless of the thermocouple temperature before the furnace was turned on. The reproducibility of the flame temperature rise was good. Hence, the temperature rise rather than the temperature itself was counted more meaningful. After radiation correction was made on the measured thermocouple temperature by the method described in Chapter IV, the final furnace augmented flame temperature of a run was calculated by adding the difference between the corrected initial flame temperature and the furnace-augmented flame temperature of the run to the averaged initial flame temperature of many runs carried out at the same experimental conditions.

2. Extinguishment Pressure with External Energy Supply

The go/no-go test was inadequate to determine the low pressure deflagration limit with energy supply because it would need the

exposure of a sample to the incident radiant heat flux for too long a time. The depressurization method was adopted with a rate of depressurization slow enough to give a minimum pressure, the necessary rate of depressurization thus depending upon the propellant kind. An extensive study on this subject was made and the results are reported in the next chapter. For the normally burning propellants considered, the rate of depressurization required was about 0.042 sec^{-1} for UFA, 0.006 sec^{-1} for UED, and 0.075 sec^{-1} for UEK, respectively. The rate of depressurization was not determined by the orifice size alone. It was affected by many other factors, principally the pressure-dependent gas generation rate, the flow rate of cooling nitrogen, and the dump-tank pressure as the extinguishment pressure approached the dump-tank pressure. The situation became further complicated by a limitation on the allowable exposure time of samples under furnace heating. Thus, some preliminary investigation of sample preheating was needed.

The effect of sample preheating on the extinguishment pressure was investigated and the result is discussed in Appendix A, Section 4. It is concluded that to limit the error in extinguishment pressure within 5 percent, the sample center temperature should not be allowed to increase more than 10°C . The sample heating rate was measured for various furnace wall temperatures and sample sizes. The results are shown in Table C.II. It is shown that a cylindrical strand of 1.43 cm diameter and 2.54 cm long is heated up from 21°C to 31°C in 56 seconds when the furnace temperature is 750°C . The sample used in this study was a parallelepiped of 1.25 cm X 1.25 cm X 2.40 cm which is similar to the sample tested above. Thus, the contribution by an increase in strand temperature would be negligible if the burning

of a sample is brought to extinguishment within approximately one minute after the furnace power is turned on. This conclusion is also supported by the burning rate measurement as described in the previous section.

Further standardization was needed for the purging rate of cooling nitrogen. As is discussed in Appendix A, Section 3, the effect of nitrogen cooling was significant. To be consistent with the standardized method for deflagration limit measurement, a quiescent nitrogen environment would be needed. This condition could not be met because the purging of nitrogen was needed to minimize the sample preheating. A faster rate of cooling nitrogen would be more effective for the cooling purpose alone. However, a flow rate more than 4 liters per minute was not adoptable because it appreciably raised the system pressure limit. Thus, 4 liters per minute was chosen for a standard rate of nitrogen purging.

It was understood that to get any meaningful data from extinguishment tests in the furnace, two rather conflicting experimental conditions must be met: the rate of depressurization should be sufficiently slow, as discussed in Part B.2 of this chapter, and the propellant burning should be brought to extinguishment within one minute after the furnace power was turned on. These conditions were easily met for the faster burning propellants such as UEK and UFA for which relatively high rates of depressurization may be used. For UED propellant, which has the slowest burning rate among the propellants considered in this study, the results are least reliable.

The extinguishment tests for UFA, UED, and UEK propellants were carried out by the following sequence:

- (1) The desired furnace temperature was set at the controller.
- (2) An orifice of proper size to meet the critical depressurization was chosen and mounted (refer to Table C.III, Appendix C).
- (3) The initial chamber pressure was chosen to be approximately two times as high as the expected extinguishment pressure (refer to Chapter VII).
- (4) A sample of 1.25 cm X 1.25 cm X 2.40 cm was mounted on the force transducer and the combustion chamber was filled with nitrogen.
- (5) The cooling nitrogen was introduced at a previously determined rate; the nitrogen flow rate was adjusted before a series of tests to give 4 liters per minute when the chamber pressure was 0.067 atms.
- (6) The hand exhaust valve was adjusted to give a constant chamber pressure with the introduction of purging nitrogen.
- (7) The sample was ignited by a heated nichrome wire (0.011 gage) and the chamber was depressurized by opening the main exhaust valve. Both the weight and the pressure signals were recorded on a Speedomax two-pen recorder.
- (8) The furnace power was turned on when the chamber pressure reached a level slightly higher than the P_{dl} measured for the propellant without furnace heating.

- (9) If the rate of depressurization was too slow to extinguish the burning within one minute, the test was repeated with a bigger orifice.

The tests on the TPF 1006 propellant which has a very high P_{dl} were made with a fixed orifice size of 0.318 cm. The furnace power was on before the depressurization was started. Since the rate of depressurization by the 0.318-cm orifice was still relatively high for this slow burning propellant, the extinguishment pressures measured would not be the limiting values independent of the depressurization rate. As the extinguishment occurred, in most cases, at pressures before the orifice was dechoked, the extinguishment pressures were determined by the fractional rate of depressurization as well as the energy supplied.

C. RESULTS AND DISCUSSION

1. Transient Response of Low Pressure Burning to External Heat Flux

On Figure VI.2 are shown the transient responses of the burning rate and the flame temperature of a PU propellant at a pressure slightly below its pressure deflagration limit. An apparent overshoot of the burning rate and the flame temperature is noted when the furnace temperature reaches the pre-assigned value. The burning rate change follows the furnace wall temperature closely and attains a maximum value. There is a time lag of 3 to 5 sec - considerably less than the relaxation time of the thermal wave. After staying the maximum level for a while, the burning rate suddenly drops to a final steady state value which is appreciably lower than the maximum. The same trend is found in the response of the flame temperature. This

strange burning behavior was a characteristic of PU propellants, being more distinct when the furnace wall temperature was less than 600°C. For furnace wall temperatures more than 700°C, the difference between the maximum and the final burning rate became less pronounced.

This peculiarity in the burning response of PU propellants is likely attributable to the existence of the surface layer formed by polymer melting and cross-linking as described in Chapter IV. The overall deflagration distance during the transient response estimated from Figure VI.2 is approximately 1.1 mm which is comparable to the deflagration distance during a long-period oscillation for the same propellant burning at about the same pressure. Also, this deflagration distance is almost the same as the thickness of the surface layer measured from a quenched sample. Thus, the explanation offered for this phenomenon, compatible with the explanation of intrinsic instability, is as follows.

The surface layer containing large AP particles, polymer melt, and cross-linked polymer decomposition products is slightly oxidizer-rich and in a marginally stable state. It burns away rapidly when additional energy is supplied, actually overshooting the new steady state which is established later. This fast-burning state is thought to be oxidizer-rich (relative to the propellant as a whole) on the evidence of the transient increase in flame temperature. When the external heat flux is rather strong, perhaps comparable to the heat feedback from the intensified flame, the available oxidizer is not sufficient to overshoot the more remote final steady state. Possibly the flux provided by the furnace at 400°C is comparable in magnitude to the flux excursions associated with oscillatory burning.

2. Augmented Burning Rates and Flame Temperatures by External Heat Flux

The dependencies of the burning rate and the flame temperature on augmenting flux were measured for two PU propellants, a catalyzed one, UFA, and an uncatalyzed one, UED, at pressures slightly above their low pressure deflagration limits. Figure VI.3 shows the burning rate data for UFA propellant. A large increase in burning rates is achieved by relatively weak external heat fluxes. As much as 45 percent enhancement in burning rate is attained with a moderate heat flux, $0.84 \text{ cal/cm}^2\text{sec}$. One striking feature is that the rate of the burning rate increase, measured by the slope of the curve, also increases as the external flux level is increased. This is contrary to the expectation that a finite increment of external heat flux would constitute a smaller increment of the total feedback heat flux for a higher burning rate. A possible explanation is found in the fact that the external heat flux also stimulates a large gain in the flame temperature which brings an extra heat feedback to the burning surface.

On Figure VI.4, similar information on burning rate augmentation is given for an uncatalyzed PU propellant. It is notable that a moderate external heat flux, $0.84 \text{ cal/cm}^2\text{sec}$ increases the burning rate as much as 140 percent at 0.05 atms, a pressure just below the deflagration limit of this propellant. The initial burning without external heat flux was barely sustained by the ignition aides. At 0.05 atms, the acceleration of the burning rate increase is not exhibited, whereas it is at 0.06 atms. At the higher pressure, a burning rate increase by 84 percent is induced by the same external heat flux, $0.84 \text{ cal/cm}^2\text{sec}$.

Figure VI.5 shows the enhanced flame temperatures of UFA propellant under the furnace heating. Those data were taken simultaneously with the burning rates. Radiation corrections and the data-reducing procedures as described early in this chapter have been made for those flame temperatures. Straight lines represent the data satisfactorily and the flame temperature is raised by 200°C at 0.05 atms and by 160°C at 0.06 atms respectively, with an external heat flux of $0.84 \text{ cal/cm}^2\text{sec}$. It is noted that the flame temperatures for two pressures approach each other as the higher heat flux is imposed. The combustion efficiencies at both pressure levels appear to be much improved and approach each other at those higher external fluxes.

The difference between the flame temperature of UED propellant (Figure VI.6) at 0.05 atms and 0.06 atms is large, being as much as 400°C when no external flux is introduced, whereas only 60°C difference is exhibited by UFA propellant. A marked increase in flame temperature, as much as 700°C , is observed for UED propellant burning at 0.05 atms with an external heat flux $0.84 \text{ cal/cm}^2\text{sec}$. It is understandable that an increase in the energy feedback to the burning surface, either due to the increase in system pressure or by the added external heat flux, have a more significant effect on the burning of a slow-burning propellant than that of a fast-burning propellant. The UFA propellant has a larger burning rate without external flux and probably a greater combustion efficiency to start with.

3. Further Interpretation of Burning Rate and Flame Temperature Data under Furnace Heating

In the previous section, a qualitative explanation has been offered for the observed burning rate behavior under furnace heating.

An attempt is made in this section to find values for thermochemical and kinetic parameters from the data. Some fundamental difficulties are expected in applying a phenomenological combustion model to these experimental data. One of the major problems is our ignorance about the combustion inefficiency which accompanies low pressure burning. Another problem comes from the possibility that the external heat flux might not only augment the burning rate but also alter the burning mode at the low pressures. There is, however, no unambiguous evidence for this possibility. It is nevertheless felt that some analysis with simplified models may be justified.

a. Activation Energy for Gas Phase Reaction

Denison and Baum's simplified model, which assumes a laminar flame in the gas phase, is adopted. Coates [30] has shown the adequacy of the simplification and some success has been claimed by Coates and Horton [31, 32] in their application of the model to the extinguishment of solid propellants by rapid depressurization. Coates and Kwak [33] also applied this theory in correlating their experimental data on the augmentation of burning rates by external heat flux. Further justification is provided by the fact that the very low pressure considered in this work makes less objectionable the application of a laminar flame theory for premixed gases to poorly mixed gases; the rate of diffusion becomes faster than the rate of reaction at very low pressures.

According to Denison and Baum, the gas-phase reaction rate is expressed by the following equation:

$$r = C p^n T_f^{n+1} e^{-E_f/2RT_f} \quad , \quad (VI-1)$$

where C is a constant and the other symbols are as defined in the previous chapter. In the steady state, the gas phase reaction rate should be the same as the deflagration rate of the condensed phase. Thus, the gas phase reaction rate can be substituted for by the regression rate of the condensed phase. Eq. (VI-1) suggests that the plot of $\log [\tau/(p^n T_f^{n+1})]$ versus the reciprocal of T_f would give a straight line of slope $(-E_f/4.606 R)$.

This is done in Figure VI.7 for both UFA (catalyzed) and UED (uncatalyzed) PU-fueled propellants. The data for UFA propellant both at 0.05 atms and at 0.06 atms are fairly well together, while a considerable discrepancy exists between two sets of data for UED propellant. There is some doubt that Eq. (VI-1) is a good representation of the data for either propellant. It is, however, seen that a straight line of $E_f = 25$ kcal/mole correlates the UED data at 0.06 atms. In contrast, a straight line fails to fit UED data for 0.05 atms. A better representation would be a curve gradually leveling off as the flame temperature is decreased. A similar and clearer tendency is shown by UFA data for both pressures. The curves could perhaps be represented by two straight lines, a declining line and a horizontal line, as the flame temperature about 1160°C as a breaking point. When the flame temperature is higher than this temperature, the straight line of $E_f = 20$ kcal/mole correlates the data for both pressures reasonably well. The data for flame temperatures lower than 1160°C are better represented by a straight line of zero slope.

An explanation is offered for this sharp change in the apparent activation energy of gas phase reactions. A modification of the burning mechanism is suggested to occur during the course of increasing

external heat flux, as speculated previously. For flame temperatures lower than the critical value (1160°C for UFA, about 1800°C for UED), controlling processes for the low-pressure burning may exist in the condensed phase, and the gas phase reaction rate becomes limiting for the flame temperatures higher than the critical value. The augmenting external heat flux required to increase the flame temperature to the critical level is in the range of 0.4 to $0.6 \text{ cal/cm}^2\text{sec}$ for UFA propellant and is about $0.8 \text{ cal/cm}^2\text{sec}$ for UED propellant. The increased burning rate at the same augmenting flux level for each propellant is about 0.16 mm/sec for UFA and 0.11 mm/sec for UED, respectively (Figures VI.3 and VI.4) which corresponds to the flux-unassisted burning rate at the pressure about 0.07 atms for UFA and 0.1 atms for UED respectively (Figure IV.1). From these results, one may infer that propellant burning becomes controlled by condensed-phase processes from a pressure slightly higher than the P_{dl} .

b. Net Heat of Gasification

Another application of the furnace-augmented burning rate and temperature data is to estimate the net heat of gasification as done by Muhlfeith, et al. [87]. For their experimental conditions, they assumed the change in the flame temperature was negligible under the irradiation by external heat flux, which turned out to be not true in our case. Horton and Youngberg [62] included the contribution of the flame temperature rise in their computation of the net heat of gasification. However, their employment of a rough energy feedback law makes their method less attractive. There is no direct way to measure the net heat of gasification. Values computed from temperatures and

rate measurements are, as pointed out by Mihlfeith, et al., a function of the assumption made.

Nevertheless, the computation of the net heat of gasification was made using the method adopted by Mihlfeith, et al., hoping that a comparison could be made with their results. The heat balance at the burning surface gives

$$f = r\rho[c(T_s - T_o) + q] \quad (\text{VI-2})$$

$$\left(\frac{\partial r}{\partial f}\right)_{T_s} = \frac{1}{\rho[c(T_s - T_o) + q]} \quad (\text{VI-3})$$

$$q = \frac{1}{\rho(\partial r / \partial f)_{T_s}} - c(T_s - T_o) \quad (\text{VI-4})$$

where f is the total energy incident on the burning surface and q is the net heat of gasification. If the quantity $(\partial r / \partial f)_{T_s}$ can be determined experimentally, Eq. (VI-4) provides a means to compute the net heat of gasification. In this work it was found that the burning rate is influenced not only by the direct heat flux but also by the additional heat flux from the gas-phase flame of increased temperature. Although the latter effect is probably not negligible, it is, for the present purpose, assumed to be so. The burning rate-external flux relationship, though not linear, is taken as linear. With these simplifications, the net heat of gasification was calculated for each case and is listed in Table VI.1. When the burning surface temperature is about 300°C which corresponds to $c(T_s - T_o) = 100$ cal/g, the net heat of gasification is barely exothermic (q negative). With the higher surface temperature assumed, the net heat of gasification becomes more

exothermic. Due to the severe assumptions introduced, the absolute values of the heat of gasification cannot be concluded from these results but we infer that the surface decomposition reactions are, taken together, slightly exothermic.

4. Extinguishment under Furnace Heat Flux

The dependency of the extinguishment pressure on the external heat flux was measured for five typical propellants. The result for four of them are discussed in detail in this chapter. Propellants chosen are representative of a group of propellants which have similar burning characteristics: an extremely slow-burning, uncatalyzed PU propellant, UED; a catalyzed PU propellant, UFA, as a representative of propellants of the intermediate burning rates; a fast-burning PBAA propellant, UEK, which ejects a large amount of AP particles; and two high- P_{dl} propellants, TPF 1006 and UDF. For four propellants, UDF being the exception, the extinguishment pressure could be lowered to the system limit with the external heat-flux level attainable in the apparatus. The fuel-rich PU propellant, UDF, behaved strangely. Even with the maximum heat flux of the system, $1.64 \text{ cal/cm}^2 \text{ sec}$, a steady burning could not be achieved for this propellant at a pressure below its deflagration limit without augmenting flux. Instead, this propellant exhibited a repeated sequence of ignition, deflagration, and extinguishment when exposed to augmenting flux. A detailed description of this phenomenon is found in Appendix D.

On Figure VI.8, the deflagration limit of UFA propellant is presented as a function of external heat flux. The extinguishment pressure is lowered when the external heat flux is supplied. When the external heat flux is greater than $0.7 \text{ cal/cm}^2 \text{ sec}$, the propellant

burning cannot be brought to extinguishment at the least pressure attainable. Linear extrapolation indicates that the propellant would burn at zero pressure when the external heat flux exceeded about $1.0 \text{ cal/cm}^2\text{sec}$. If, of course, one could further reduce the pressure, other, as yet unobtrusive, effects would become prominent, and the extinguishment pressure vs. external flux curve would deviate from the simple extrapolation. There are three examples of processes which might occur when the pressure approaches zero: (1) surface reaction between oxidizing gases (from AP) and polymer would cease as the mean free path approaches the distance between AP particles; (2) AP would evaporate and escape at sub-ignition temperature; (3) the behavior of UDF (intermittent burning). But the extrapolated minimum flux for what appears to be near-ordinary burning is important. It is the least net surface flux at which ordinary burning could occur. The corresponding furnace temperature, 650°C for UFA, is the least effective temperature for burning.

Figure VI.9 displays the effect of external flux on the extinguishment pressure of UED propellant. The scattering of data is due to the difficulty of experimentation with slow-burning propellant, as discussed earlier in this chapter. Because of the sample preheating problem, the higher values of extinguishment pressure for a given flux are considered the more accurate. The extinguishment pressure for zero heat flux to be 0.063 atms was determined with cooling nitrogen passed around the sample at a rate of 4 liters per minute, so that it is appreciably higher than the P_{d1} of this propellant, 0.052 atms as determined by the standard method. Less pronounced effects of cooling

nitrogen on the extinguishment pressure was observed for faster burning propellants such as UFA and UEK.

Again, interestingly, linear extrapolation of the data to zero extinguishment pressure gives a corresponding external heat flux about 0.9 to $1.0 \text{ cal/cm}^2\text{sec}$, supporting the interpretation applied to UFA propellant.

It appears that the augmented burning rate stabilizes the combustion to give the near-linear drop of extinguishment pressure with respect to the external heat flux. In Figures VI.10 and VI.11, the heat flux-augmented burning rates are compared at the pressures near the extinguishment values for UFA and UED propellant respectively. The data were taken from the weight transducer signals recorded during the tests for determining extinguishment pressures. Filled symbols indicate the burning rate taken near the extinguishment pressure. Note that the burning rates at the extinguishment pressures are nearly the same for all the external flux levels considered, although a slight decrease is experienced as the heat flux level is increased. The limiting burning rate is approximately 0.1 mm/sec for UFA propellant and 0.045 mm/sec for UED respectively. The near-constant limiting burning rate is taken as an empirical fact useful for further interpretation of the extinguishment data.

Based on the assumption of the limiting burning rate, termed r_{dl} , a mathematical description is attempted for the extinguishment data under the furnace heat flux. Additional assumptions are needed to predict the lowering of the extinguishment pressure by external heat flux based on the burning rate augmentation data near the flux-unassisted deflagration limit of a propellant. It is postulated that

the same functional dependency of the burning rate on the external flux exists even at pressures below the deflagration limit and the burning rate increases linearly with the external heat flux. Also assumed is that the same burning rate law holds at pressures lower than the deflagration limit of the propellant. A burning rate law adopted is

$$r_{dl} = ap_{dl}^n \quad (VI-5)$$

By the assumptions as above, the burning rate of a propellant at a certain pressure, being augmented by an external flux, f_r , is,

$$r = ap^n + \beta f_r \quad (VI-6)$$

where β is the slope of burning rate-external flux curve, termed the heat flux coefficient for convenience and f_r is external heat flux.

By the assumption of limiting burning rate, extinguishment occurs when r equals to r_{dl} . Thus, from Eqs. (VI.5) and (VI.6), the pressure deflagration limit under furnace heating, P_f , becomes

$$P_f = P_{dl} \left(1 - \frac{\beta f_r}{r_{dl}} \right)^{1/n} \quad (VI-7)$$

Eq. (VI-7) suggests that the more significant effect is produced when the heat flux coefficient is bigger and the limiting burning rate and the burning rate exponent are smaller. The deflagration limit under the external heat flux can be predicted by Eq. (VI-7) with the heat flux-augmented burning rate data at low pressure deflagration limit. Applying Eq. (VI-7) to data for UFA and UED propellants, one finds that this linearized correlation predicts higher values of extinguishment pressures than experimentally measured ones for UFA

propellant and slightly lower values for UED propellant. The simplifying assumptions are probably responsible for those discrepancies. However, Eq. (VI-7) does correctly predict the qualitative nature of the phenomenon such as the slope of the curve being steeper for UED propellant.

Due to the severe assumptions involved in its derivation, the application of Eq. (VI-7) should be limited to a rather small external heat flux. Eq. (VI-7) cannot be applied when P_f approaches zero, as shown by the following argument. Differentiating Eq. (VI-7) with respect to f_r , we come up with the following equation:

$$\frac{dP_f}{df_r} = -\frac{1}{n} \frac{\beta}{r_{dl}} P_{dl} \left(1 - \frac{\beta f_r}{r_{dl}}\right)^{1/n - 1} \quad (VI-8)$$

Eq. (VI-8) indicates that the slope of the curve (dP_f/df_r) at $P_f = 0$ becomes zero or minus infinity depending on whether n is smaller or bigger than one, which seems hardly credible.

On Figure VI.12 are shown the extinguishment data for UEK propellant. This propellant needs more than $1.0 \text{ cal/cm}^2\text{sec}$ to reduce the extinguishment pressure below the system limit. With an external heat flux more than $1.05 \text{ cal/cm}^2\text{sec}$, the propellant burned out at the system limiting pressure without showing a visible flame, which indicates that the flame temperature is very low. At these very low pressures and with high external heat fluxes, the condensed phase regression rate of this propellant stays high as a result of the high regression rate of the continuous phase (polymer and fine AP particles), most of the large AP particles being ejected. The reaction rate in the gas phase is very low, which appears to be the cause of the very low

flame temperature. This new phenomenon is presumed to make this propellant behave differently from UFA and UED propellants. However, we find the extinguishment data below external heat flux $0.8 \text{ cal/cm}^2\text{sec}$, where the new phenomenon is not significant, resembles those of UFA and UED propellants. Linear extrapolation gives a minimum heat flux about $1.1 \text{ cal/cm}^2\text{sec}$ which is not very far off from about $1.0 \text{ cal/cm}^2\text{sec}$ for UFA propellant.

The extinguishment data for a fluorocarbon propellant, TPF 1006, are shown in Figure VI.13. This propellant has a high P_{dl} of about 5 atms. The burning of this propellant was seen to be very erratic when the external heat flux was less than $0.3 \text{ cal/cm}^2\text{sec}$. Also, the burned surface was very irregular and concave. The increased heat flux above that value gave a normal burning and a flatter burning surface. The burning surface became perfectly flat when the external heat flux was $0.7 \text{ cal/cm}^2\text{sec}$ and had a tendency to be convex for still higher heat fluxes. On a semi-logarithmic coordinate, a straight line approximates the data of this propellant well. Noticeably, air does not provide a detectable effect in those high extinguishment pressures when it replaces nitrogen as an ambient gas, while the effect of cooling nitrogen is still observed.

Because the chemistry of this propellant is very much different from that of the other propellants, comparison of the extinguishment data is not attempted. We do note very large change in extinguishment pressure with external heat flux.

CHAPTER VII

EXTINGUISHMENT DURING DEPRESSURIZATION

A. BACKGROUND

In the early phase of this program, the slow depressurization method was used to determine the low pressure deflagration limit as the asymptotic extinguishment pressure approached as slower rates of depressurization were employed. It was observed that even very small rates of depressurization had a significant effect on the extinguishment pressure, though a lesser effect than observed when extinguishment was achieved by rapid depressurization.

The object of this subprogram is two-fold. One is to develop a suitable way of determining the low-pressure limit and to see how the low-pressure limit changes as less severe pressure transients are imposed. Another object is to broaden our understanding of the extinguishment during depressurization using the relatively easy controllability of experimental conditions at low pressures. Although the burning behavior and the extinguishment mechanism at low pressures could be much different from those at high pressures, we presume the difference is in the relative influences of sub-processes that are common to combustion at all pressures.

Notwithstanding much effort devoted to understand the extinguishment during rapid depressurization, the mechanism of extinguishment is not well understood. Both theoretical and experimental difficulties

appear. From the theoretical point of view, the relatively well-developed transient burning theories based on linear perturbational analysis are not applicable to this situation, because large excursions from steady-state behavior are induced. The inadequate understanding of the steady-state burning mechanism itself is an obstacle.

Experimentally, several problems have been encountered, although the extinguishment itself is easily achieved, one being the difficulty of the instrumentation for the rapid depressurization test. Some investigators [134, 135] report difficulty in determining the extinguishment point accurately enough. The exact pressure of extinguishment is an essential datum for judging the adequacy of predictive theories. Only a few investigators [67, 68, 129] have attempted to determine the point of extinguishment precisely. Most other workers have relied on the conventional go/no-go type of test which supplies only very rough information on extinguishment mechanism. Another experimental attack on this problem which has a poor yield of understanding is an attempt to measure the transient burning rates during depressurization. If successfully measured, the rate transient would give critical information on the extinguishment mechanism. Fletcher and Bunde [50] deduced the transient burning rate by a mass balance, using the pressure-time history of a propellant-containing chamber during depressurization. For some cases, they inferred that the transient burning rate first rapidly increases above the initial steady-state value before eventually decreasing to zero. Their conclusion is not widely accepted because of many uncertainties involved in their calculation, such as the nozzle opening time, the

gas temperature inside the combustor and the nozzle coefficient of discharge. A technique using microwave reflection from the surface has been adopted by several investigators, and some results have been reported [117]. However, the reliability of those data are still also in doubt. Recently, Yin and Hermance [137] have measured the transient burning rate by continuously monitoring the electrical capacitance across the burning surface. Their results show that the burning rate at any pressure during depressurization is higher than the steady-state value at the corresponding pressure. As the capacitance across the flame is the least reliable quantity to be measured, their results also remain uncertain. Thus, there is no generally accepted way to measure the transient burning rate during depressurization.

Experimental difficulties arise from the strong dependency of the extinguishment process on the experimental conditions. The burning rate becomes small at the last stage of the extinguishment process, so that it could be strongly affected by heat loss and flow conditions around the burning surface. Two types of experimental apparatus have been used for extinguishment tests: a subscale motor with variable venting, and a rarefaction tube in which propellant strands are burned. A motor may generate data of practical value, but the results are of little use for testing extinguishment theories. The pressure-time relationship is complicated by the coupling between the combustion and the nozzle flow. Additionally, in motor tests there are the effects of erosive burning and the external heat flux coming from the heated hardware which surely promotes reignition. In rarefaction-tube runs or in modified strand

bomb tests, the pressure-decay rates are little affected by the strand burning. However, heat loss from the strand burning to the cold surroundings promotes extinguishment. Those effects of the experimental conditions introduce unavoidable errors which preclude close examination of any existing theory.

In the following paragraphs, some of the related work is reviewed. At first, the von Elbe-type theories are examined. Von Elbe-type models lead to Eq. (II-1), $(r^2/\alpha)/[-(d \ln p)/dt] = n/\Lambda$ which could readily be inferred from dimensional analysis, but has a basis in physical reasoning. Rather severe assumptions are introduced in deriving the equation: a constant burning surface temperature, a chemically inert solid phase, and a quasi-steady heat feedback law. Furthermore, the solution is basically obtained by a perturbational approach which is valid only if the deviation from the steady state is small. However, if only the resultant equation is examined, one can rationalize its occasional success. It is interpreted as expressing that when the characteristic time of the change in process conditions (represented by pressure) is less than the time required for the thermal wave adjustment, which is the slowest process, then departure from steady-state increases. In the case of depressurization, the departure is in the direction of starving the precombustion processes of needed energy, with the consequence of extinguishment. Eq. (II-1) implies that the extinguishment is determined only by the instantaneous rate of depressurization. However, the experimental results (for example, [83]), indicate that not only a certain rate of depressurization but also a finite pressure drop is needed

to quench a propellant burning. Hence, Eq. (II-1) is considered to constitute the condition for the onset of instability as Cohen [35] viewed, not to represent the termination point as the original derivations imply.

Although Eq. (II-1) does not adequately describe extinguishment, it has been applied, with some success, in correlating the extinguishment data. Ciepluch [27, 28, 29] was the earliest investigator who made a systematic experimental study of rapid-depressurization extinguishment. Using a subscale motor, he investigated the extinguishment of PBAA and PU propellants during rapid depressurization and of the occasional subsequent reignition. He reported that the minimum pressure decay rate for extinction linearly increased as the initial chamber pressure was increased [27]. He later represented his data in terms of the critical time required for the pressure to decrease to one-half its initial value. A mild effect of initial pressure on this critical time was observed [28]. His observations for the compositional effect on the extinguishment requirement are summarized in Table VII.2 in comparison with the results of other investigators. The mild effect of initial pressure for extinction requirement is a tendency supporting von Elbe's representation. Later, von Elbe [128] applied his theory to Ciepluch's experimental data, assuming reasonably a depressurization history deduced from the ballistic equation. His analysis indicates that the theory yields a critical vent ratio only about 20 percent smaller than the experimentally determined ratio.

An advanced interpretation of the von Elbe-type model has been made by Cohen [35]. He viewed Eq. (II-1) as defining the requirement

for the initiation of extinguishment. He further believed that both the L^* extinguishment and the rapid depressurization extinguishment are the same phenomenon caused by self-induced and externally induced pressure perturbations, respectively. The permanence of extinguishment is hypothesized to be achieved only if the pressure falls from the initiation pressure to below the low pressure ignition threshold level within the corresponding chemical induction time for reignition. His view on the completion of extinguishment is questioned due to the introduction of quantities of vague physical meaning, the ignition threshold limit and chemical induction time. He reports that Eq. (II-1) well predicts the rate of depressurization required for extinguishment.

Investigators at the University of Utah [26, 44, 83] have used a rarefaction tube as a tool to quench the propellant burning. Blow-down and first-rarefaction-wave pressure reduction were utilized to extinguish the strand burning. They found that the initial tube pressure has no effect on the extinguishment in blow-down runs and, therefore, the fractional rate of pressure decay, $-(d \ln p)/dt$, is the determining factor for extinguishment. Their results on the blow-down type of extinguishment tests are summarized in Table VII.I. The pressures at the moment of extinguishment were not detected so that the direct comparison with the von Elbe-type theories is not possible. However, as the fractional rate of pressure decay is nearly constant in a blow-down type of run until the nozzle is de-choked, Eq. (II-1) is best checked at the minimum pressure where the nozzle remains choked. This minimum pressure would be about twice the pressure in the region into which the gases are vented [26]. With

this postulated extinction pressure, the fractional rate of depressurization required for extinguishment is computed by Eq. (II-1) and compared with the experimentally-determined value. It is seen that the experimental results are well within the predictions of Eq. (II-1) except for F propellant, which is a catalyzed bimodal PBAA propellant. F propellant requires as much as eight times faster rate of pressure decay for extinguishment than theoretically predicted (based on $\Lambda = 1$). However, the Utah investigators have taken the severe test of permanent extinguishment as the extinguishment-nonextinguishment criterion. Since F propellant has strong tendencies to reignite, they may have judged the equation too harshly.

Mantyla [83] estimated the net heat of gasification, using his data for extinguishment by the first rarefaction wave. His computation was based on a hypothetical critical pressure ratio, the ratio of the final pressure to the initial pressure, which would be required to extinguish a propellant by an infinite rate of pressure decay.

The problems associated with extinguishment in motor firings were also noted by von Elbe and McHale [129]. They avoided the complicated problems by using a modified strand bomb. With the aid of a simultaneously recorded photocell signal, the actual extinguishment pressure was determined on the recorded pressure-time curve. The instantaneous depressurization rate was also obtained from the tangent to the actual pressure-time curve at the point of extinguishment. They have reported that an excellent agreement exists between von Elbe's theory and experimental data for a PVC-fueled propellant, whereas the data for PBAA propellants show a fair agreement with the theory in the intermediate pressure range, but definite departure

from theory at the highest and lowest depressurization rates. They have concluded that von Elbe's theory is a good first approximation for predicting extinguishment of solid propellants.

An extensive experimental study of extinguishment by rapid depressurization was made by Jensen [67, 68] using two large-volume, small-grain motors, with end-burning and tubular grains. He also obtained the extinguishment data from the actual pressure history of a motor. He has found that the von Elbe equation with $\Lambda = 1$ correlates the extinguishment data for most of the propellants considered. The CTPIB propellant data show disagreement with the theory at the highest and lowest depressurization rates, as von Elbe and McHale noted for PBAA. Jensen also observed that the extinguishment was easier when a vacuum exhaust pressure was used. He concluded that the von Elbe type of combustion extinguishment model provided a rough guideline for motor development work.

There is experimental evidence supporting the view that the extinguishment during depressurization is not determined primarily by the initial or mean rate of depressurization, but rather is governed by the last part of the pressure history, over a small pressure range. Schulz [112] and later Baer, et al. [4] observed that extinguishment by rapid depressurization was determined by the final dump tank pressure rather than by the initial pressure. Schulz's results show that a four-fold variation in initial pressure (from 1.4 atms to 5.4 atms) does not produce a change in critical dump tank pressure more than 0.02 atms for a fixed nozzle. Baer, et al. made an extension of Schulz's work and found that the final

dump tank pressure determined the extinction criterion within 0.01 atms when the initial pressure was changed from 6 atms to 13 atms.

More rigorous analysis has been attempted by various investigators [32, 60, 86, 135] to overcome the shortcomings of the von Elbe-type models. Horton, et al. [60] solved the transient heat conduction equation in the solid numerically with the assumptions of quasi-steady heat feedback law and constant surface temperature to predict the depressurization extinguishment. They also allowed a finite amount of endothermic net heat of gasification in their model. Their model was claimed to predict their experimental data better than Eq. (II-1). The numerical values of the net heat of gasification, however, are very much uncertain. Mantyla [83] has shown that their model predicts depressurization rates for extinguishment three to ten times greater than those actually needed.

Woolridge, et al. [135], Merkle, et al. [86] and Coates and Horton [32] have improved Horton's earlier technique of solving the heat conduction equation in the condensed phase to predict the extinction criterion with less drastic assumptions. All those investigators have allowed the variations of surface temperature with the burning rate in Arrhenius fashion. Both Woolridge, et al. and Coates and Horton employed Denison and Baum's transient heat feedback law. Besides, Woolridge, et al. included two kinds of the condensed phase heat release, one pressure-dependent and another pressure-independent. Thus, their model needs five more parameters to be assigned in addition to the surface temperature at a reference pressure. The model by Merkle, et al. is based on the granular diffusion flame theory. Besides the surface temperature at a given pressure, two more

parameters are needed, the heat of decomposition and activation energy for solid phase reaction. They assumed that the extinguishment was actually achieved when the surface temperature reached 600°K. Coates and Horton circumvented the uncertainty in the heat of decomposition by directly applying the Denison and Baum's heat feedback law, which implicitly includes the heat involved in the solid surface decomposition. With the surface temperature known at a given pressure, their model also needs two more parameters, the activation energies for the gas phase and the solid phase reactions. They postulated that extinguishment would occur when the transient burning rate dropped to 0.0127 cm/sec for all propellants. All the investigators who devised more sophisticated models claim good prediction of extinguishment conditions with their estimated values of the parameters; however, the arbitrariness in the numerical value of those parameters needs further justification.

In testing any existing extinguishment theory with the experimental data available, one finds that those data are too rough for critical evaluation. One reason is the variation in propellant compositions studied by the various laboratories. Experimental procedures are different also. In Table VII.11, some of the extinguishment data are compared. Some investigators report that no significant effect of the binder kind, while others say differently. Considerable disagreement is shown to exist in the effect of oxidizer particle size, the content of aluminum and the inclusion of catalysts.

What may be an invalidating defect in one-dimensional extinguishment theories is suggested by the experimental observations by Schulz [112] and Steinz and Selzer [121, 122]. Schulz observed by infra-red

spectrometry that the ratio of oxidizer to binder species in the gas phase increases at the earlier stage of depressurization and later decreases below the steady-state value. Steinz and Selzer have reported that at a medium depressurization rate, the quench of the first flame is followed by a development of a second flame which preferentially consumes the oxidizer before dying out. There are grounds for doubting the validity of any theory which does not account for the compositional heterogeneity of composite propellants.

In this program, the accurate extinguishment data are gathered to examine the existing theories. The transient burning rates during depressurization are also measured. A comparison is made between the low pressure deflagration limit measured by a go/no-go test at fixed pressure and that obtained by employing successively lower rates of depressurization.

B. EXPERIMENTAL PROCEDURE

1. Extinguishment During Depressurization

As seen by the literature survey, close control of the experimental conditions is the key to reproducible, extinguishment data. In order to attain a sure control of the thermal surroundings, the combustion chamber was used as a tool for depressurization extinguishment. Instead of attempting to simulate the adiabatic condition for strand burning, fixed thermal surroundings were provided. For this purpose, the nichrome-ribbon furnace was replaced by the cooling coil described in Chapter III, Section C. All the extinguishment tests were carried out with samples of 1.25 cm X 1.25 cm cross-section, 2.4 cm long under a quiescent nitrogen environment. The sides of the sample were inhibited by Krylon.

The various rates of depressurization [as $-(d \ln p)/dt$], ranging from 5.0 sec^{-1} to 0.003 sec^{-1} , were attained by connecting the combustion chamber and the main dump tank with a line in which orifices of eleven different sizes would be placed. In Table C.III in Appendix C, the orifices and the corresponding fractional rates of depressurization, which were calculated theoretically with the assumption of the ideal nozzle and no gas generation in the combustion chamber, are shown. Without the propellant burning inside the chamber, the pressure decay was fairly well approximated as exponential when the nozzle was choked. The actual rates of blow-down had values between the predicted rates for isentropic and isothermal blow-down. Even when a propellant sample was burning inside the chamber, the history of pressure changes was well represented by an exponential decay as shown in Figure C.7. It is also shown that the actual rates of depressurization compare well with the theoretical predictions when the orifice size is larger than 0.318 cm. The gas evolution by propellant burning, however, becomes significant when the orifice size is smaller than 0.318 cm and the pressure is low. Although the theoretical prediction of depressurization rate is not possible for this case, the constant fractional rate of pressure decay still well represents the pressure history when the orifice is choked.

The detection of the extinguishment point was achieved by a photocell (1N2175) or by the force transducer, depending upon the rate of depressurization. When both sensors were used, they signaled extinguishment at the same time. The pressure signal was picked up by a pressure transducer (Statham PA731TC-25-350). The light and the force signals were recorded either by a camera-equipped

oscilloscope (Tektronix Model 564) or by a strip-chart recorder (Leeds and Northrup Speedmax Series XL600 Recorder), depending on the depressurization rate. When an orifice larger than 0.635 cm was used, the extinguishment point was detected by a photocell and the oscilloscope was utilized for recording signals. For the 0.635 cm orifice or smaller ones, the depressurization rate was slow enough that the weight transducer and the strip-chart recorder served better.

Since it was intended to correlate the extinguishment pressure in terms of the instantaneous rate of depressurization, a preliminary study was made to determine if the initial portion of the pressure decay affects the extinguishment pressure. The results for a catalyzed PU propellant are shown in Figure VII.2. It is noted that for the two orifices tested, the pressure at which depressurization is begun does not affect the extinguishment pressure provided that it exceeds the latter at least by a factor of two. This observation holds for the other propellants studied. For the other data taken during depressurization and reported here, the initial pressure used was, accordingly, more than twice the extinguishment pressure.

To establish a steady combustion before the depressurization was started and to solve the difficult ignition problem at low pressures, special procedures were needed. When the depressurization was made from the combustion chamber alone to the large vacuum tank, the propellant was ignited at a high enough pressure that ignition was fast, then the chamber was slowly depressurized by venting to the auxiliary dump tank originally kept at a pressure slightly lower than the desired initial test pressure. An auxiliary

orifice was chosen such that the propellant was not quenched during this preliminary depressurization. When the auxiliary dump tank was coupled to the combustion chamber so that the extremely low rates of depressurization could be used, the ignition was made at the low initial test pressure. Not only was the auxiliary dump tank unavailable for the first stage depressurization but too long a time was needed to depressurize the chamber from a large pressure at which ignition is easy. In this case ignition was slow; the deflagration was allowed to proceed more than 10 mm before the test depressurization was begun in order that the thick thermal wave generated by the ignition wire was consumed and a true steady state attained. In this preparation step the chamber pressure was maintained at a constant level by adjusting the hand exhaust valve.

The extinguishment tests were carried out in an automatic sequence preset on two control timers. The first timer set the time for ignition and deflagration before the first-stage depressurization was started. The second was designed to control the interval required for the first-stage depressurization and steady burning before the main exhaust line was opened. A third timer was hooked up to the main control sequence to trigger the oscilloscope, if necessary.

With procedures as described above, the extinguishment tests were carried out in the following sequence:

- (1) An initial pressure and auxiliary orifice size were selected which were adequate for the extinguishment tests with the main orifice. Atmospheric pressure

was, if possible, preferably chosen for the initial pressure in most cases.

- (2) The main dump tank pressure was kept at the lowest system pressure, about 0.02 atms, by continuously operating a vacuum pump during a run.
- (3) When needed, the auxiliary dump tank pressure was set at a pressure being 0.02 atms lower than the desired initial pressure.
- (4) The timers were set at appropriate times estimated for the initial steady burning and oscilloscope triggering.
- (5) A sample was mounted on the weight transducer and the cooling coil was put above the sample.
- (6) When needed, the photocell was located inside the cooling coil at a position about 3 cm from the sample so that it viewed the flame.
- (7) When necessary, the chamber pressure was adjusted to a reference pressure, which was recorded by the oscilloscope camera along with the zero output of the photocell signal. Then, the oscilloscope and camera were prepared for a run.
- (8) The combustion chamber was evacuated to the lowest system pressure before it was filled with nitrogen gas to a preignition pressure.
- (9) A run was initiated by pushing the starting button. The sequence was as follows: ignition, preparatory

burning, first stage depressurization and steady burning at a constant pressure (initial test pressure), the triggering of the oscilloscope, and the opening of the main exhaust valve.

2. Measurement of Transient Burning Rate During Depressurization

To measure the transient burning rate during depressurization, the force transducer was utilized along with the recoil force compensator as described in Chapter III. An obstacle was encountered during the first efforts to measure the transient burning rate with the force transducer. As the sensor element of the force transducer was contained inside a confined case, the signal of the force transducer was sensitive to pressure changes. Much improvement was realized when a vent hole was drilled through the wall of the transducer case at a position opposite to the sensor hole; even then, the influence of depressurization was detectible when the rate of depressurization was greater than about 0.5 sec^{-1} . Accordingly, the successful employment of the force transducer as a tool for measuring the transient burning rate was limited to the depressurization rate lower than 0.5 sec^{-1} .

Most of the steps of the experimental procedure for extinguishment tests were also employed for the transient burning rate measurement. The changes were that cylindrical samples 1.0 cm in diameter and 2.5 cm long were used in the burning rate tests, and the cooling coil was removed to make room for the recoil force compensator.

C. EXPERIMENTAL RESULTS

1. Extinguishment During Depressurization

Figure VII.1 shows oscilloscope traces for two typical depressurization runs. For both runs, the same fractional rate of depressurization, 4.80 sec^{-1} , was employed. A slow-burning, non-catalyzed UEF propellant (polyurethane-fueled) is shown to be extinguished above atmospheric pressure, while the fast-burning, catalyzed UEZ propellant (PBAA-fueled) is not quenched until the pressure reaches a very low value. Another difference noted between the oscilloscope traces of UEF and UEZ propellant is the manner the extinguishment point is approached. The luminosity of UEF propellant burning, measured by the photocell, dropped very sharply to zero, whereas the luminosity of UEZ propellant burning approached zero gradually, making determination of extinguishment pressure difficult. It appears that there may be a difference in the extinguishment processes of these two propellants.

As briefly discussed in the previous section, the effect of initial chamber pressure on the extinguishment pressure observed was checked for UFA propellant and the result is shown in Figure VII.2. For the two orifices employed, the initial pressure did not influence on the extinguishment pressure when it exceeded the latter by a factor of two or more. When the initial pressure was less than twice the extinguishment pressure, the latter decreased as the initial pressure was lowered, indicating that a finite pressure drop is needed for extinguishment along with a certain rate of depressurization. The pressure drop was more conveniently represented by the pressure ratio between extinguishment pressure and the initial pressure

when the latter affected the former. It is interesting that this pressure ratio appears to remain at a constant value, approximately 0.5 for UFA propellant. Similar tests were made for UEG propellant, which showed the ratio of extinguishment pressure and initial pressure to be approximately 0.8, a value larger than the one for UFA propellant (the experimental results are not shown in this report). It appears that the required pressure ratio for extinguishment is dependent on the propellant kind. If the pressure ratio is interpreted in terms of time, one may say that there is a finite time required for extinguishment, a time needed for the completion of extinguishment after a propellant burning is brought to an unstable condition. This extinguishment time is longer for UFA propellant than UEG propellant. In the experiments reported hereafter, the initial pressure always exceeded the extinguishment pressure by more than a factor of two.

The extinguishment data are presented in terms of extinguishment pressure and the instantaneous fractional rate of depressurization in Figures VII.3, VII.4 and VII.5. The fractional rate of depressurization was obtained by dividing the actual rate of depressurization at extinguishment ($-dp/dt$) by the extinguishment pressure. The reader may refer to Table G.II for the detailed information on the extinguishment tests for all the propellants considered. At least two runs were carried out at each experimental condition. In general, the reproducibility was quite good.

The extinguishment data for polyurethane-fueled propellants are summarized in Figure VII.3. For each propellant considered, a straight line correlates the extinguishment data at extinguishment

pressures exceeding the asymptotic minimum by more than about a factor of two. At very small depressurization rates, the rate no longer affects the extinguishment pressure which, for these propellants, approaches an asymptotic value in the neighborhood of 0.05 atms. It is inferred that the existence of two distinct regimes of extinguishment signifies the existence of two distinct mechanisms. It should be noted that for a given extinguishment pressure in the high-rate regime, the rate of depressurization required to produce extinguishment is very much dependent upon the propellant kind, being greater for the faster-burning propellant, UFA, than the slower-burning propellants, UED, UFC, and UEF propellants; and being least for the propellant containing the most polymer, UEF.

The extinguishment data for the high-rate regime strongly suggest the applicability of the von Elbe-type expressions as represented by Eq. (II-1), $(r^2/\alpha)/[-(d \ln p)/dt] = n/\Lambda$, which implies that a single parameter, the ratio of characteristic times, provides the extinguishment criterion. It is predicted by the von Elbe-type models that the faster-burning UFA propellant requires a higher rate of depressurization than the slower-burning propellants for extinguishment at the same pressure. However, they fail to explain why the slower burning UED and UFC propellants require more stringent extinguishment stimuli than the faster-burning UEF propellant. Von Elbe's criterion must be applied with caution.

Similar extinguishment data for HTPB and PBAA propellants are given in Figures VII.4 and VII.5, respectively. The quenching curves for these propellants show the same general features as those for PU

propellants. Since the burning rates of these propellants are greater than those of PU propellants, only limited portions of high-depressurization-rate regimes are shown.

Because of the popularity of von Elbe's criterion, the extinguishment data are further reduced to compute the ratio of characteristic times, $-(d \ln p)/(r^2/\alpha)$, corresponding to each extinguishment pressure and the results are listed in Table G.II for all the propellants considered. Also, the data for PU propellants are plotted in Figures VII.6 and VII.7. To conform with von Elbe-type models, the ratio of characteristic times should be a constant (0.5, 1, or 2) divided by the burning rate exponent, and therefore should increase slightly as the extinguishment pressure increases because the burning rate exponent decreases as the pressure is raised at subatmospheric pressure. Thus, n times of the ratio of characteristic times might be a better coordinate than the ratio itself. This adjustment of the ratio is not made in Figures VII.6 and VII.7, but the numerical values of n at the extinguishment pressure are given in Table G.II for all data points.

The extinguishment data presented in Figure VII.6 are for two PU propellants containing more polymer. In the high-rate regime, where the criterion should be applicable, the critical ratio of the characteristic times remains at an almost constant level for each propellant, approximately 2.3 for catalyzed UFA propellant and 0.5 for uncatalyzed UEF propellant. It appears that a critical ratio of characteristic times is a good extinguishment criterion for a high-fueled PU propellant, but the value of the critical ratio is a property of the particular propellant.

A slightly different response to pressure transients is indicated on Figure VII.7 for PU propellants with less polymer: a plain propellant (UED) and an aluminized propellant (UFC). The ratio of characteristic times at extinguishment varies greatly, from more than 2.6 to about 1.3 in the high-rate regime. The multiplication of the critical ratio by the burning rate exponent yields only a slight approach to constancy. The von Elbe-type expression is less satisfactory in correlating extinguishment data for these propellants than for the more fuel-rich propellants, but is still judged to be a fair extinguishment criterion for these propellants. Note that there is a tendency for the critical value of the ratio of characteristic times to increase as the pressure increases.

A similar, but more severe, variation of the critical ratio of characteristic times with pressure is shown by all HTPB and PBAA propellants tested (refer to Table G.II, Appendix G). Similar to PU-fueled propellants, the variation is less for propellants containing more polymer (UEV, UEX, UEM, and UFB): the most variation is recorded by the propellants containing the most oxidizer (UEW and UEK). The von Elbe-type criterion is still useful, but only marginally, for describing the extinguishment of HTPB and PBAA propellants.

2. Transient Burning Rates

Figure VII.8 shows the burning rate as a function of pressure for an uncatalyzed PBAA propellant (UEN). The solid line was obtained for steady burning at fixed pressure. The data are for two different tests for which the pressure was reduced at the fractional rate of 0.075 sec^{-1} . The steady state curve is followed by the transient

data down to a pressure about 0.1 atms. As the pressure drops further, there is a marked difference between steady and transient rates until about 0.05 atms where extinguishment occurs (filled symbol). Clearly, for the experiment depicted in Figure VII.8, the burning of UEN propellant is responding very sluggishly to the changing conditions as extinguishment is approached.

Measurement of transient burning rates was attempted for other PBAA propellants, and similar results were obtained. However, due to experimental limitations on the depressurization rate, the extinguishment could be induced only in the low-rate regime where most PBAA propellants exhibit erratic burning behavior. Consequently, the burning rates taken from the force signal are of poor accuracy. A similar problem was encountered with HTPB propellants. This difficulty notwithstanding, the force transducer signaled the onset of unsteady burning and indicated how slowly the extinguishment point is reached.

The extinguishment process occurred with less departure from normal burning when tests were made with high-fueled uncatalyzed PU propellants. Figure VII.9 displays the burning rate of a high-fueled PU propellant (UEG). It is remarkable that, for each of two tests, the transient burning rate follows the steady state rate faithfully all the way to extinguishment (filled symbols). Even when the extinguishment of this propellant was induced near its low pressure deflagration limit, the transient burning behavior was almost the same as at higher pressures. A PU propellant containing more oxidizer (UED) showed slightly sluggish extinguishment behavior near its P_{dl} when the flame was visually observed but no significant

departure of the transient burning rate from the steady state rate was detected. The sluggishness of burning rate response to pressure transients appears to depend primarily on the nature of fuel type and perhaps also on the pressure.

3. Comparison of Limiting Extinguishment Pressures Measured by Depressurization Tests and the Pressure Deflagration Limit Determined by Go/No-Go Tests

An extremely interesting observation is that the extinguishment pressure attained in slow depressurization tests was often lower than the pressure deflagration limit determined by the constant-pressure (i.e., zero depressurization rate) go/no-go test described in Chapter IV. This anomaly is most pronounced with PBAA propellants, a catalyzed one in particular. The extinguishment pressure produced by slow depressurization (P_E) is compared with the pressure deflagration limit of each propellant determined by go/no-go tests (P_{dl}) in Figures VII.10, VII.11 and VII.12, for PU, HTPB, and PBAA propellants, respectively. In the case of every propellant, a smaller P_E was attained when a slower rate of depressurization was applied. Thus, it should be noted that for HTPB and PBAA propellants, there was a significant range of low rates for which P_E was less than P_{dl} .

For PU propellants, Figure VII.10, the least P_E values agree well with P_{dl} values. However, only for the UFA propellant it is assured that the asymptotic least value of P_E was actually attained, according to Figure VII.3. Quite possibly, the anomaly exists for PU propellants also. All HTPB propellants exhibit least P_E values less than the P_{dl} . Still more pronounced differences are seen for

PBAA propellants. The catalyzed PBAA propellant, UEZ, shows an extinguishment pressure as low as 0.024 atms compared with its low pressure deflagration limit, 0.037 atms.

An explanation is needed for this apparently contradictory phenomenon that propellant burning can be extended to lower pressures than the steady-combustion limit by slowly depressurizing the system pressure and lower extinguishment pressure is attained by lower rate of depressurization.

D. DISCUSSION OF RESULTS

The experimentally determined quenching curves (extinguishment pressure vs. fractional rate of depressurization) of various propellants are seen to consist of two distinct portions: a straight-line portion with a non-zero slope for high rates of depressurization, and another straight-line with a zero slope for low rates. There is also a hybrid intermediate portion. For convenience and as inferred previously, we term them the high-rate regime, the low-rate regime, and the transition regime, respectively. The two extreme regimes indicate that there exist two different mechanisms of extinguishment.

1. Extinguishment in the High-Rate Regime

As already pointed out, the sloped straight-line relationship between the extinguishment pressure and the fractional rate of depressurization indicates a tendency to support von Elbe-type extinguishment concept. From Eq. (II-1), $(r^2/\alpha)/[-(d \ln p)/dt] = n/\Lambda$, if Vielle's law ($r = ap^n$) holds for the pressure range considered, a straight line is resulted between $\log P_E$ and $\log -(d \ln p)/dt$ with the slope of $1/2n$. The approximate applicability of Eq. (II-1)

is shown by experimental results, suggesting that in the high-rate regime the relative magnitudes of the rate of the externally-imposed pressure reduction and the rate of thermal-wave adjustment largely determine extinguishment.

The limitation of von Elbe-type expressions is obvious by the fact that in order to fit the experimental data the critical value of the characteristic time ratio should be allowed to be a property of each propellant and also to vary with pressure. Certainly, processes other than thermal-wave adjustment also come into action during extinguishment. The justification of the usefulness of Eq. (II-1) is based on the observation that the experimentally-determined values of Λ are in a rather limited range, about 0.5 to 3.0, for most propellants. Conclusively, the starvation of energy in the thermal wave by externally-imposed transient action is the major process of extinguishment in the high-rate regime.

2. Extinguishment in the Low-Rate Regime

As lower rates of depressurization are used, the log-log plot of P_E vs. $-(d \ln p)/dt$ deviates from the simple straight line relationship (transition regime) and P_E approaches a limiting minimum value unaffected by further reduction in $-(d \ln p)/dt$ (low-rate regime). The limiting P_E would be expected to be the least pressure, P_{dl} , at which combustion can be sustained at fixed pressure. An anomaly occurs that the limiting P_E is less than P_{dl} for many propellants. Thus, the low-rate regime is characterized by an action of pressure reduction to stabilize propellant burning rather than to destabilize it as in the high-rate regime. The observed anomaly is certainly a

consequence of the finiteness of the depressurization rate. If the rate approaches zero (i.e., is infinitely slow), P_E should be equal to P_{dl} . Thus, we expect a minimum in P_E exists for a certain small value (smaller than employed in this study) of the fractional rate of depressurization.

We attribute extinguishment in P_{dl} experiments to an intrinsic instability as discussed in Chapter V. Somehow a small but finite $-(c \ln p)/dt$ inhibits the instability mechanism. A difference between the experiments is noted. In P_{dl} experiments, propellant burns prior to extinguishment through an energy-rich zone obtained during slow ignition while in P_E experiments propellant burns prior to extinguishment through normal zones, since depressurization time is considerably bigger than the thermal-wave relaxation time. But still, there is a slight deficiency of energy in the thermal wave in P_E tests. The more energy-rich wave may become a factor facilitating the onset of intrinsic instability in P_{dl} tests or the slight deficiency of energy in the thermal wave may suppress the instability. One may recall that a deep thermal wave in the condensed phase is inferred to be the origin of oscillatory burning behavior near the P_{dl} in Chapter V.

Another view is that there is a pressure-independent characteristic time of extinguishment. Note that the most lowering of P_E below P_{dl} is observed for PBAA propellants. It is proposed that there is a longer characteristic time of flame-out for PBAA propellants than HTPB or PU propellants. Also, it is longer in the low-rate or transition regime as the transient burning rate tests indicate. From the quenching curves, one may note that the low-rate regime is fully

established for PBAA and HTPB propellants and not for most FU propellants considered. The long characteristic time of flame-out for PBAA propellants is probably ascribed to the non-melting and AP-ejecting characteristics of PBAA binder. The interfacial reactions between PBAA binder and the oxidizer may exist beneath the large AP particles after the system pressure reduced below the P_{dl} and momentarily stabilize local burning.

CHAPTER VIII

RAPID DEPRESSURIZATION EXTINGUISHMENT AND REIGNITION

A. BACKGROUND

In previous chapters, there have been discussed the combustion and extinguishment of composite propellants at pressures not far removed from their low pressure deflagration limits. Two distinct regimes were noted when extinguishment occurred during pressure drop: the high-rate regime, where a critical ratio of characteristic times is a good criterion for extinguishment during depressurization; and the low-rate regime, where the externally imposed pressure transient defers the onset of the intrinsic instability which eventually extinguishes the flame. The maximum depressurization rate attainable in the strand bomb was 5 sec^{-1} , too small to extinguish some fast-burning propellants burning initially at high pressure. An extension of the extinguishment study to the higher pressure range was carried out with a small-L* (compared to the chamber used previously) blow-down chamber described in Chapter III, Section D. This blow-down chamber allowed the use of fractional rates of pressure decay up to about 350 sec^{-1} . One of the objectives of this investigation was to determine whether the extinguishment criterion, the critical ratio of characteristic times, is applicable to extinguishment by depressurization near atmospheric pressure; and if not, what other factors affect the extinguishment at pressures well above the low pressure deflagration limit.

Another motivation for this investigation was to study the reignition phenomenon occurring after depressurization extinguishment, a serious problem in the development of controllable motors. For all its practical importance, little progress has been made in the research on the reignition phenomenon, largely because it is so dependent upon experimental conditions. For example, it is certain that the reignition should be strongly influenced by the thermal surroundings of a temporarily-extinguished propellant grain. Reignition was observed in rarefaction tube tests by Baer, et al. (4). They reported that a catalyzed bimodal PBAA propellant could not be permanently extinguished with a fractional rate of pressure decay rate as great as 100 sec^{-1} . Their catalyzed PBAA propellant required a very large fractional rate of pressure decay for permanent extinguishment, and they speculated that this propellant might have an exceptional propensity for reignition. An examination of this behavior of PBAA propellants was intended.

Other investigators have been concerned with the reignition problem. Ciepluch [29] has made a systematic study on the reignition phenomenon of aluminized and non-aluminized PBAA propellants. His results show that the temporary flame-out is determined by the rate of pressure decay and little influenced by the ambient pressure level. In contrast, success in achieving permanent extinguishment at the same rate of pressure decay is determined by the ambient pressure level. Ciepluch reasoned that the existence of the reignition limit, which is far higher than the deflagration limit of the propellant, is due to the limitation of the available residual energy for reignition since the threshold energy flux required for propellant ignition increases sharply as the pressure is decreased in the subatmospheric pressure

range. He explains that the radiant energy flux from the heated chamber wall is not sufficient to cause reignition and the energy for reignition is derived from a combination of the residual energy in the thermal wave and in the combustion gases. He also reports that the reignition time, the time duration between flame-out and reignition, increases as either the depressurization rate is increased or the ambient pressure is lowered, being in the range from one second to more than 20 seconds. An aluminized propellant is observed to have the lowest reignition pressure limit.

Wooldridge, et al. [133, 134] investigated the extinguishment of PU propellants burned in a chamber vented to a vacuum tank. Their reports indicate that the extinguishment with depressurization at a low rate is more dependent on the pressure in the vacuum tank than on the rate of depressurization [133]. Like Ciepluch they observe that the reignition time increases as the dump tank pressure is decreased until it reaches a pressure at which no reignition takes place. The presence of aluminum is observed to shorten the reignition time. They also write that tubular grains are less prone to reignition than are end-burning grains, and, if reignition occurs, require a longer time for reignition than end-burning charges. They attribute the difference to radiation from the heated hardware in the chamber.

The effect of grain shape on reignition observed by Jensen [68] is different from that noted by Wooldridge, et al. He reports that a swing-nozzle motor in which a tubular grain is burned experiences more frequent reignition than a windowed chamber in which end-burning grains are burned. It is evident that chamber size and geometry are important factors. A valid comparison of propellants requires that

similarly shaped grains be burned in the same chamber. Jensen also reports that the addition of catalyst in aluminized propellants containing carboxyl-terminated polybutadiene or polyisobutylene greatly enhances the reignition tendency. He was able to prevent the reignition by purging the chamber with nitrogen immediately after depressurization.

During motor extinguishment tests in a chamber vented to the atmosphere, Merkle, et al. [78] also observed frequent reignition phenomena. They adopted the temporary extinguishment as a criterion of depressurization extinguishment to examine their theoretical extinguishment model. They considered a model for reignition including the effect of depressurization. Because the heat flux from the surroundings to the propellant surface was not known, their theoretical prediction could not be compared with experimental results.

From a literature survey, one infers that the reignition depends not only on the intrinsic properties of a propellant but also strongly on the experimental conditions. The standardization of experimental procedures is necessary if propellants are to be compared. However, most investigators report that the factors influencing reignition are the final dump-tank pressure, the rate of depressurization, the propellant composition, sample and motor geometry. In this investigation, it was intended to minimize the effect of chamber geometry by using a small- L^* blow-down tube whose wall temperature was controlled and by burning strands or hollow grains small compared to the chamber volume. Because the accuracy of pressure measurement was much decreased when the rapid depressurization rate was employed and because the reignition was very sensitive to the final dump tank

pressure, the final dump tank pressure and orifice size were chosen as major control variables in this study. Extinguishment tests were undertaken with four selected propellants: an uncatalyzed HTPB propellant, a catalyzed PU propellant, and a catalyzed and an uncatalyzed PBAA propellants.

B. EXPERIMENTAL PROCEDURE

The small-L* blow-down chamber described in Chapter III was connected to the main dump tank replacing the large combustion chamber for rapid depressurization tests. Since the volume of the blow-down chamber was small, the depressurization history was significantly affected by combustion generated hot gases and the variation of gas temperature inside the chamber during a test. Only the initial part of the pressure-time curve could be represented as an exponential decay. The combustion-unaffected depressurization history desired was not attained.

Square grains, 1.25 cm X 1.25 cm cross-section and 2.4 cm long, and tubular grains, 0.64 cm i.d., 2.2 cm o.d., and 2.4 cm long, were prepared and used. Tubular grains were cast in sections of stainless steel tubing of the same length with 0.64 cm diameter rods at the center. An extinguished tubular sample was used again when sufficient web thickness was left after a run. In some cases, a tubular grain was used three times. A re-used tubular grain had an increased diameter and, accordingly, produced a slightly different pressure history.

At first, there was an attempt to maintain a constant pressure for the steady combustion before depressurization. Later the attempt was

discontinued as unnecessary. The preparatory propellant combustion in the pressurizing environment was thought close to steady state since the characteristic time of pressurization was very much greater than the thermal wave adjustment time at the initial pressures employed. The maximum pressure during initial steady burning before depressurization was taken as the initial pressure of an extinguishment test.

The desired initial pressure was obtained by choosing an appropriate pre-ignition pressure and initial burning time before depressurization was started. The initial burning time was controlled by a pressure switch and a timer. The pressure switch activated the timer when the chamber pressure, being increased by propellant burning, reached the pre-set level. Several trial tests were needed to determine the appropriate level of pre-ignition pressure, pressure switch and timer setting for a desired initial pressure.

The pressure in the tube was monitored either by a Statham Model PA 285 TC-150-350 absolute pressure transducer with an Accudata 120 DC Amplifier when the maximum tube pressure was less than 10 atms or by a Kistler PZ 14 quartz crystal transducer with a Kistler Model S/N 166 charge amplifier when the maximum pressure was higher than 10 atms. The dump tank pressure was read from a mercury manometer before and after a run.

The light signal was detected by an RCA 1P40 infrared-sensitive gas photodiode which was mounted on the window of the rarefaction tube so that it could directly look across the flame. The light signal was amplified up to 50 times by a CRC AMPLI-VOLT DC amplifier to sense the low-intensity flame near extinguishment at low pressures. The circuit diagram for the photocells is shown in Figure C.5.

The pressure and light signals were amplified to volt level to record by a Precision Instrument Model 1207 tape recorder. Since the tape recorder was adjusted to record a maximum input 3V r.m.s., the portion of light signal larger than 3V was chopped off by a silicon voltage regulator diode (Texas Instruments Model 4372A) before being fed to the tape recorder. The tape recorder was pre-calibrated for each channel and for each recording speed. The recording speed was chosen out of 15, 30, and 60 ips depending on the depressurization rate. The recording was made in FM mode. The pressure and light signals were also photographed on the screen of a Tektronix Model 564 memory oscilloscope.

After a series of tests, the recorded pressure and light signals were reproduced on the Tektronix Model 564 dual beam oscilloscope by playing the recorder back at 7-1/2 ips speed and photographed by a C-12 model oscilloscope camera. Two photos were taken for each run; one in slow scan to determine reignition time and another in fast scan to determine the extinguishment pressure and the rate of depressurization from the pressure trace.

C. EXPERIMENTAL RESULTS AND DISCUSSIONS

For the four propellants selected, approximately 250 runs were conducted, emphasizing the dependency of reignition and reignition time on the final dump-tank pressure.

Figure VIII.1 shows the oscilloscope traces of a typical test in which extinguishment is followed by reignition. From the fast scan, upper picture, the extinguishment pressure was determined. It is noted that complete extinguishment occurs at a pressure very near the

final dump-tank pressure. Also noted is that the pressurization rate of the chamber due to pre-depressurization combustion is very slow on the time scale of interest. As seen in the lower picture, the re-development of flame follows about 0.25 sec after the original flame is quenched.

1. The Effect of Initial Pressure on Extinguishment Requirements

In the previous chapter, it was shown that the initial pressure does not affect the extinguishment pressure during depressurization in a lower pressure range when it exceeds the latter at least by a factor of two. It was intended to determine if the same is true for higher pressures and higher rates of depressurization. Figure VIII.2 shows the effect of initial pressure on the critical dump-tank pressure needed for extinguishment of the strands of a catalyzed polyurethane propellant. The orifice size is rather small so that extinguishment occurs at low pressures which are, however, in the high-rate regime as defined previously. The change of initial pressure from 0.8 to 20 atms does not produce any detectable change in the critical dump-tank pressure, about 0.2 atms, which may not be exceeded if burning is to be extinguished. Also noted is that the pressure at which extinguishment actually occurs is 0.25 atms, regardless of the initial pressure. Extinguishment occurs when the orifice flow is subsonic, and therefore is sensitive to the final dump tank pressure. Accordingly, the final dump-tank pressure becomes a factor in depressurization extinguishment.

Similar extinguishment data for a larger vent orifice are plotted in Figure VIII.3, also for catalyzed polyurethane propellant. At the higher rate we find that the initial pressure has a detectable

influence on the extinguishment phenomenon. The least severe extinguishment condition, as measured inversely by dump-tank pressure, is for an initial pressure about 5 atms, while more severe extinguishment requirements are shown for higher and lower initial pressures. The same tendency was observed by previous Utah investigators [26]. Another point to be noticed from the figure is that the extinguishment of hollow grains requires a lower dump tank pressure than end-burning strands. Reignition is rarely observed for this catalyzed PU-propellant at the experimental conditions adopted. In tests with strands, reignition is only observed when the initial pressure is about 2 atms. The range of final dump-tank pressures for reignition is, however, very narrow.

The decided effect of initial pressure on extinguishment, as shown just above, is contradictory to the earlier findings when a smaller vent orifice was used. Further examination is considered to resolve this contradiction. When one characterizes the severity of extinguishment conditions by the final dump-tank pressure, he supposes that the same pressure-time history is followed in the period in which the pressures are common for the cases with different initial pressures if the critical final dump-tank pressure is the same. In other words, he assumes that the rate of depressurization is a function only of the system pressure, the dump-tank pressure, and orifice diameter.

To check the validity of the assumption, the pressure histories for tests at three different initial pressures and at near critical dump-tank pressure but with the same vent orifice are displaced on Figure VIII.4, such that the initial point of each lower-pressure run

is on the pressure-time curve for the run starting at the highest pressure. Obviously, our assumption is not supported. The initial pressure affects the pressure histories below about 2.3 atms, even though the pressure is higher than 1.7 atms, where the orifice flow is expected to be sonic for all tests: at a given pressure, the pressure drops more slowly when a test is begun at higher pressures. The same trend persists even at subsonic-nozzle conditions until the system pressure is very close to the dump-tank pressure. As shown, extinguishment occurs when the system pressure is below 1 atms where the orifice flow is subsonic for all tests. The tests at a higher initial pressure simply need a lower critical dump-tank pressure to give the necessary rate of depressurization for extinguishment at the observed flame-out pressure. The role of the dump-tank pressure in determining extinguishment is to influence the rate of depressurization when the orifice is dechoked. The pressure histories of the tests with the initial pressure of 5 atms are also checked (not shown) and found to be very close to but to decrease slightly faster than those at initial pressure about 2.2 atms. The influence of initial pressure on the depressurization history appears to come from the difference in the temperature histories of the gases inside the burner chamber for the different initial pressures.

It is noted in Figure VIII.3, however, that the pressure at extinguishment appears to become independent of the initial and dump-tank pressures if the former is large enough, and the latter small enough.

2. The Effect of Grain Shape on Extinguishment Requirements

The actual histories shown in Figure VIII.5, confirms the observation of Figure VIII.3, that a much lower dump-tank pressure is required by hollow grains than by strands. For the same orifice size and the same initial pressure, the rate of pressure decay is noted to be much slower when hollow grains are used. The total mass burning rate has a decided effect on the depressurization history at low pressures. It is interesting to note that the rate of pressure decay in Run 235 is faster than that in Run 234 for most parts of the pressure history, except the very last portion. Extinguishment is, however, recorded in Run 234. Note that below 0.5 atms, the orifice is dechoked earlier in Run 235 and therefore the rate of depressurization is expected to be lower than that in Run 234 for the same pressure. The notably higher mass burning rate in Run 234 at higher pressures is due to the use of a sample which has once before extinguished and, accordingly, had a larger burning surface area than the sample used in Run 235.

3. Temporary and Permanent Extinguishment Requirement of Various Propellants

With the observation made above, it is acknowledged that the representation of extinguishment data by the initial pressure and the initial rate of depressurization, which is fairly well represented by the orifice size (or, more precisely, by the ratio of its area to tube volume), is not satisfactory. The actual pressure history should be used to test any extinguishment theory. For an approximate characterization of depressurization to permanent extinguishment, the orifice size and final dump-tank pressure would make better but still approximate descriptors.

In Table VIII.I, the experimental data are summarized in terms of final dump-tank pressure for a given orifice size and initial pressure.

A number of tests were carried out to determine the reignition time with the experimental conditions producing reignition. Reignition was rarely observed in uncatalyzed HTPB and catalyzed PU propellants. PBAA propellants, however, both catalyzed and uncatalyzed, showed reignition over a broad range of experimental conditions. In most tests, the final dump-tank pressure was kept at subatmospheric pressure. From Table VIII.I, one may notice that for UEW and UFA propellants, the dump-tank pressures for permanent and temporary extinguishment are very close. In general, hollow grains are shown to require lower dump-tank pressure wither for the burned out-reignition boundary or for the reignition-permanent extinguishment boundary. As discussed previously, the main reason that hollow grains need a lower critical dump-tank pressure for extinguishment is probably the slower rate of depressurization at low pressures.

Extinguishment results for a catalyzed PBAA propellant, of interest because of its broad range of reignition conditions, are summarized in Figure VIII.6. The dump-tank pressure needed permanent extinguishment is greater for end-burning grains than for hollow grains and dependent on the rate of depressurization. Hollow grains exhibit almost a constant critical dump-tank pressure for permanent extinguishment for a wide range of depressurization rates. When the fractional rate of depressurization is lower than 50 sec^{-1} , the propellant could not even be temporarily extinguished with the final dump-tank pressure as low as 0.075 atms. The final dump-tank pressure appears to be a most influential factor on reignition as was remarked by Ciepluch [29].

4. The Effect of Final Dump Tank Pressure on Reignition Time

In Figure VIII.7, the reignition times of UEZ, a PBAA-containing propellant, are plotted as a function of final dump-tank pressure for various experimental conditions. Although some data scattering is noticed, the general trend is that the reignition time decreases as the final dump-tank pressure is increased. This result is consistent with the observations of Ciepluch [29] and Woolridge, et al. [135], although they observed longer reignition times, from one second to about 20 seconds. Sometimes almost immediate reignition was observed after flame-out when the final dump-tank pressure was high. Generally, strands show slightly longer reignition time than hollow grains at the same experimental conditions, indicating that heat loss plays a role. The initial pressure and the rate of depressurization do not seem to have a sufficient effect on the reignition time to be discerned through the data scatter.

5. The Unusual Reignition Tendency of a Catalyzed PBAA Propellant

The unusual reignition capability of a catalyzed bimodal PBAA propellant reminds one of the several peculiar burning and extinguishment characteristics of this propellant: exceptionally fast burning rate at low pressures, ejection of a large amount of AP at low pressure, and long characteristic time of flame-out near the limiting pressure. Uncatalyzed PBAA propellants also show similar reignition behavior. The reignition under the cold surrounding conditions arranged in this study is presumably caused by the unique characteristics of PBAA propellants. Note that the propellants fueled with PU and HTPB binders rarely show reignition in the same experimental conditions.

It may be that the difference between PBAA and PU (and HTPB has PU characteristics) propellants is the same as that between the polymeric fuels. As described in Chapter IV, the PU binder melts, while the PBAA binder does not. On an extinguished surface, molten PU polymer flows into small crevices between AP particles and binder, but these crevices remain on PBAA surface, and are the hot spots for reignition. AP ejection at low pressure may have the same explanation, with reaction at the interface gap eating under the particle.

6. The Representation of Extinguishment Data by the Critical Ratio of Characteristic Times

To determine the applicability of the critical ratio of characteristic times for extinguishment, the extinguishment pressure, in both the temporary and the permanent extinguishment cases, is plotted with respect to the instantaneous fractional rate of depressurization at the moment of extinguishment along with the extinguishment data obtained from combustion-chamber tests in Figures VIII.8, VIII.9 and VIII.10 for UFA, UEM, and UEZ, respectively. The data from the small- L^* blow-down chamber on those figures show extinguishment pressure for first extinguishment regardless of whether reignition occurs and whether the orifice is sonic or not.

The extinguishment data obtained by the small- L^* blow-down chamber are much less accurate than those taken in the combustion chamber. In some cases, probably, the error in taking the slope of the pressure-time curve could be a factor of two. The large scatter of the data is presumably due to the inaccuracy involved in data acquisition and reduction procedures. The first thing to be noted from these figures is that differences are not detectable in the temporary-extinguishment

requirements between the hollow grain and the strand, suggesting that heat loss does not play a role for high-pressure first extinguishment.

It is also noted that straight lines, adequately correlating the combustion-chamber extinguishment data in the high-rate regime studied in the large chamber, match the low-pressure bound of the data for the small- L^* chamber for UFA and UEM propellants, respectively, implying that a critical ratio of characteristic times particular to a given propellant constitutes a rough guideline for motor design with the propellant. The line of the low-pressure bound represents the conditions for sure extinguishment. The critical ratio of characteristic times for UFA and UEM propellants happens to be a value approximately corresponding to $\Lambda = 2$ for the von Elbe-type criterion. For reference, the lines representing the von Elbe-type criterion with $\Lambda = 2$ are plotted in Figures VIII.8 and VIII.9. The UEZ propellant, for which high-rate data in the combustion chamber are very limited, lacks the extinguishment data for the intermediate rates of depressurization needed to interrelate the two sets of data as above. Roughly, a straight line corresponding to a Λ value slightly less than two make the low-pressure bound of the data for the small- L^* blow-down chamber but the von Elbe-type expression with the same value does not correlate the combustion-chamber data. The lines corresponding to $\Lambda = 1$ and 2 are drawn in Figure VIII.10 for reference.

6, Summary of Results

The findings in this chapter can be summarized as follows:

- (1) The presentation of extinguishment conditions in terms of initial pressure and initial rate of

depressurization is not satisfactory. The actual pressure history should be measured to determine extinguishment conditions.

- (2) The critical final dump-tank pressure is a very important parameter in the extinguishment process because it governs the final phase of the depressurization history, which actually determines the extinguishment. Moreover, reignition is very sensitive to the final dump-tank pressure.
- (3) The sample geometry does not have significant effect on temporary extinguishment although hollow grains have a greater tendency to reignite.
- (4) Reignition is very much dependent on the polymer fuel. PBAA propellants are most prone to reignition. Reignition is rarely observed for HTPB and FU propellants in the experimental conditions considered.
- (5) Reignition time is observed to be less than 1.6 seconds for the experimental conditions employed and increases as the final chamber pressure is decreased.
- (6) The critical ratio of characteristic times appears to be roughly applicable to temporary extinguishment even at higher pressures.

CHAPTER IX

SUMMARY AND CONCLUSIONS

Each of the Chapters IV through VIII contains its own discussion of a study which is, in large degree, independent of the others. Few cross references are made. This final chapter is an attempt to draw, from the five preceding chapters, selected items of information which, taken together, bear importantly on the following four topics:

A, Mechanisms of Extinguishment; B, Effect of Heat Losses on the Combustion and Extinguishment; C, Influence of Binder Chemistry on Low-Pressure Combustion; D, Status of Unsteady Combustion Theory.

A. MECHANISMS OF EXTINGUISHMENT

1. Experimentally-determined (by depressurization) quenching curves (Figures VII.3, VII.4, and VII.5) indicate that there are two distinct extinguishment regimes (the high-rate regime and the low-rate regime as defined in Chapter VII, Section D), signifying two different extinguishment mechanisms.
2. The sloped-straight-line relationship between the extinguishment pressure and the fractional rate of depressurization in the high-rate regime suggests that the ratio of characteristic times (depressurization and thermal-wave adjustment) determines extinguishment in

the high-rate regime. The starvation of energy in the zone of initial reactions is believed to be the mechanism of extinguishment in this regime. The high-rate regime extends to still higher pressures and depressurization rates, as shown by the data taken with small- L^* below-down chamber (Figures VIII.8, VIII.9, and VIII.10). Consequently, von Elbe-type extinguishment criterion is, at least to a first approximation, applicable in this regime with the Λ value taken as a property of the propellant.

3. The extinguishment pressure takes the limiting minimum value independent of the rate of depressurization when the rate is slow enough (low-rate regime). Extinguishment in the low-rate regime (Chapter VII) has the same mechanism as the extinguishment in the P_{dl} experiment (Chapters IV and V). Self-excited, intrinsic instability, manifested as oscillations in burning rate, develops in the combustion wave and eventually leads to the extinguishment. An anomaly occurs at this low-rate regime. The limiting extinguishment pressure observed during depressurization is often lower than the P_{dl} of the propellant determined by go/no-go tests (Figures VII.10, VII.11, and VII.12). We suggest two possible explanations. One is that the slight deficiency of energy in the thermal wave in depressurization extinguishment tests may have the

effect of delaying the onset of the intrinsic instability. Another view is that there is a pressure-independent characteristic time of extinguishment, whose value depends on propellant chemistry.

B. EFFECT OF HEAT LOSSES ON THE COMBUSTION AND EXTINGUISHMENT

1. The large augmentation of the burning rate (Figures VI.3 and VI.4) and flame temperature (Figures VI.5 and VI.6) and the significant lowering of the P_{dl} (Figures VI.8, VI.9, VI.12, and VI.13) by a moderate external flux indicate that heat losses from the burning surface have a significant effect on the combustion and extinguishment of solid propellants near their P_{dl} .
2. The analyses of the burning rate and flame temperature data show that the surface decomposition reaction is slightly exothermic (Table VI.I) and the activation energy for the gas-phase reaction (as defined for the Denison-Baum model) is approximately 20 kcal for a catalyzed PU propellant and 25 kcal for an uncatalyzed PU propellant (Figure VI.7).
3. It is clear that the low-pressure burning behavior of propellants is strongly influenced by the thermal environment of the combustion chamber. Meaningful investigation of the combustion characteristics requires knowledge or control of that environment.

4. The limiting extinguishment pressure drops almost linearly with the supplemental external heat flux (Figures VI.8 and VI.9). The extrapolated minimum flux corresponding to the zero pressure is about $1.0 \text{ cal/cm}^2\text{sec}$. It is the least net surface heat flux at which the ordinary burning could occur. The corresponding effective furnace temperature, about 650°C , is interpreted as the least effective surface temperature for burning.

C. INFLUENCE OF BINDER CHEMISTRY ON LOW-PRESSURE COMBUSTION

1. Low-pressure burning conditions such as the low burning rate, the low surface temperature, and the low heating rate of the binder polymer, permit the details of the polymer chemistry to emerge as important variables by allowing polymers to undergo combustion-modifying changes (Chapter IV). The effect of polymer chemistry is noted in the burning rate behavior (Figure IV.4), in the P_{dl} (Figures IV.5 and IV.6), in the oscillatory burning behavior (Figures V.4, V.5, and V.6), and in the extinguishment during depressurization (Figures VII.10, VII.11, and VII.12).
2. The high P_{dl} of polyurethane and PLMA-fueled propellants (Figures IV.5 and IV.6) is due to the melting of the binder polymers. The melting of these polymers is inferred to accompany depolymerization. The HTPB binder

is also a polyurethane but the effect of melting is less pronounced due at least in part to the lower concentration of urethane bonds, and therefore, the higher melting temperature.

3. The observed insensitivity of the P_{dl} of propellants fueled with PBAA binder to the oxidizer particle size (Figure IV.5) is due to the non-melting and the reactivity of this binder. The same characteristics presumably account for the large amount of AP ejection from PBAA-bimodal-AP propellants. Also the exceptional propensity for reignition following rapid depressurization extinguishment (Chapter VIII) appears to support the same reasoning.
4. The PBAA propellants and highly-oxidized PU and HTPB propellants containing the bimodal AP show a strange burning behavior near the P_{dl} : a more fuel-rich propellant has a higher burning rate at the same pressure and thus, a lower P_{dl} (Figures IV.1, IV.2, IV.3, and IV.4). The explanation offered is that the large AP particles, decomposing slowly, provide a relatively inert, energy-absorbing surface layer for PU propellants. Large AP particles are ejected by PBAA propellants burning at very low pressure. The more fuel-rich propellants eject a much smaller fraction of their AP, and are thought to be actually the less fuel-rich as measured by concentrations of reacting species in the combustion zone. The

actual combustion efficiency is therefore inferred to be better in the more fuel-rich propellant.

D. STATUS OF UNSTEADY COMBUSTION THEORY

1. The observed oscillatory burning behavior of solid propellants near their low pressure limit supports a view that the extinguishment at the P_{dl} should be attributed to an intrinsic instability (Chapter V).
2. The so-called "one dimensional" theories of propellant combustion instability presume a homogeneous propellant. They treat instability as a coupling response of combustion to an external pressure (or energy flux) perturbation, and therefore can describe an intrinsic instability only as a limiting case in which the amplitude of the driving perturbation vanishes (Chapter V). Denison and Baum's theory, one of this kind, fails to predict the observed periods of the oscillation in burning rate with reasonable values of kinetic and thermochemical parameters (Chapter V). That theory does, however, predict the observed fixed ratio of oscillation period to the relaxation time of the thermal wave in the propellant.
3. The above-mentioned successful prediction by the theory is not regarded as validating the theory. It is merely taken as evidence that any successful theory must account for the energy capacitance of the thermal wave.

4. To consider intrinsic instability as a special case of ~~externally stimulated~~ instability is to adopt much too narrow a perspective. The processes providing the coupled stimulus and response must all occur in the flame, surface, and subsurface preheat zones, and, further, should all be describable without reference to external conditions.
5. It is proposed that a successful theory start with the proposition, which has a respectable experimental foundation, that the oscillating gasification rates of the two main propellant ingredients are out of phase. The relative surface availability of the ingredients would necessarily vary, as would the feedback energy flux, and the thermal wave would provide a capacitive element in the cycle of events.

NOMENCLATURE

<u>Symbols</u>	<u>Definition</u>	<u>Units</u>
A	parameter in pressure response function	
A_b, A_{ox}	Arrhenius frequency factors for the decomposition processes of binder and oxidizer	
A_n	nozzle throat area	cm^2
a	burning-rate coefficient in Vielle's burning-rate law	$\text{cm}/[\text{sec atm}^n]$
a_0	initial speed of sound at p_0 and T_0	cm/sec
B	parameter in pressure response function	
C	constant in Denison-Baum model	$\text{cm}/[\text{sec atm}^n \text{ } ^\circ\text{K}^{n+1}]$
c	heat capacity of solid	$\text{cal}/\text{gm } ^\circ\text{K}$
c_i	heat capacity of i^{th} ingredient	$\text{cal}/\text{gm } ^\circ\text{K}$
c_p	heat capacity of gas at constant pressure	$\text{cal}/\text{gm } ^\circ\text{K}$
D	bead diameter of thermocouple	cm
D_i	diameter of i^{th} oxidizer particle size	cm
D'_i	characteristic distance associated with an oxidizer particle of D_i diameter	cm
D_0	diameter of oxidizer particle in general	cm
E_b, E_{ox}	activation energies for the decomposition processes of binder and oxidizer	$\text{cal}/\text{gm mole } ^\circ\text{K}$
E_f	activation energy for gas phase reaction	$\text{cal}/\text{gm mole } ^\circ\text{K}$
E_s	activation energy for surface reaction	$\text{cal}/\text{gm mole } ^\circ\text{K}$

F_i	frequency of oscillations	Hz
f	total heat feedback flux	$\text{cal/cm}^2 \text{ sec}$
f_r	external heat flux	$\text{cal/cm}^2 \text{ sec}$
G	$g_+ g_- / g_0$	
g	$1 + A(1 - B)$	
g_+, g_-, g_0	statistical weights [Eq. (F-1)]	
h	distance crystal protrudes above or is recessed below the propellant surface	cm
i	$(-1)^{1/2}$	
K	equilibrium constant	
K_i	ratio of the i^{th} oxidizer particle size to the associated characteristic distance	
k	thermal conductivity of propellant	$\text{cal/cm}^\circ \text{K sec}$
k_a	thermal conductivity of the continuous phase in a composite solid	$\text{cal/cm}^\circ \text{K sec}$
L^*	ratio of the free chamber volume to nozzle throat area	cm
M	molecular weight of gas	gm/gm mole
m, m'	mass flux and its perturbation	$\text{gm/cm}^2 \text{ sec}$
m_b, m_{ox}	mass decomposition rates of binder and oxidizer	$\text{gm/cm}^2 \text{ sec}$
Nu	Nusselt number	
n	pressure exponent in Vielle's burning rate law	
P_{dl}	pressure deflagration limit	atm
P_E	extinguishment pressure	atm
P_f	pressure deflagration limit under furnace heating	atm
Pr	Prandtl number	

p, p'	pressure and its perturbation	atm
P_o	initial chamber pressure	atm
q	net heat of gasification	cal/gm
R	gas constant	cal/gm mole °K
R'	gas constant	gm cm ² /sec gm mole °K
Re	Reynolds number	
r	linear burning rate	cm/sec
\bar{r}	averaged linear burning rate	cm/sec
r_b, r_{ox}	linear burning rates of binder and oxidizer	cm/sec
r_{dl}	limiting burning rate	cm/sec
S_b, S_{ox}	decomposition surface areas of binder and oxidizer	cm ²
T	temperature	°K
T_a	temperature of the surroundings	°K
T_c	thermocouple temperature	°K
T_f	flame temperature	°K
T_o	initial temperature of propellant	°K
T_o	initial gas temperature in the chamber	°K
T_s	surface temperature of burning propellant	°K
$T_{s,b}, T'_{s,b}$	surface temperature of decomposing binder and its perturbation	°K
$T_{s,ox}, T'_{s,ox}$	surface temperature of decomposing oxidizer and its perturbation	°K
t	time	sec
t_{ign}	ignition delay time	sec
U	ionization potential	cal/gm mole

V	chamber volume	cm^3
w_i	weight fraction of the i^{th} ingredient	
X	photograph magnification	
X_i	weight fraction of i^{th} oxidizer particle size in total propellant weight	
X_T	total oxidizer weight fraction	
x	fraction of ionized molecules	
α	thermal diffusivity	cm^2/sec
β	heat flux coefficient, $\partial r / \partial f_r$	cm^3/cal
β	constant dependent on heat-capacity ratio	
γ	heat-capacity ratio	
ϵ	emissivity of thermocouple bead	
η	volume fraction of the discontinuous phase	
ζ	volumetric ratio of oxidizer to binder in propellant	
Λ	constant in von Elbe-type criterion	
λ	characteristic root of solid phase energy equation [see Eq. (V-2)]	
ν	ratio of the thermal conductivities of the discontinuous phase to that of the continuous phase	
ρ, ρ_b, ρ_{ox}	densities of propellant, binder, and oxidizer	gm/cm^3
τ	period of oscillatory burning	sec
τ	defined by Eq. (C-3)	sec
τ_i	period of oscillations associated with i^{th} oxidizer particle size	sec
ϕ, ϕ'	ratio of the mass decomposition rates of the oxidizer to that of the binder and its perturbation	

ψ, ψ'	ratio of the decomposing surface areas of the oxidizer to that of the binder and its perturbation	
$\Omega, \Omega_r, \Omega_i$	dimensionless frequency parameter and its real and imaginary parts	
Ω_0	resonance dimensionless frequency parameter	
ω	angular frequency	rad/sec

Abbreviations

AP	ammonium perchlorate
CB	carbon black
CC	copper chromite catalyst
CTFB	carboxyl-terminated polybutadiene
CTPIB	carboxyl-terminated polyisobutylene
FC	fluorocarbon polymer
TPB	hydroxyl-terminated polybutadiene
PBAA	poly(butadiene co acrylic acid)
PBAA-AN	poly(butadiene co acrylic acid co acrylonitrile)
PLMA	poly(lauryl methacrylate)
PVC	poly(vinyl chloride)

REFERENCES

1. Adams, G. K., Newman, B. H., and Robins, A. B., "The Combustion of Propellants Based upon Ammonium Perchlorate," *Eighth Symposium (International) on Combustion*, p. 693, The Williams and Wilkins Company, Baltimore (1962).
2. Arden, E. A., Powling, J., and Smith, W. A. W., "Observations on the Burning of Ammonium Perchlorate," *Combustion and Flame*, 6, 21 (1962).
3. Avery, J., "Radiation Effects in Propellant Burning," *J. Phys. Chem.*, 54, 917 (1950).
4. Baer, A. D., Chien, W. P., and Ryan, N. W., "Transient Flame Temperature and Depressurization Extinguishment of Composite Propellant Strands," *7th JANNAF Combustion Meeting*, CPIA Publication No. 204, Vol. I, p. 369 (Feb. 1971). Also Chien, W. P., "Solid Propellant Flame Temperatures during Depressurization," M. S. Thesis, Department of Chemical Engineering, University of Utah (October 1970).
5. Baer, A. D., Schulz, E. M., and Ryan, N. W., "Spectra and Temperature of Propellant Flames During Depressurization," *AIAA J.*, 9, 869 (1971).
6. Barrère, M. and Nadaud, L. "Combustion of Ammonium Perchlorate Spheres in a Flowing Gaseous Fuel," *Tenth Symposium (International) on Combustion*, The Combustion Institute 1381 (1965).
7. Barrère, M. and Williams, F. A., "Analytical and Experimental Studies of the Steady State Combustion Mechanism of Solid Propellants," *Advances in Tactical Rocket Propulsion*, AGARD Conference Proceedings No. 1, p. 49, April, 1965, edited by S. S. Penner, Maidenhead, England, Technivision Services (Aug. 1968).
8. Bastress, E. K., Hall, K. P., and Summerfield, M., "Modification of the Burning Rates of Solid Propellants by Oxidizer Particle Size Control," *ARS Solid Propellant Rocket Conference*, Salt Lake City, Utah, Feb. 1-3, 1961.
9. Beckstead, M. W., "Non-acoustic Combustion Instability of Solid Propellants," Ph. D. Thesis, Department of Chemical Engineering, University of Utah (June, 1965).
10. Beckstead, M. W., Derr, R. L., and Price, C. F., "A Model of Composite Solid-Propellant Combustion Based on Multiple Flames," *AIAA J.*, 8, 2200 (1970).

11. Beckstead, M. W., Derr, R. L., and Price, C. F., "The Combustion of Solid Monopropellants and Composite Propellants," *Thirteenth Symposium (International) on Combustion*, p. 1047, The Combustion Institute (1971).
12. Beckstead, M. W. and Hightower, J. D., "Surface Temperature of Deflagrating Ammonium Perchlorate Crystals," *AIAA J.*, 5, 1785 (1967).
13. Beckstead, M. W., Ryan, N. W., and Baer, A. D., "Nonacoustic Instability of Composite Propellant Combustion," *AIAA J.*, 4, 1622 (1966).
14. Bircumshaw, L. L. and Newman, B. H., "The Thermal Decomposition of Ammonium Perchlorate I," *Proc. Roy. Soc. (London)*, A227, 115 (1954).
15. Bircumshaw, L. L. and Newman, B. H., "The Thermal Decomposition of Ammonium Perchlorate II," *Proc. Roy. Soc. (London)*, A227, 228 (1955).
16. Boggs, T. L., "Deflagration Rate, Surface Structure, and Sub-surface Profile of Self-Deflagrating Single Crystals of Ammonium Perchlorate," *AIAA J.*, 8, 867 (1970).
17. Boggs, T. L. and Beckstead, M. W., "Failure of Existing Theories to Correlate Experimental Nonacoustic Combustion Instability Data," *AIAA J.*, 4, 626 (1970).
18. Boggs, T. L., Mathes, H. B., Price, E. M., Kraeutle, K. J., Dehority, G. L., Crump, J. E., and Culick, F. E. C., *Combustion of Solid Propellants and Low Frequency Combustion Instability Progress Report*, NWC TP 4749, Naval Weapons Center (June 1969).
19. Boldyrev, V. V., Alexandrov, V. V., Boldyreva, A. V., Gritsan, V. I., Karpenko, Yu. Ya., Korobeinichev, O. P., Panfilov, V. N., and Khairtdinov, E. F., "On the Mechanism of the Thermal Decomposition of Ammonium Perchlorate," *Combustion and Flame*, 15, 71 (1970).
20. Bouck, L. S., Baer, A. D., and Ryan, N. W., "Pyrolysis and Oxidation of Polymers at High Heating Rates," *Fourteenth Symposium (International) on Combustion*, p. 1177, The Combustion Institute (1973). Also Bouck, L. S., "A High-Heating Rate Thermal Analysis of Solid-Propellant Reactions," Ph. D. Thesis, Department of Chemical Engineering, University of Utah, (August 1971).
21. Carslaw, H. S. and Jaeger, J. C. *Conduction of Heat in Solids*, 2nd ed., Oxford University Press, London, (1959).

22. Caveny, L. H. and Pittman, C. Y., "Contribution of Solid-Phase Heat Release to AP Composite Propellant Burning Rate," *AIAA J.*, 6, 1461 (1968).
23. Chaiken, R. F., "A Model for Low Pressure Extinction of Solid Rocket Motors," *AIAA J.*, 3, 1144 (1965).
24. Chaiken, R. F., "Implications of a Steady State Solid Propellant Combustion Model to a Low Pressure Deflagration Limit," *WSCI-69-5*. Presented at Western States Section of the Combustion Institute, U. S. Naval Weapons Center, China Lake, Ca., April 28-29, 1969.
25. Cheng, J. T., "Thermal Effects of Composite-Propellant Reactions." Ph. D. Thesis, Department of Chemical Engineering, University of Utah (August 1967).
26. Cheng, J. T., Bouck, L. S., Keller, J. A., Baer, A. D., and Ryan, N. W., "Ignition and Combustion of Solid Propellants," Technical Report under Air Force Grant AFOSR 40-65, Department of Chemical Engineering, University of Utah (1965).
27. Ciepluch, C. C., "Effect of Rapid Pressure Decay on Solid Propellant Combustion," *ARS J.*, 31, 1584 (1961).
28. Ciepluch, C. C., "Effect of Composition on Combustion of Solid Propellants During a Rapid Pressure Decrease," NASA TN D-1559 (1962).
29. Ciepluch, C. C., "Spontaneous Reignition of Previously Extinguished Solid Propellants," NASA TN D-2167 (March 1964).
30. Clemmow, D. M. and Huffington, J. D., "An Extension of the Theory of Thermal Explosion and Its Application to the Oscillatory Burning of Explosives," *Trans. Faraday Soc.*, 52, 385 (1956).
31. Coates, R. L., "An Analysis of a Simplified Laminar Flame Theory for Solid Propellant Combustion," *Combustion Science and Technology*, 4, 1 (1971).
32. Coates, R. L. and Horton, M. D. "Prediction of Conditions Leading to Extinguishment," *6th ICRPG Combustion Conference*, CPIA Publication No. 192, Vol. I, 399 (December 1969).
33. Coates, R. L. and Horton, M. D., "Further Evaluation of a Simplified Theoretical Model for Solid Propellant Extinguishment," *7th JANNAF Combustion Meeting*, CPIA Publication No. 204, Vol. I, 369 (February 1971).
34. Coates, R. L. and Kwak, S., "Effect of External Radiation on the Burning Rates of Solid Propellants," *J. Spacecraft*, 9, 742 (1972).

35. Cohen, N. S., "A Theory of Solid Propellant Extinguishment by Pressure Perturbation," *ICRPG 2nd Combustion Conference (1965)*, CPIA Publication No. 105, 677 (May 1966).
36. Cohen, N. S., Fleming, R. W., and Derr, R. L., "Role of Binder in Solid Propellant Combustion," *AIAA Paper No. 72-1121*, AIAA/SAE 8th Joint Propulsion Specialist Conference, New Orleans, Louisiana, Nov. 29 - Dec. 1, 1972.
37. Cookson, R. E. and Fenn, J. B., "Strand Size and Low Pressure Deflagration Limit in a Composite Propellant," *AIAA Paper No. 69-144*. Presented at AIAA 7th Aerospace Science Meeting, New York City, New York, Jan. 20-22, 1969.
38. Cordes, H. F., "An Estimate of the Melting Point of Ammonium Perchlorate," *AIAA J.*, 7, 1193 (1969).
39. Coward, H. F. and Jones, G. W., *U. S. Bureau of Mines Bull.* No. 279 (Revised) (1938).
40. Culick, F. E. C., "A Review of Calculations for Unsteady Burning of a Solid Propellant," *AIAA J.*, 6, 2241 (1968).
41. Culick, F. E. C., "An Elementary Calculation of the Combustion of the Solid Propellants," *Astronautica Acta*, 14, 171 (1969).
42. Denison, M. R. and Baum, E., "A Simplified Model of Unstable Burning in Solid Propellants," *ARS J.*, 31, 1112 (1961).
43. Dixon-Lewis, G. N. and Isles, G. L., "Limits of Inflammability," *Seventh Symposium (International) on Combustion*, p. 475, Butterworths Scientific Publications, London (1959).
44. Donaldson, A. B., Baer, A. D., Ryan, N. W., and Ryan, P. W., "Extinguishment of Composite Propellants by Rapid Depressurization," *2nd ICRPG Combustion Conference*, CPIA Publication No. 105, Vol. I, 697 (May 1966).
45. Dyer, E. and Wright, G. C., "Thermal Degradation of Alkyl N-Phenylcarbamates," *J. Am. Chem. Soc.*, 81, 2138 (1959).
46. Egerton, A. C., "Limits of Inflammability," *Sixth Symposium (International) on Combustion*, p. 4, Reinhold Publishing Corporation, New York (1957).
47. Eisel, J. L., "Flame Spectra of Solid Propellant during Unstable Combustion," Ph. D. Thesis, Department of Chemical Engineering, University of Utah (June 1972).
48. Eisel, J. L., Horton, M. D., Price, E. W., and Rice, D. W., "Preferred Frequency Oscillatory Combustion of Solid Propellants," *AIAA J.*, 2, 1319 (1964).

49. Feinauer, L. R., "Burning of Composite Ammonium Perchlorate Based Propellants Near Their Extinction Pressure," *AIAA Student J.*, 3, 125 (1965).
50. Fletcher, E. A. and Bunde, G. W., "Gas Evolution from a Solid Rocket Propellant During Depressurization to Produce a Quench," *AIAA J.*, 4, 181 (1966).
51. Frazer, A. H., *High Temperature Resistant Polymers*, p. 108, p. 132, Inter Science Publishers, A Division of John Wiley & Sons, New York (1968).
52. Friedman, R., Nugent, R. G., Rumbel, K. E., and Scurlock, A. C., "Deflagration of Ammonium Perchlorate," *Sixth Symposium (International) on Combustion*, p. 612, Reinhold Publishing Corporation (1957).
53. Goring, R. L. and Churchill, S. W., "The Conductivities of Heterogeneous Materials," *Chem. Eng. Prog.*, 57, 53 (1961).
54. Guirao, C. and Williams, F. A., "A Model for Ammonium Perchlorate Deflagration between 20 and 100 atm," *AIAA J.*, 9, 1345 (1971).
55. Guth, E. D., Land, J. S., and Schlesinger, G., "Model for the Burning Rate and Extinction of Aluminized Polybutadiene Ammonium Perchlorate Composite Propellants," AD 706 033, U. S. Department of Commerce/National Bureau of Standards (December 1969).
56. Hawkins, W. L. Editor, *Polymer Stabilization*, Wiley-Interscience, a Division of John Wiley & Sons, Inc., New York (1972).
57. Hermance, C. E., "A Model of Composite Propellant Combustion Including Surface Heterogeneity and Heat Generation," *AIAA J.*, 4, 1629 (1966).
58. Hertzberg, J., "The Free-Laminar and the Laser-Induced Combustion of Ammonium Perchlorate," *Combustion Science and Technology*, 1, 449 (1970).
59. Hightower, J. D. and Price, E. W., "Combustion of Ammonium Perchlorate," *Eleventh Symposium (International) on Combustion*, p. 463, The Combustion Institute, Pittsburgh, Pa. (1967).
60. Horton, M. D., Bruno, R. S., and Graesser, E. C., "Depressurization Induced Extinction of Burning Solid Propellant," *AIAA J.*, 6, 292 (1968).
61. Horton, M. D. and Price, E. W., "Deflagration of Pressed Ammonium Perchlorate," *ARS J.*, 32, 1745 (1962).

62. Horton, M. D. and Youngberg, L. Z., "Effect of radiation Energy on the Burning Rate of a Composite Solid Propellant," *AIAA J.*, 8, 1738 (1970).
63. Huffington, J. D., "The Unsteady Burning of Cordite," *Trans. Faraday Soc.*, 50, 942 (1954).
64. Inami, S. H., Rosser, W. A., and Wise, H., "Dissociation Pressure of Ammonium Perchlorate," *J. Phys. Chem.*, 7, 269 (1963).
65. Jacobs, P. W. M. and Russell-Jones, A., "On the Mechanism of the Decomposition of Ammonium Perchlorate," *AIAA J.*, 5, 829 (1967).
66. Jacobs, P. W. M. and Whitehead, H. M., "Decomposition and Combustion of Ammonium Perchlorate," *Chemical Reviews*, 69, 551 (1969).
67. Jensen, G. E., "A Start-Stop Study of Solid Propellants," NASA CR-66488 Nov. 1967.
68. Jensen, G. E., "An Experimental Study of Solid Propellant Extinction by Rapid Depressurization," NASA CR-66747, Final Report, Contract No. NAS 1-7815, United Technology Corporation, March 1969.
69. Johns, W. F., "New Results on the Low Pressure Deflagration and Reignition Limits of Solid CMDB Propellants," *3rd Combustion Conference*, CPIA Publication No. 138, Vol. I, 181 (February 1967).
70. Johnson, W. E. and Nachbar, W., "Deflagration Limits in Steady Linear Burning of a Monopropellant with Application to Ammonium Perchlorate," *Eighth Symposium (International) on Combustion*, p. 678, The Williams and Wilkins Company, Baltimore (1962). Also Technical Note AFOSR TN 60-700, Lockheed Missiles and Space Division (August 1960).
71. Kaskan, W. E., "The Dependence of Flame Temperature on Mass Burning Velocity," *Sixth Symposium (International) on Combustion*, p. 134, Reinhold Publishing Corporation, New York (1957).
72. Keller, J. A., "Studies of Ignition of Ammonium Perchlorate-Based Propellants by Convective Heating," Ph. D. Thesis, University of Utah, 1965; Technical Report, "Ignition of Ammonium Perchlorate-Based Propellants by Convective Heating," under Grant AF AFOSR 40-63 and 64, Department of Chemical Engineering, University of Utah, August 1, 1966.
73. Konev, E. V., "Influence of Light Radiation on Burning Rate of N Powder," *Combustion, Explosion, and Shock Waves*, Vol. 1, No. 2, 53 (1965).

74. Konev, E. V. and Khlevnoi, S. S., "Burning of a Powder in the Presence of Luminous Radiation," *Combustion, Explosion, and Shock Waves*, Vol. 2, No. 4, 21 (1966).
75. Law, R. J., Personal communications with N. W. Ryan, University of Utah, Salt Lake City, Utah (1973).
76. Lengelle, G., "Thermal Degradation Kinetics and Pyrolysis of Vinyl Polymer," *AIAA J.*, 8, 1989 (1970).
77. Levy, J. and Friedman, F., "Further Studies of Pure Ammonium Perchlorate Deflagration," *Eighth Symposium (International) on Combustion*, p. 663, The Williams and Wilkins Company, Baltimore (1962).
78. Lewis, B. and Von Elbe, G., *Combustion, Flames, and Explosions, of Gases*, 1st Edition, p. 369, Academic Press, New York (1951).
79. Lewis, B. and Von Elbe, G., *Combustion, Flames and Explosions, of Gases*, 2nd Edition, p. 310, Academic Press, New York (1961).
80. Linnett, J. W. and Simpson, J. S. M., "Limits of Inflammability," *Sixth Symposium (International) on Combustion*, p. 20, Reinhold Publishing Corporation, New York (1957).
81. Madorsky, S. L., *Thermal Degradation of Organic Polymers*, Interscience Publishers, New York (1964).
82. Manelis, G. B. and Strunin, V. A., "The Mechanism of Ammonium Perchlorate Burning," *Combustion and Flame*, 17, 69 (1971).
83. Mantyla, R. G., "Extinguishment of Solid Propellants by First Rarefaction Waves," M. S. Thesis, Department of Chemical Engineering, University of Utah (1968). Also Mantyla, R. G., Baer, A. D., and Ryan, N. W., "Extinction by Rapid Depressurization: A Means to Other Ends," *3rd ICRPG Combustion Conference*, CPIA Publication No. 138, Vol. 1, 227(1966).
84. Marshakov, V. N. and Leipunskii, O. I., "Burning and Quenching of a Powder in the Pressure of a Rapid Pressure Drop," *Combustion, Explosion, and Shock Waves*, 3, 144 (1967).
85. Mastrolia, E. J. and Klager, K., "Solid Propellants Based on Polybutadiene Binders," *Propellant Manufacture, Hazards, and Testing, Advances in Chemistry Series No. 88*, p. 122, American Chemical Society, Washington, D. C. (1969).
86. Merkle, C. L., Turk, S. L., and Summerfield, M., "Extinguishment of Solid Propellants by Depressurization: Effects of Propellant Parameters," *AIAA Paper No. 69-176*. Presented at AIAA 7th Aerospace Sciences Meeting, New York, New York (January 1969); Princeton University Aerospace Mechanical Science Report No. 880 (July 1969).

87. Muhlfeith, C. M., Baer, A. D., and Ryan, N. W., "Propellant Combustion Instability as Measured by Combustion Recoil," *AIAA J.*, 10, 1280 (1972). Also Muhlfeith, C. M., "Some Experiments on the Effect of Thermal Radiation on Composite Rocket Propellants," Ph. D. Thesis, Department of Chemical Engineering, University of Utah (June 1971).
88. Nachbar, W., "Steady Linear Burning of a Monopropellant with a General Surface Condition," Paper 69-22, *Spring Meeting Western State Section/The Combustion Institute*, China Lake, Calif., (April 1969).
89. Novikov, S. S., Pikhil, P. F., and Ryazantsev, Yu. S., "Modern Ideas on the Mechanism of Combustion of Condensed Systems: A Review," *Combustion, Explosion, and Shock Waves*, 4, 469 (1968).
90. Novozhilov, B. V., "Stability of the Stationary Regime for Powders Burning in a Semiconfined Space," *Combustion, Explosion, and Shock Waves*, 3, 19 (1967).
91. Oberth, A. E. and Bruenner, R. S., "Polyurethane Based Propellants," *Propellant Manufacture, Hazards, and Testing, Advances in Chemistry Series*, No. 88, p. 84, American Chemical Society, Washington, D. C. (1969).
92. Ohlemiller, T. J. and Summerfield, M., "Radiation Augmented Burning of a Solid Propellant," *Aerospace and Mechanical Sciences Rept. No. 799*, Princeton University (November 1967).
93. Osborn, J. R., Burick, R. J., and Ho, P. Y., "Techniques for the Continuous Measurement of Solid Propellant Burning Rates," Final Report Grant AF-AFOSR 207-64, Report No. F-66-3, Jet Propulsion Center, Purdue University (February 1966).
94. Parker, K. H. and Summerfield, M., "Response of the Burning Rate of a Solid Propellant to a Pressure Transient," *AIAA Preprint No. 66-683*. Presented at the AIAA Propulsion Joint Specialist Conference, Colorado Springs, Colorado (June 1966).
95. Paul, B. E., Cohen, N. W., and Fong, L. Y., "Solid Propellant Burning Rate under Transient Heating and Extinguishment via L^* Instability," *Proceedings of the 1st ICRPG Combustion Conference*, CPIA Publication No. 68, 491 (January 1965).
96. Paul, B. E., Lovine, R. L., and Fong, L. Y., "A Ballistic Explanation of the Ignition Pressure Peak," *AIAA Preprint 64-121*. Presented at the Fifth AIAA Solid Propellant Rocket Conference, Palo Alto, California (January 1964).

97. Pearson, G. S., "Perchlorate Oxidizers," *Oxidation and Combustion Reviews*, 4, 9 (1969).
98. Penner, S. S. and Olfe, D. B., "The Influence of Radiant-energy Transfer on Propellant Burning Rates and Ablation Rates Controlled by an Intense Radiation Field," *Astronautica Acta*, 11, 65 (1965).
99. Peterson, J. A., Reed, R., and Cornia, R. P., "Comparative Extinction Characteristics of Fluorocarbon and Conventional Propellants," *4th ICRPG Combustion Conference*, CPIA Publication No. 162, Vol. I, 389 (December 1967).
100. Peterson, J. A., Reed, R., and McDonald, A. J., "Control of Pressure Deflagration Limits of Composite Solid Propellants," *AIAA J.*, 5, 764 (1967).
101. Powling, J., "The Combustion of Ammonium Perchlorate-Based Composite Solid Propellants: A Discussion of Some Recent Experimental Results," E. R. D. E. Report No. 15/R/65, (July, 1965).
102. Powling, J., "Experiments Relating to the Combustion of Ammonium Perchlorate-Based Propellants," *Eleventh Symposium (International) on Combustion*, The Combustion Institute, Pittsburgh, 447 (1967).
103. Powling, J., and Smith, W. A. W., "Measurement of the Burning Surface Temperatures of Propellant Compositions by Infra-red Emission," *Combustion and Flame*, 6, 173 (1962).
104. Powling, J. and Smith, W. A. W., "The Surface Temperature of Ammonium Perchlorate Burning at Elevated Pressures," *Tenth Symposium (International) on Combustion*, The Combustion Institute, 1373 (1965).
105. Price, E. W., "Review of the Combustion Instability Characteristic of Solid Propellants," *Advances in Tactical Rocket Propulsion*, AGARD Conference Proceedings No. 1, April 1965, Edited by S. S. Penner, Maidenhead, England, Technivision Services, pp. 141-149 (August 1968).
106. Rabinovitch, B., "Regression Rates and the Kinetics of Polymer Deflagration," *Tenth Symposium (International) on Combustion*, The Combustion Institute, 1395 (1965).
107. Ranz, W. E. and Marshall, W. R., Jr., "Evaporation from Drops," *Chem. Eng. Prog.*, 48, 141-146, 173-180 (1952).
108. Reed, R., Cornia, R. P., Miller, R., and Munson, W. O., "Some Effects of Coated AP and Finely Divided Oxidizers on the Extinction Characteristics of Polyurethane Propellants," *AIAA Paper* No. 70-657. Presented at AIAA 6th Propulsion Joint Specialist Conference, San Diego, California (June 1970).

109. Reed, R., Nelson, C., McDonald, A., and Ramnarace, J. "Extinction Characteristics of Carboxyl Terminated Polybutadiene Propellants," *3rd Combustion Conference*, CPIA Publication No. 138, Vol. 1, 187 (February 1967).
110. Rosen, J. B., "Stability of Ozone Flame Propagation," *Sixth Symposium (International) on Combustion*, p. 236, Reinhold Publishing Corporation, New York (1957).
111. Ryan, N. W., "Comments: Experimental Solid Rocket Combustion Instability," *Tenth Symposium (International) on Combustion*, p. 1081, The Combustion Institute, Pittsburgh, Pa. (1965).
112. Schulz, E. M., "Propellant-Flame Spectra During Depressurization." Ph. D. Thesis, Department of Chemical Engineering, University of Utah (1969).
113. Sehgal, R. and Strand, L., "A Theory of Low Frequency Combustion Instability in Solid Rocket Motors," *AIAA J.*, 2, 696 (1964).
114. Selzer, H., "The Temperature Profile Beneath the Burning Surface of a Composite Ammonium Perchlorate Propellant," *Eleventh Symposium (International) on Combustion*, The Combustion Institute, Pittsburgh, Pa. 439 (1967).
115. Selzer, H., "Depressurization Extinguishment of Composite Solid Propellants: Influence of Composition and Catalysts," *AIAA Paper No. 72-1136*. AIAA/SAE 8th Joint Propulsion Specialist Conference, New Orleans, La., November 29 - December 1, 1972.
116. Shannon, S. J. and Erickson, Y. E., "The Thermal Decomposition of Composite Solid Propellant Binders," *Sixth ICRPG Combustion Conference*, CPIA Publication No. 192, 519 (1969).
117. Shelton, S., a paper presented at 3rd ICRPG/AIAA Joint Propulsion Conference, Atlantic City, N. J. (1968), cited by Culick, F. E. C., "Remarks on Extinguishment and the Response Function for a Burning Solid Propellant," *AIAA J.*, 7, 1403 (1969).
118. Silla, H., "Burning Rates of Composite Solid Propellants at Subatmospheric Pressure," *ARS J.*, 31, 1277 (1961).
119. Spalding, D. B., "A Theory of Imflammability Limits and Flame-quenching," *Proc. Roy. Soc.*, A240, 831 (1957).
120. Spalding, D. B., "The Theory of Burning Solid and Liquid Propellants," *Combustion and Flame*, 4, 59 (1960).
121. Steinz, J. A. and Slezer, H., "Depressurization Extinguishment of Composite Solid Propellants: Flame Structure, Surface Characteristics, and Restart Capability," *Combustion Science and Technology*, 3, 25 (1971).

122. Steinz, J. A. and Selzer, H., "Depressurization Extinguishment for Various Starting Pressures and Solid Propellant Types," *AIAA Paper* No. 71-631, AIAA/SAE 7th Propulsion Joint Specialist Conference, Salt Lake City, Utah (June 1971).
123. Steinz, J. A., Stang, P. L., and Summerfield, M., "The Burning Mechanism of Ammonium Perchlorate-Based Composite Solid Propellants," *Aerospace and Mechanical Sciences* Dept. No. 830, Princeton University (February 1969).
124. Strand, L. D., "Summary of a Study of the Low-Pressure Combustion of Solid Propellants" JPL Technical Report 32-1242 (April 1968).
125. Summerfield, M., Caveny, L. H., Battista, R. A., Kubota, N., Gostintsev, Yu. A., and Isoda, H., "Theory of Dynamic Extinguishment of Solid Propellants with Special Reference to Non-steady Heat Feedback Law," *AIAA Paper* No. 70-667. Presented at AIAA 6th Propulsion Joint Specialist Conference, San Diego, California (June 1970).
126. Thompson, C. L., Jr. and Suh, N. P., "The Interaction of Thermal Radiation and M-2 Double-Base Solid Propellant," *Combustion Science and Technology*, 2, 59 (November 1970).
127. Varney, A. M., "An Experimental Investigation of the Burning Mechanism of Ammonium Perchlorate Composite Solid Propellants," Ph. D. Thesis, School of Aerospace Engineering, Georgia Institute of Technology (May 1970).
128. Von Elbe, G., "Theory of Solid Propellant Ignition and Response to Pressure Transients," *Bull. Interagency Solid Propulsion Meeting (Conf.)*, Seattle, Washington, Vol. III, p. 92 (July 1963). Also "Solid Propellant Ignition and Response of Combustion to Pressure Transients," *AIAA Paper* No. 66-668. Presented at AIAA Second Propulsion Joint Specialist Conference, Colorado Springs, Colorado (June 1966).
129. Von Elbe, G. and McHale, E. T., "Extinguishment of Solid Propellants by Rapid Depressurization," *AIAA J.*, 6, 1417 (1968).
130. Waesche, R. H. A. and Wenograd, J., "Calculation of Solid Propellant Burning Rates from Condensed-Phase Decomposition Kinetics," *AIAA Paper* No. 69-145, AIAA 7th Aerospace Sciences Meeting, New York City, New York, Jan. 20-22, 1969.
131. Watt, D. M., Jr. and Petersen, E. E., "Relationship between the Limiting Pressure and the Solid Temperature for the Deflagration of Ammonium Perchlorate," *J. Chem. Phys.*, 50, 2196 (1969).
132. Williams, F. A., *Combustion Theory*, p. 191, Addison-Wesley Publishing Company, Inc. (1965).

133. Wooldridge, C. E. and Dickinson, L. A., "Review of Soviet Transient Combustion Research," Volume of Preprints from *ICRPG/AIAA 2nd Solid Propulsion Conference*, Anaheim, California, 104 (June 1967).
134. Wooldridge, C. E., Marxman, G. A., and Capener, E. L., "Propellant Combustion Phenomena During Rapid Depressurization," NASA CR-66500, Final Report, Stanford Research Institute, October 1967; *AIAA J.*, 6, 471 (1968).
135. Wooldridge, C. E., Marxman, G. A., and Krier, R. J., "A Theoretical and Experimental Study of Propellant Combustion Phenomena During Rapid Depressurization," NASA CR-66733, Final Report, Contract No. NAS 1-7349, Stanford Research Institute (February 1969).
136. Wong, T. L., "L-Star Instability," Ph. D. Thesis, Department of Chemical Engineering, University of Utah (June 1969).
137. Yin, C. F. and Hermance, C. E., "Continuous Measurement of Transient Burning Rates of a Composite Propellant Undergoing Rapid Depressurization," *AIAA Paper* No. 71-173, AIAA 9th Aerospace Science Meeting, New York, January 25-27, 1971.
138. Yount, R. A. and Angelus, T. A., "Chuffing and Non-Acoustic Instability Phenomena in Solid Propellant Rockets," *AIAA J.*, 2, 1307 (1964).

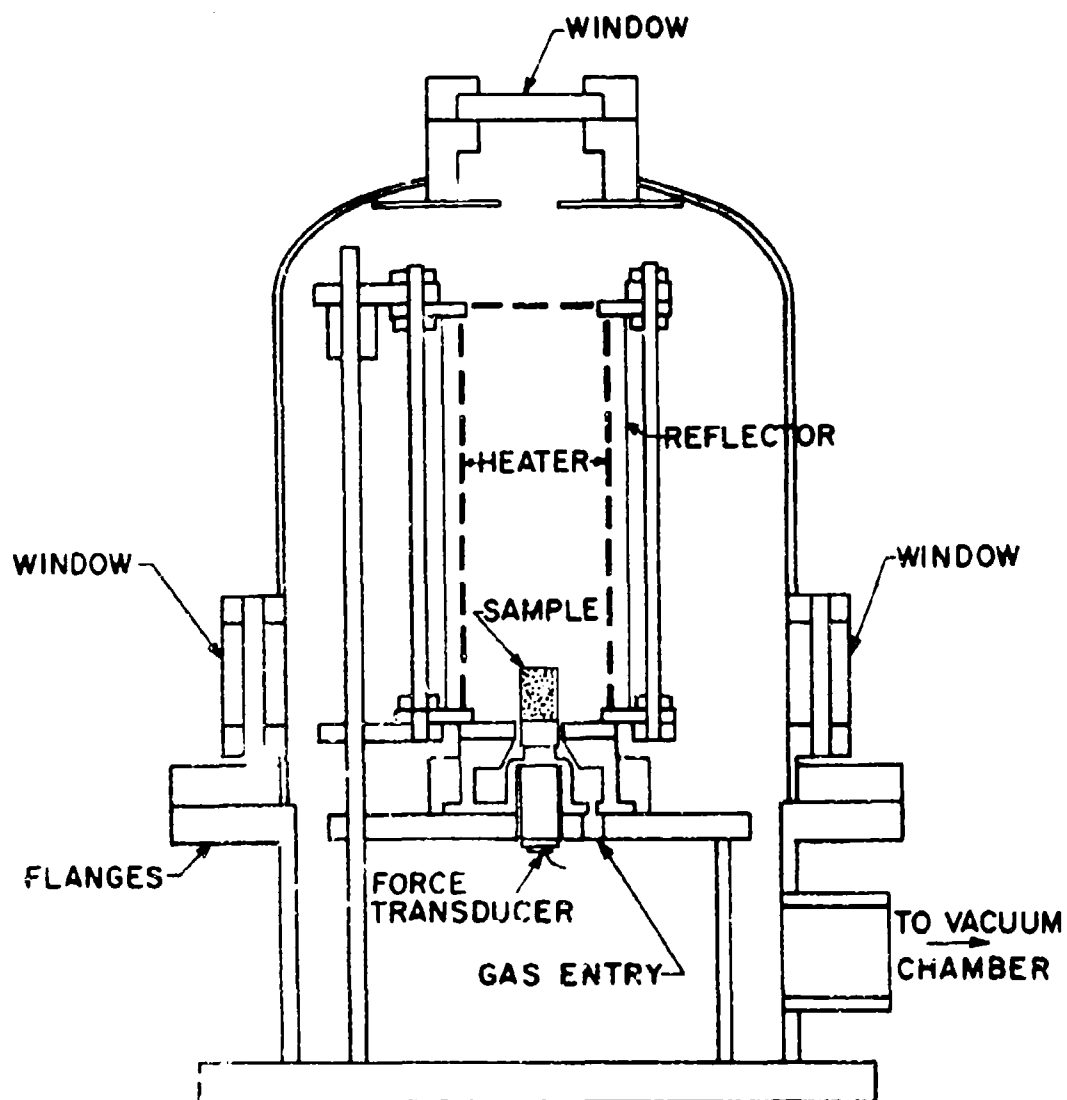


Figure III.1. A Schematic Diagram of the Combustion Chamber.

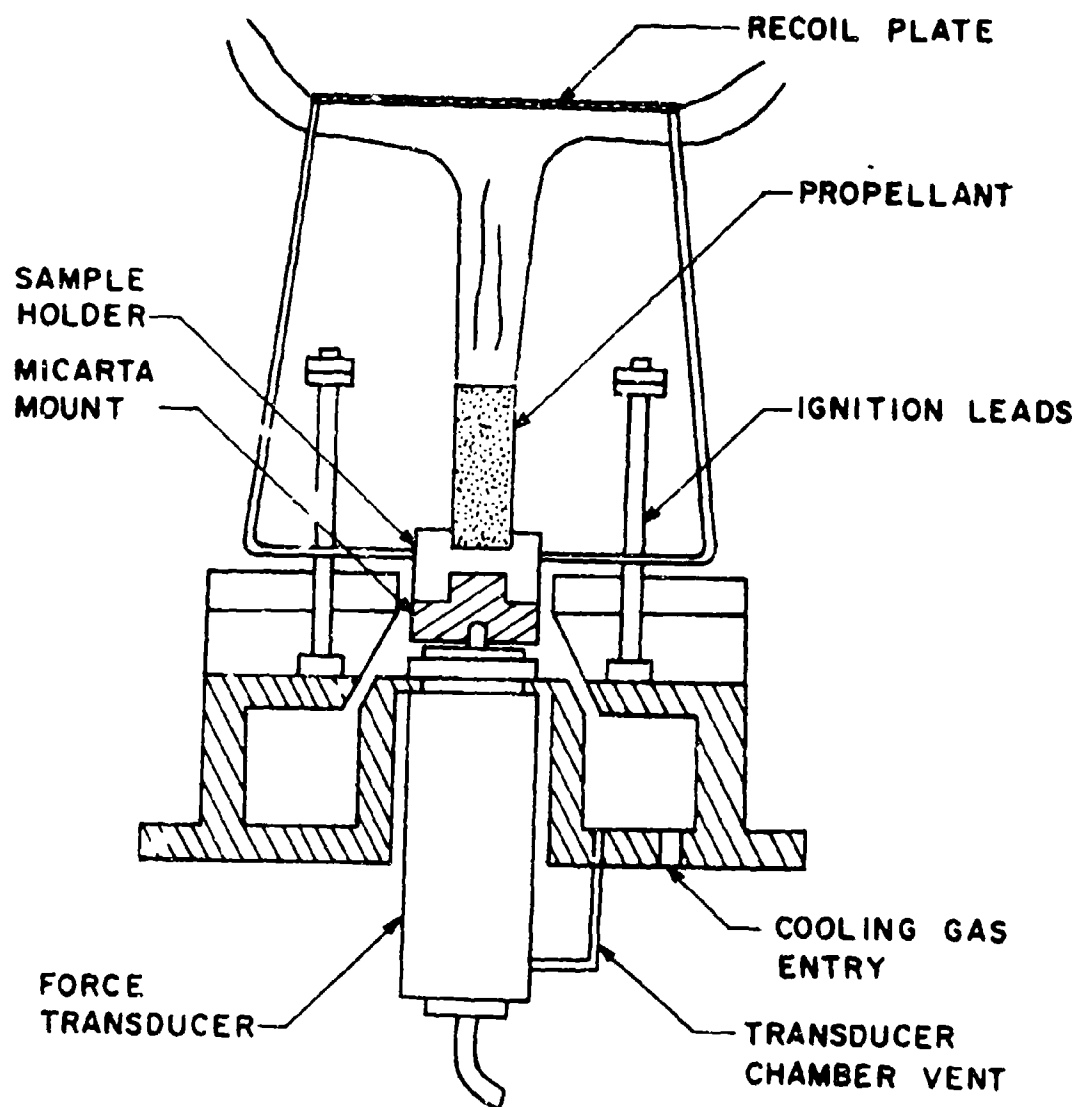


Figure III.2. A Schematic Diagram of the Force Measurement Assembly.



Figure III.3. An Overview Photograph of the Combustion Chamber (With Dome Lifted to Show Nichrome Ribbon Furnace) and Accessories.



Figure III.4. A View of the Remote Control Panel and the Data Acquisition and Processing Equipment..

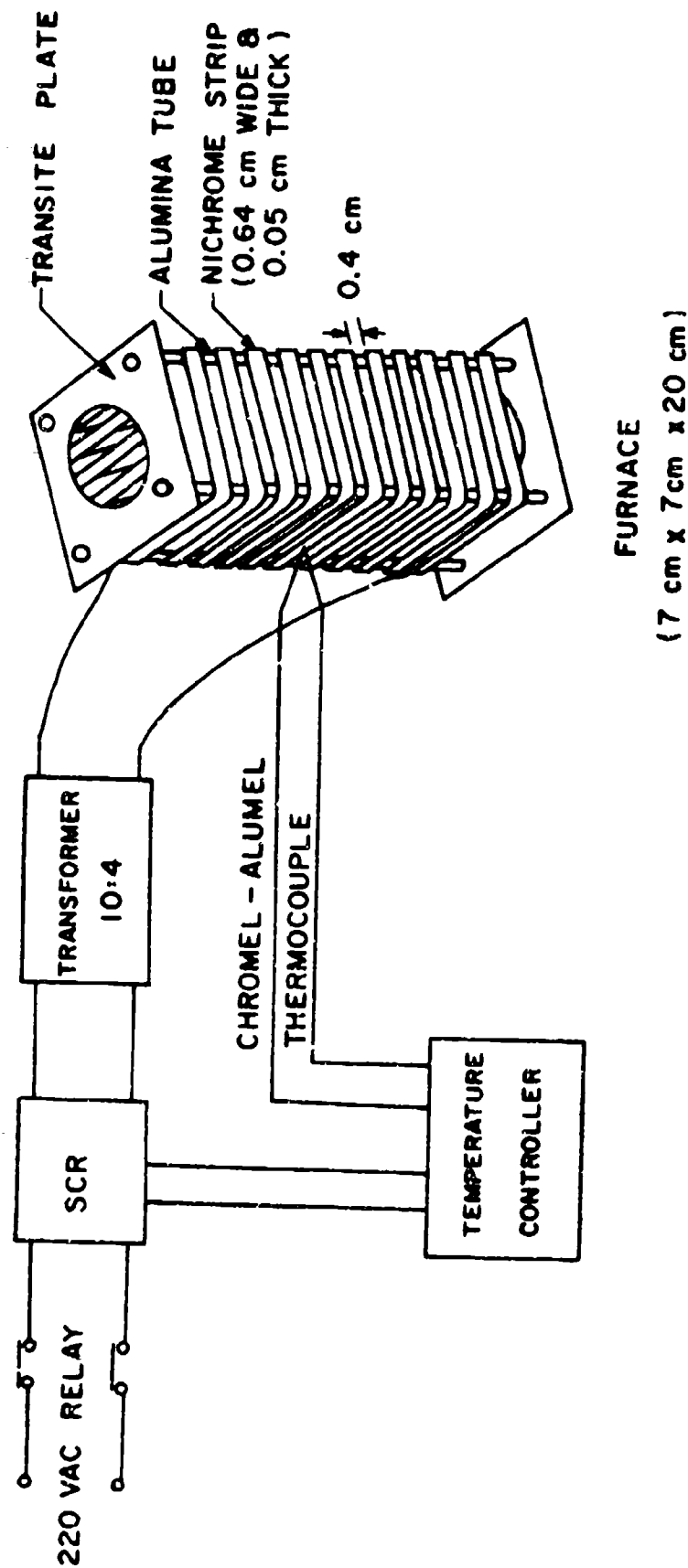


Figure III.5. A Schematic Diagram of the Quick Heating Furnace and Its Electrical Circuit.

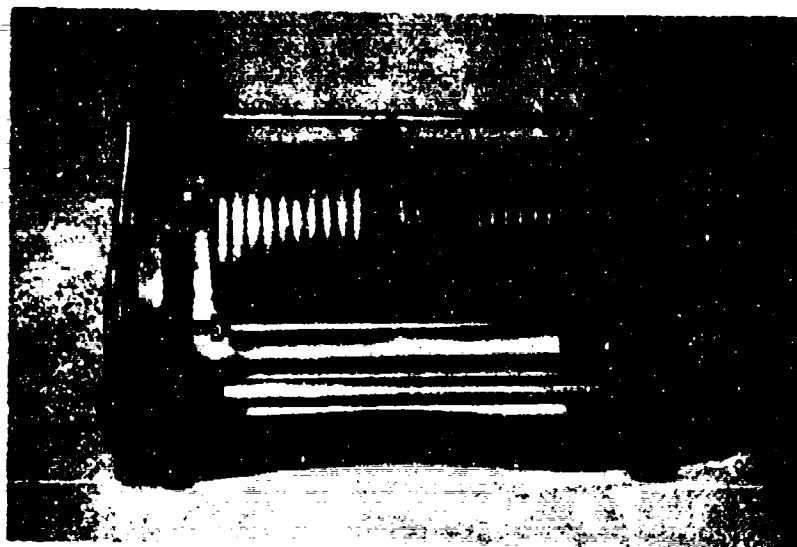


Figure III.7. A Photograph of the Cooling Coil.

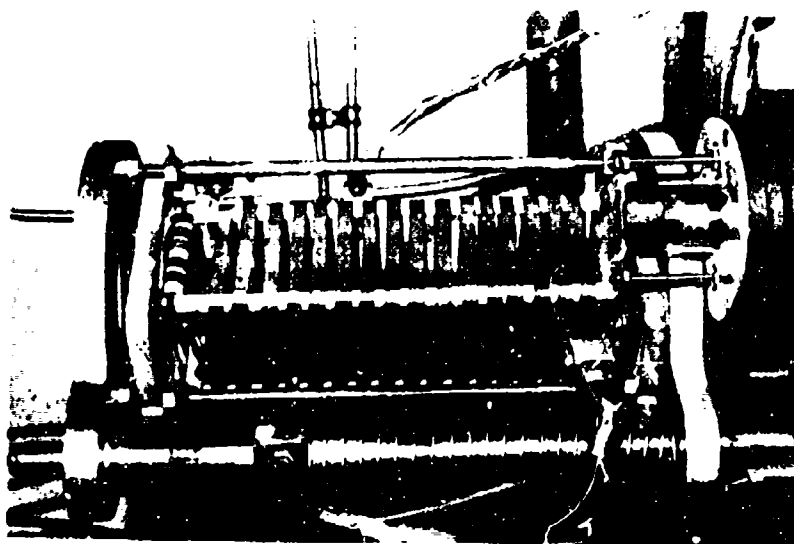


Figure III.6. A Photograph of the Quick Heating Furnace.

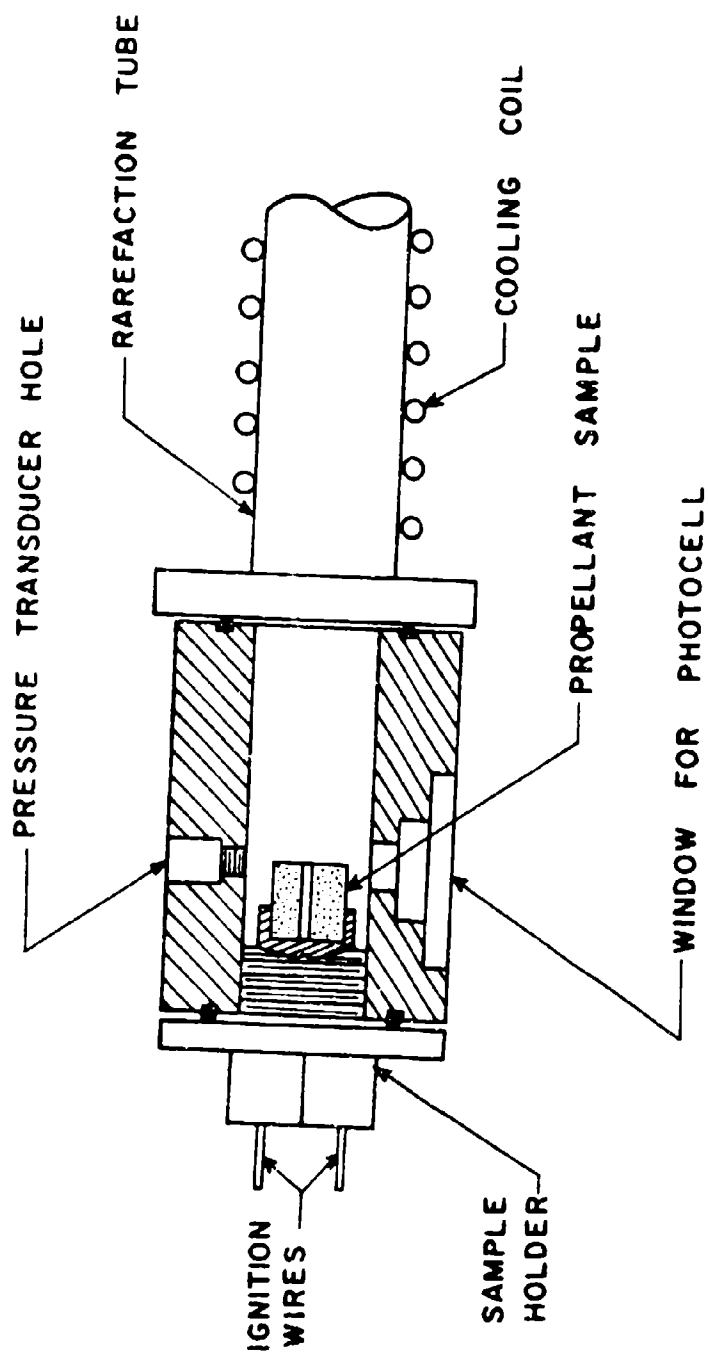


Figure III.8. A Sectioned View of the Small-L* Blow-down Chamber Showing Sample Mounting.

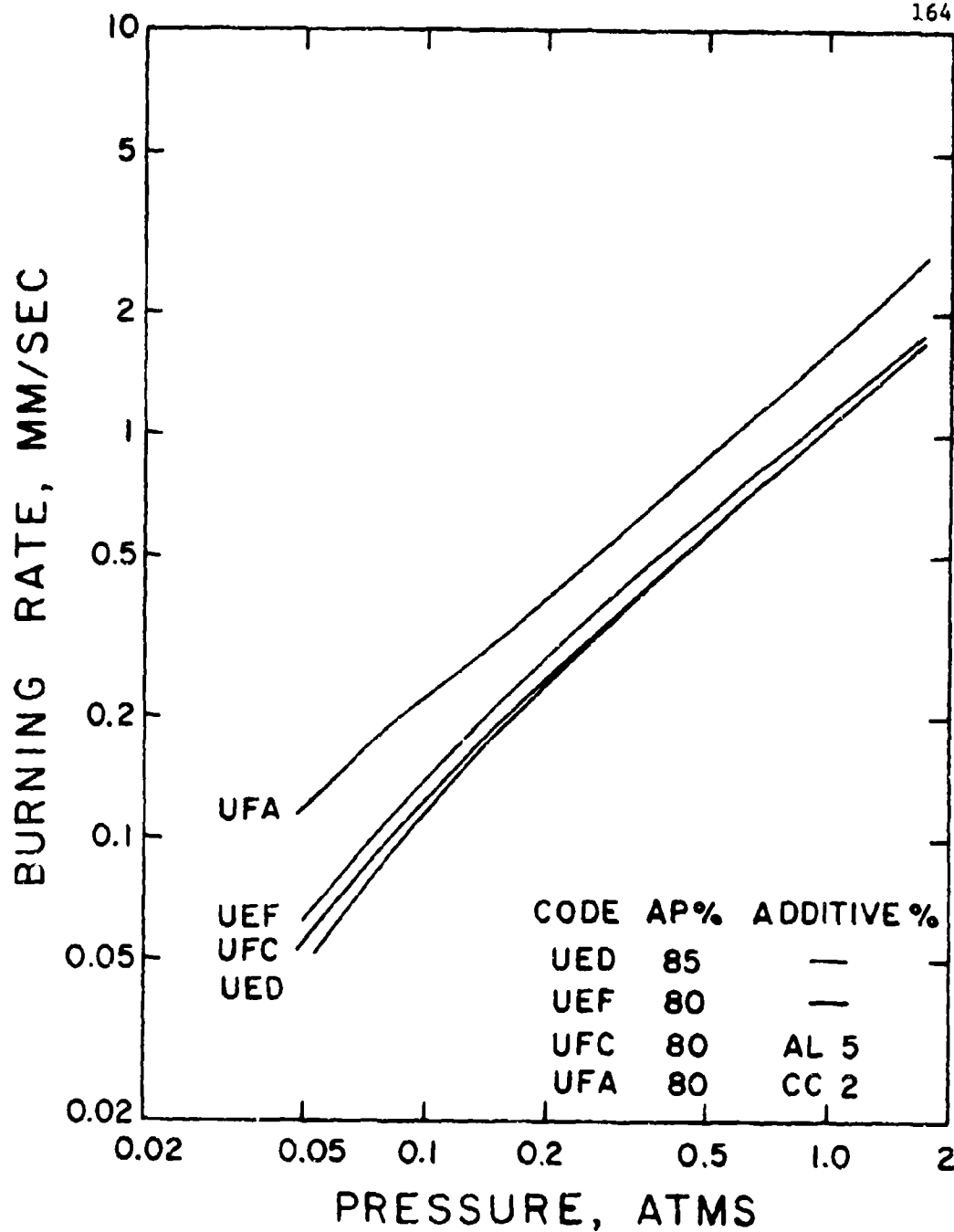


Figure IV.1. Burning Rate Behavior of Bimodal (60/40)-AP, PU-fueled Propellants at Low Pressures. The Lines were Drawn Through the Averaged Values of at Least Two Runs. All Propellants Contained 1% Carbon Black. CC Denotes Copper Chromite Catalyst.

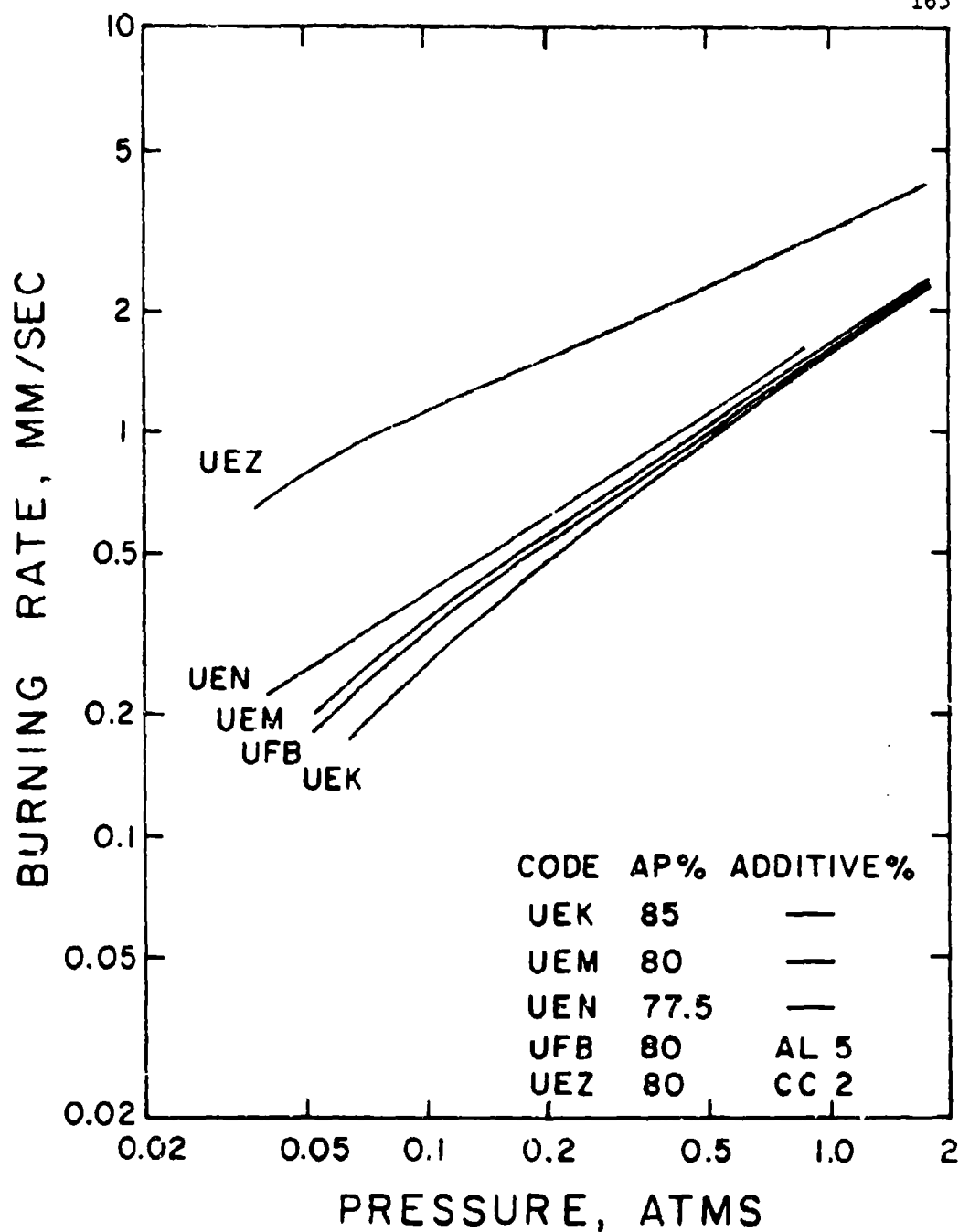


Figure IV.2. Burning Rate Behavior of Bimodal (60/40)-AP, PBAA-fueled Propellants at Low Pressures. Supplementary Captions are the Same as for Figure IV.1.

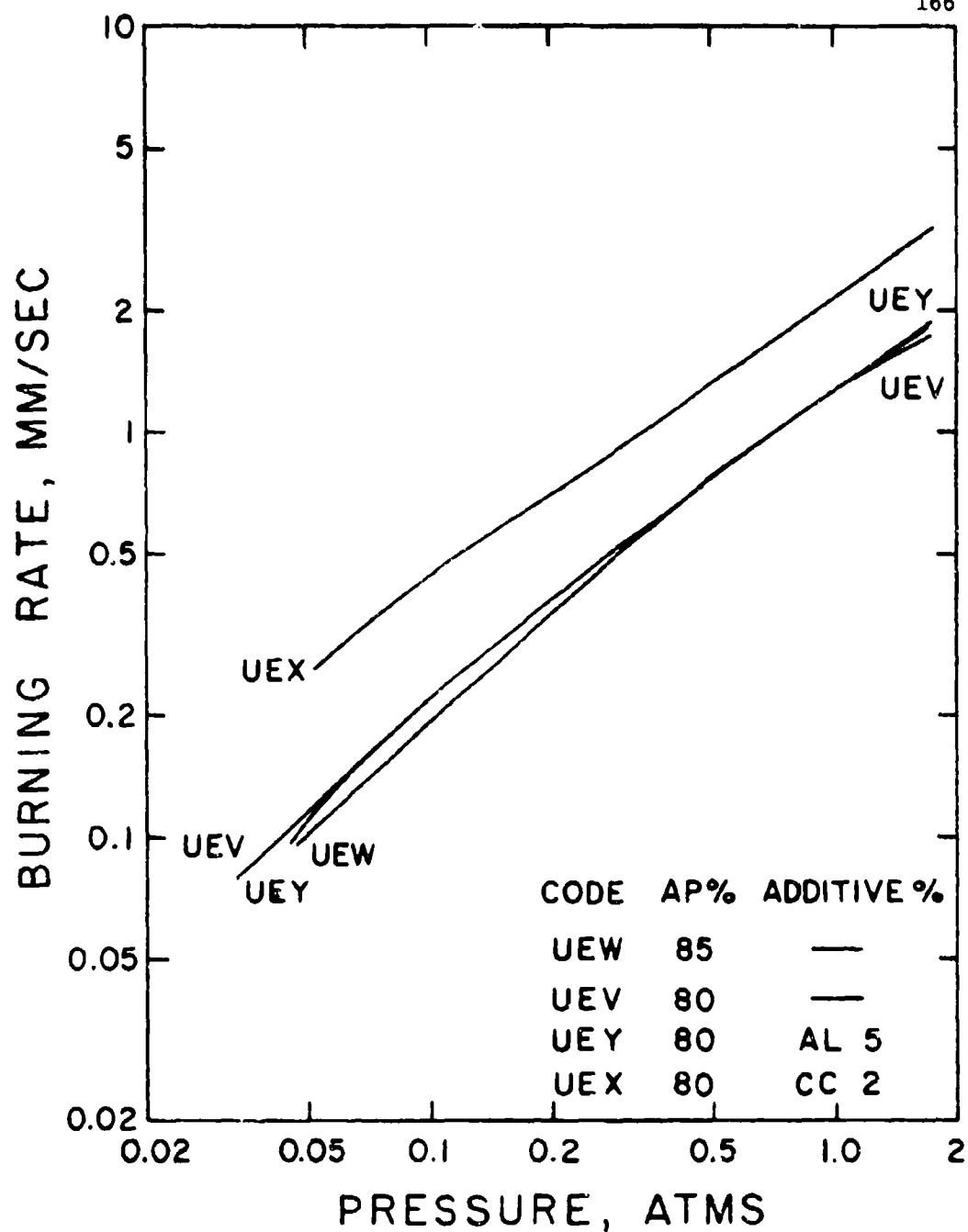


Figure IV.3. Burning Rate Behavior of Binodal (60/40)-AP, HTPB-fueled Propellants at Low Pressures. Supplementary Captions are the Same as for Figure IV.2.

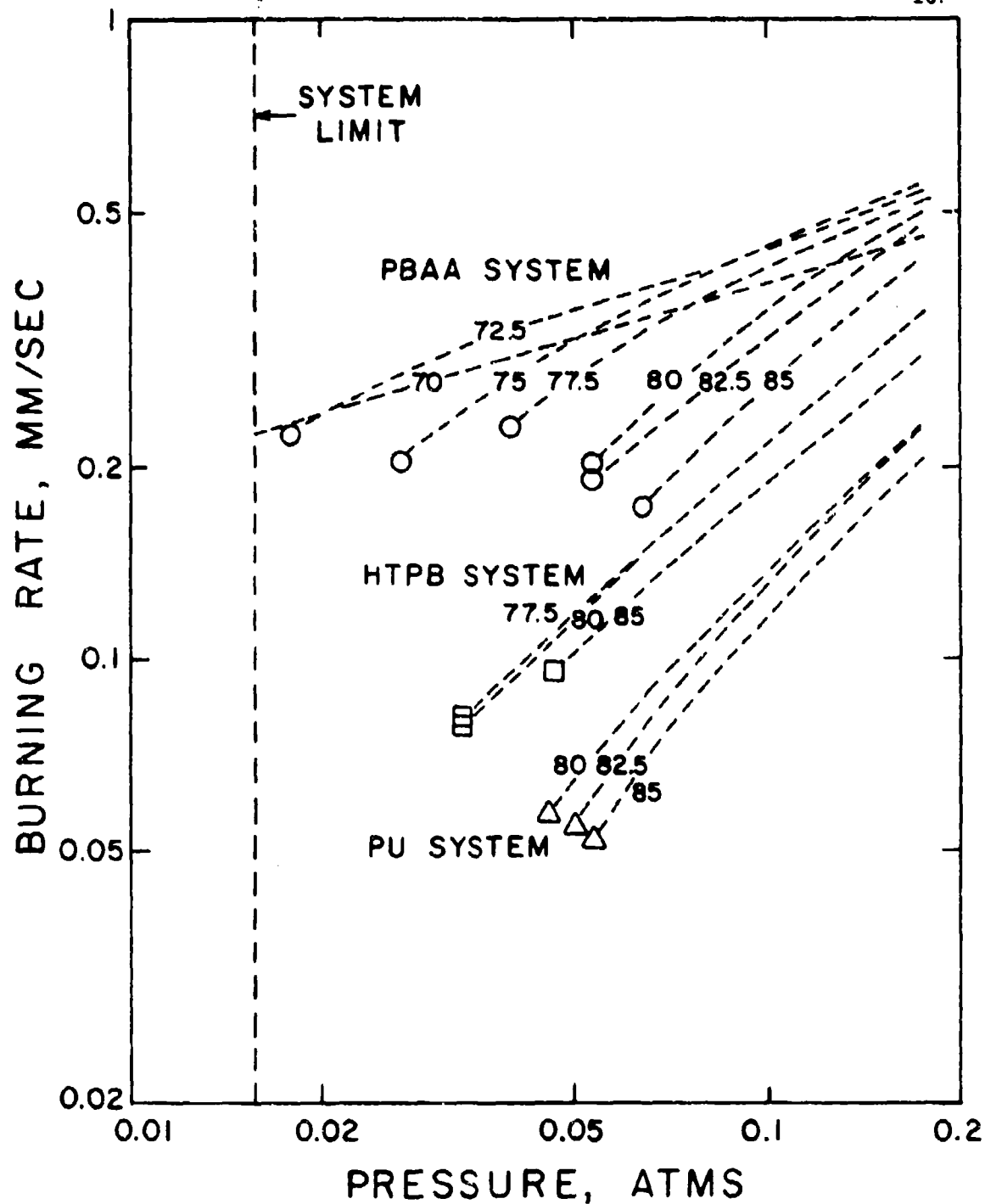


Figure IV.4. Burning Rate Behavior of Many Bimodal-AP Propellants Below 0.2 atms. The Numbers Denote AP Weight Percent and the Terminal Symbols Indicate the Deflagration Limits.

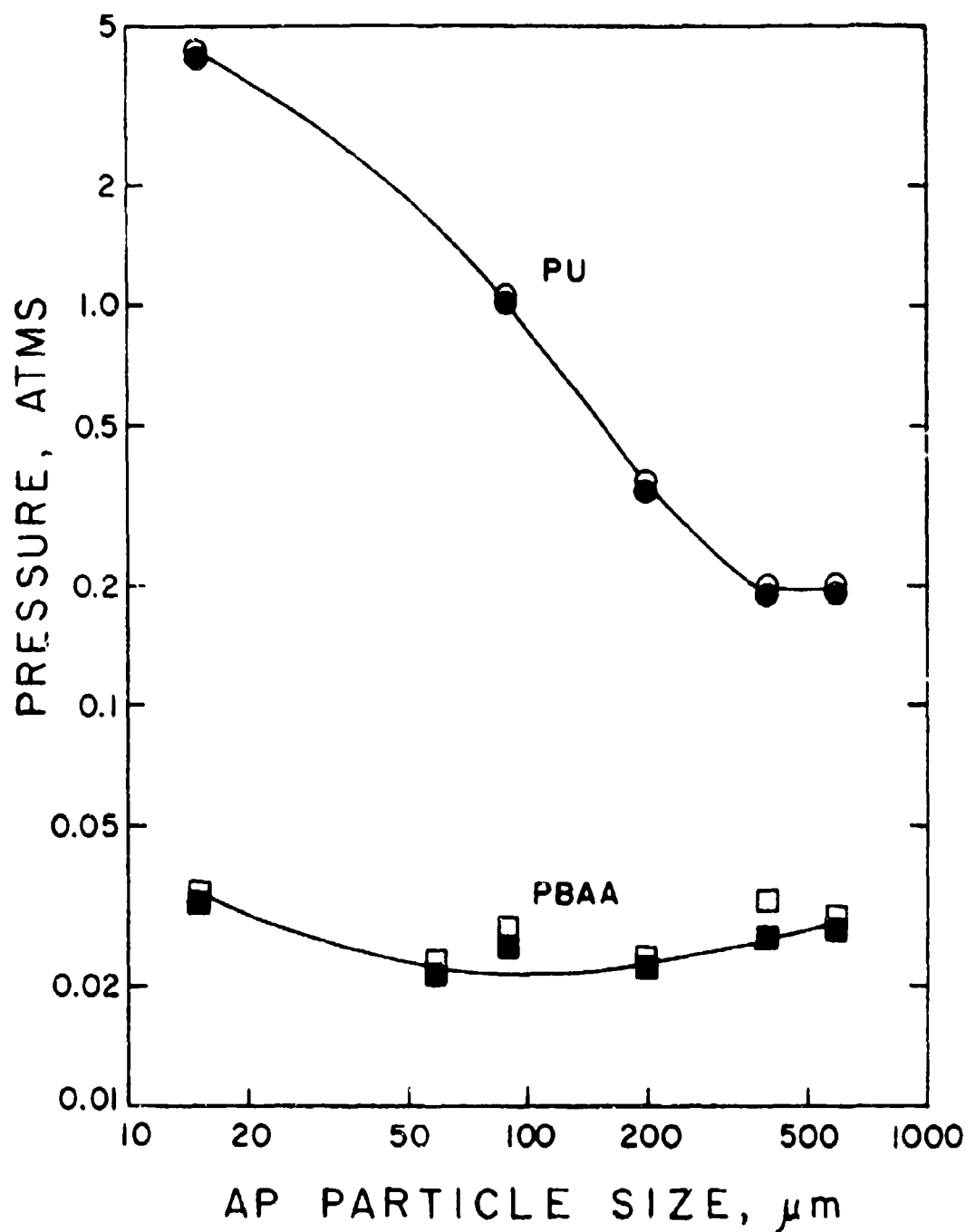


Figure IV.5. Effect of the AP Particle Size on the Low Pressure Deflagration Limit. Each Propellant Contained 75% AP and 1% Carbon Black. The Open Symbols Indicate Conditions in Which Strands Completely Burned, While the Filled Symbols Indicate Conditions in Which Strands Were Not Consumed.

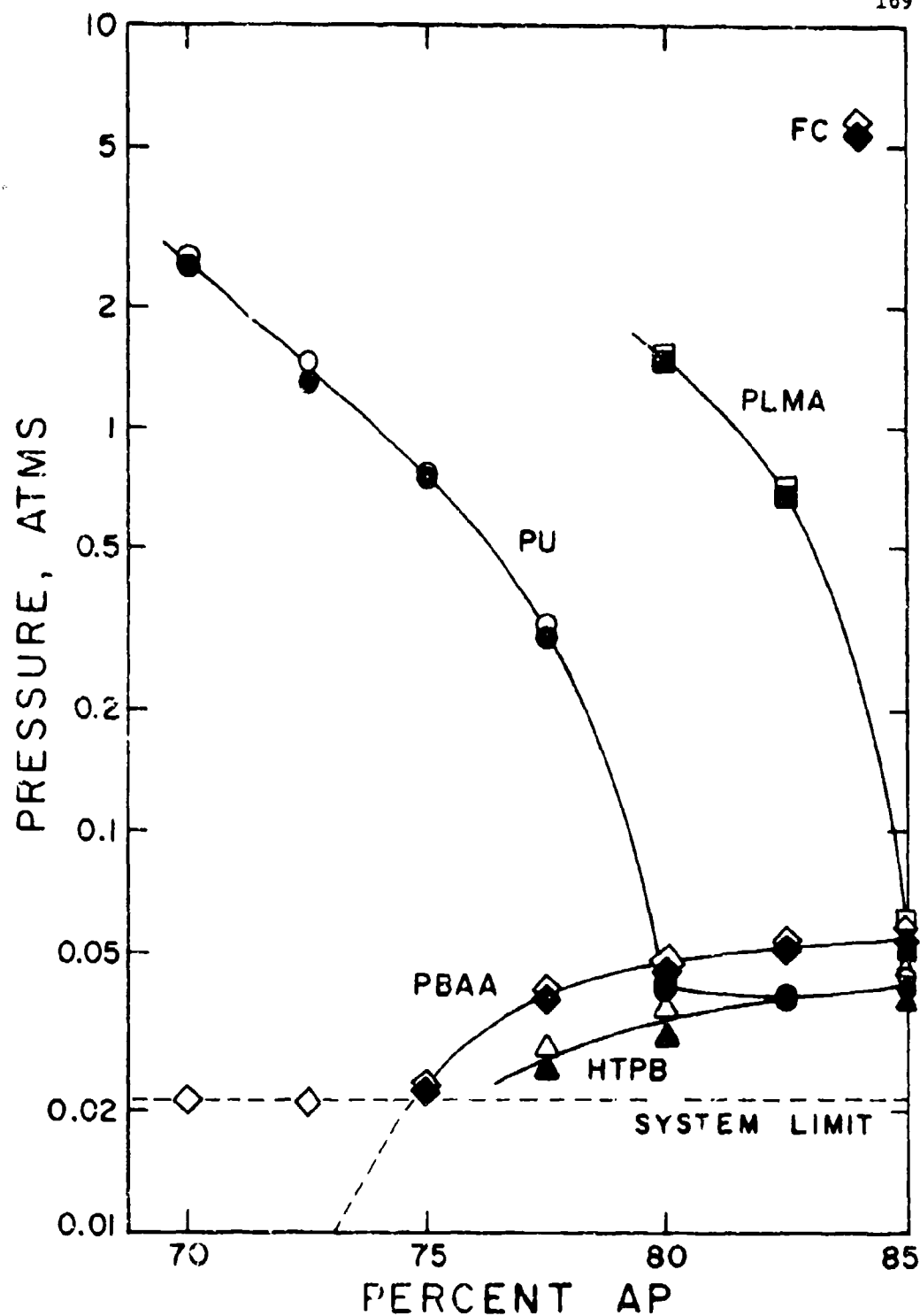


Figure IV. 6. Effect of AP Level on the Low Pressure Deflagration Limit for Series of Bimodal AP Propellants Fueled with Various Polymers. All Propellants Except the FC Propellant Contained 1% Carbon Black. The Interpretation of the Symbols is as for Figure IV.5.

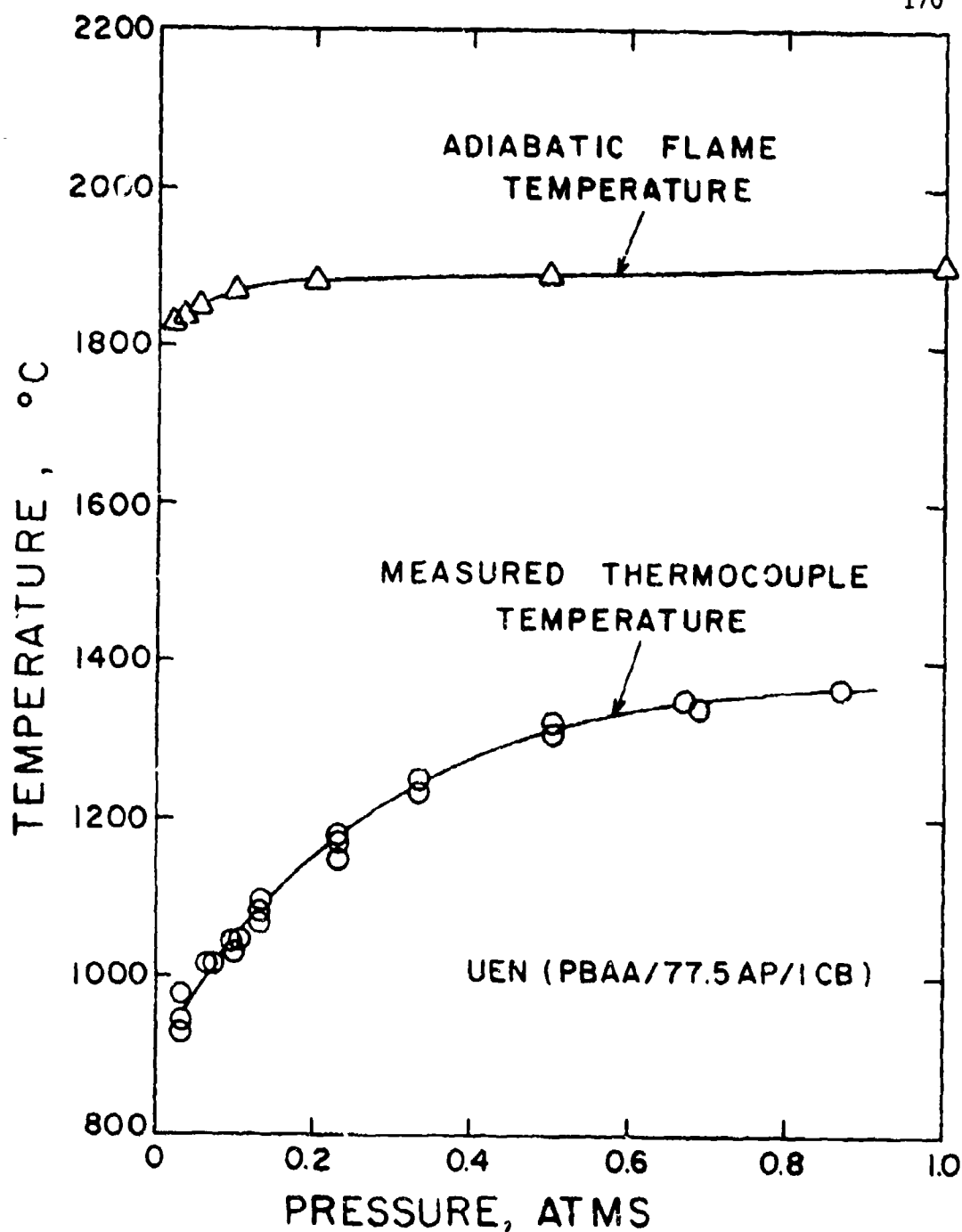


Figure IV.7. Flame Temperatures of a PBAA Propellant at Subatmospheric Pressures. Silica-coated Thermocouples of 0.8 mm Diameter were Used. Radiation Corrections were Not Made for the Measured Thermocouple Temperatures.

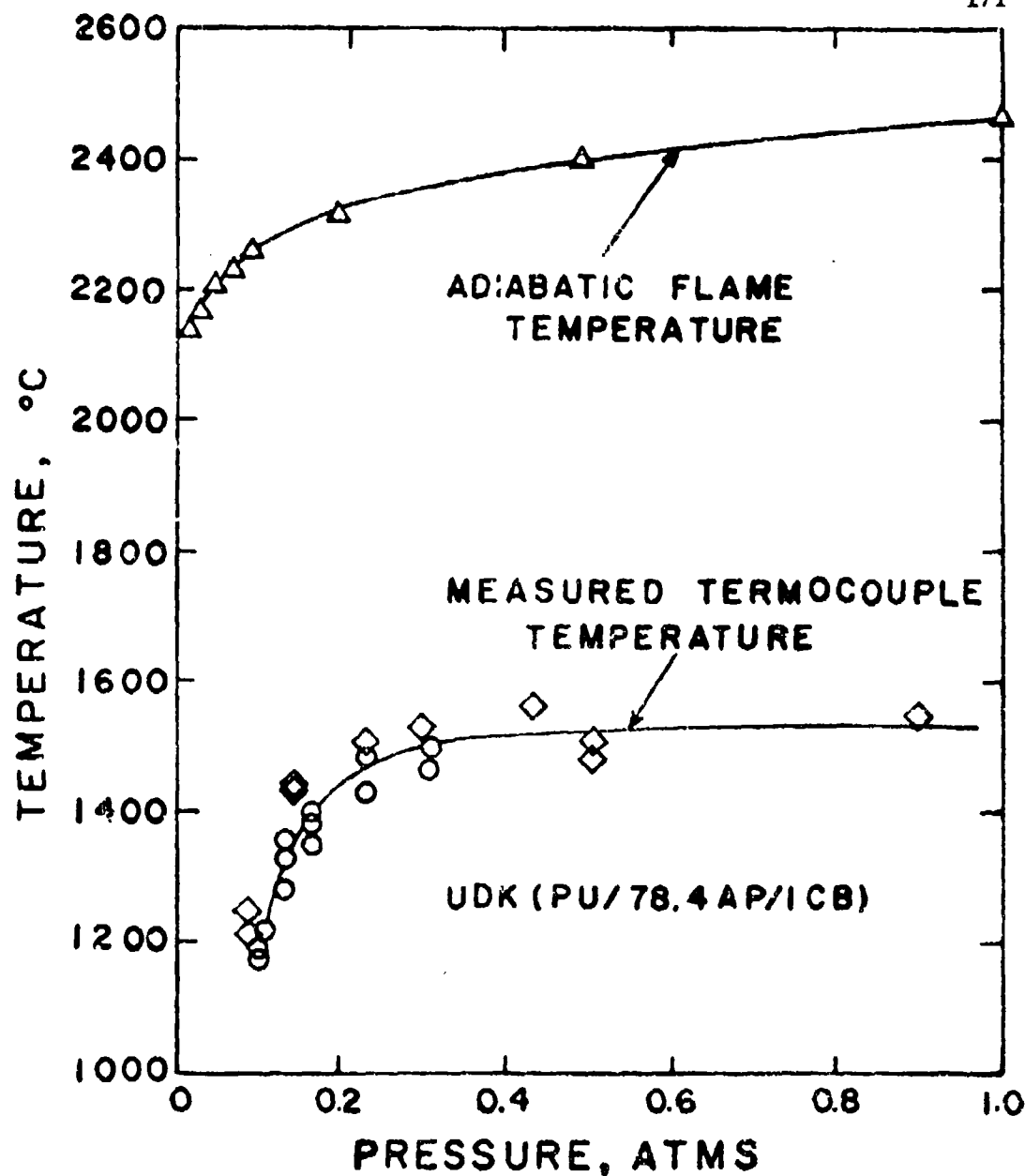


Figure IV.8. Flame Temperatures of a PU Propellant at Subatmospheric Pressures. The Circles Indicate the Tests Conducted with Uncoated Thermocouples (0.58 mm Diameter), While the Diamonds Indicate Those with Alumina-Coated Thermocouples (0.8 mm Diameter). Radiation Corrections Were Not Made for the Measured Thermocouple Temperatures.

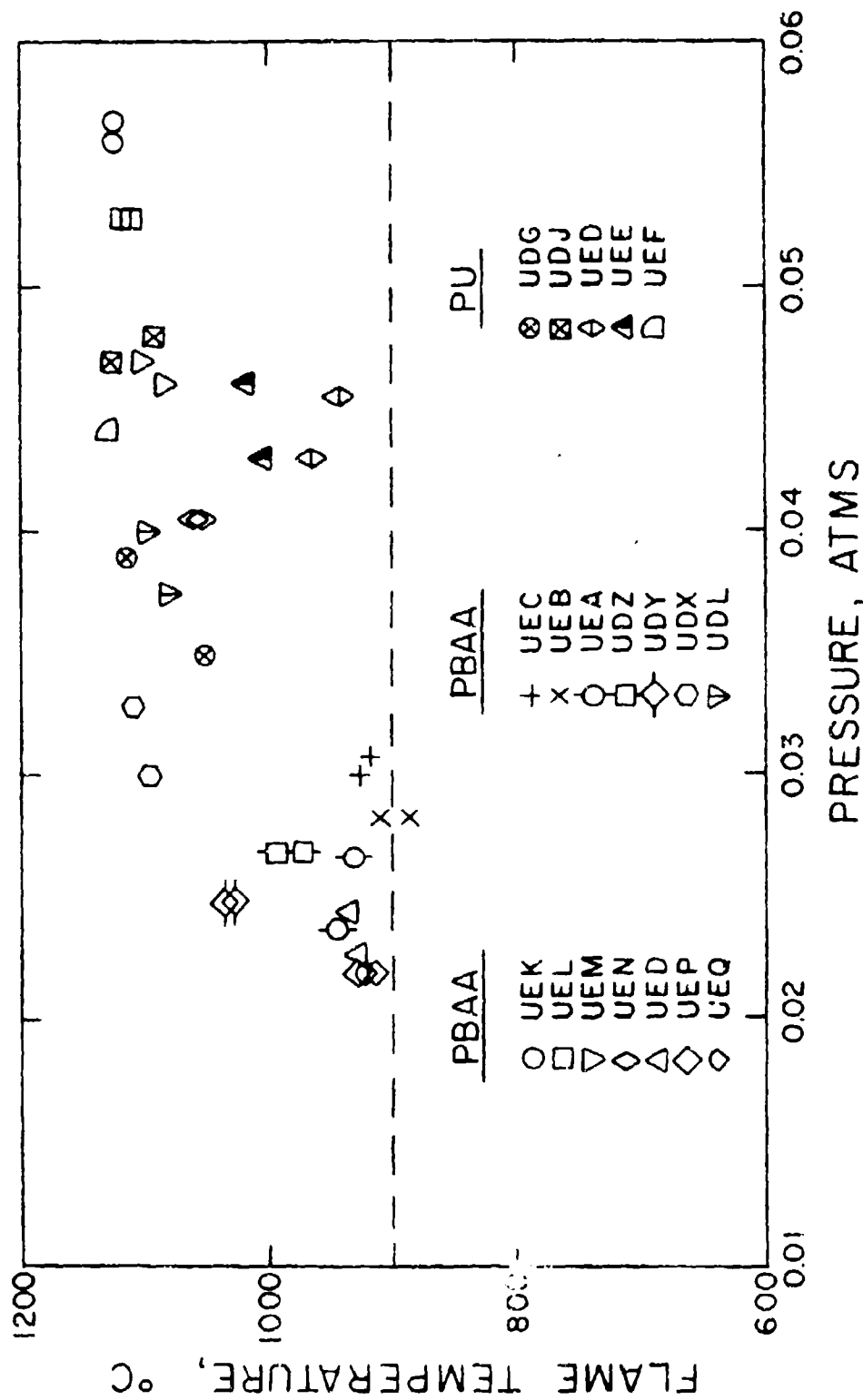


Figure IV.9. Flame Temperatures of Many Propellants near Their Low Pressure Deflagration Limits. Silica-coated Thermocouples of 0.58 mm Diameter Were Used. Radiation Corrections Were Not Made for the Measured Thermocouple Temperatures.

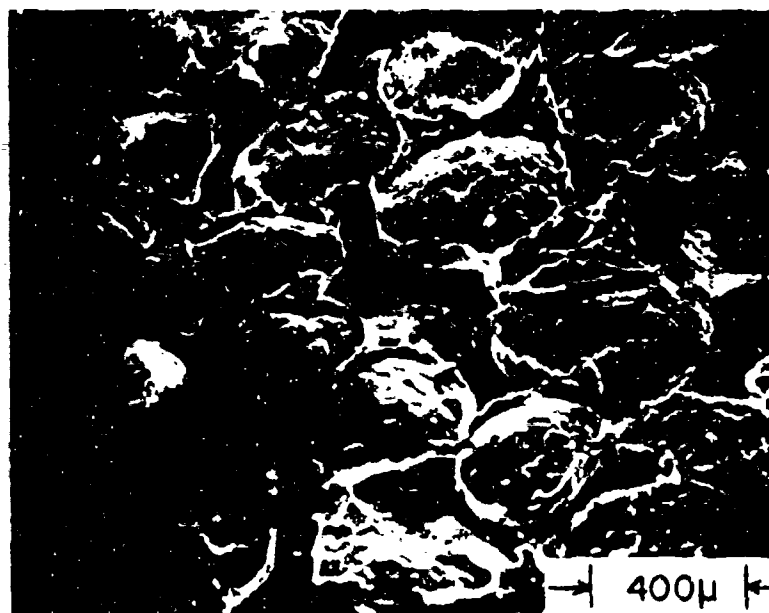


Figure IV.10. Scanning Electron Microscope Micrograph of the Extinguished Surface of a Unimodal-AP (400 μ) PU Propellant (UDV) Burned near Its P_{dl} (55X).

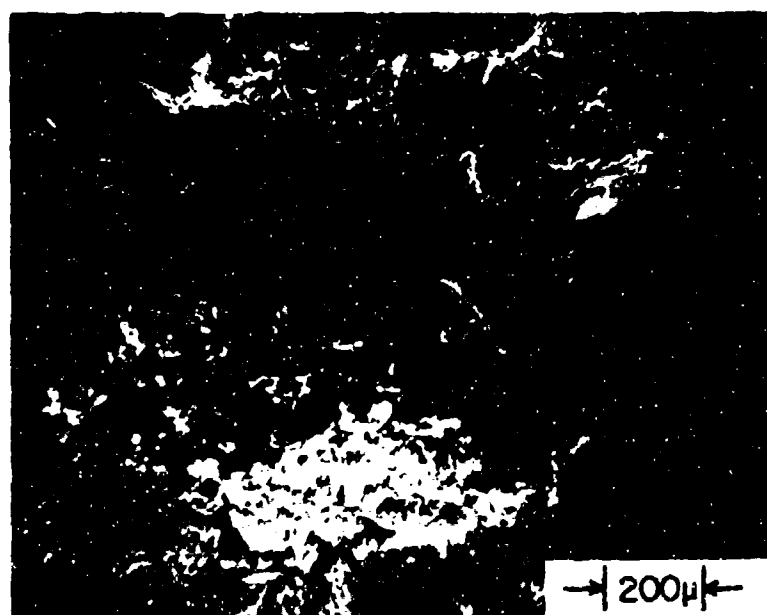


Figure IV.11. Scanning Electron Microscope Micrograph of the Extinguished Surface of a Bimodal-AP (200 μ /15 μ) PU Propellant Burned near Its P_{dl} (70X).

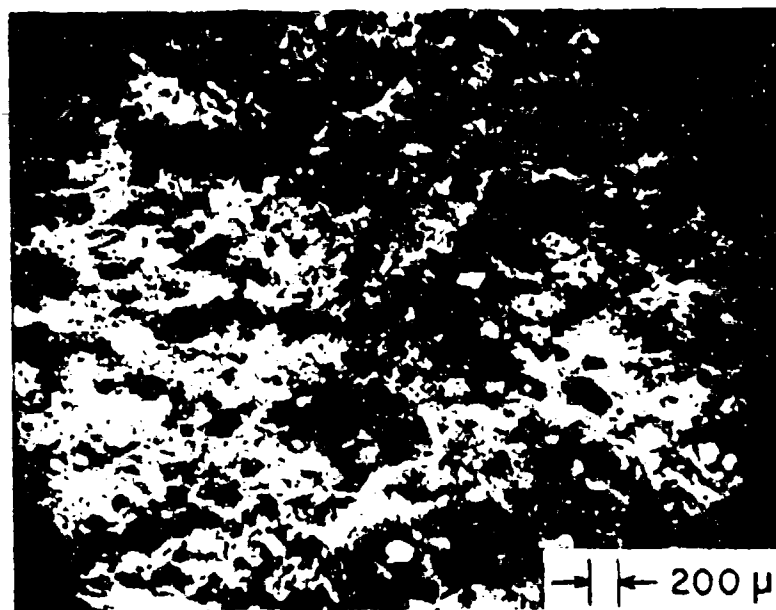


Figure IV.12. Scanning Electron Microscope Micrograph of the Extinguished Surface of a Bimodal-AP (200μ/15μ) PBAA Propellant (UDL) Burned near Its P_{dl} (20X).

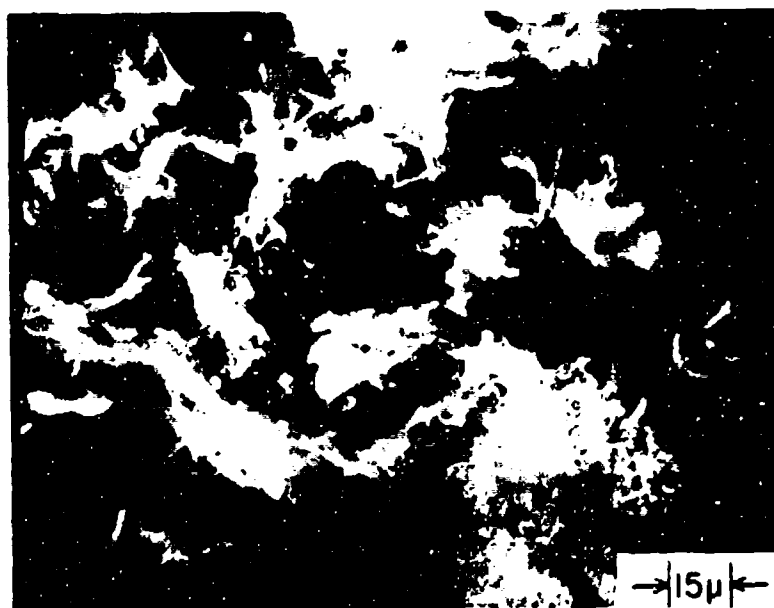


Figure IV.13. Scanning Electron Microscope Micrograph of the Extinguished Surface of a Unimodal-AP (15μ) PBAA Propellant (UDX) Burned near Its P_{dl} (600X).

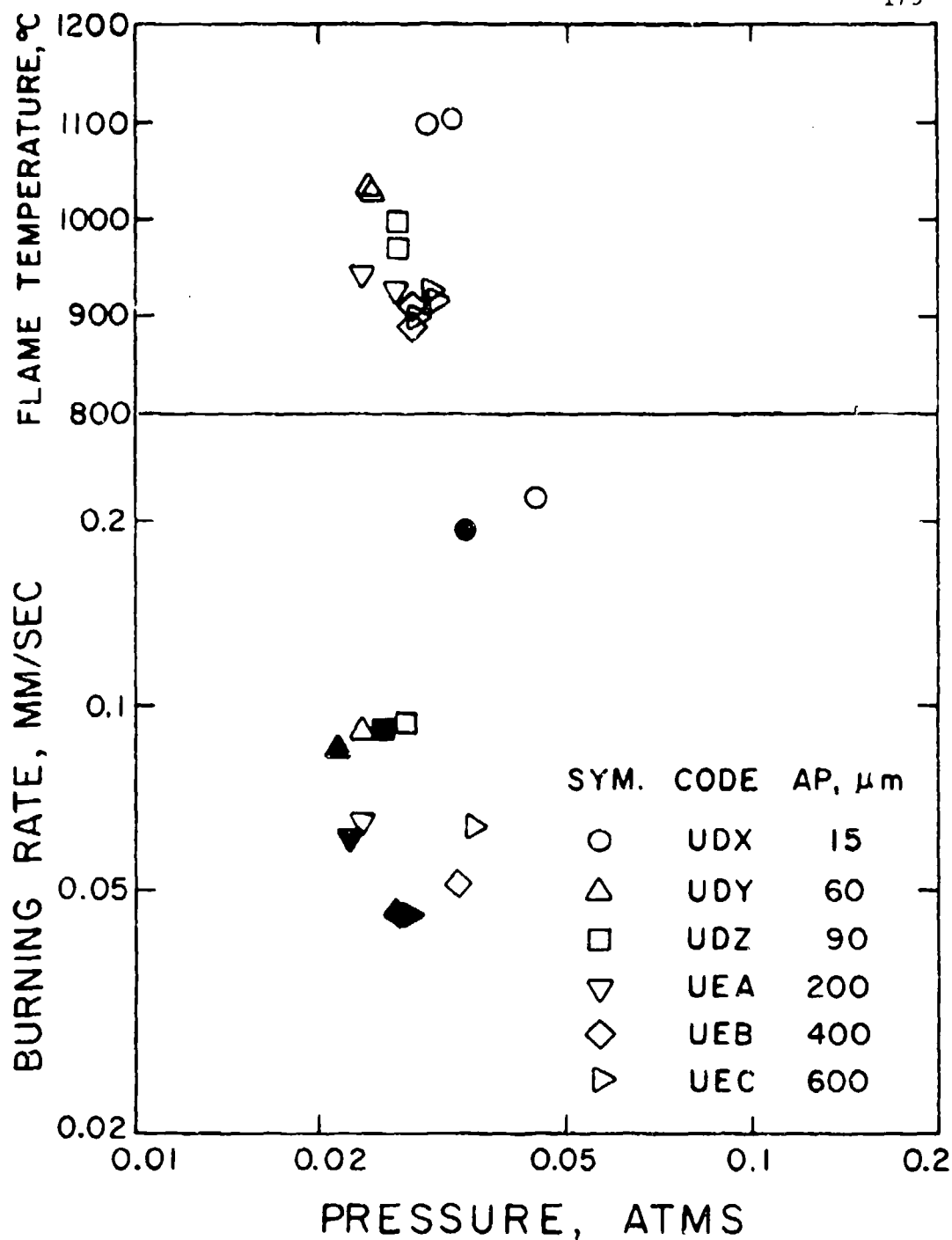


Figure IV.14. Burning Rates and Flame Temperatures of a Series of Unimodal PBAA Propellants near Their Low Pressure Deflagration Limits. All Propellants Contained 75% AP and 1% Carbon Black. The Filled Symbols Indicate Conditions in Which Strands Were Not Consumed.

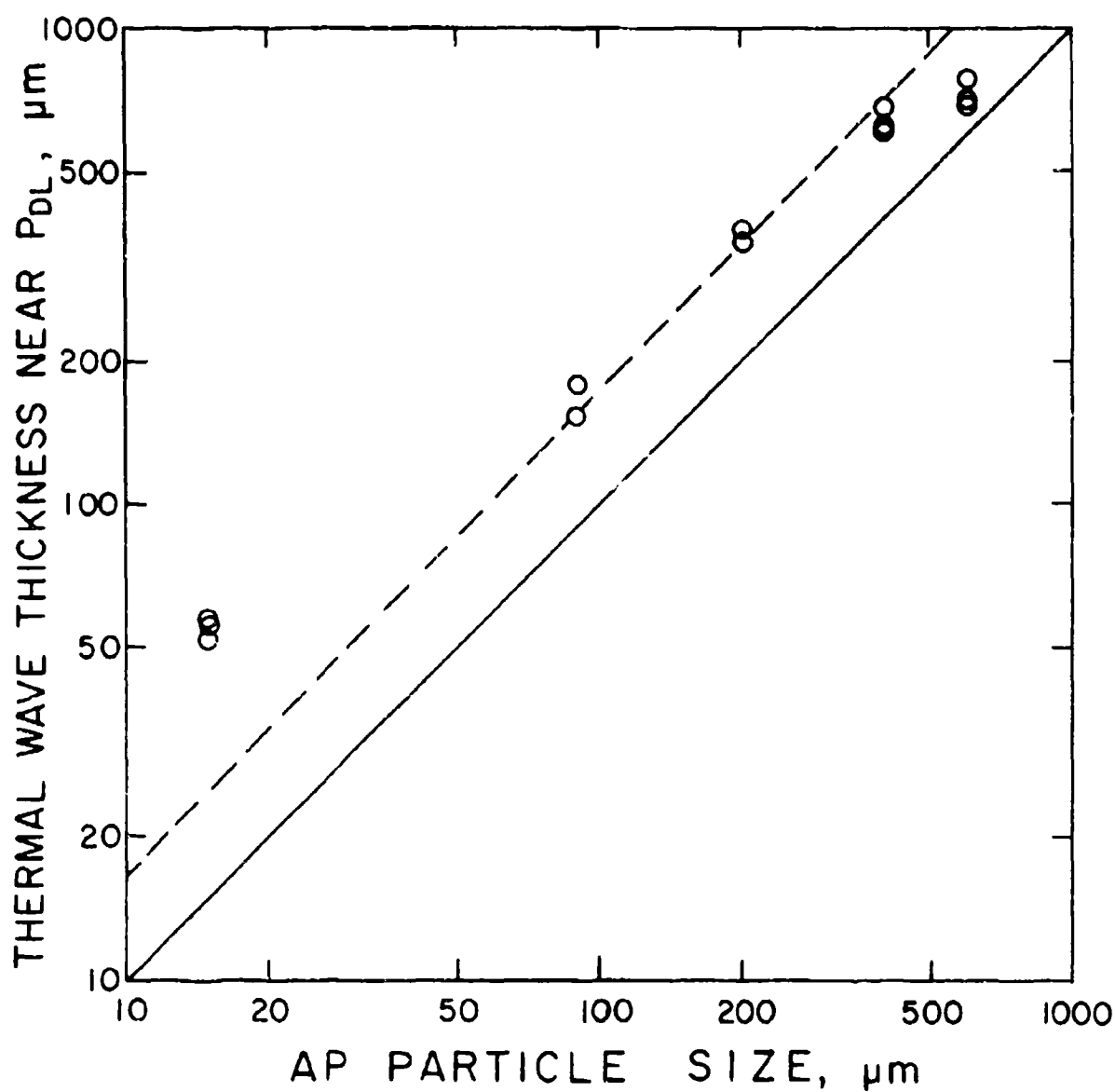


Figure IV.15. Comparison of Thermal Wave Thickness near the P_{dl} and the AP Particle Size for a Series of Unimodal PU Propellants. All Propellants Contained 75% AP and 1% Carbon Black.

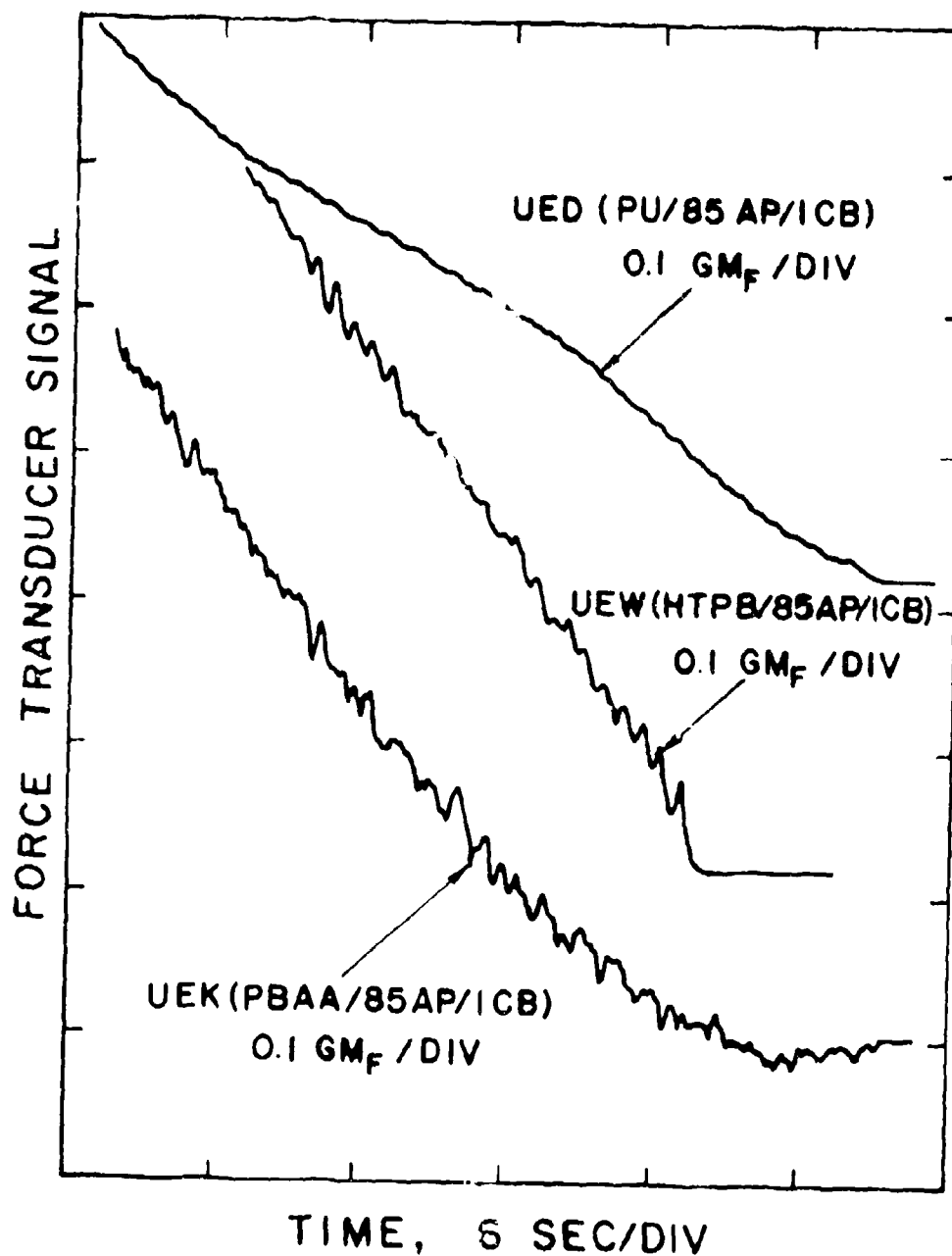


Figure V.1. Force Transducer Signals for Bimodal PU, HTPB, and PBAA Propellants Burned and Extinguished near Their P_{dl} Showing Oscillatory Burning Behavior.

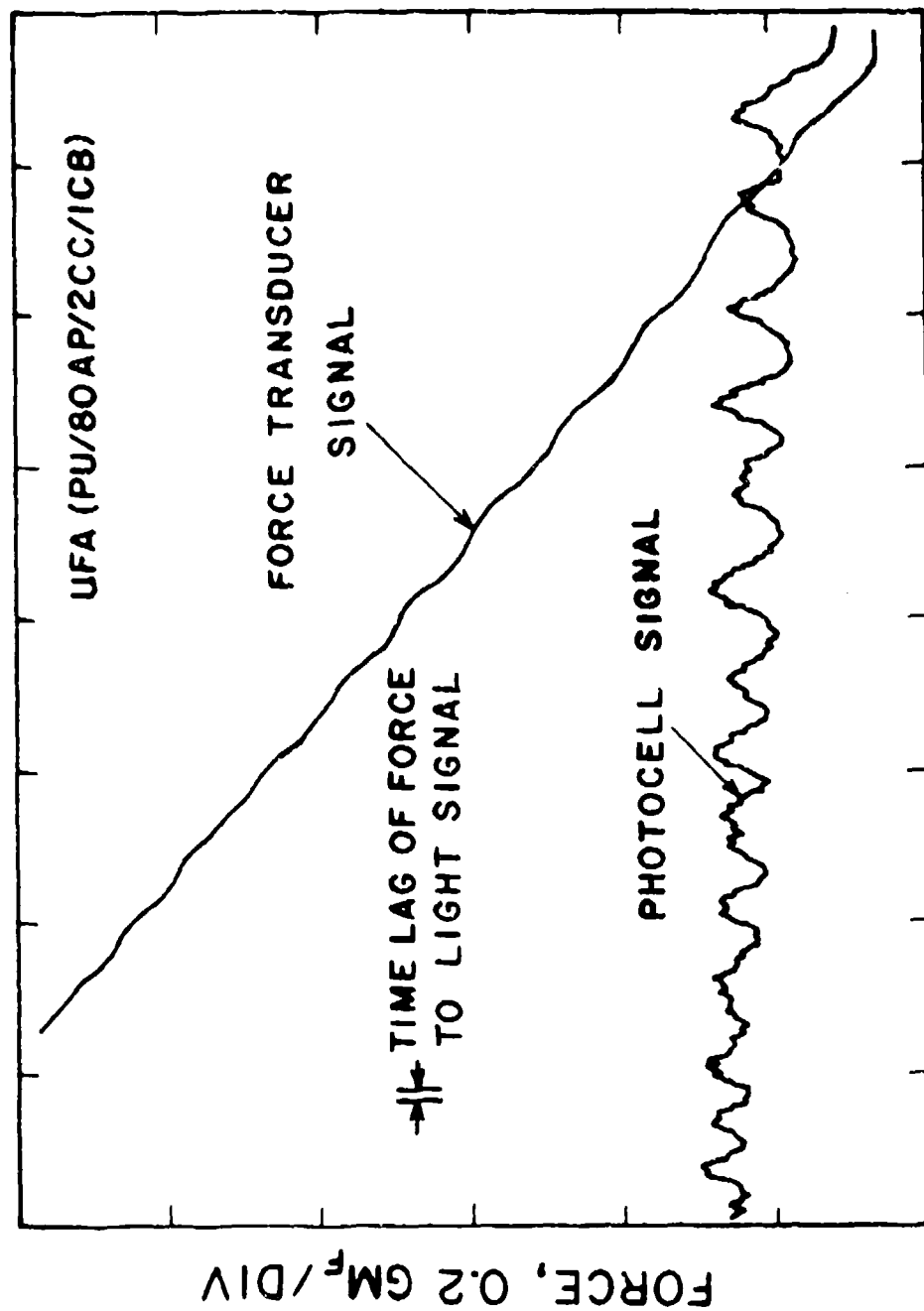


Figure V.2. Force and Light Signals Recorded Simultaneously During Low-Pressure (near P_{d1}) Oscillatory Burning of a Catalyzed Bimodal PU Propellant.

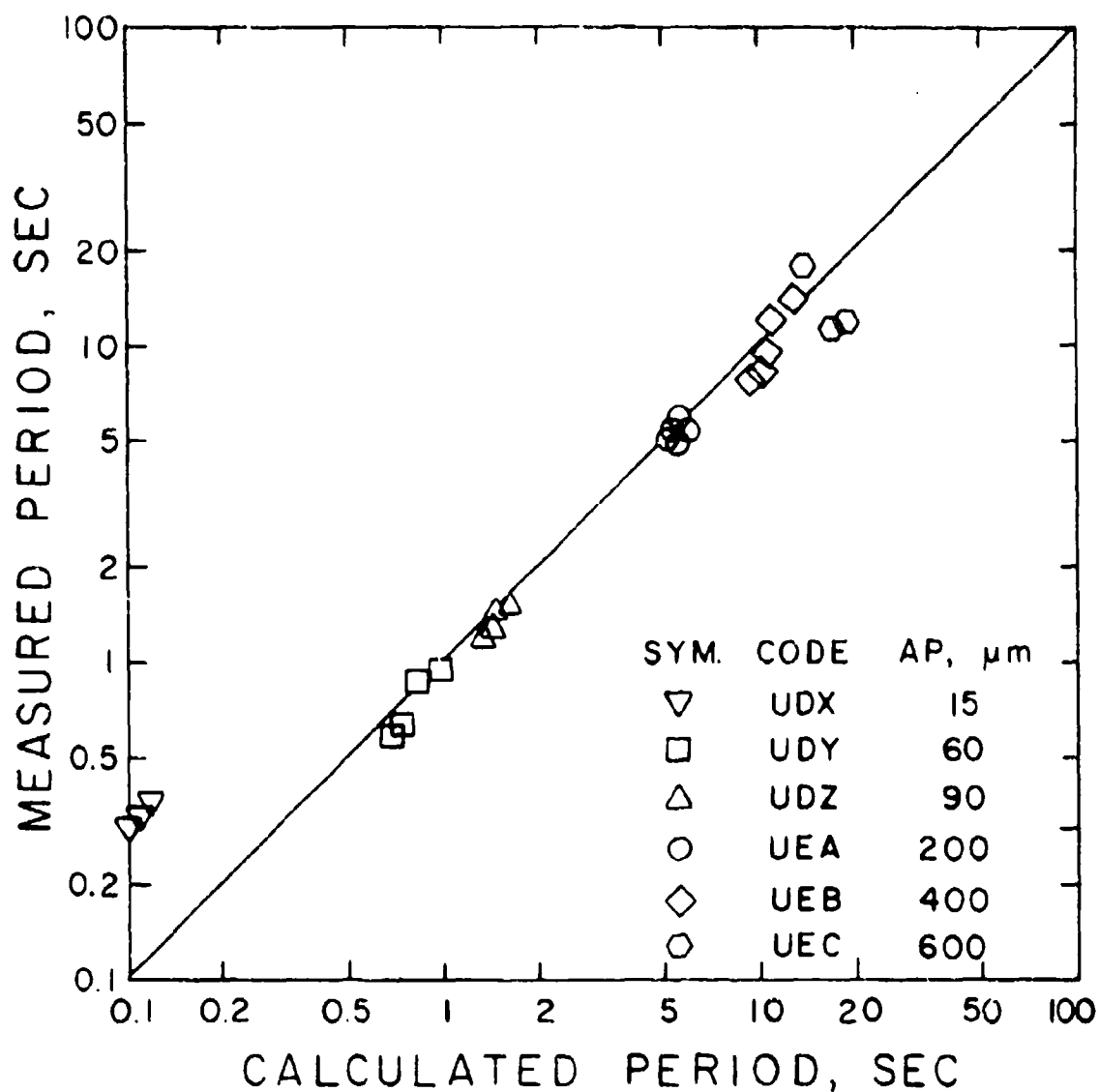


Figure V.3. Comparison Between the Measured Period of Oscillations and the Period Calculated by Boggs and Beckstead's Theory for a Series of Unimodal PBAA Propellants. All Propellants Contained 75% AP and 1% Carbon Black.

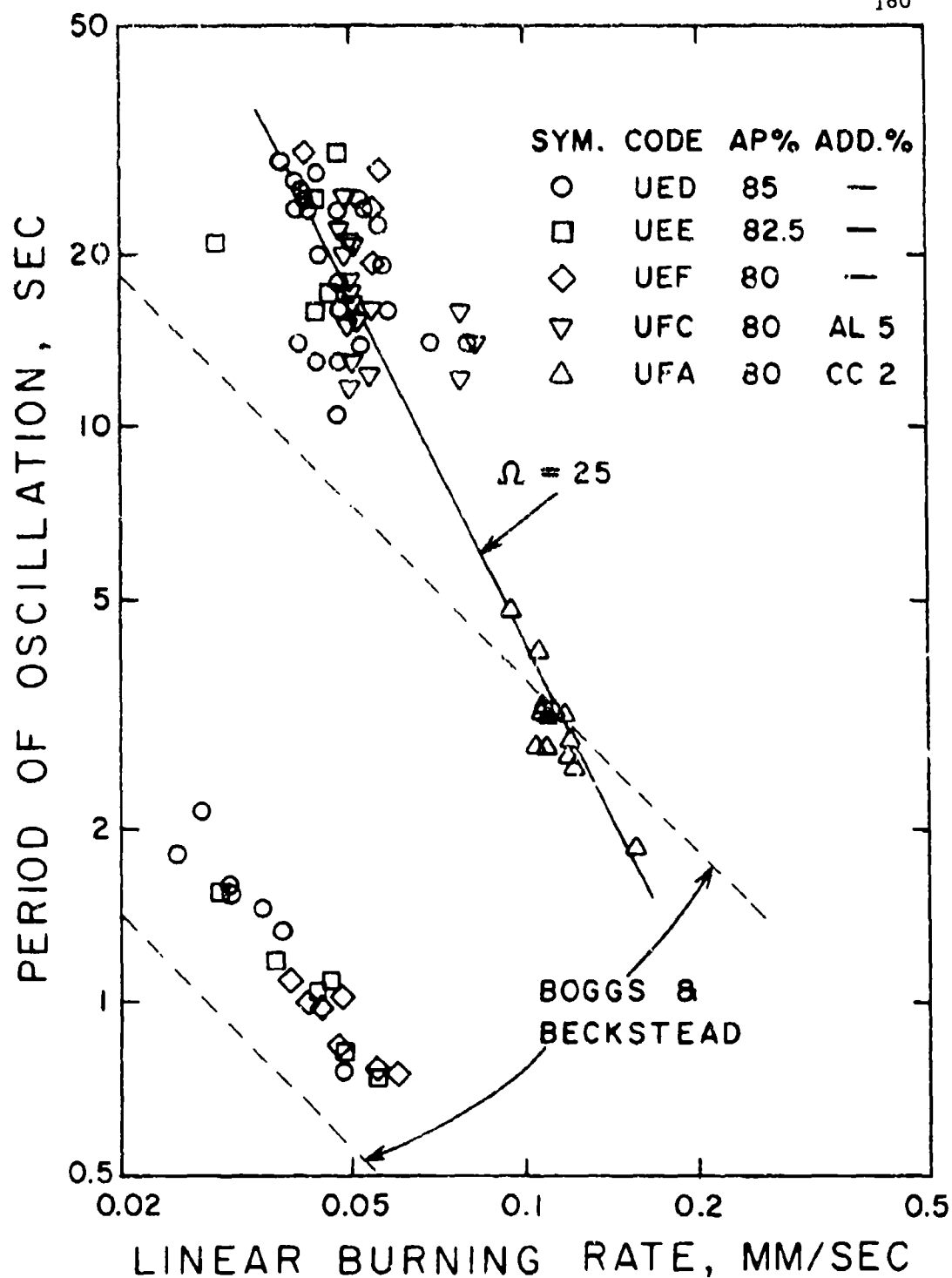


Figure V.4. Low-Pressure (near P_{d1}) Oscillatory Burning Data for
 PU Propellants Containing Bimodal AP (60/40, 200 μ /15 μ).
 The Solid Line Represents the Relationship, $\Omega = \alpha_L / r^2$,
 While Dotted Lines Represent $F_1 = K_1 r / D_1$.

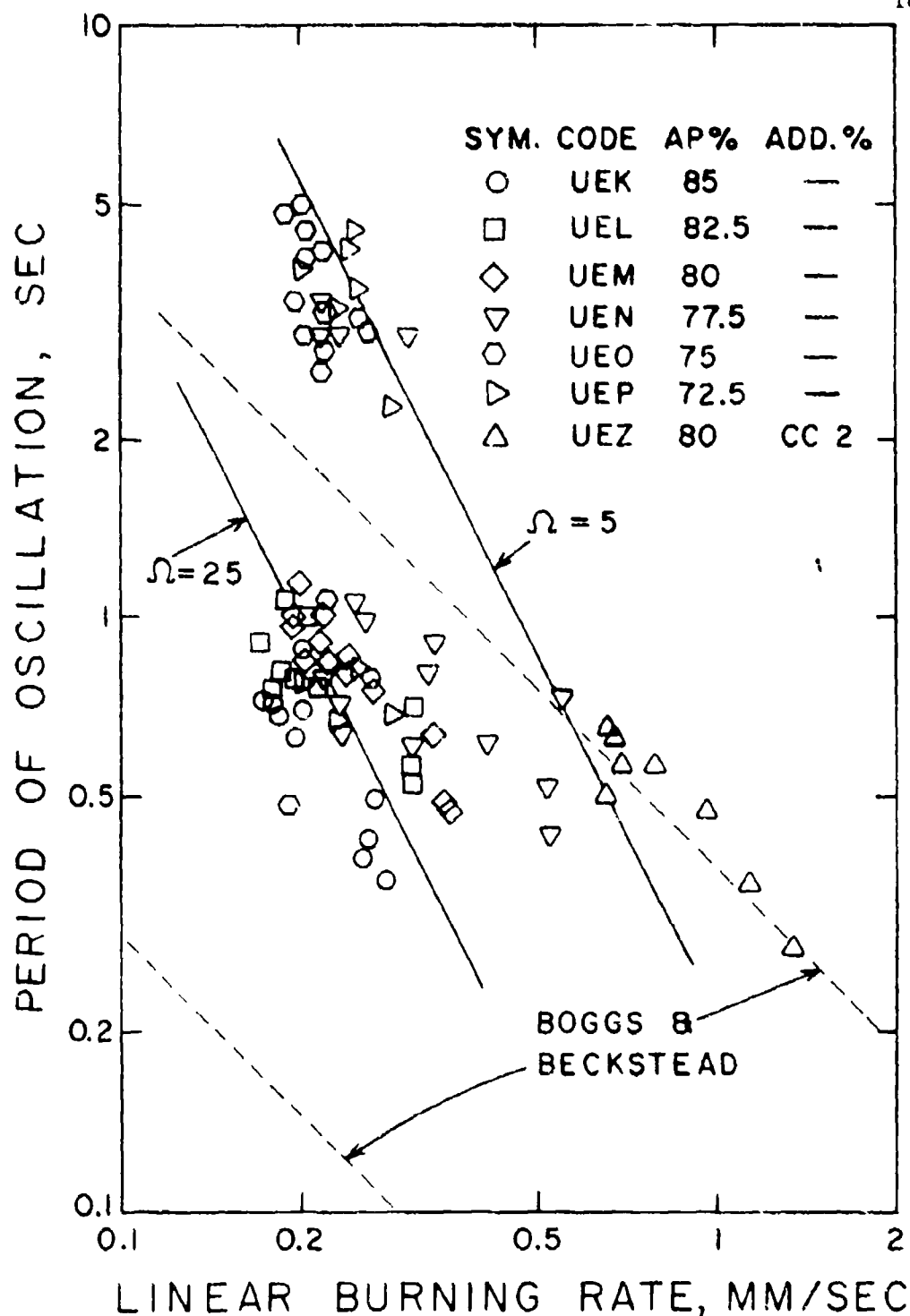


Figure V.5. Low-Pressure (near P_{dl}) Oscillatory Burning Data for PBAA Propellants Containing Bimodal AP (60/40, 200/15 μ). The Solid Lines Represent the Relationship, $\omega = \omega_0/r^2$, while Dotted Lines Represent $F_1 = K_1 r/D_1$.

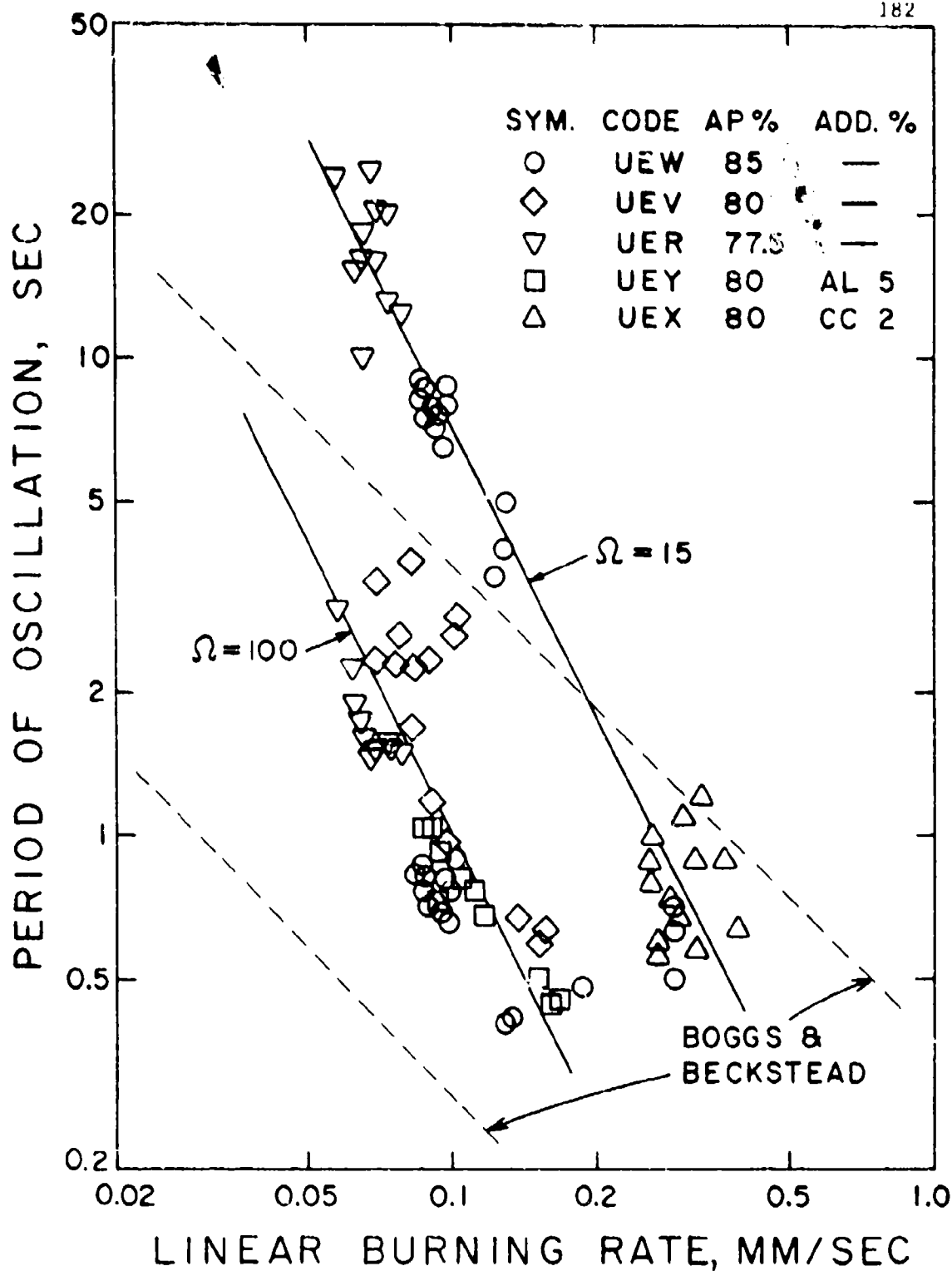


Figure V.6. Low-Pressure (near P_{d1}) Oscillatory Burning Data for HTPB Propellants Containing Bimodal AP (60/40, 200 μ /15 μ). The Solid Lines Represent the Relationship, $\omega = \alpha\omega/r^2$, While Dotted Lines Represent $F_1 = K_1 r/D_1$.

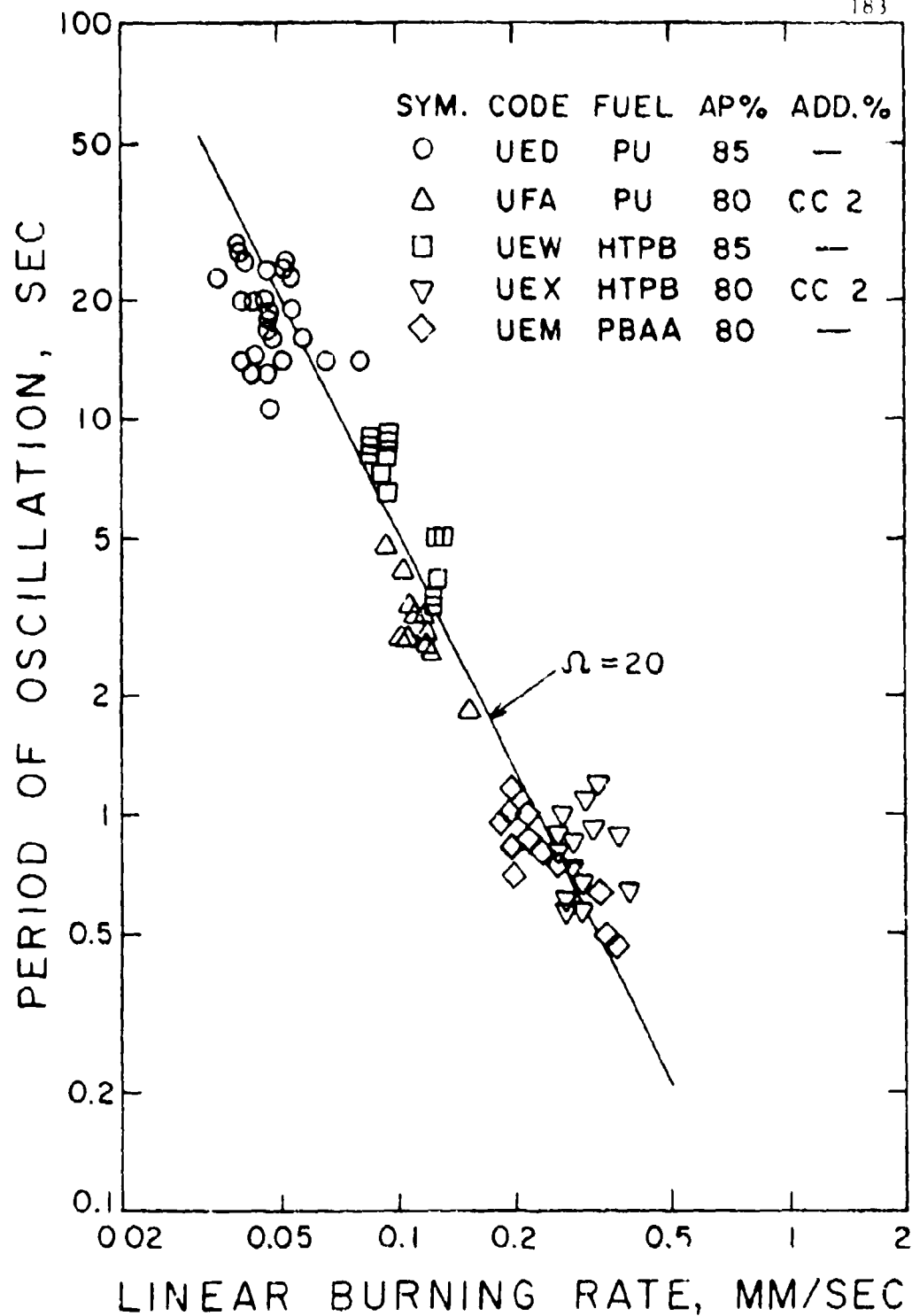


Figure V.7. Summary of Long-Period Data Being Representative of Each Binder System. The Solid Line Represents the Relationship $\Omega = \omega/r^2$.

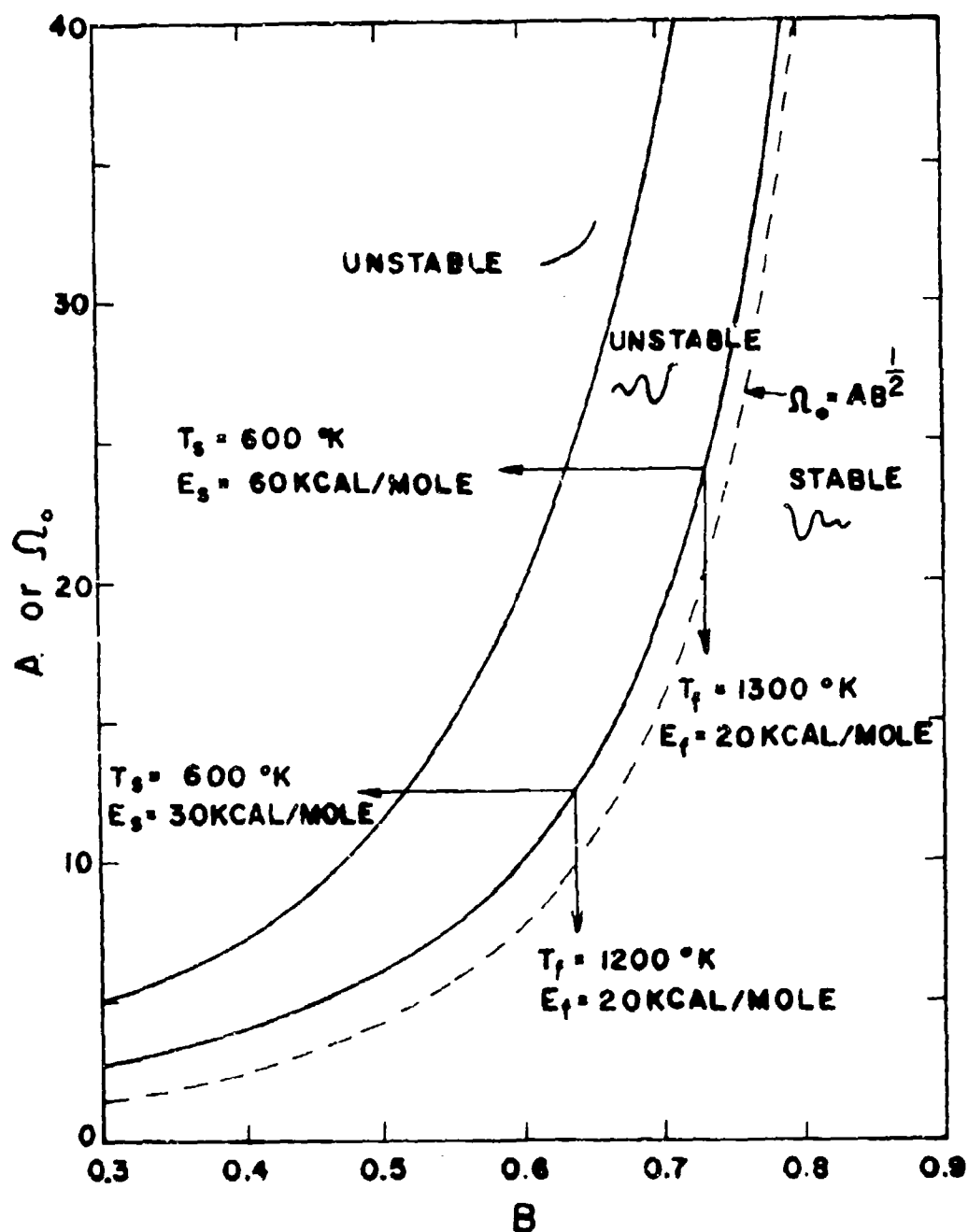


Figure V.8. Parametric Study on the Denison and Baum-Type Stability Diagram to Fit the Observed Periods of Oscillations.

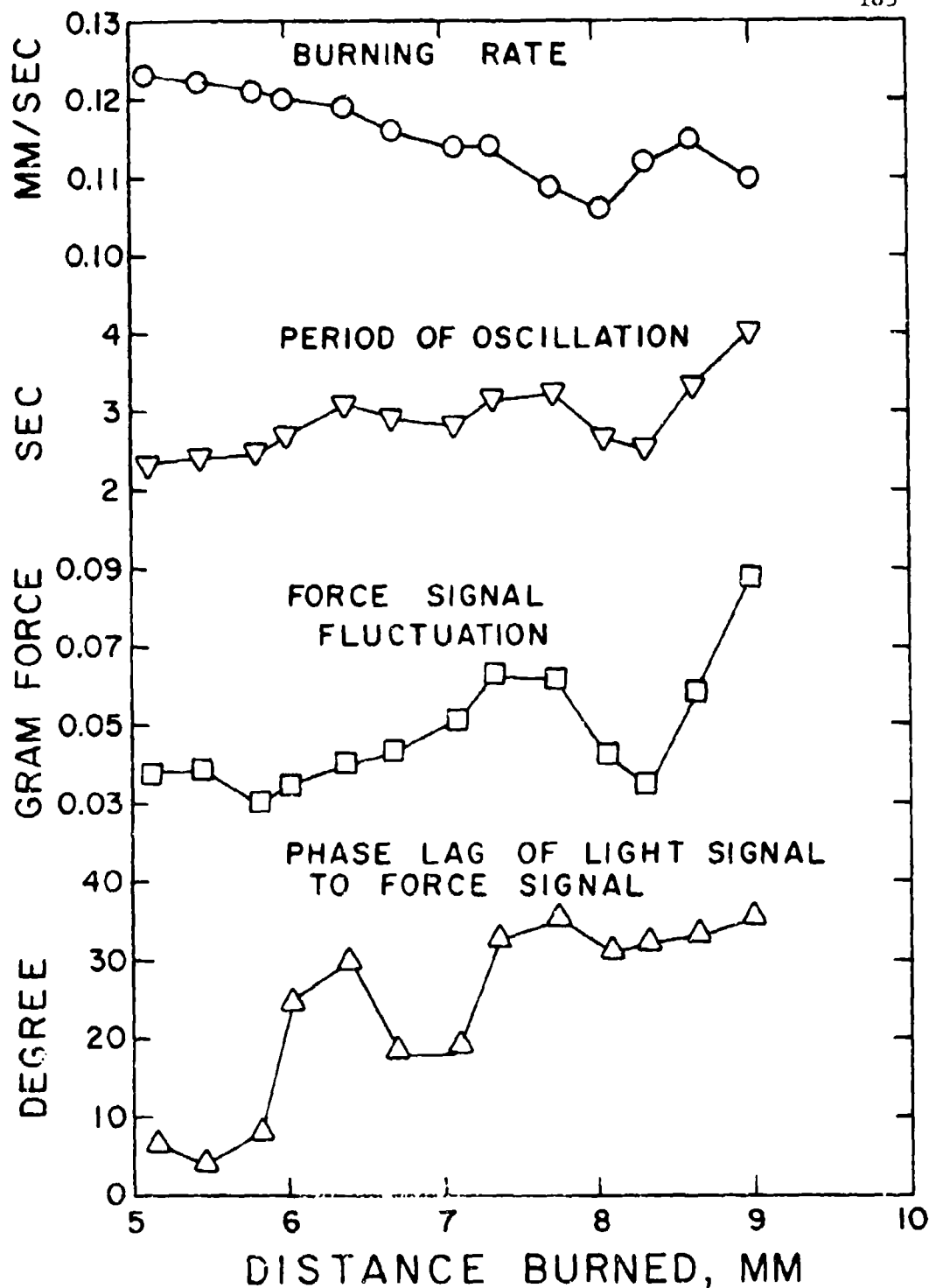


Figure V.9. This Figure Shows How the Averaged Burning Rate, Period and Amplitude of Oscillation, and the Phase Lag of Light Signal to Force Signal Changed During an Oscillatory Burning of a Catalyzed PU Propellant (UFA) Which Burned Just Below the P_{dl} and Eventually Self-Extinguished.

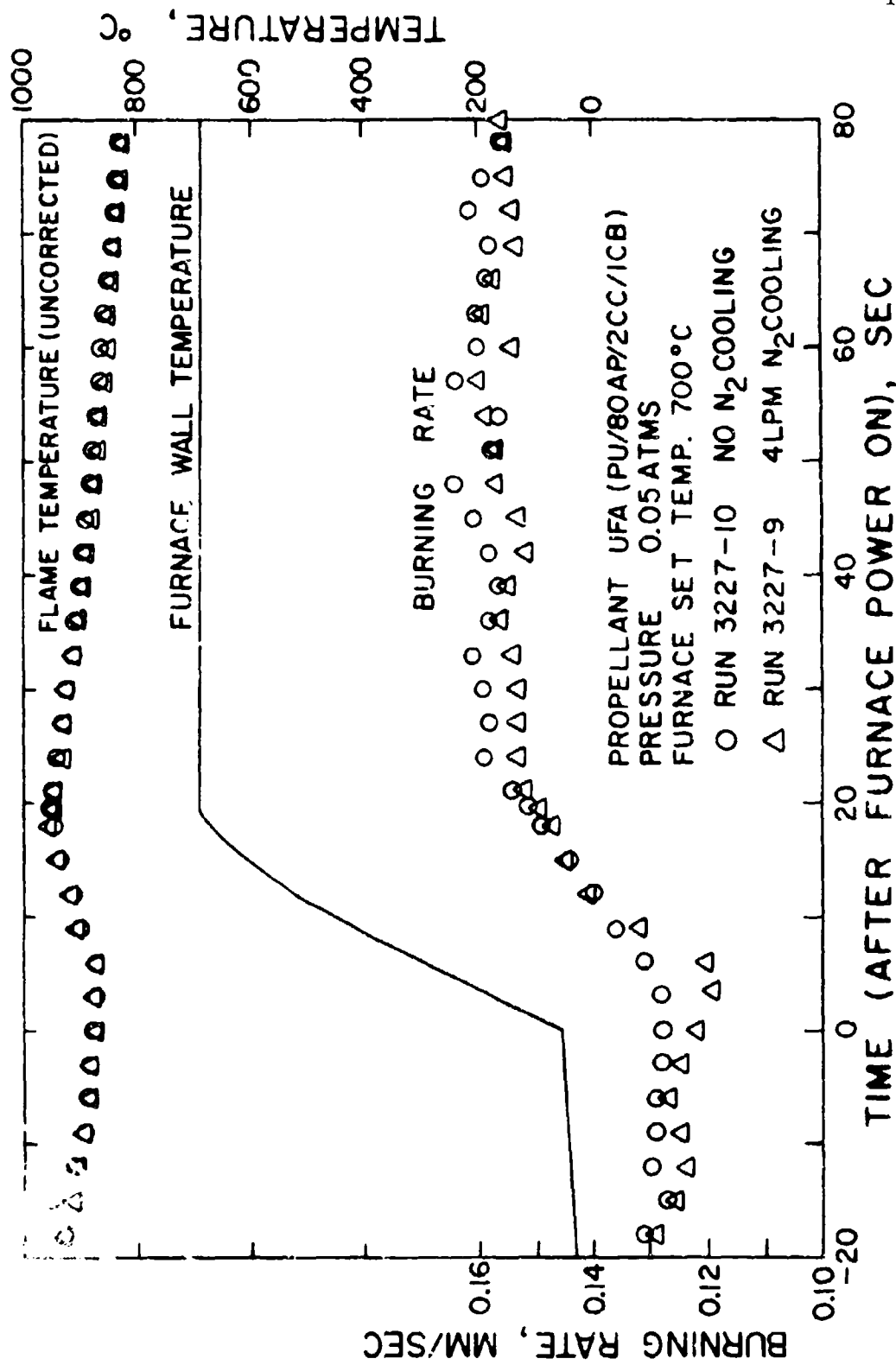


Figure VI.1. Transient Responses of the Burning Rate and the Flame Temperature of a Catalyzed PU Propellant (UFA) to Furnace Heating.

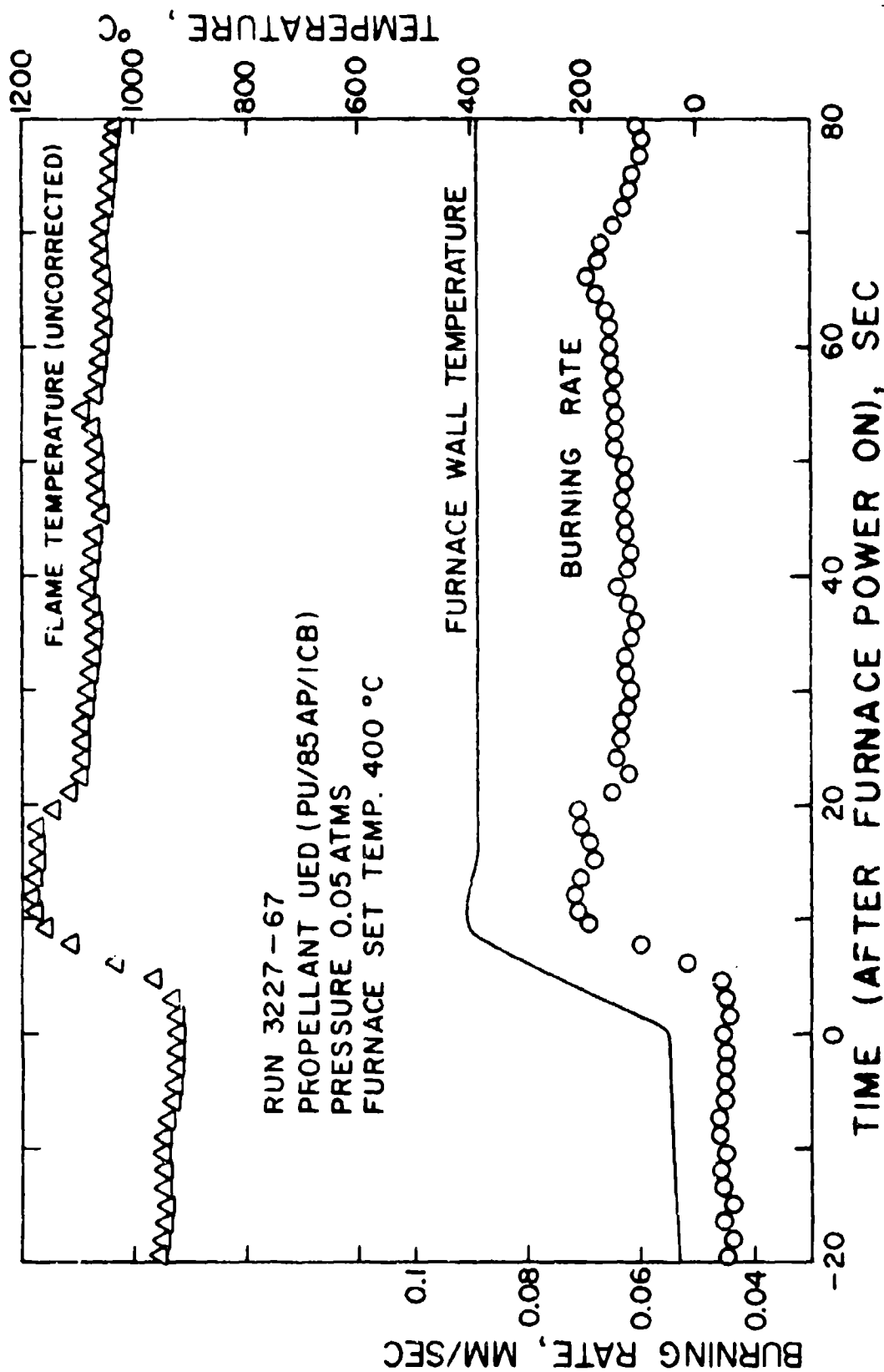


Figure VI.2. Transient Responses of the Burning Rate and the Flame Temperature of an Uncatalyzed PU Propellant (UED) to Furnace Heating.

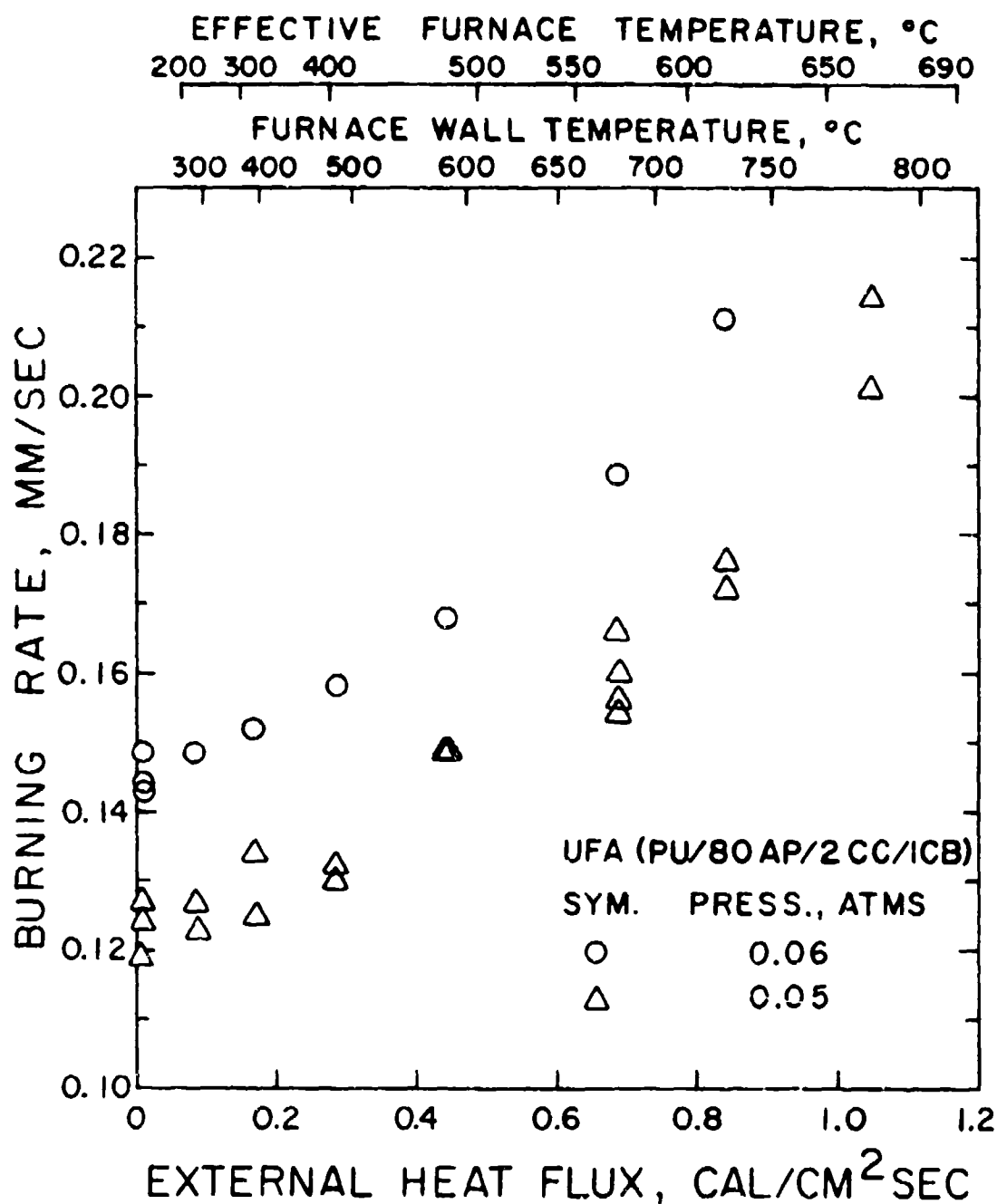


Figure VI.3. Effect of the External Heat Flux on the Burning Rate of a Catalyzed PU Propellant (UFA).

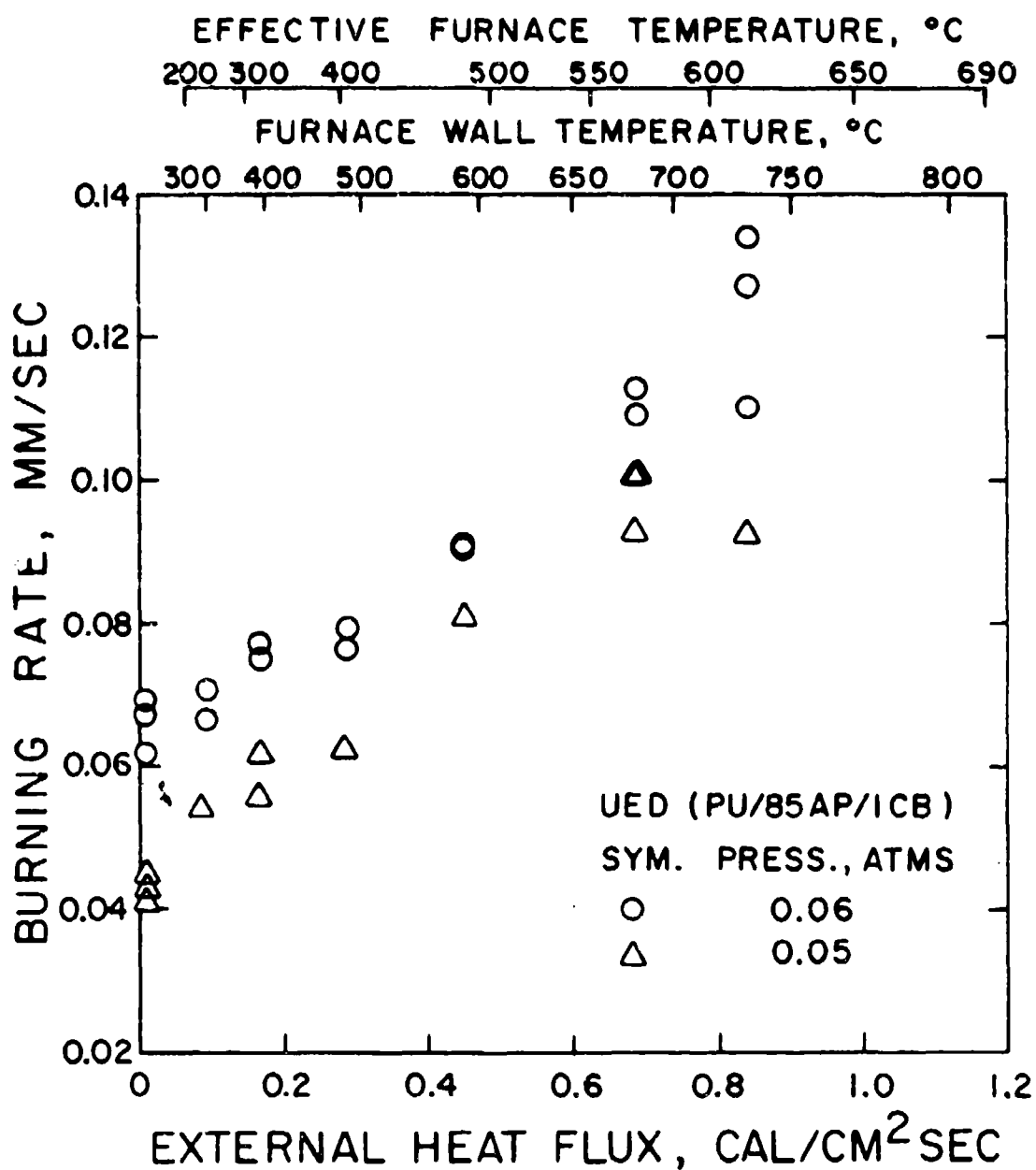


Figure VI.4. Effect of the External Heat Flux on the Burning Rate of an Uncatalyzed PU Propellant (UED).

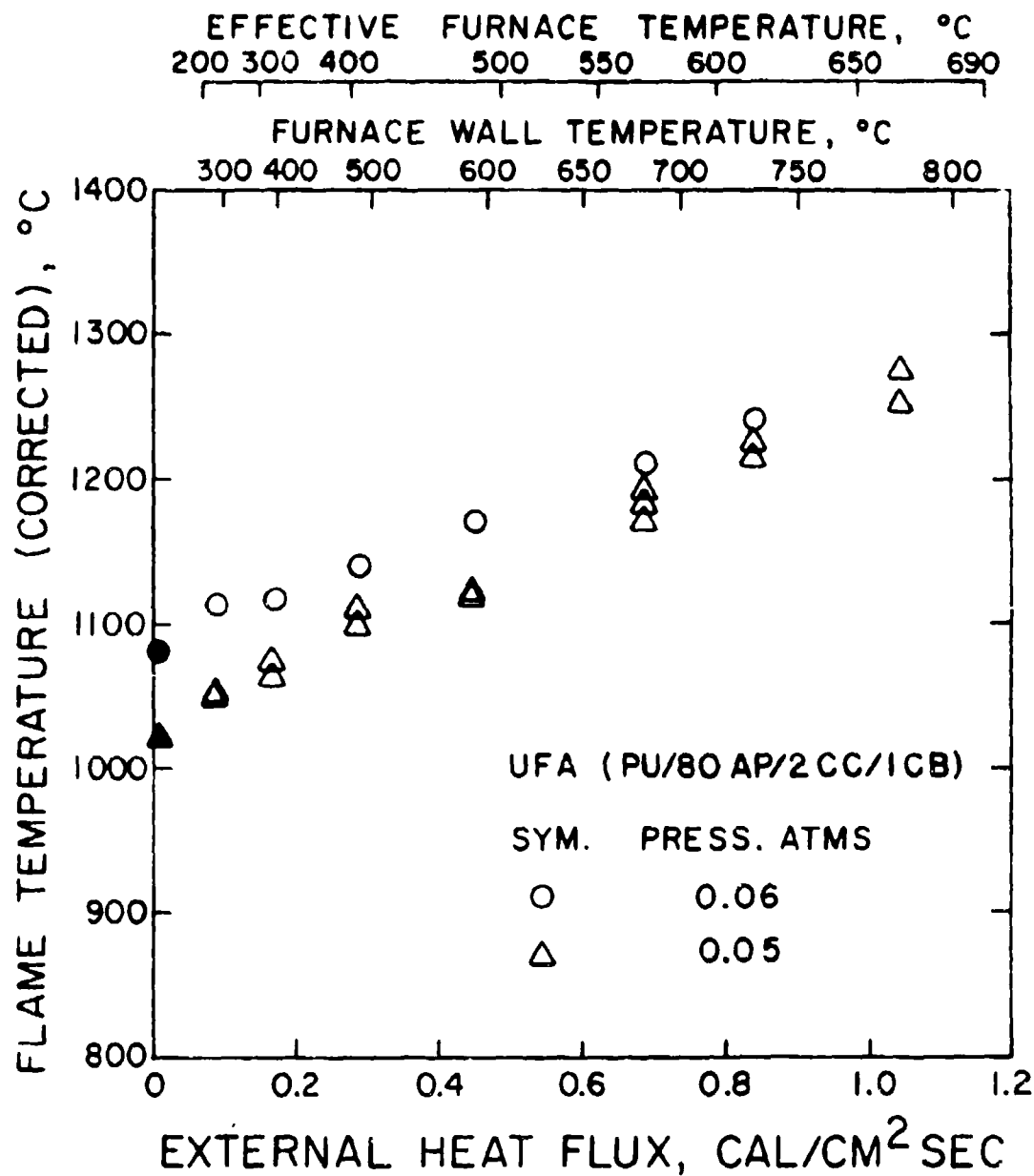


Figure VI.5. Effect of the External Heat Flux on the Flame Temperature of a Catalyzed PU Propellant (UFA). Radiation Corrections Were Made for the Flame Temperatures. Filled Symbols Indicate the Averaged Values of Many Runs at the Same Test Conditions.

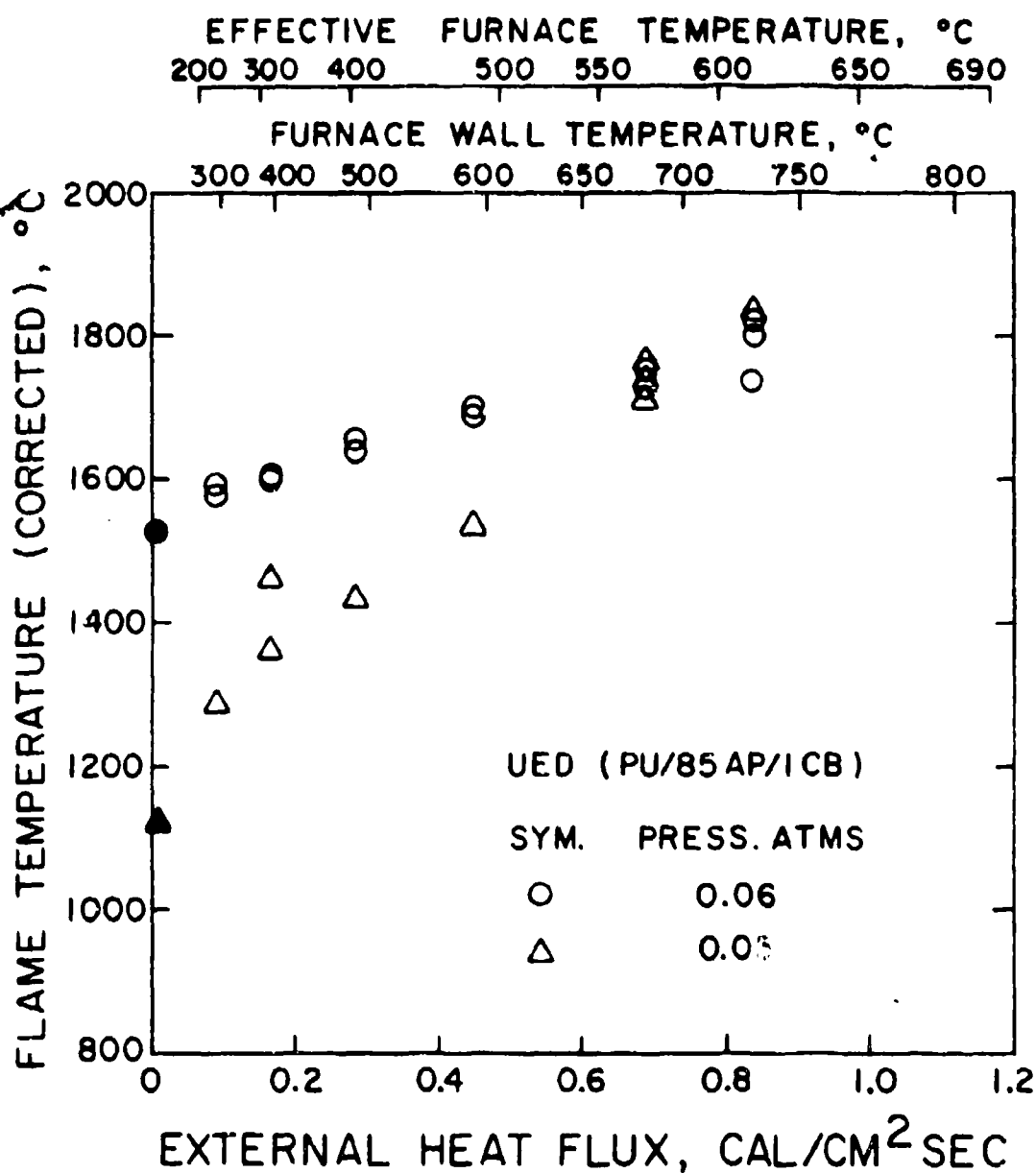


Figure VI.6. Effect of the External Heat Flux on the Flame Temperature of an Uncatalyzed PU Propellant (UED). Radiation Corrections Were Made for the Flame Temperatures. Filled Symbols Indicate the Averaged Values of Many Runs at the Same Test Conditions.

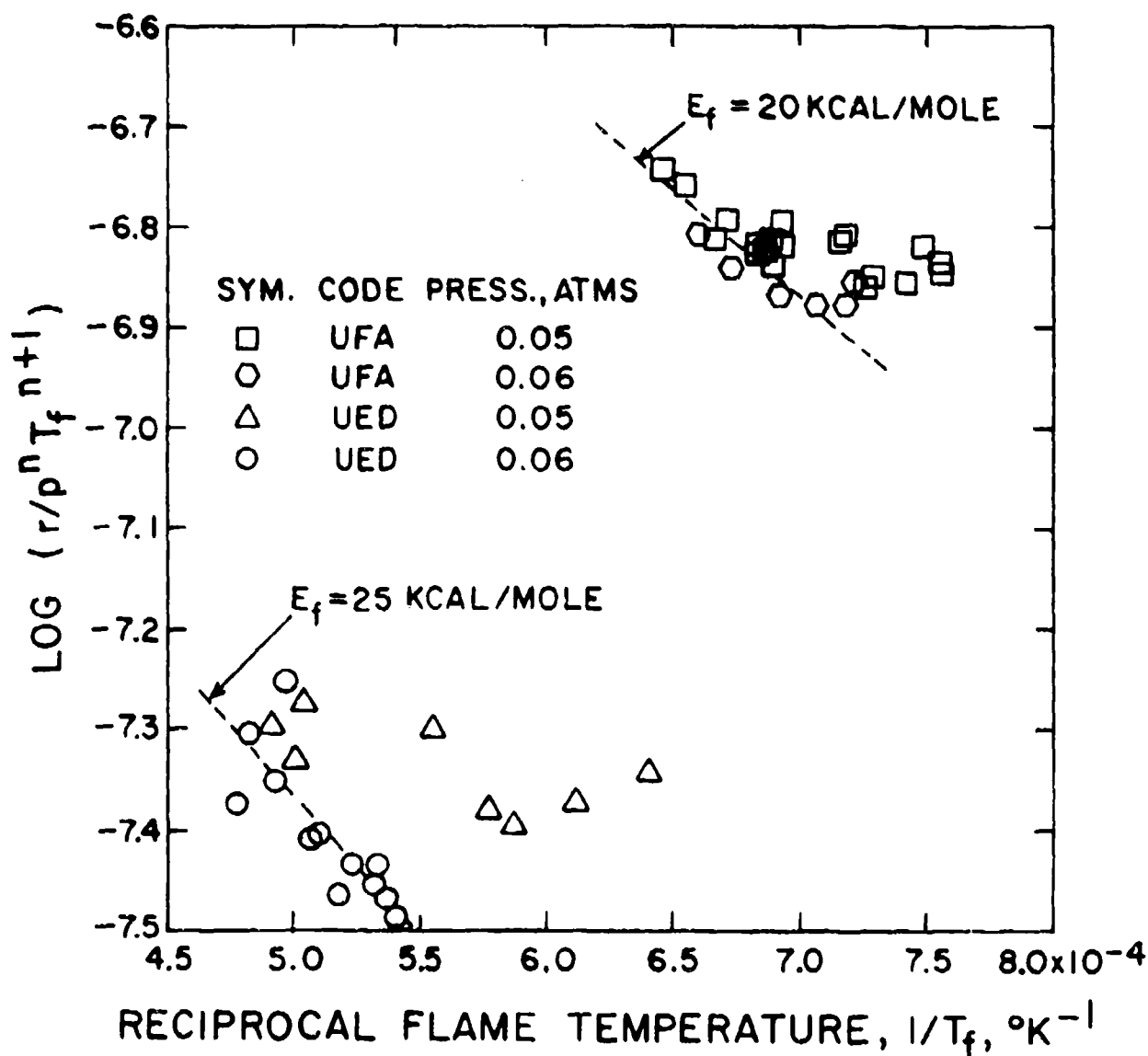


Figure VI.7. Determination of the Activation Energy of Gas Phase Reaction Using Denison and Baum's Model for a Catalyzed (UFA) and an Uncatalyzed (UED) PU Propellants. The Value of n Was Taken to be One.

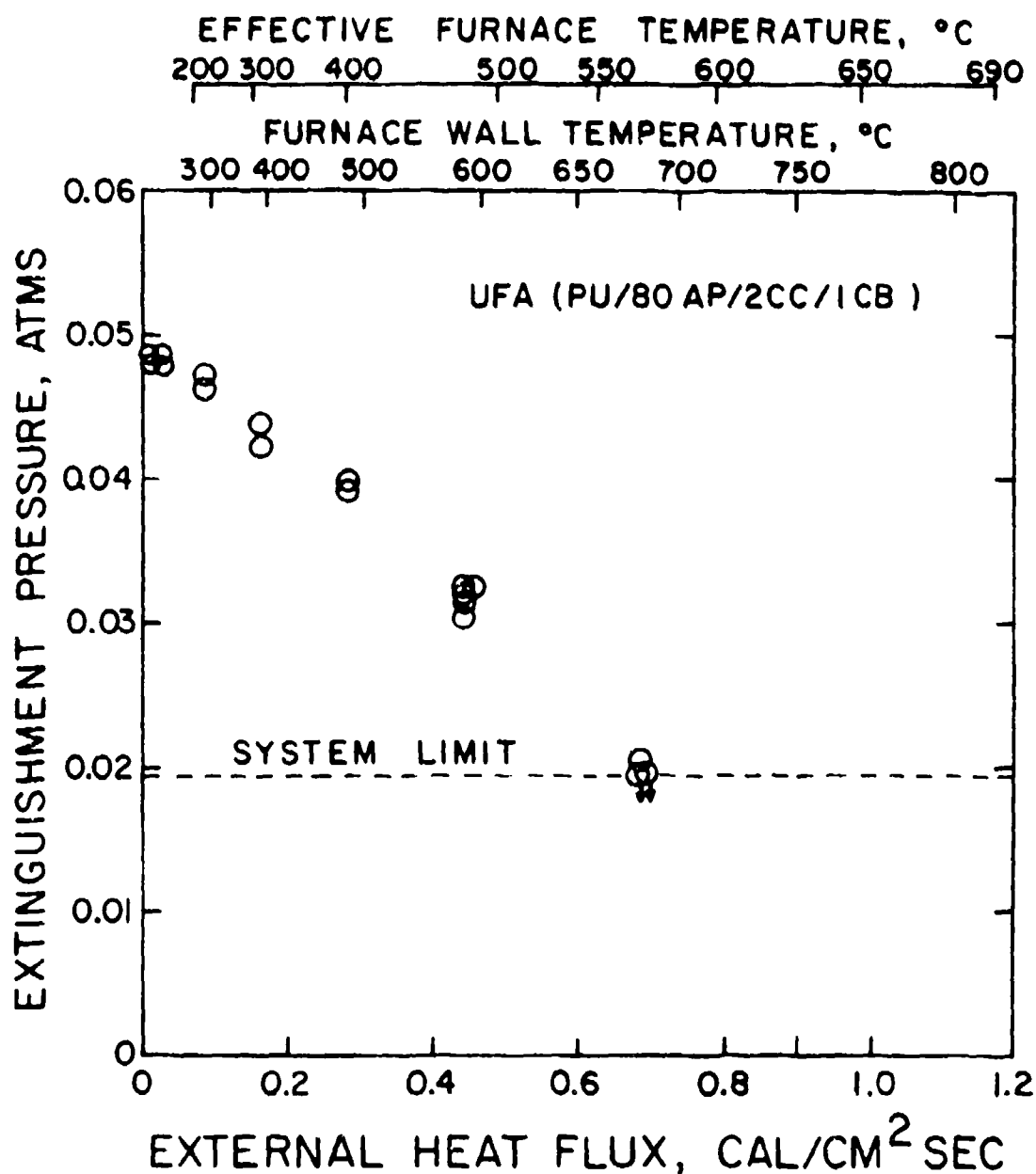


Figure VI.8. Effect of the External Heat Flux on the Limiting Extinguishment Pressure of a Catalyzed PU Propellant (UFA). The Slow-Depressurization Method Was Used.

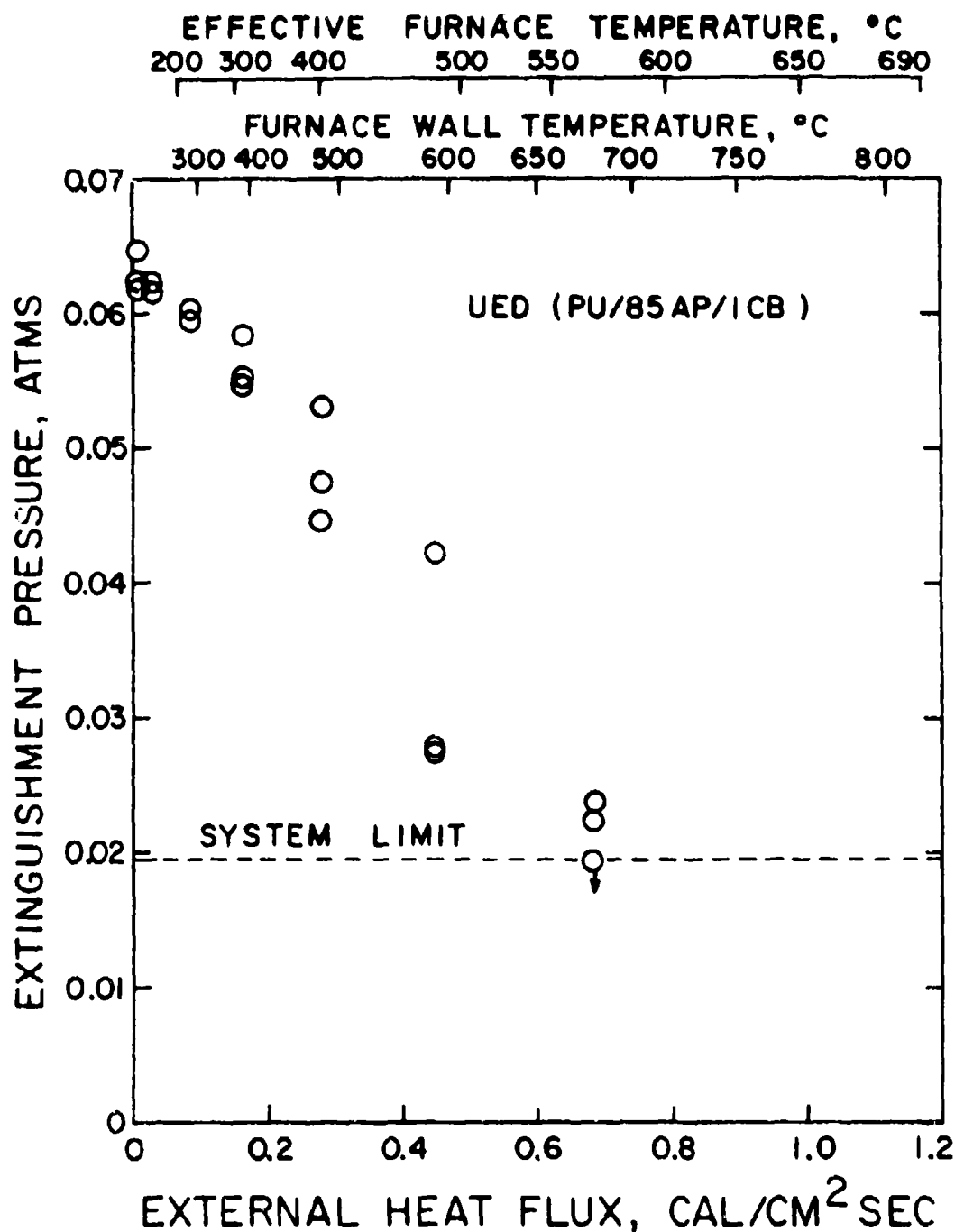


Figure VI.9. Effect of the External Heat Flux on the Limiting Extinguishment Pressure of an Uncatalyzed PU Propellant (UED). The Slow-Depressurization Method Was Used.

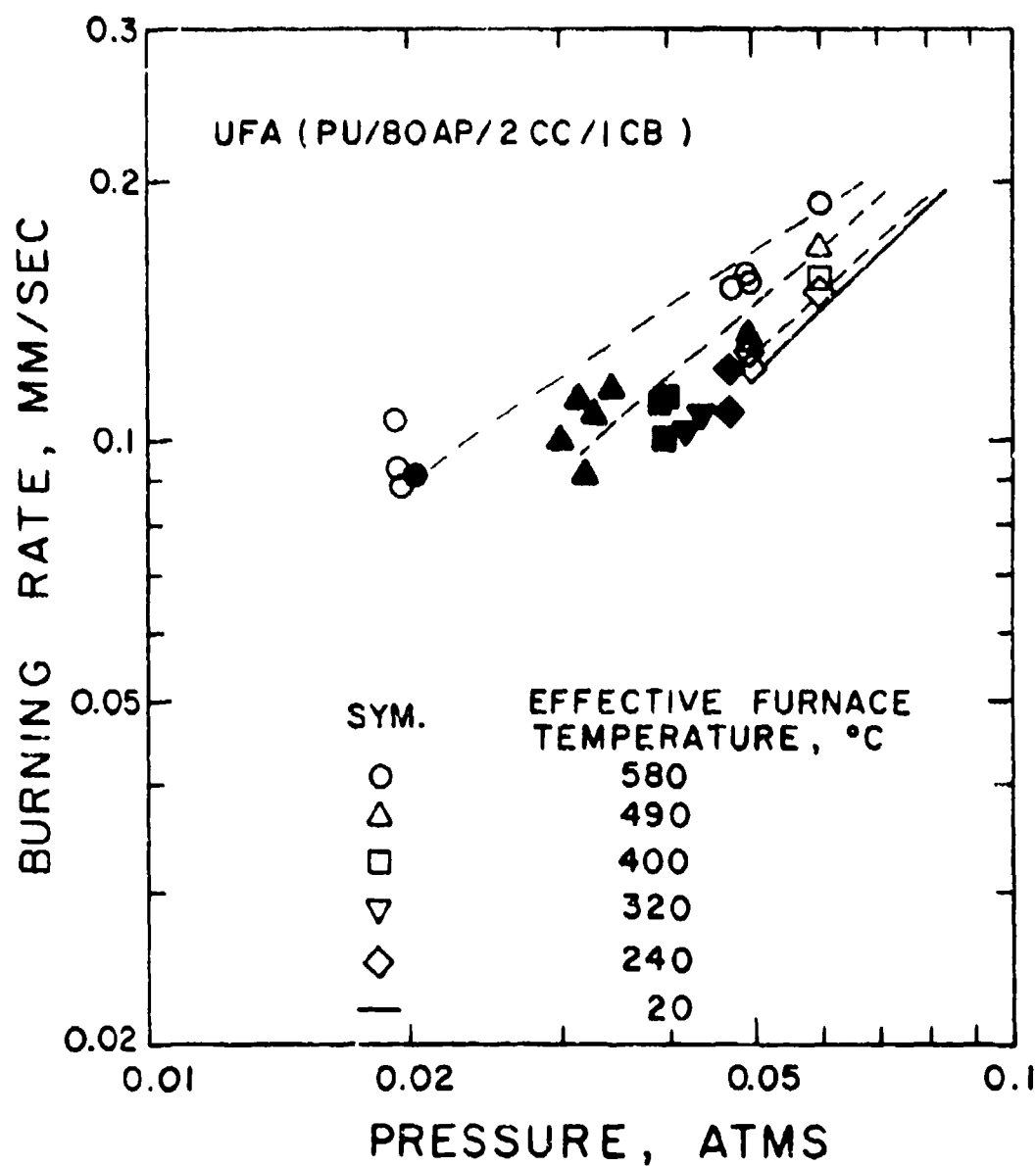


Figure VI.10. Heat Flux-Augmented Burning Rate Data of a Catalyzed PU Propellant (UFA) near the Limiting Extinguishment Pressures. Filled Symbols Indicate the Conditions in Which the Extinguishment Occurred.

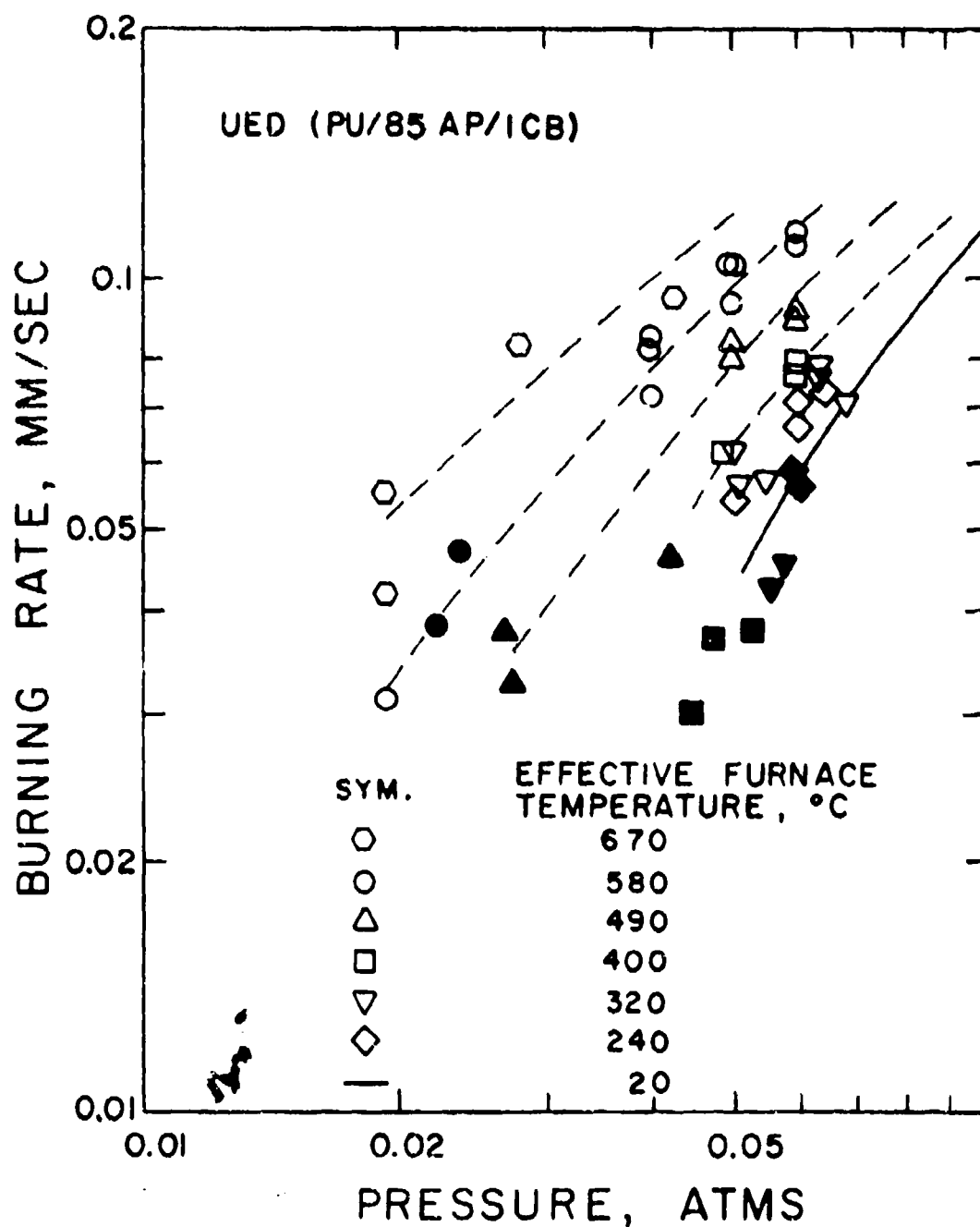


Figure VI.11. Heat Flux-Augmented Burning Rate Data of an Uncatalyzed PU Propellant (UED) near the Limiting Extinguishment Pressures. Filled Symbols Indicate the Conditions in Which the Extinguishment Occurred.

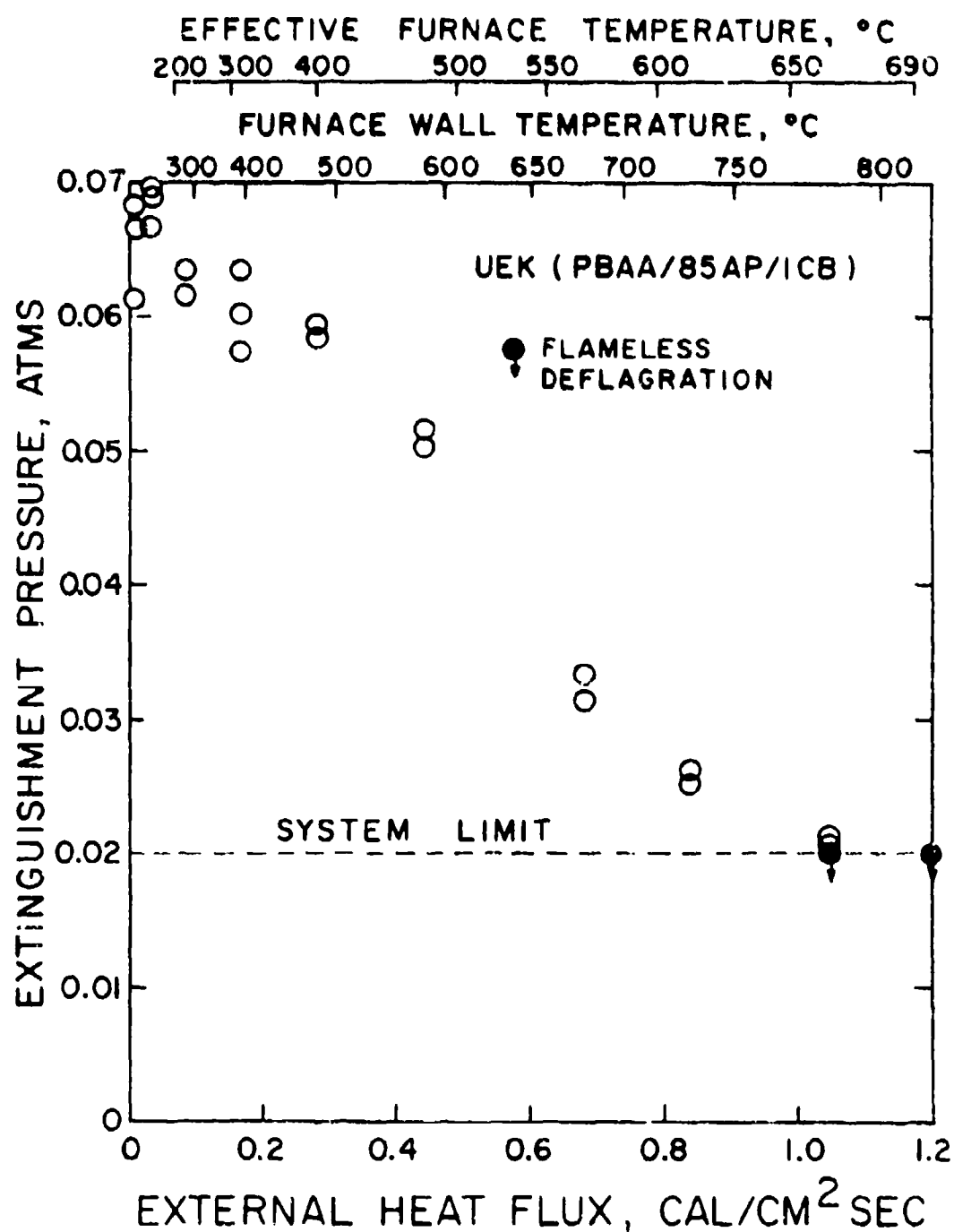


Figure VI.12. Effect of the External Heat Flux on the Limiting Extinguishment Pressure of an Uncatalyzed PBAA Propellant (UEK). The Slow-Depressurization Method Was Used.

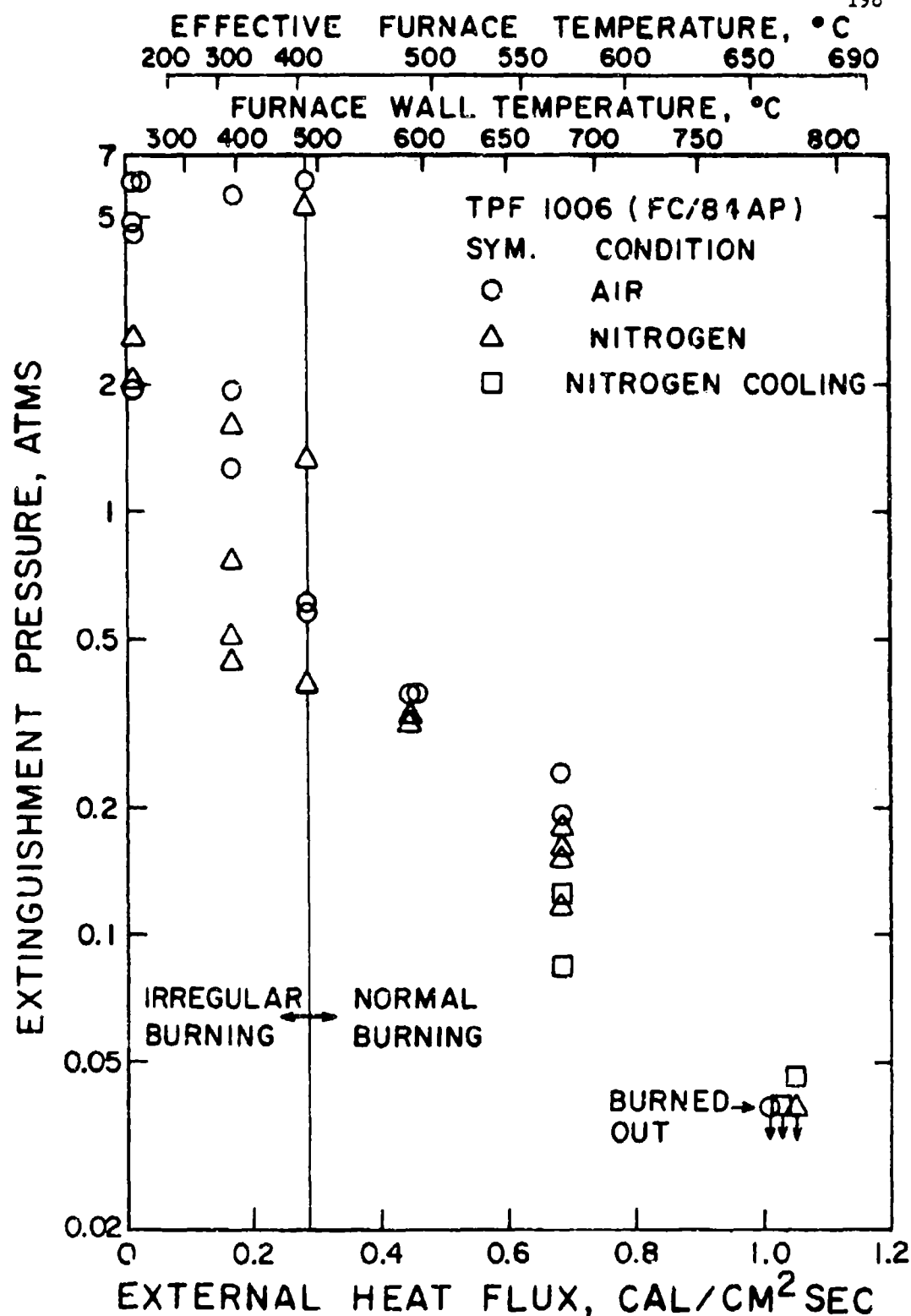
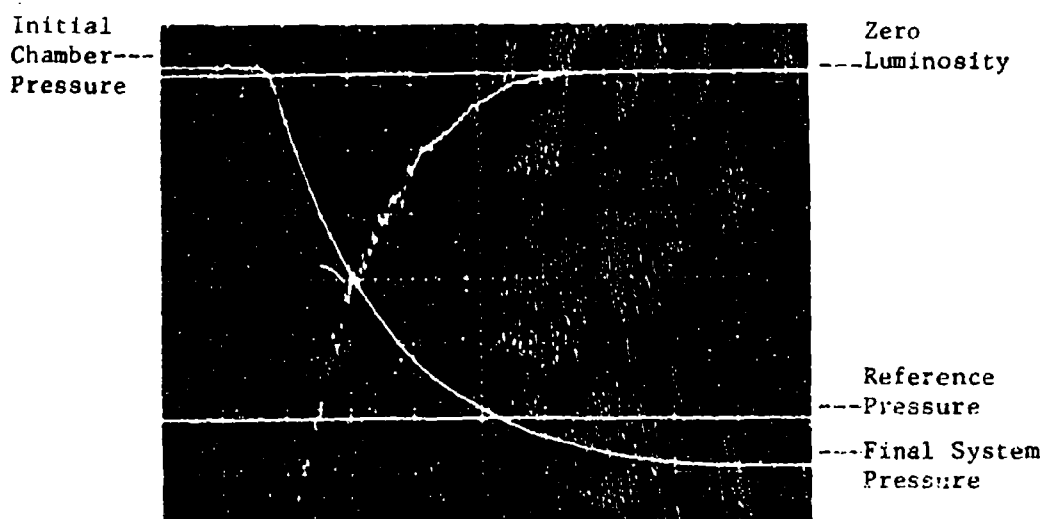


Figure VI.13. Effect of the External Heat Flux on the Extinguishment Pressure of a Fluorocarbon Propellant (TPF 1006). The Slow-Depressurization (with 0.318-cm Orifice) Method was Used.



Run No.: 21106-47, Propellant: UEF, Orifice: 2.54 cm, Initial Chamber Pressure: 1.40 atms, Reference Pressure: 0.85 atms, Vertical Scale: 0.13 atms/division, Horizontal Scale: 0.1 sec/division.



Run No.: 21106-55, Propellant: UEZ, Orifice: 2.54 cm, Initial Pressure: 0.85 atms, Reference Pressure: 0.13 atms, Vertical Scale: 0.13 atms/division, Horizontal Scale: 0.1 sec/division.

Figure VII.1. Oscilloscope Traces of Typical Depressurization Extinguishment Tests Using the Combustion Chamber.

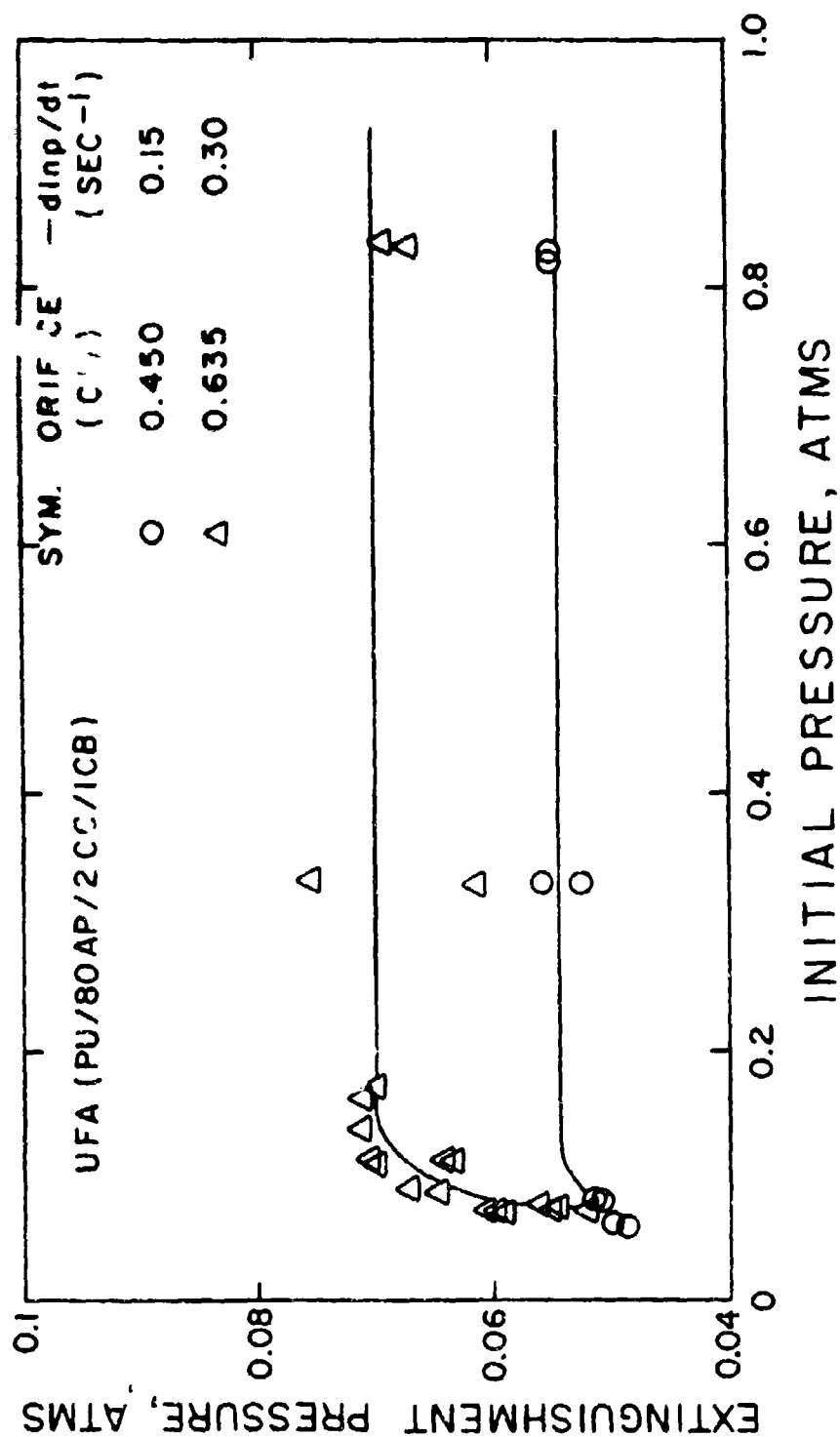


Figure VII.2. Effect of the Initial Pressure on the Extinguishment Pressure for a Catalyzed PU Propellant (UFA) During Depressurization.

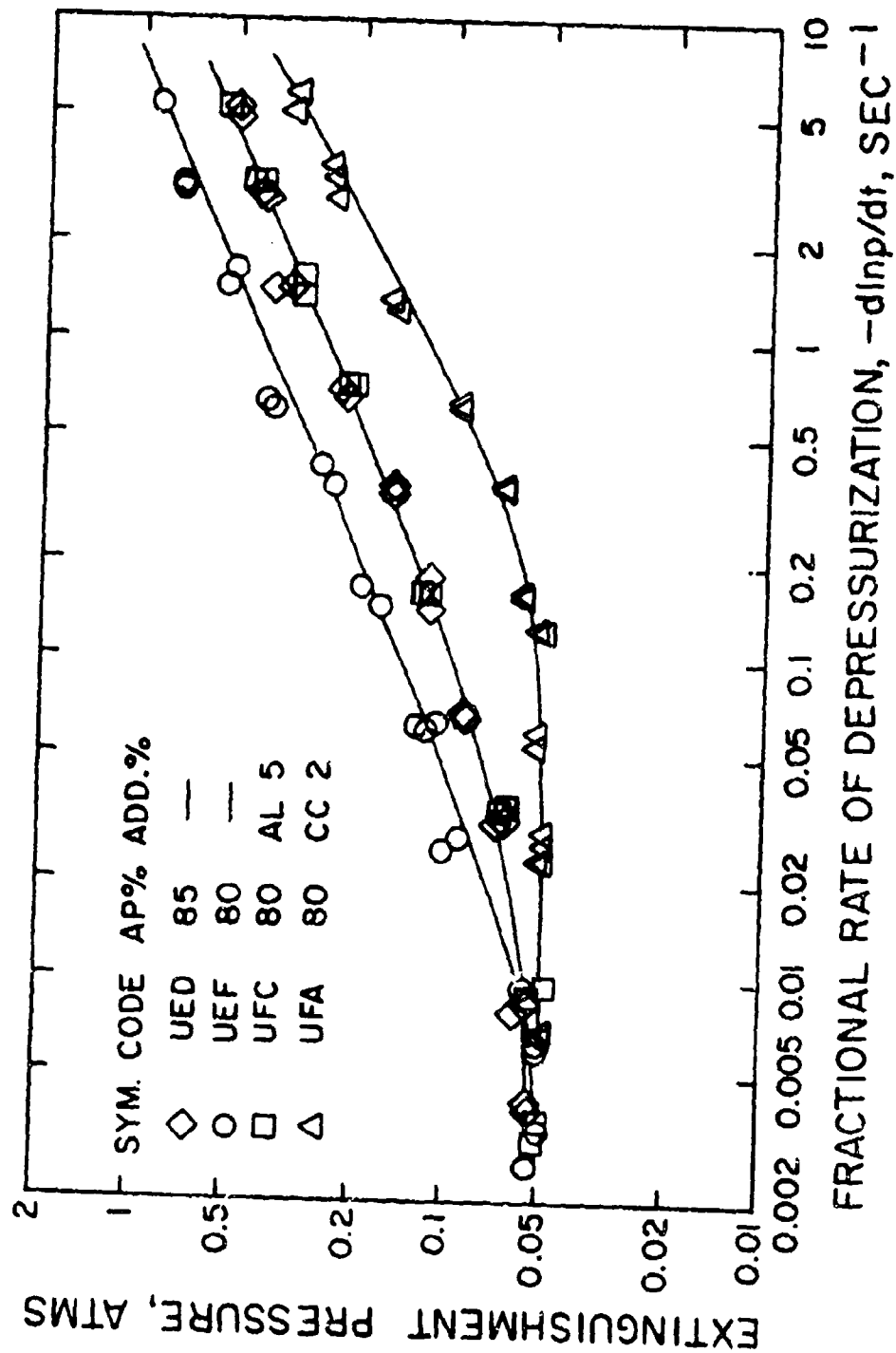


Figure VII.3. Effect of the Depressurization Rate on the Extinguishment Pressure of PU Propellants.

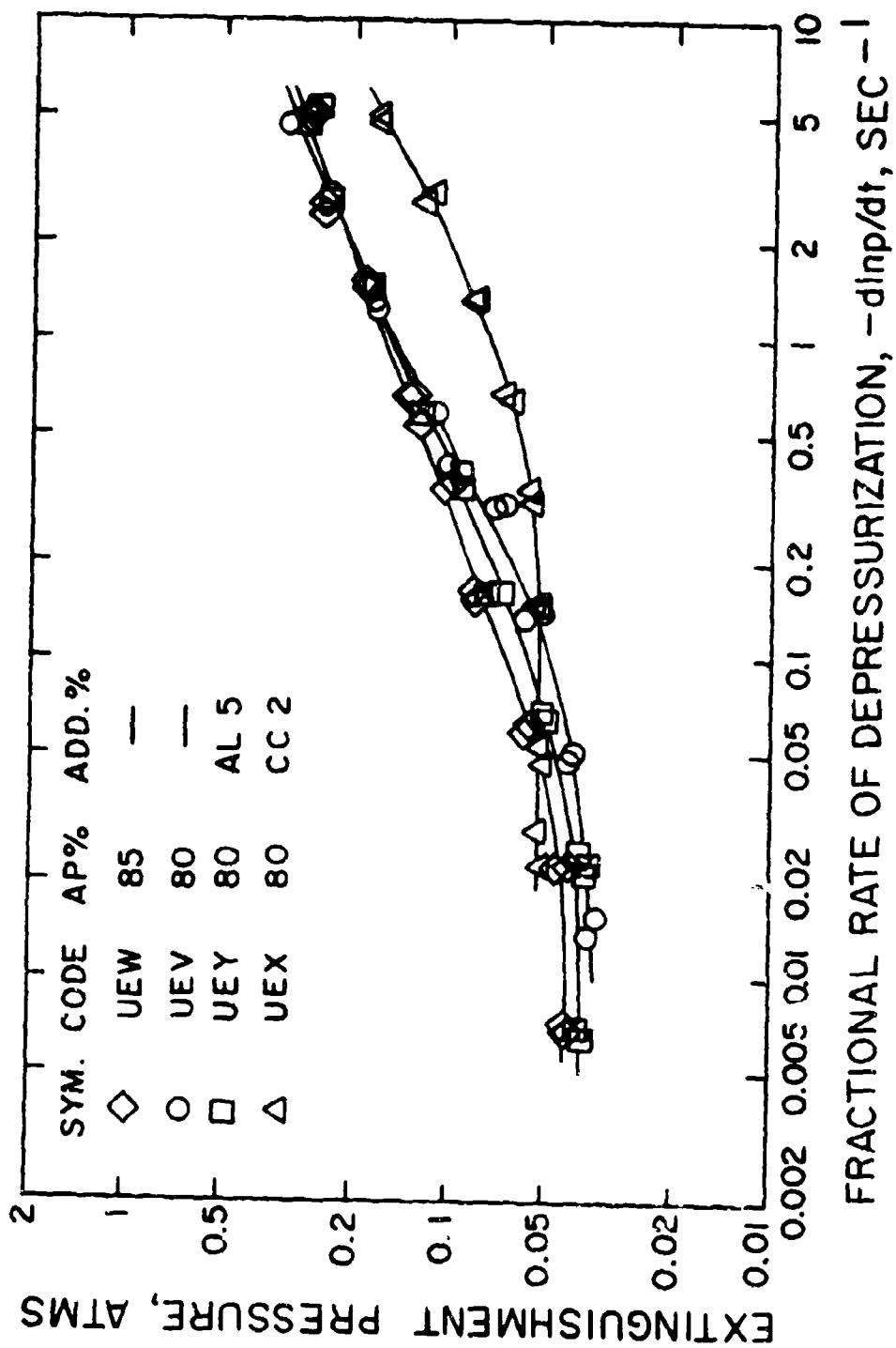


Figure VII.4. Effect of the Depressurization Rate on the Extinguishment Pressure of HTPB Propellants.

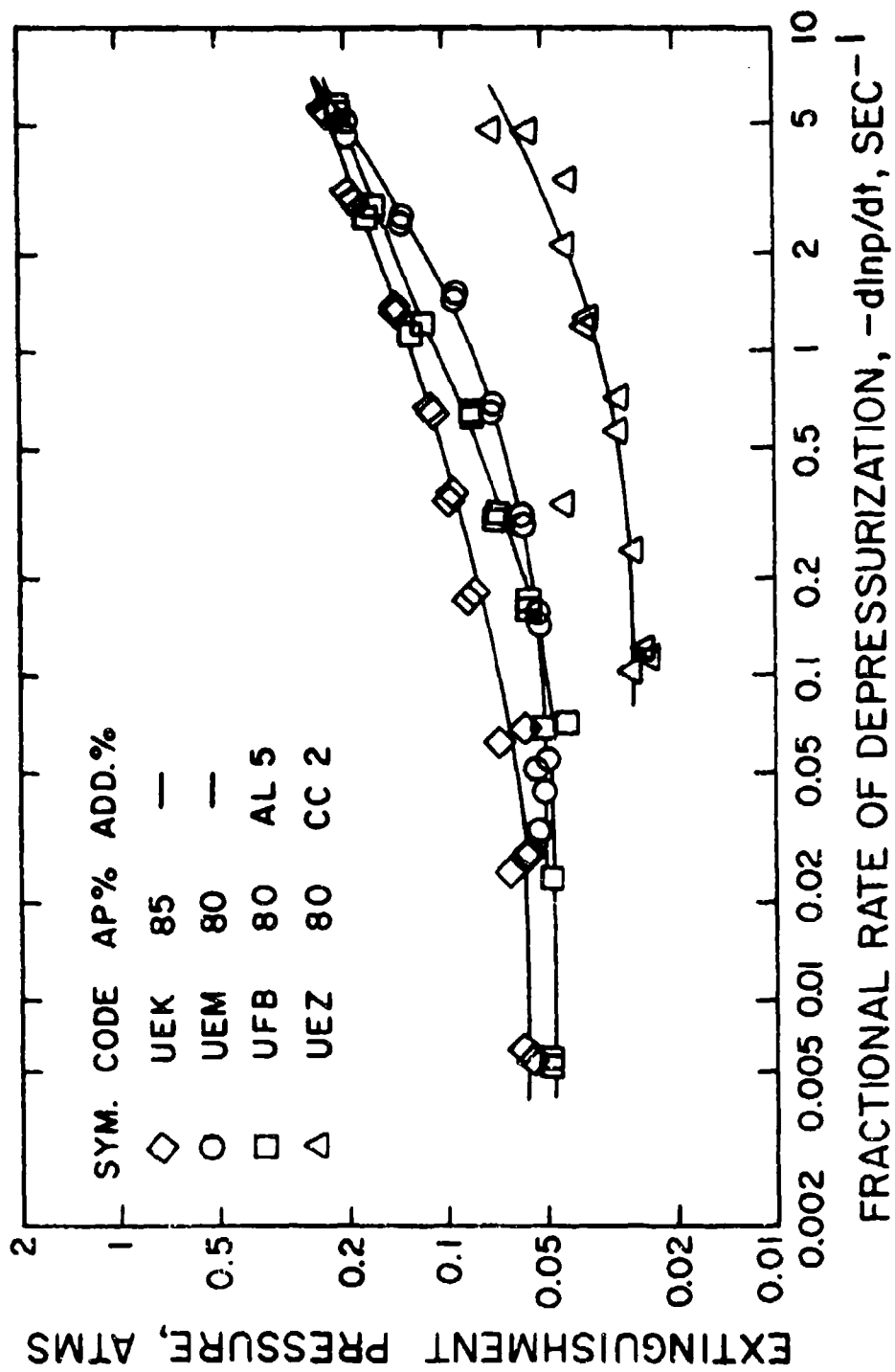


Figure VII.5. Effect of the Depressurization Rate on the Extinguishment Pressure of PBAA Propellants.

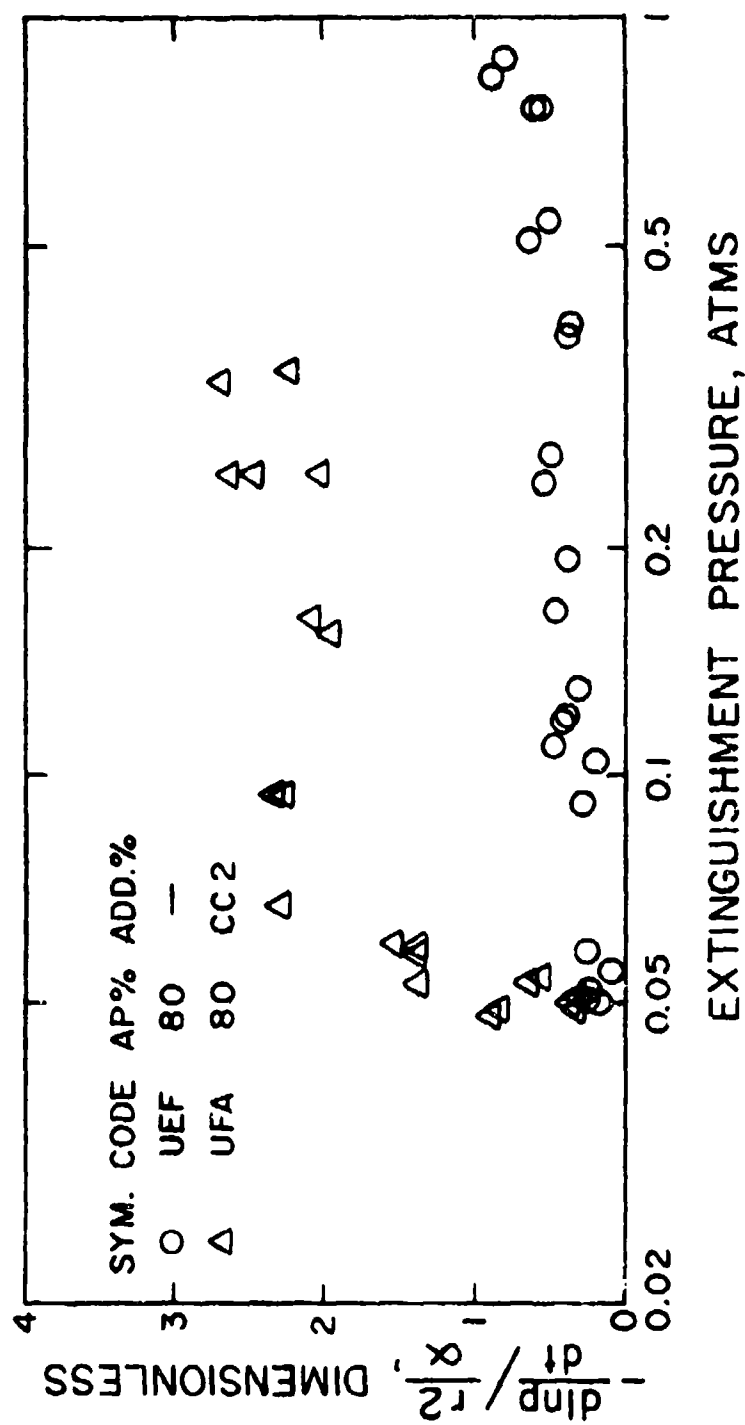


Figure VII.6. The Critical Ratio of Characteristic Times as a Function of the Extinguishment Pressure for Two PU Propellants of Higher Fuel Loading.

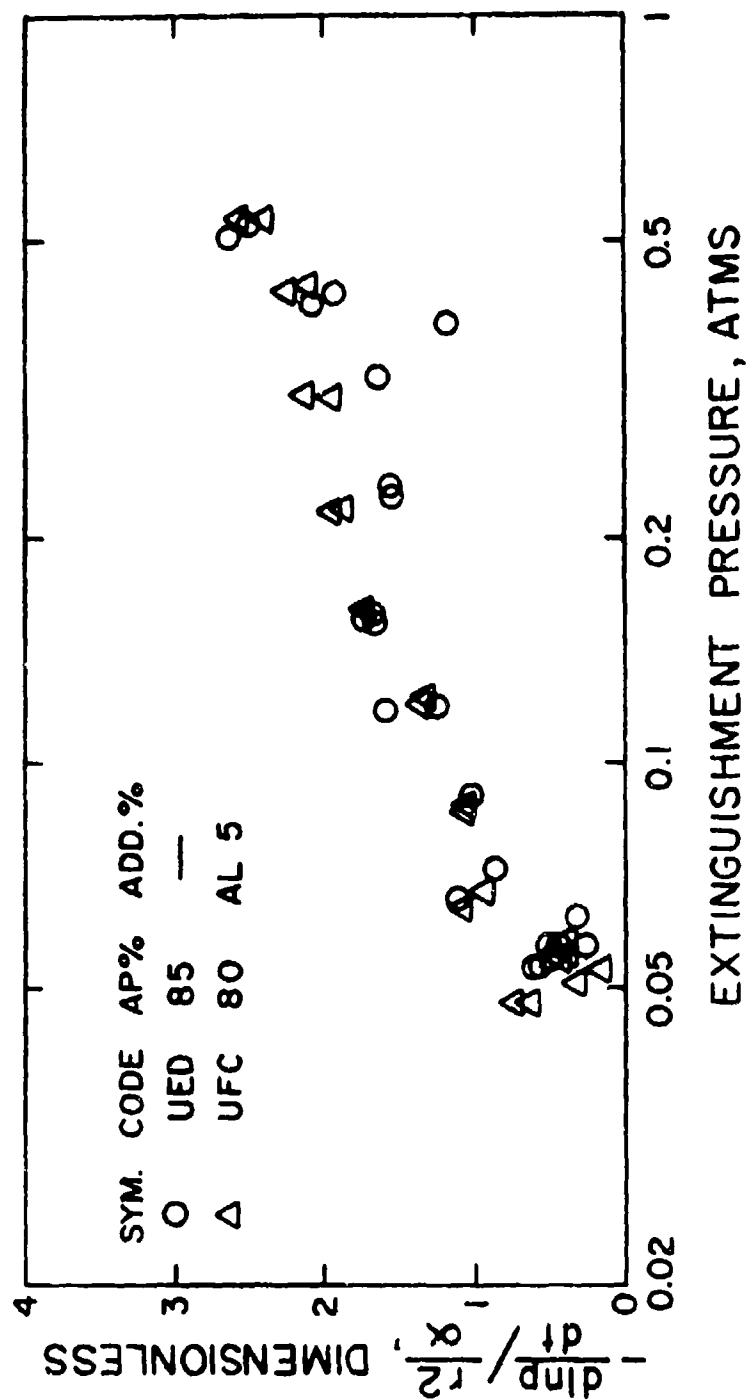


Figure VII.7. The Critical Ratio of Characteristic Times as a Function of the Extinguishment Pressure for Two PU Propellants of Lower Fuel Loading.

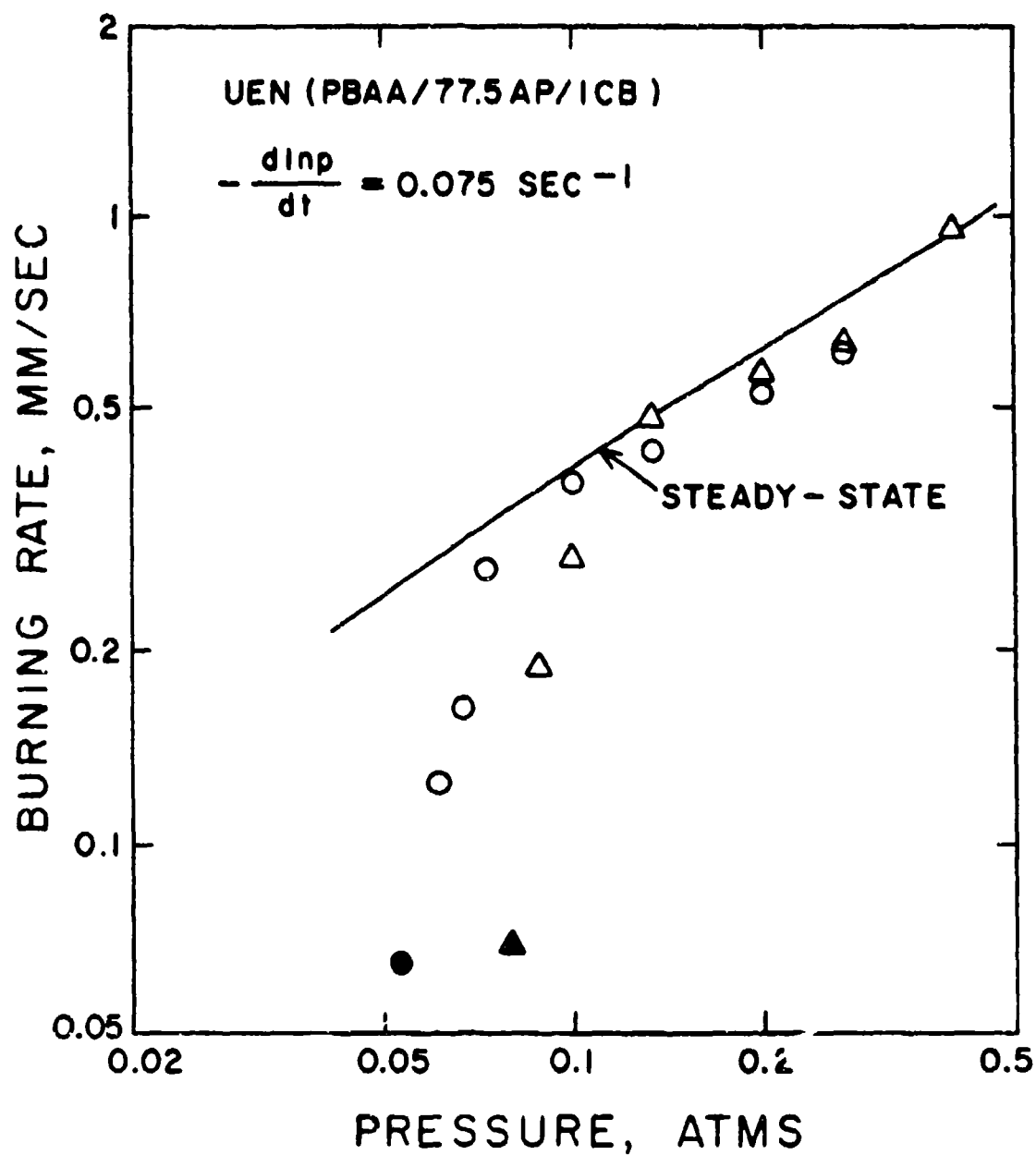


Figure VII.8. Transient Burning Rates During Depressurization at Low Pressures for a PBAA Propellant.

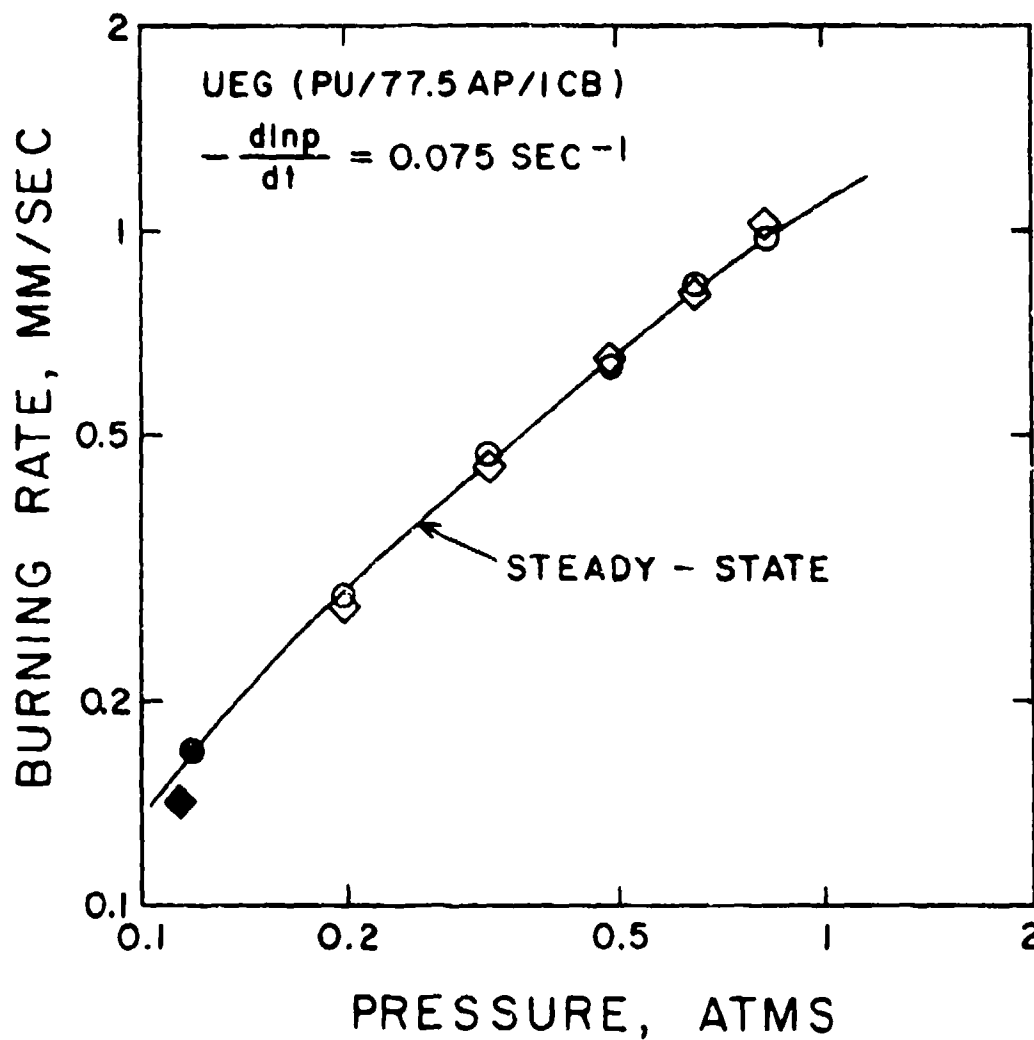


Figure VII.9. Transient Burning Rates During Depressurization at Low Pressures for a PU Propellant.

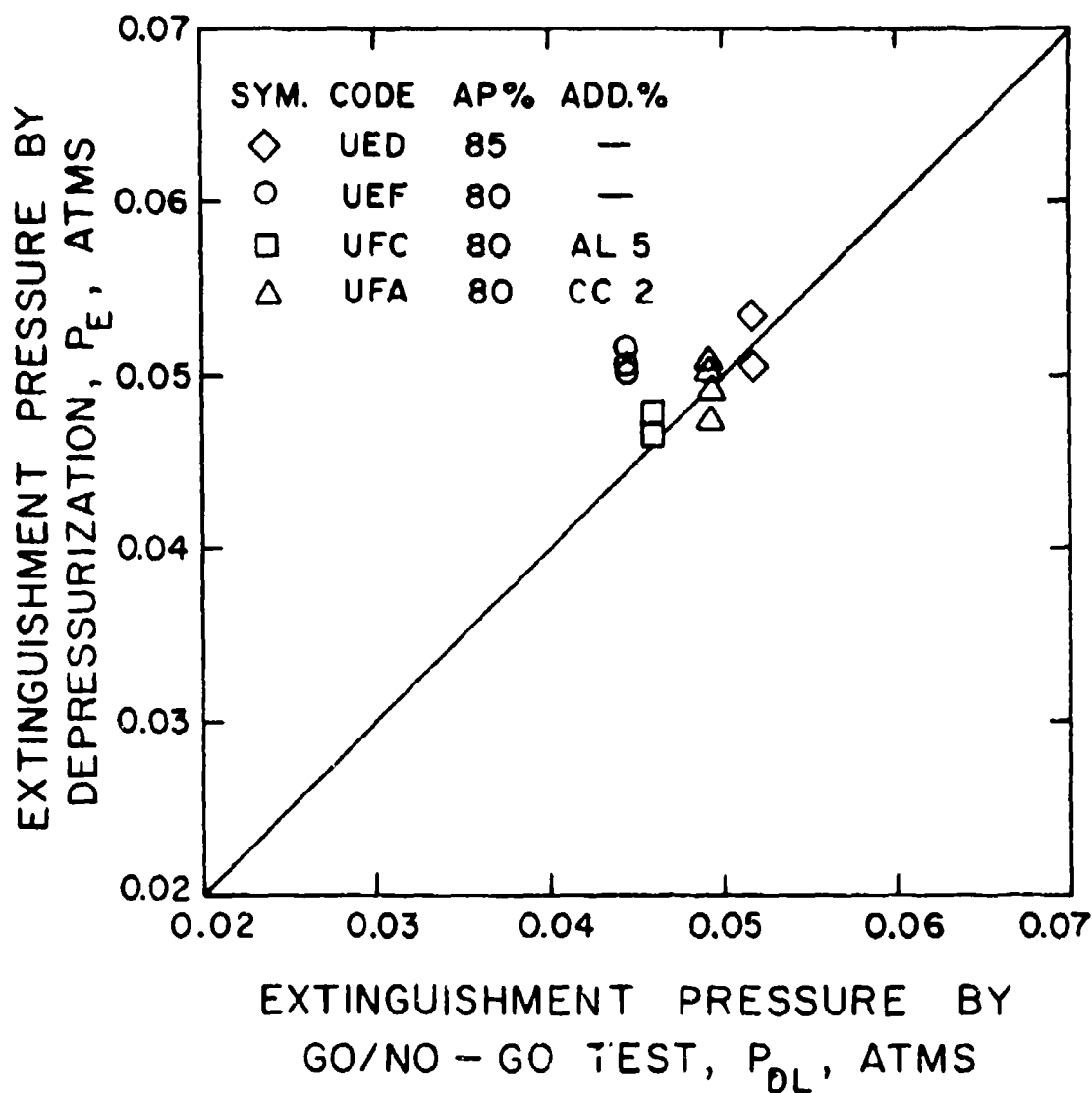


Figure VII.10. Comparison of Near-Limiting Extinguishment Pressures Measured by Depressurization Tests (P_E) and the Pressure Deflagration Limit Determined by Go/No-Go Tests (P_{dl}) for PU Propellants. In the Case of Every Propellant, a Smaller P_E Was Attained When a Slower Rate of Depressurization Was Applied.

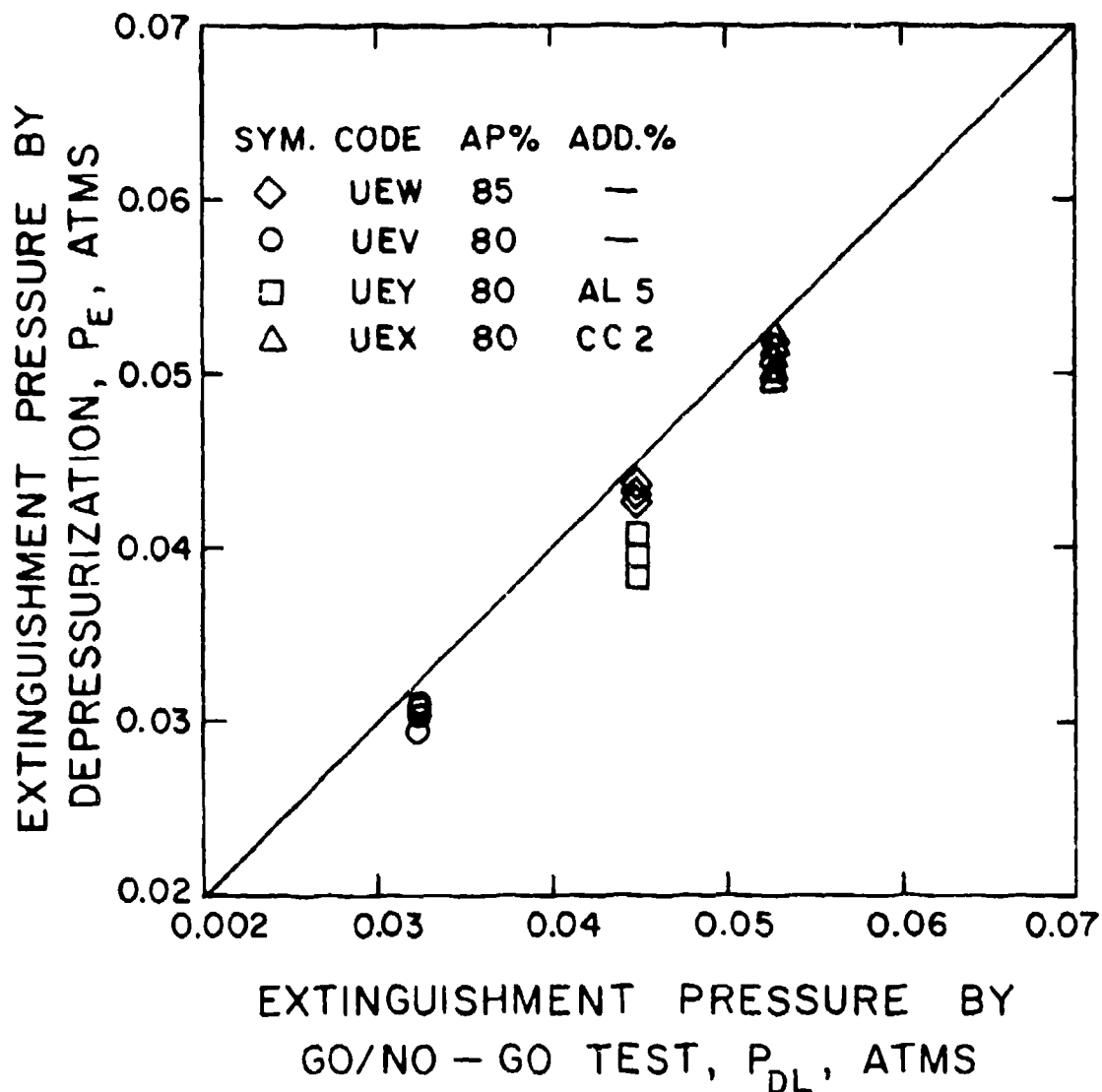


Figure VII.11. Comparison of Near-Limiting Extinguishment Pressures Measured by Depressurization Tests (P_E) and the Pressure Deflagration Limit Determined by Go/No-Go Tests (P_{dl}) for HTPB Propellants. In the Case of Every Propellant, a Smaller P_E Was Attained When a Slower Rate of Depressurization Was Applied.

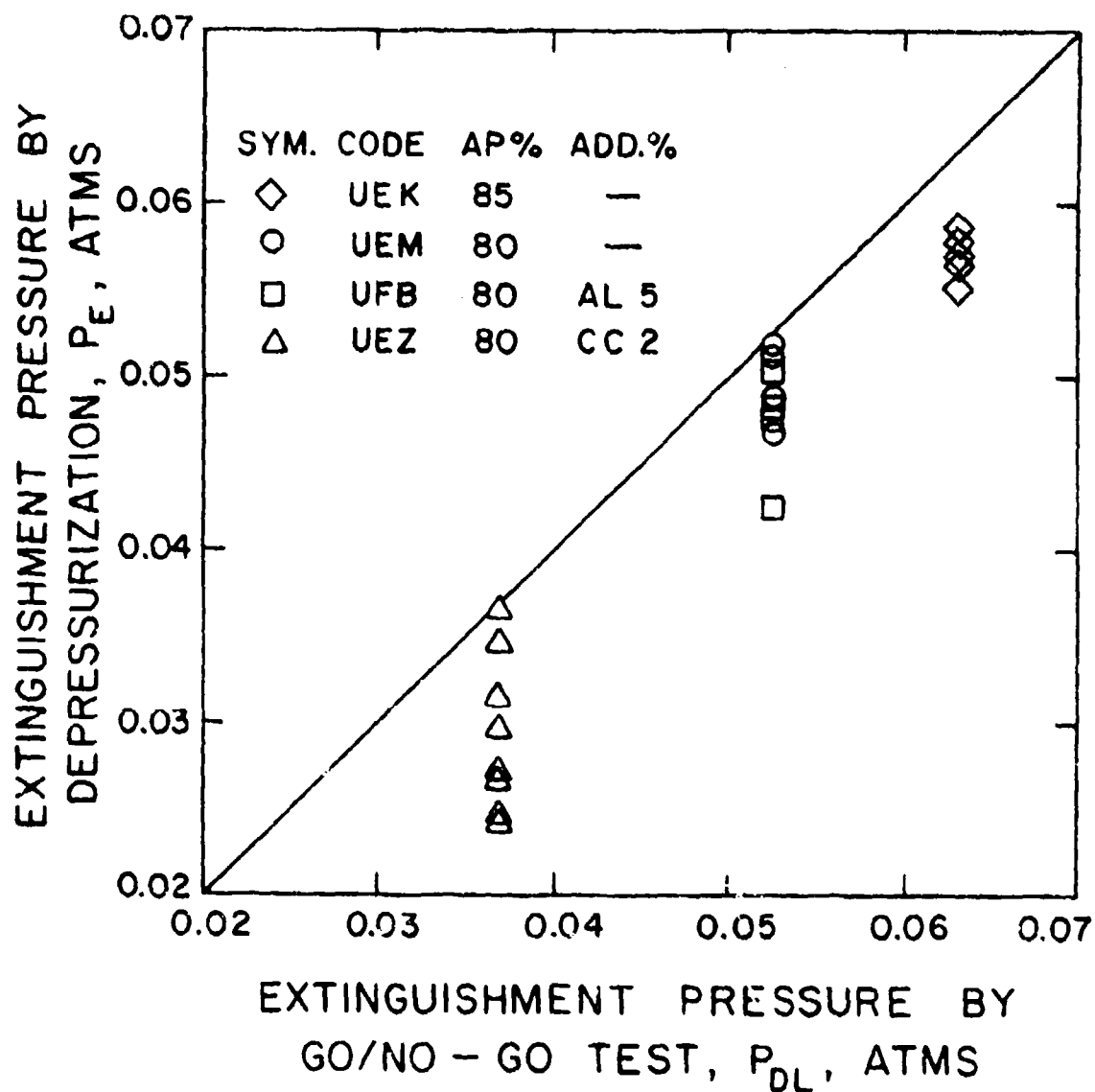
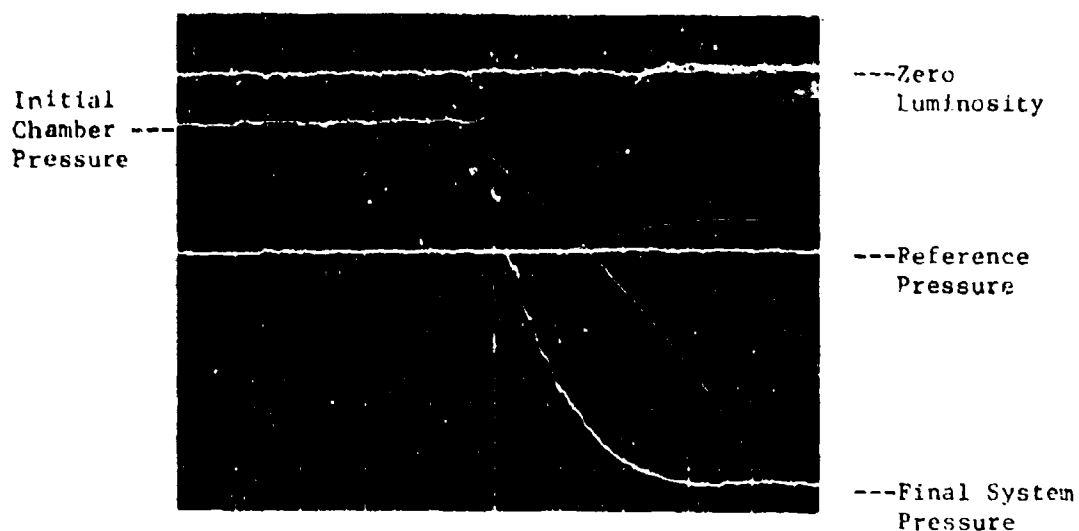


Figure VII.12. Comparison of Near-Limiting Extinguishment Pressures Measured by Depressurization Tests (P_E) and the Pressure Deflagration Limit Determined by Go/No-Go Tests (P_{DL}) for PBAA Propellants. In the Case of Every Propellant, a Smaller P_E Was Attained When a Smaller Rate of Depressurization Was Applied.



Run No.: 2813-133, Propellant: UEZ, Sample Shape: Strand.

Initial Chamber Pressure: 19.6 atms, Reference Pressure: 13.8 atms.

Initial Dump-Tank Pressure: 0.68 atms, Final Dump-Tank Pressure: 0.71 atms.

Tape Recorder Recording Speed: 60 inches/sec.

Play Back Speed: 7.5 inches/sec.

Vertical Scale: 3.40 atms/division.

Horizontal Scale: 6.25 msec/division (above),
0.0625 sec/division (below).

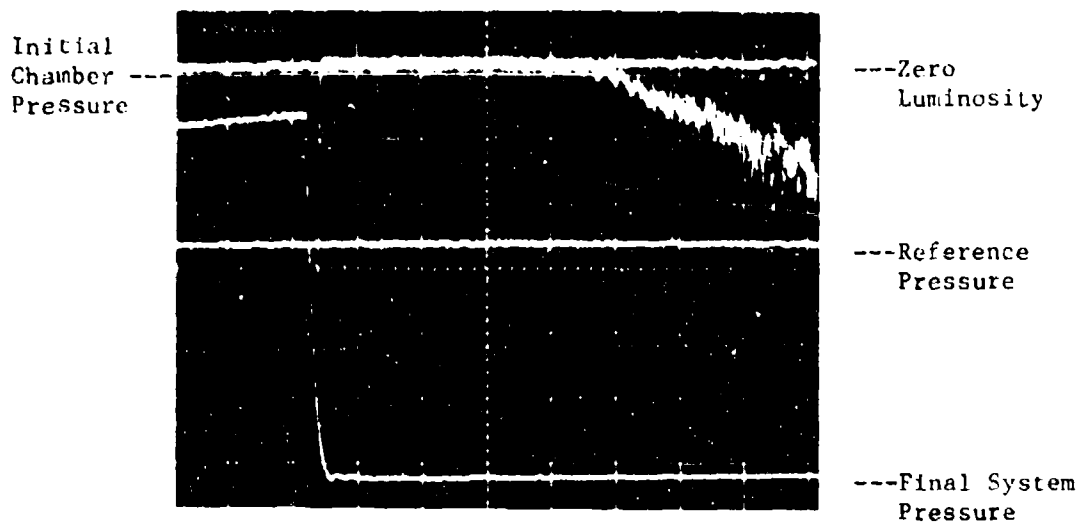


Figure VIII.1. Oscilloscope Traces of a Typical Rapid-Depressurization Extinguishment Test Followed by Reignition.

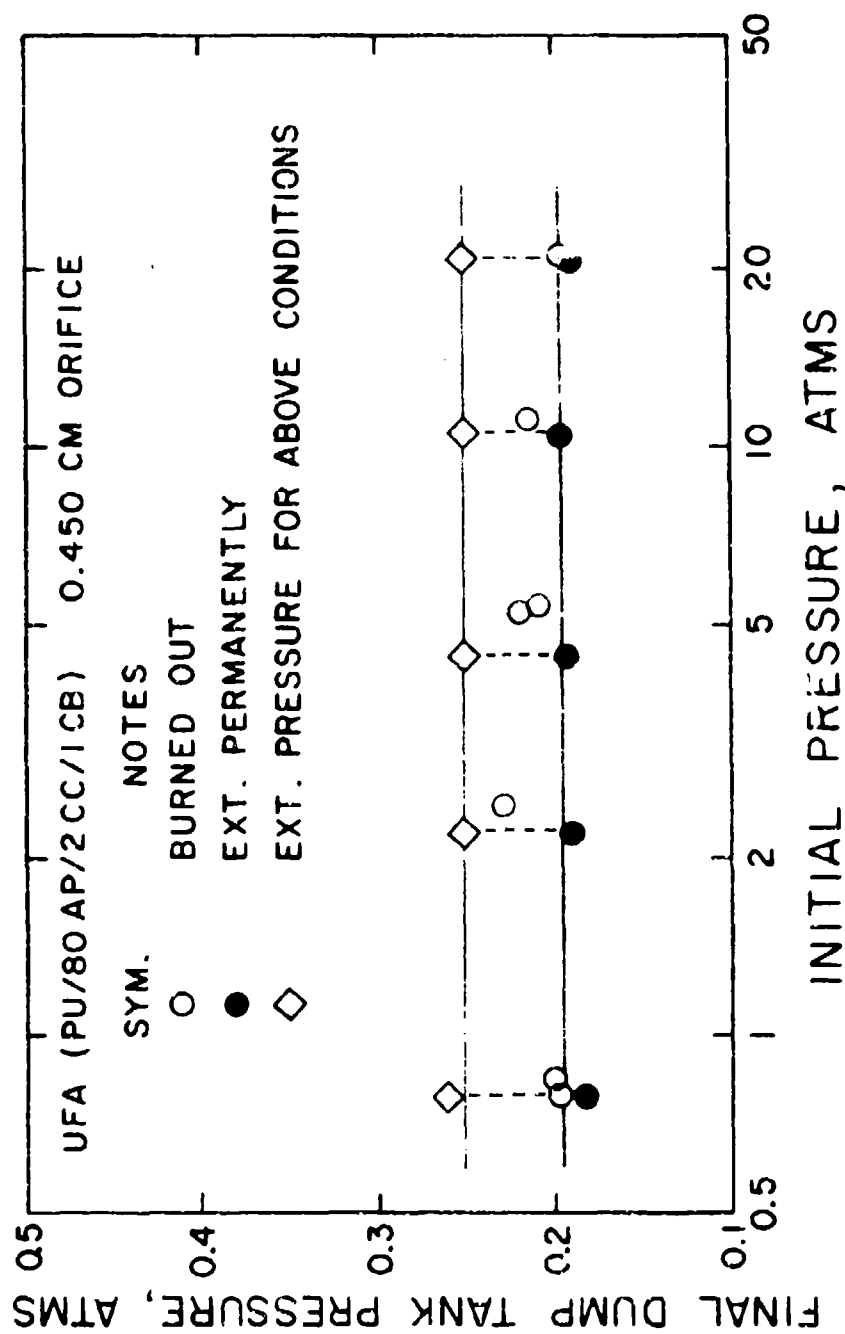


Figure VIII.2. Effect of the Initial Pressure on the Critical Dump-Tank Pressure for the Extinguishment of a Catalyzed pu Propellant (UFA) During Rapid Depressurization When the 0.450-cm Orifice Was Used [$-(d\lambda_{up})/dt = 3.1 \text{ sec}^{-1}$]. Diamond Symbols Indicate the Chamber Pressures at Which Extinguishment Actually Occurred During Depressurization.

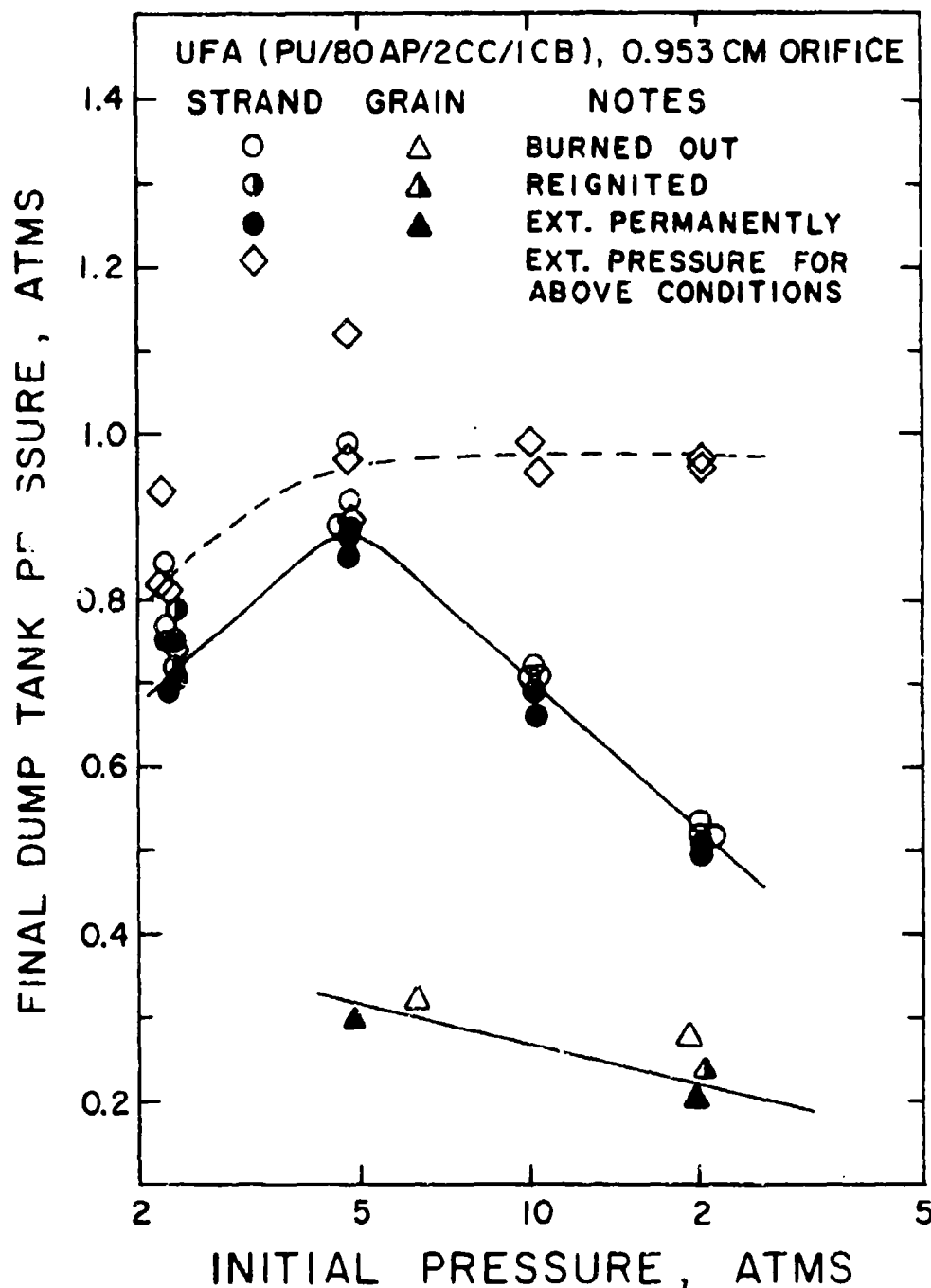


Figure VIII.3. Effect of the Initial Pressure on the Critical Dump-Tank Pressure for the Extinguishment of a Catalyzed PU Propellant (UFA) During Rapid Depressurization When the 0.953 cm Orifice Was Used [$-(d \ln p)/dt = 13.9 \text{ sec}^{-1}$]. Diamond Symbols Indicate the Chamber Pressures at Which Extinguishment Actually Occurred During Depressurization.

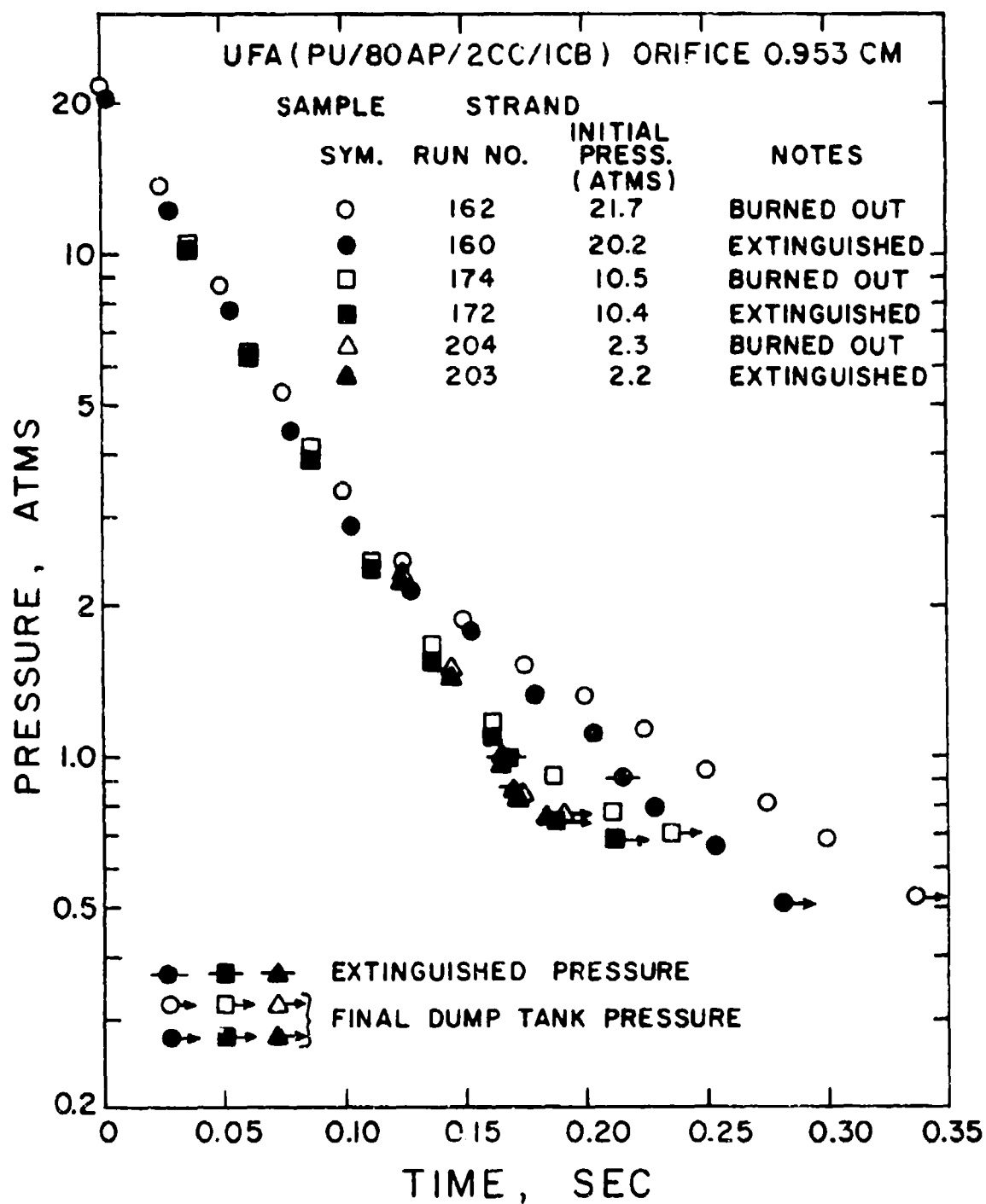


Figure VIII.4. Influence of the Initial Chamber Pressure on the Pressure Histories During Rapid-Depressurization Extinguishment Tests.

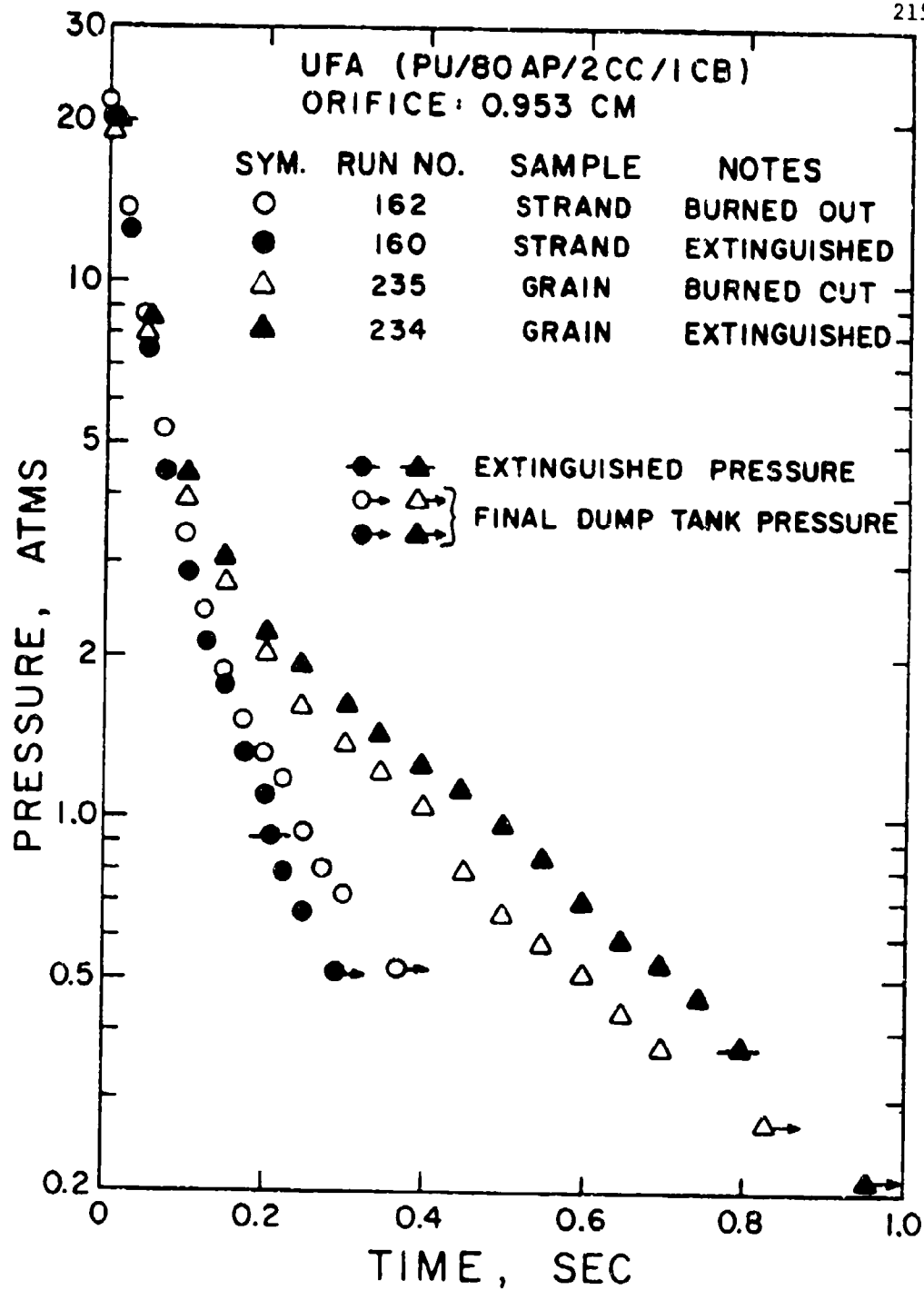


Figure VIII.5. Influence of the Sample Shapes on the Pressure Histories During Rapid-Depressurization Extinguishment Tests.

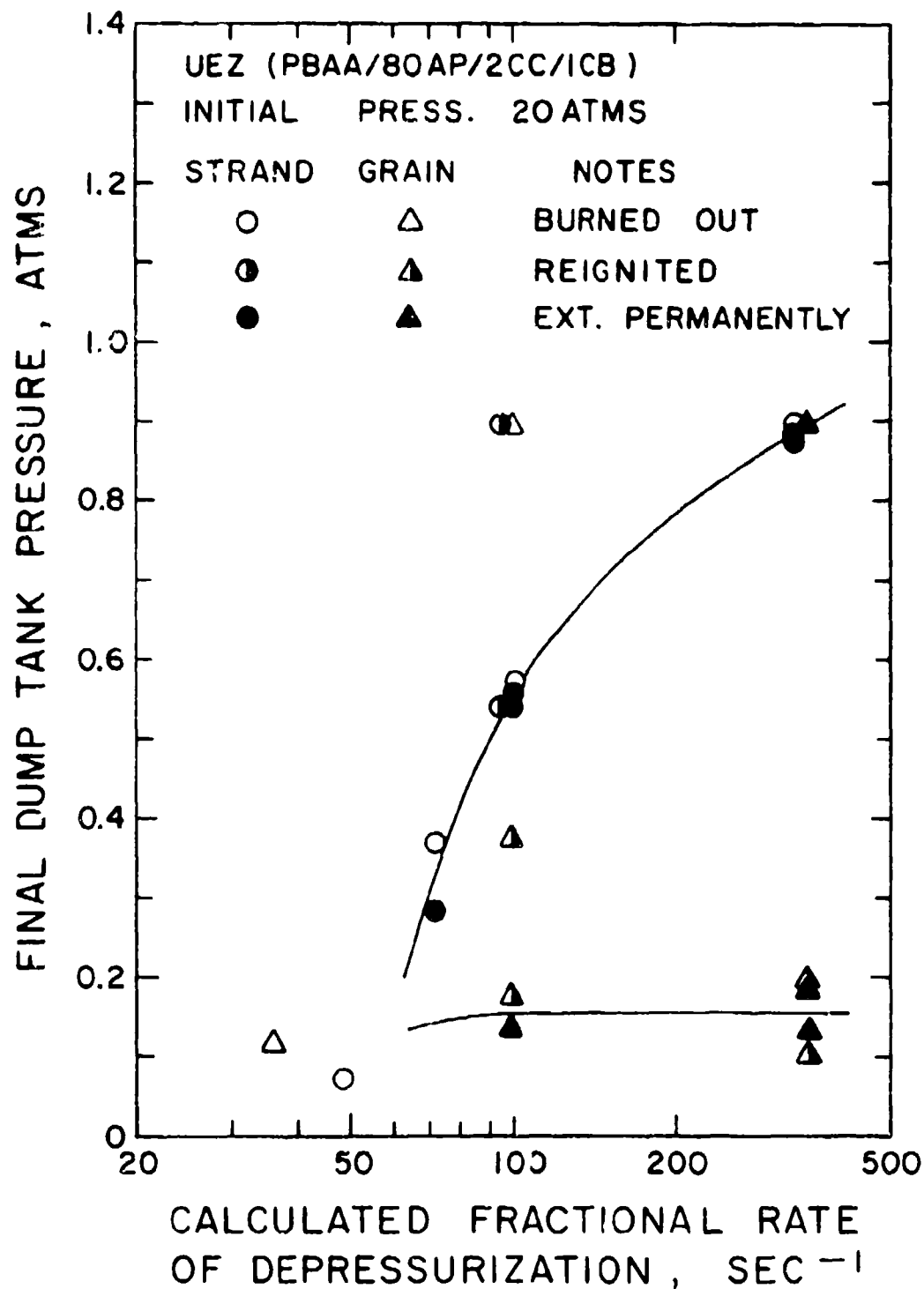


Figure VIII.6. Temporary and Permanent Extinguishment Requirements for a Catalyzed PBAA Propellant (UEZ).

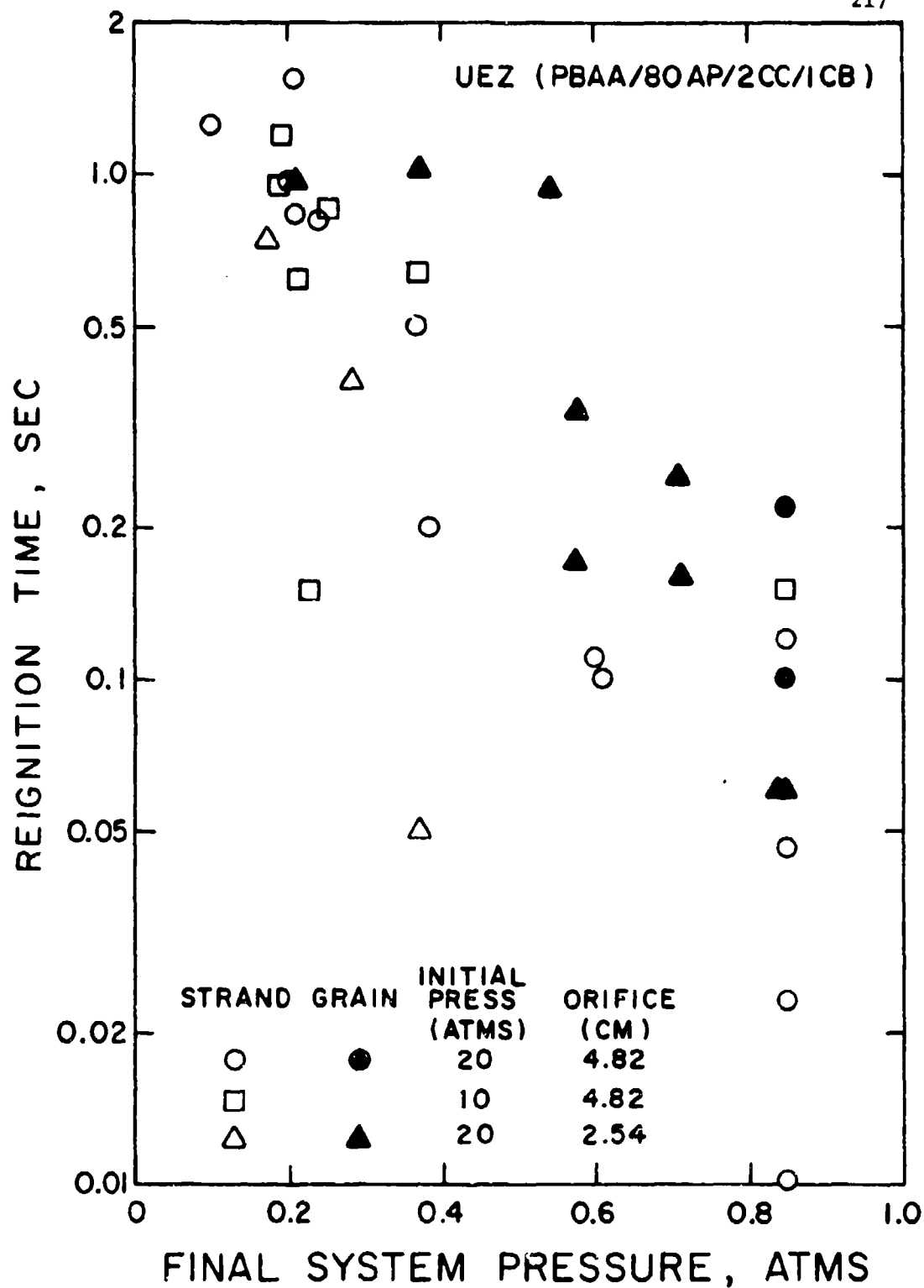


Figure VIII.7. Reignition Time as a Function of Final Dump-Tank Pressure for a Catalyzed PBAA Propellant (UEZ).

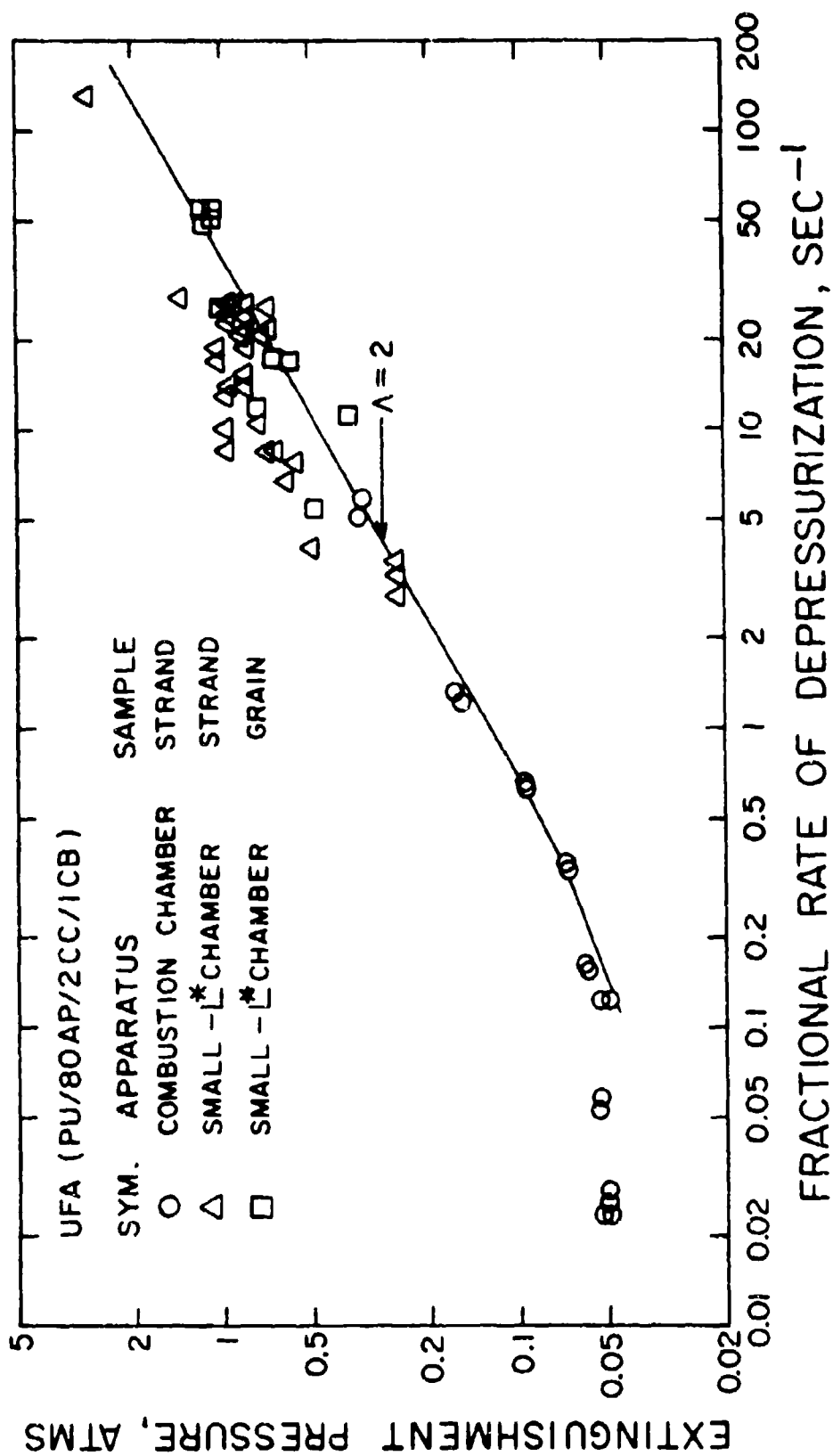


Figure VIII.8. Comparison of von Elbe-Type Theories and Extinguishment Data for a Catalyzed PU Propellant (UFA).

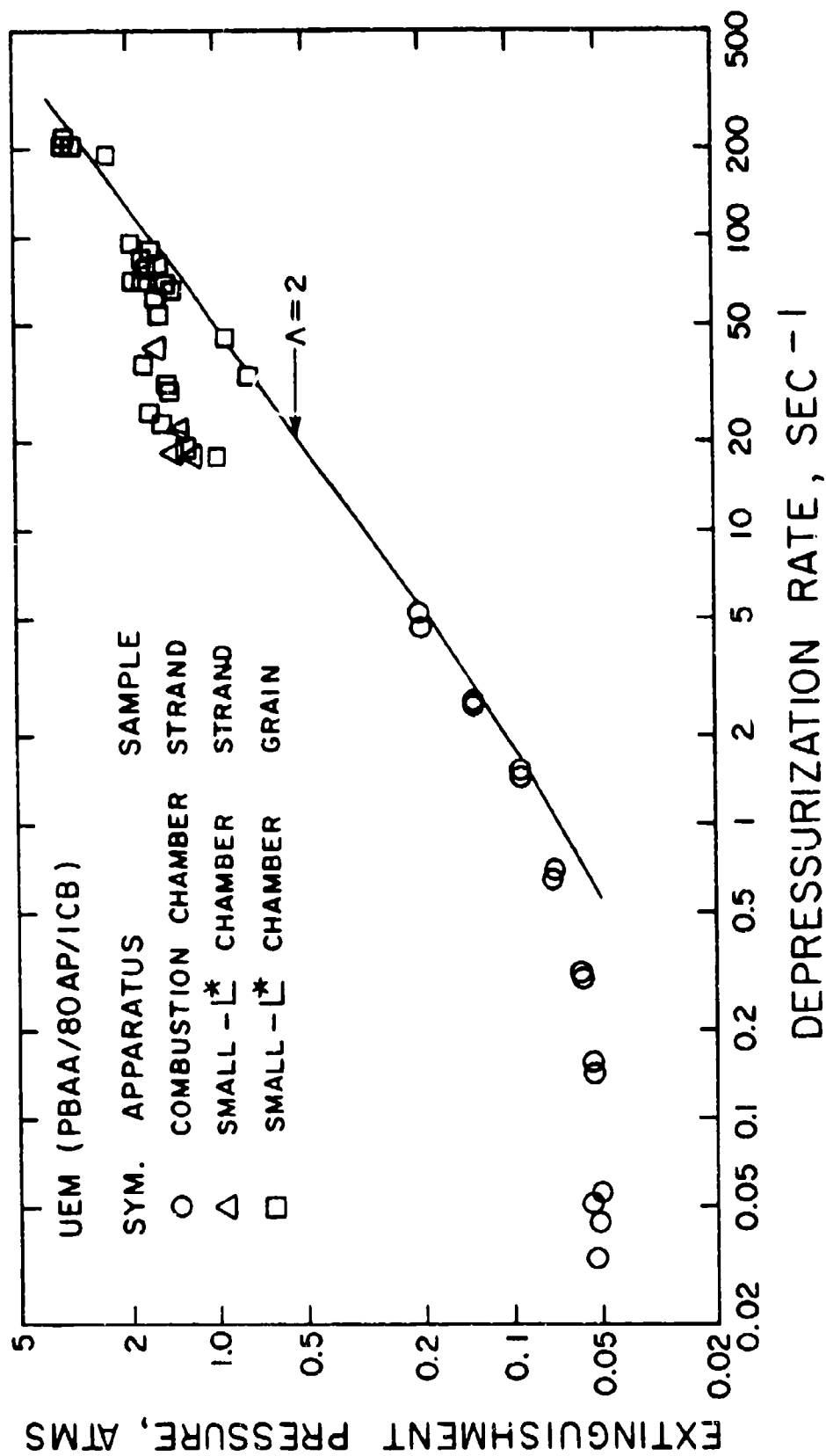


Figure VIII.9. Comparison of von Elbe-Type Theories and Extinguishment Data for an Uncatalyzed PBAA Propellant (UEM).

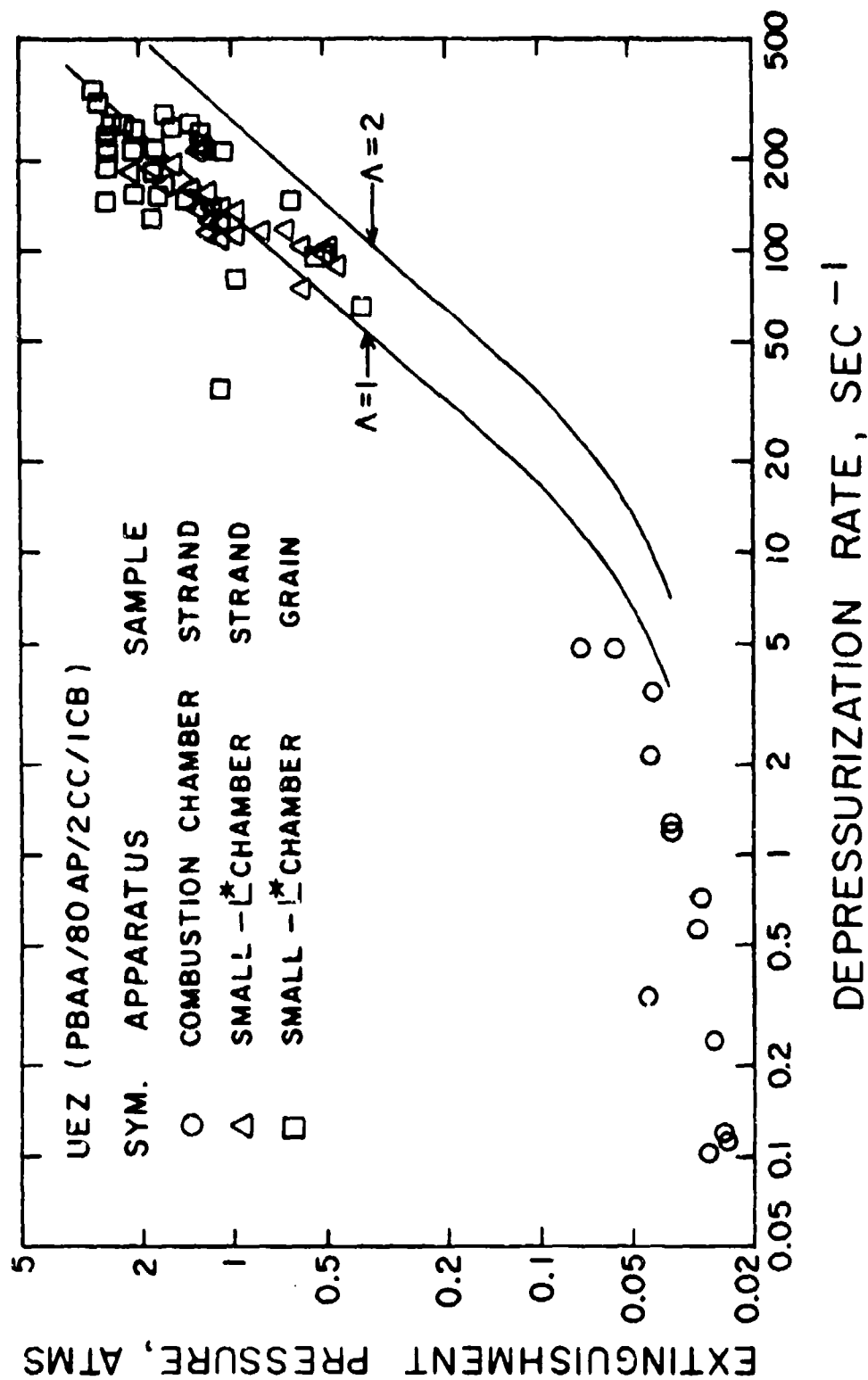


Figure VIII.10. Comparison of von Elbe-Type Theories and Extinguishment Data for a Catalyzed PBAA Propellant (UEZ).

Table VI.I. Net Heat of Gasification Calculated Using Heat-Flux-Augmented Burning Rate Data

Propellant Code	Pressure atms	$\frac{\partial r}{\partial f}$ cm ³ /cal	$\frac{1}{\rho \left(\frac{\partial r}{\partial f} \right)}$ cal/g	Net Heat of Gasification (cal/g) When c (T _s -T _o) is		
				100	130	160
UED	0.05	0.00728	81	-19	-49	-79
UED	0.06	0.00650	91	- 9	-39	-69
UFA	0.05	0.00608	97	- 3	-33	-63
UFA	0.06	0.00654	90	-10	-40	-70

Table VII.1. Summary of Blowdown-Type Extinguishment Data Using a Rarefaction
Tube Taken from the Previous Works at the University of Utah [26,83]

Propellant	Binder	%AP	AP Size μm	Additives	n	r (1.7 atms) cm/sec	α cm^2/sec	r^2/α sec^{-1}	Experimental $-(d \ln p)/dt$ sec^{-1}
UC	PU	80	200, 15	None	0.72	0.106	1.73×10^{-3}	9.0	12.7 - 12.9
AH	PBAA	75	15	None	0.57	0.175	1.66	32.5	40 - 60
G	PBAA	82	200, 15	None	0.52	0.173	1.73	33.1	40 - 60
UA	PBAA	73	15	2% Cu-0202P	0.57	0.373	1.63	150	200 - 250
F	PBAA	80	200, 15	2% CU-0202P	0.57	0.312	1.70	101	600 - 800

Table VII.11. Comparison of Others' Data Concerning Compositional Effect on Depressurization Extinguishment

Investigators	Test Apparatus	Test Conditions			Compositional Effect on Extinguishment				
		Initial Pressure atms	Exhaust Pressure	Criterion for Extinguishment	More Difficult to Extinguish When				
					Binder	Ap Level	Ap Size	AI	Catalyst
Ciepluch (27, 28, 29)	Motor	27-68	Atm. and Vacuum	Permanent and Temporary Ext.	PBAA-PU	Increased	Larger	Included	----
Ryan et al. (26) Mantyla (83)	Strand in Rarefaction Tube	2-12	Atm.	Permanent Ext.	P3AA-PU	----	Larger (Catalyzed)	----	Cu-0202P Included
Wooldrige et al. (134, 135)	Motor	20-70	Atm. and Vacuum	Permanent and Temporary Ext.	PU	----	----	Not Included	Iron Oxide Not Included
Jensen (67, 68)	Motor	15-70	Atm. and Vacuum	Permanent Ext.	CTPB>PU>CTPIB	Increased	Larger	Not Included for Temporary Ext.	Little Effect on Temporary Ext.
Merkle et al. (86)	Motor	15-70	Atm.	Temporary Ext.	CTPB=PEAA-PU	Increased	Smaller when Press.>20 atms Larger when Press.<20 atms	Included when Press.>27 atms Not included Press.<27 atms	----
Steinz and Seizer (122) Seizer (115)	Strand Bomb	20-100	Atm.	Permanent and Temporary Ext.	CTPB>PBAN>PU	----	Smaller	Included (CTPB)	Little Effect

Tabl. VIII.I. Summary of the Data of Rapid-Depressurization Extinguishment Tests

Propellant	Sample Shape	Orifice Size cm	Initial Pressure atm	Final Dump Tank Pressure, atm			
				Lowest Burned-out Pressure	Highest Reignition Pressure	Lowest Reignition Pressure	Highest Exinction Pressure
UEV	Hollow Grain	1.27	20				0.85
	Hollow Grain	0.953	20	0.212			0.212
	Hollow Grain	0.953	10	0.313			0.268
UEM	Hollow Grain	2.54	20				0.85
	Hollow Grain	2.54	10				0.85
	Hollow Grain	1.78	20		0.85	0.85	0.85
	Hollow Grain	1.78	10				0.85
	Hollow Grain	1.52	20		0.85	0.801	0.730
	Hollow Grain	1.52	10		0.85	0.770	0.744
	Hollow Grain	1.27	20	0.095			0.082
	Hollow Grain	0.953	10	0.108			0.086
	Strand	1.52	15		0.85	0.85	0.85
	Strand	1.27	15	0.500	0.496	0.493	0.456
UEZ	Hollow Grain	4.82	20		0.85	0.202	0.189
	Hollow Grain	4.82	10		0.85	0.192	0.178
	Hollow Grain	2.54	20	0.85	0.372	0.176	0.135
	Hollow Grain	1.52	20	0.122			
	Strand	4.82	20		0.85	0.85	0.85
	Strand	2.54	20		0.85	0.577	0.560
	Strand	2.16	20		0.85	0.372	0.279
	Strand	1.78	20	0.075			
	Strand	1.27	20				
	Strand	0.953	20	0.515			0.85
UFA	Strand	0.953	20	0.707			0.504
	Strand	0.953	10	0.891			0.694
	Strand	0.953	5	0.768	0.754	0.707	0.886
	Strand	0.953	2	0.230			0.704
	Strand	0.450	2	0.207			0.190
	Strand	0.450	5	0.214			0.193
	Strand	0.450	10	0.193			0.197
	Strand	0.450	20	0.197	0.199	0.199	0.190
	Strand	0.450	0.7				0.183
	Strand	0.450	0.7				
UFA	Hollow Grain	1.27	20	0.811	0.848	0.848	0.794
	Hollow Grain	1.27	5	0.814	0.811	0.804	0.807
	Hollow Grain	0.953	20	0.274	0.240	0.240	0.207
	Hollow Grain	0.953	5	0.327			0.294
	Hollow Grain	0.450	3	0.103			

APPENDIX A

EFFECT OF EXPERIMENTAL CONDITIONS
ON THE PRESSURE DEFLAGRATION LIMIT

It is necessary to standardize the experimental procedure if one is to measure the pressure deflagration limit of a propellant reproducibly. A preliminary study was therefore conducted to find its dependency on strand size, sample side inhibitor, environmental gas, flow rate of cooling nitrogen on the sample side, and initial strand temperature.

1. Effect of Strand Size on the Pressure Deflagration Limit

Figure A.1 shows the significant effect of sample diameter on extinguishment pressure. The form of the curve indicates an asymptotic pressure as the strand diameter increases. For the strand diameter bigger than 12 mm, little change in extinguishment pressure is noted. The results are quite similar to those reported by Cookson and Fenn [37]. It appears that the conductive and convective heat losses become insignificant when the sample diameter is bigger than 12 mm. However, the radiative heat loss from the burning surface remains, but its value per unit burning area may reasonably be assumed to be independent of strand diameter for diameters greater than 12 mm.

As suggested by Cookson and Fenn, it would be instructive to replot the same data in the coordinates of P_{dl} versus the ratio of strand diameter to cross-sectional area, which is a rough measure of the heat

losses from the burned gases relative to the radiative heat loss from the burning surface to the surroundings. This is done on Figure A.2. Contrary to their result, the data do not fall on a straight line so that the extrapolation of the line may intercept the P_{dl} ordinate at a finite value of the pressure. Instead, the straight line which best fits all the data goes through the origin. However, the data points corresponding to the three largest diameters fit a curve which extrapolates to a finite P_{dl} between 0.2 and 0.3 atms for infinite cross section. Thus, it is concluded that the conductive and convective heat losses become insignificant, and radiative losses are nearly constant, when the strand diameter is greater than 12 mm.

2. Effect of Strand Side Inhibitor and Environment Gas on Pressure Deflagration Limit

The strand burning behavior of a solid propellant at very low pressures was found to be influenced by the inhibitor material painted on the side of the strand and also by the ambient gas filling the combustion chamber. The effects were most pronounced for an uncatalyzed PU propellant, UEG, which is so formulated as to exhibit a marginal effect of binder melting (refer to Chapter IV). Other propellants were also influenced, but to a lesser degree. On Figure A.3, the experimental results for UEG propellant are summarized.

The Krylon is an acrylic solution made by Borden Inc. and Mr. Spray is a white paint made by Plasti-Kote Inc. It is noted that the white paint contains a small amount of cellulose nitrate as a vehicle. Combustion at low pressure is strongly promoted by Mr. Spray. The deflagration limit for a Krylon-inhibited strand, about 0.32 atms, is

reduced to 0.078 atms when Mr. Spray is used as an inhibitor. The use of air as an ambient gas replacing nitrogen, also promotes combustion, enabling deflagration at a pressure as low as 0.057 atms.

Different burning phenomena in different experimental conditions were also observed. A Krylon-inhibited strand burning in nitrogen exhibits periods of instability during burning near its deflagration limit. Flame quenching would start from one edge of the burning surface and propagate toward the center, leading to complete extinguishment if the chamber pressure was lower than the P_{dl} . If the chamber pressure was slightly higher than the pressure deflagration limit of the propellant, the quenching front stopped, and the flame recovered on the quenched area. The extinguished surface of Krylon-inhibited sample burned in nitrogen was always concave. This was true for all other propellants. The Mr. Spray-inhibited sample surface burned in nitrogen was flat except being slightly concave at the very center portion. A convex and rounded edge was displayed by a Krylon-inhibited sample burned in air.

As a consequence of all the above observations, it is apparent that when oxygen is available either in the ambient gas or the inhibitor, the resulting heat supply affects the deflagration limit even when the strand diameter is bigger than 12 mm. Krylon inhibitor and nitrogen environment were adopted as standard.

3. Effect of the Purging Rate of Cooling Nitrogen on Pressure Deflagration Limit

Thus far, the effect of conductive and convective heat losses on the P_{dl} has been discussed for a propellant strand burning in quiescent

ambient gases. The effect of heat losses by forced convection on the extinguishment pressure was also examined.

Figure A.4 shows the detectable effect of the rate of cooling nitrogen. The cooling nitrogen was introduced to the system to purge the force transducer and the sample side to minimize side heating in the furnace. The nitrogen gas was at ambient temperature. The extinguishment pressure monotonically increases to about 0.072 atm as the purging rate is increased to 8 liters per minute. An increase in purging rate to 15 liters per minute does not produce any more increase in extinguishment pressure. This result appears partly due to the increased combustion intensity at higher pressures and partly due to the diminishing effect of nitrogen purging rate on the forced convection in this apparatus.

Again, the importance of the conductive and convective heat losses is perceived. Since the combustion of solid propellant is so much susceptible to the external flow condition of the ambient gas, it was decided to take a quiescent ambient gas as a standardized experimental condition, except when the furnace was used.

4. Effect of Initial Strand Temperature on Extinguishment Pressure

The dependency of extinguishment pressure on the initial strand temperature was checked to construct basis for the experiments with the furnace. Cylindrical samples, 1.43 cm in diameter and 2.2 cm long, were preheated in a temperature-regulated oven for about 30 minutes. The sample temperature was continuously monitored by a thermocouple embedded at the center of the sample. When the sample center

temperature reached a desired value, the sample was mounted on a sample holder, around which nitrogen gas, regulated at the same desired temperature, was continuously purged before and during a test. The nitrogen temperature was regulated by flowing the nitrogen through a copper tube wound around a cartridge heater and by a temperature controller. In spite of these precautions, the sample temperature, continuously monitored by a copper-constantan thermocouple, failed to keep at steady level. The experiment had to be performed quickly after the sample was transferred to the test section. Extinguishment pressures were measured by depressurization methods.

The results are shown in Figure A.5. Later, the rates of depressurization adopted in these tests were found not to be small enough to give the real low pressure deflagration limit (refer to Chapter VII). As the extinguishment pressure for a same fractional rate of depressurization still could be a measure of the combustion stability, it is instructive to see the trend of extinguishment pressure as the initial temperature is increased. The data nearly fall on a straight line for a given rate of depressurization. As expected, the extinguishment pressure is lowered as the initial strand temperature is increased. The tendency, however, is mild. Only about 20% lowering in the extinguishment pressure was achieved by increasing the initial strand temperature by 40°C. If the initial temperature is maintained within 10°C of the standard, the extinguishment pressure can be measured with no more than 5% error from this source.

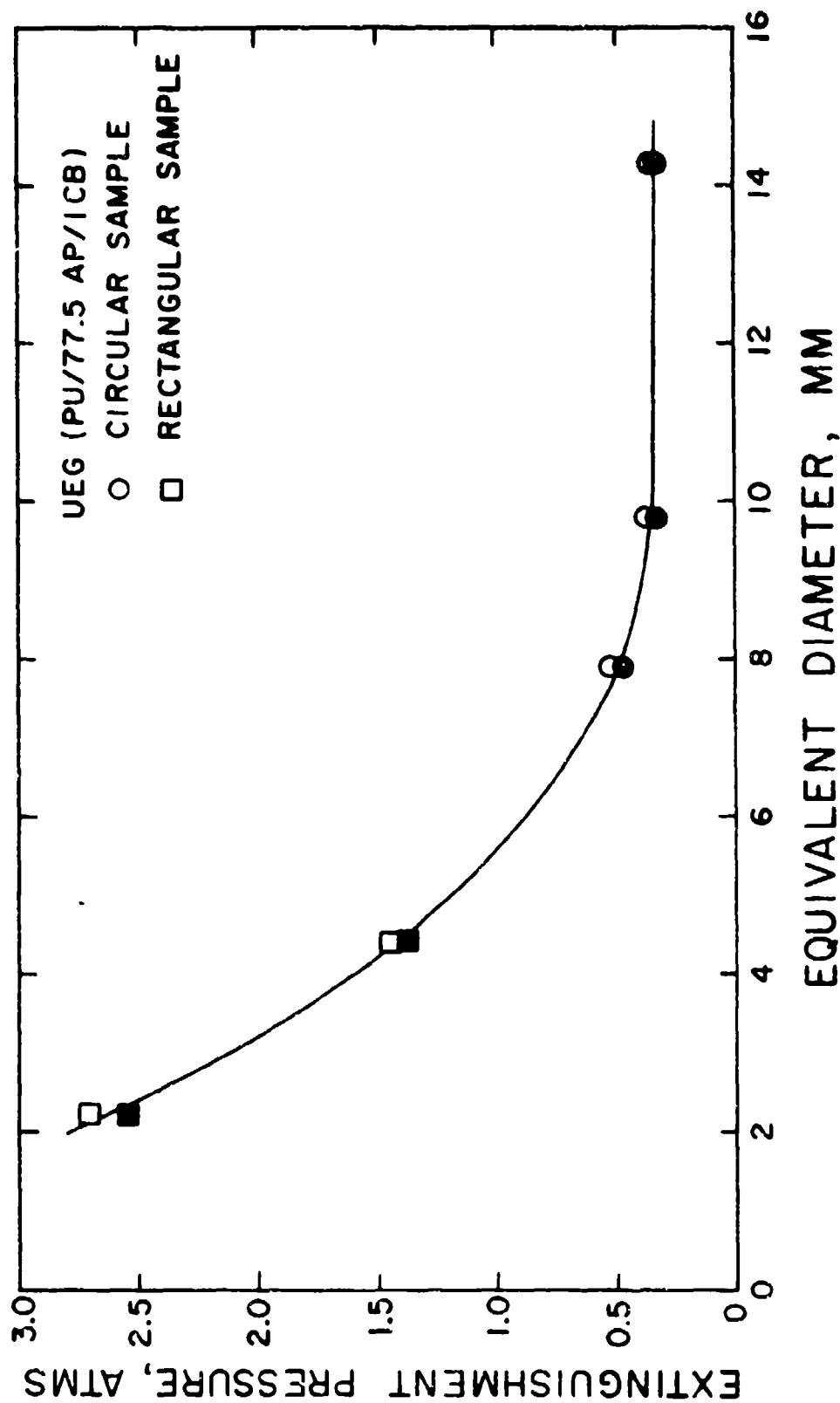


Figure A.1. Effect of Strand Size on the Pressure Deflagration Limit. Open Symbols Indicate Burned-out Conditions, While Filled Symbols Indicate the Intermediate Extinguishment. Tests Were Carried Out in a Quiescent Nitrogen Environment.

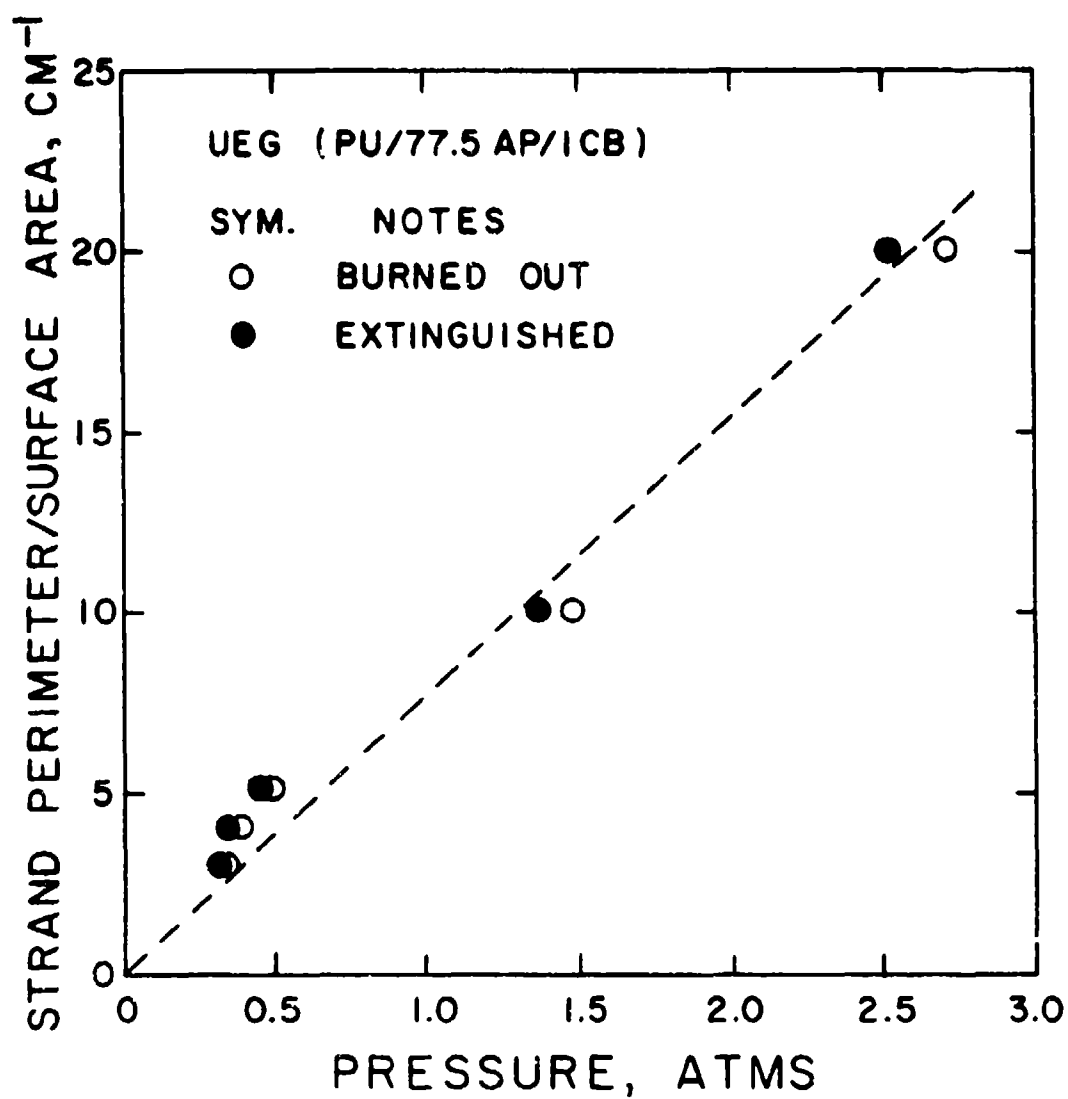


Figure A.2. Dependence of the Pressure Deflagration Limit on Strand Hydraulic Radius.

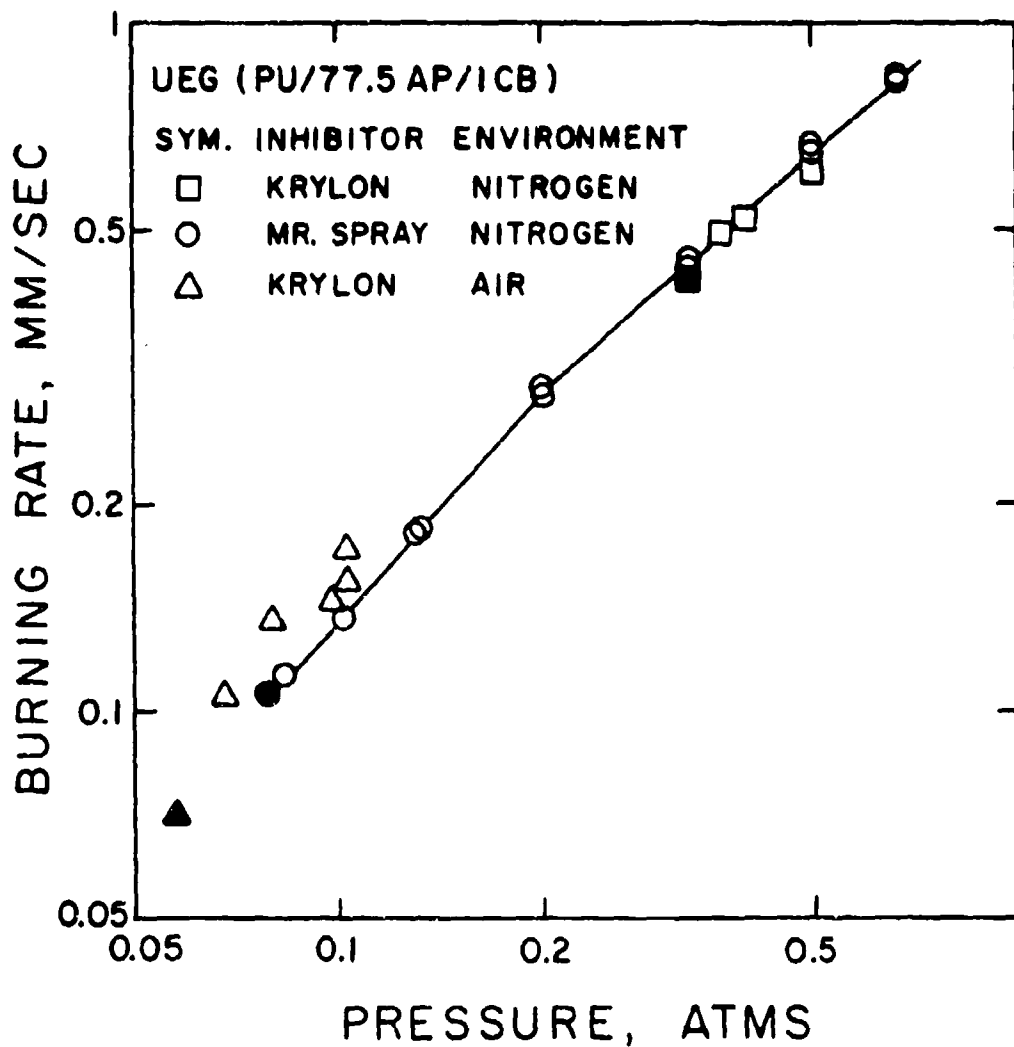


Figure A.3. Effect of Strand Side Inhibitors and Environmental Gases on the Pressure Deflagration Limit. Filled Symbols Indicate P_{dl} for the Given Conditions. Samples of 1.43-cm Diameter Were Used.

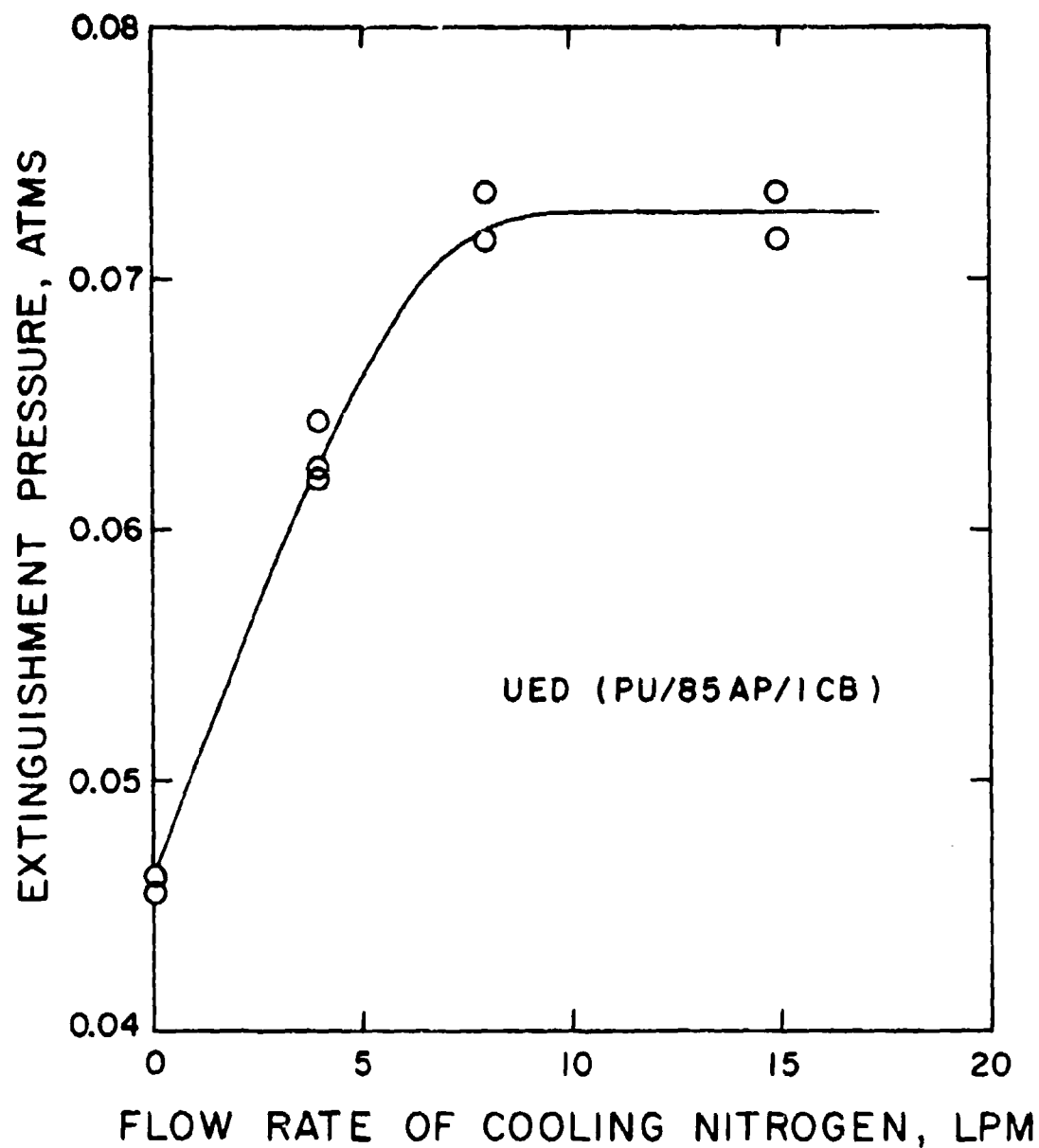


Figure A.4. Effect of the Flow Rate of Cooling Nitrogen on the Pressure Deflagration Limit. The Extinguishment Pressures Were Determined by the Slow Depressurization Method. The Rate of Depressurization Was 0.0060 sec^{-1} .

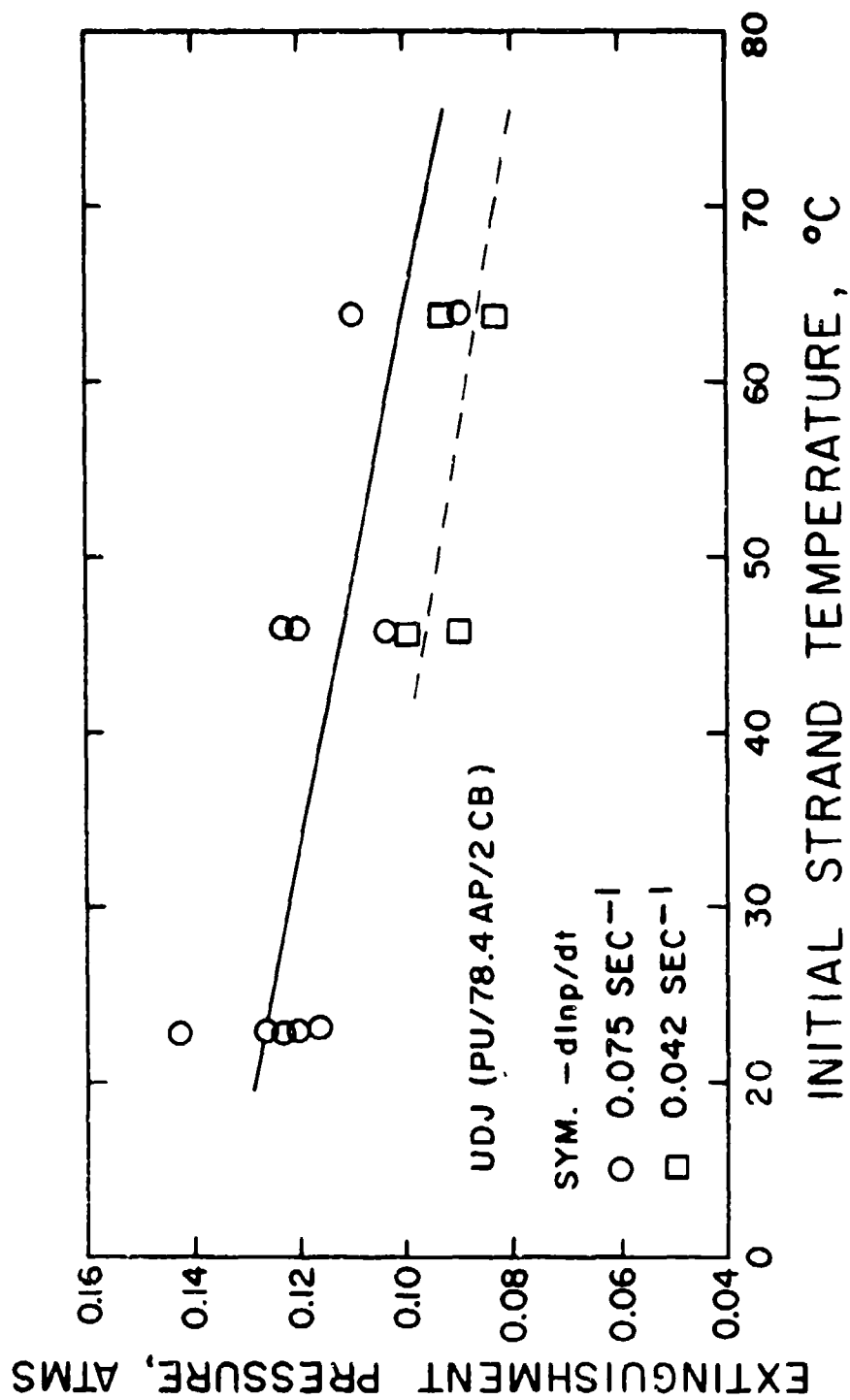


Figure A.5. Effect of the Initial Strand Temperature on the Extinguishment Pressure. The Extinguishment Pressures Were Determined by the Slow Depressurization Method.

APPENDIX B

PROPELLANT PREPARATION, COMPOSITIONS, AND PROPERTIES

1. Propellant Preparation

Because some moisture is absorbed in storage, just prior to mixing uncured binders, curatives, and ammonium perchlorate were dried for two to three hours in a vacuum oven set at 80°C. Uncured binders were dried until no more bubbles came out. Lauryl methacrylate monomer, which is readily oxidized at drying temperatures, was dried in the presence of nitrogen.

Sigma-blade mixers were used for mixing the propellant ingredients. The chosen mixer was preheated to about 60°C by circulating warm water. The propellant was mixed by the following procedure:

- (1) Weighed quantities of solid ingredients were added to the mixer in the following order: coarse AP, fine AP, and other additives.
- (2) The mixer was evacuated to about 25 torr and the solid ingredients were mixed for 15 minutes.
- (3) The vacuum was broken, the mixer opened, and the uncured polymer and the curative were added. For PLMA propellants, benzyl peroxide powder was dissolved in the lauryl methacrylate before the monomer was added to the mixer.

- (4) The mixer was evacuated to 25 torr and kept for 10 minutes, then started and operated for 20 minutes.
- (5) The mixer was stopped and opened, and the walls and blades were scraped with a spatula.
- (6) The mixer was then sealed and again evacuated, held for 5 minutes, then operated for 20 to 30 minutes.

Two types of molds were used. For slabs from which strands were later cut, shallow pans 16.5 cm x 11.4 cm in area and 1.27 cm deep were fabricated. Each pan held approximately 400 g of the propellant. Hollow grains were cast in sections of stainless steel tube, 2.2 cm i.d. and 2.38 cm long, with dowel pins of 0.635 cm in diameter arranged at the center. To cast 36 hollow grains in one mold, a total propellant mass of about 500 g was required. The inner surface of slab molds was lined with aluminum foil. Mold release agent (Rulon Spray #2, The Connecticut Hard Rubber Co.) was sprayed on the surface of the aluminum foil. The inner surface of hollow grain molds was doped with poly(vinyl alcohol) (Plastilease 512-B, Ram Chemicals, Gardena, California) so that the stainless steel hull could, after use, be easily cleaned by water. The molds were preheated to 80°C before the casting operation.

The viscous propellant mix was poured, spooned and tamped into the heated molds at atmospheric pressure. The filled molds were put in the vacuum oven maintained at 80°C temperature. After 10 minutes' warming time, the oven was evacuated to 7 torr. After about 10 minutes, the mold was taken out of the oven and the gas bubbles were worked out of the soft propellant. This vacuuming and kneading procedure was repeated two or three times until the bubbling from the propellant surface was no more significant. Then the propellant was

transferred to the main oven, for final cure at atmospheric pressure and a temperature appropriate for curing the given propellant. The surfaces of PLMA propellants were covered by high temperature wax to prevent them from air contact. The curing temperatures and times were as follows:

<u>Binder Type</u>	<u>Curing Times, Days</u>	<u>Curing Temperature, °C</u>
PBAA	5	80
PU	2	80
HTPB	4-5	57.5
PLMA	2	90-93

The cured propellant was wrapped with the aluminum foil and stored for future use. When a series of runs was planned, test specimens were cut from the slabs. Newly cut surface was coated with Krylon acrylic solution. Just before a test, the coating was trimmed away from the surface to be ignited.

The fluorocarbon propellant (TPF 1006) was supplied by the Wasatch Division of the Thiokol Chemical Corporation, Brigham City, Utah, already in the form of cured slabs 1.27 cm thick.

2. Propellant Compositions and Properties

The designations and compositions of all the propellants employed in this study are listed in Table B.I along with their low pressure deflagration limits.

The properties of propellants were mostly calculated from the properties of the ingredients. Densities were also measured by weighing specimens of measured dimensions. The measured density of a propellant

compared favorably with the theoretical value, as shown in Table B.II. Table B.II also contains the calculated thermal capacities, thermal conductivities and thermal diffusivities of various propellants which were extensively employed in this study. Using the properties of ingredients shown in Table B.III, the theoretical calculations of properties were carried out in the following ways:

Density

$$\frac{1}{\rho} = \sum_1 \frac{w_1}{\rho_1} \quad (B-1)$$

where ρ is the density of the propellant and w_1 and ρ_1 are mass fraction and density of the i^{th} ingredient respectively.

Heat capacity

$$c = \sum_1 w_1 c_1 \quad (B-2)$$

where c is the heat capacity of the propellant and c_1 is the heat capacity of the i^{th} ingredient.

Thermal conductivity

The Maxwell equation, as used by Gorrington and Churchill [51] for the calculation of thermal conductivity of heterogeneous materials and also adopted by other Utah investigators [9,68], was employed to calculate the thermal conductivity of propellants:

$$k = \frac{2 + v - 2\eta(1-v)}{2 + v + \eta(1-v)} \quad (B-3)$$

where v is the ratio of the thermal conductivities of the discontinuous phase to that of continuous phase, n is the volume fraction of discontinuous phase, k_a is the thermal conductivity of the continuous phase, and k is the conductivity of the propellant. According to references [9] and [68], Eq. (B-3) predicts the thermal conductivity within 3 to 4 percent of the measured value.

Thermal diffusivity

Thermal diffusivity was calculated by the definition,

$$\alpha = \frac{k}{\rho c} \quad (B-4)$$

Table B.1. Propellant Formulations and Their Pressure Deflagration Limits

Propellant Code	Binder ¹		Ammonium Perchlorate ²		Additive, Wt%			Pressure Deflagration Limit, atms ⁶	
	Type	Wt%	Size	Wt%	Carbon Black ³	Copper Chromite ⁴	Aluminum ⁵	Without Cooling Coil	With Cooling Coil
UG	PU	20	BM(50/50)	80				0.042	
UDE	PU	15	BM(50/50)	85				0.037	
UDF	PU	30	BM(50/50)	70				5.45	
UDG	PU	20	BM(50/50)	80			5	0.036	
UDI	PU	19	BM(50/50)	76				0.486	
UDJ	PU	19.6	BM(50/50)	78.4				0.046	
UDK	PU	19.6	BM(50/50)	78.4	2	2		0.085	
UCS	PU	50	BM(50/50)	50				10.1	
G	PBAA	18	BM(50/50)	82				0.038	
UDL	PBAA	20	BM(50/50)	80	1			4.17	
UDR	PU	24	15 μ	75	1				
UDS	PU	24	-200 +325	75	1			1.05	
UDT	PU	24	-150 +200	75	1			0.346	
UDU	PU	24	- 48 +100	75	1			0.192	
UDV	PU	24	400 μ	75	1			0.034	
UDW	PU	24	600 μ	75	1			0.022	
UDX	PBAA	24	15 μ	75	1			0.027	
UDY	PBAA	24	-200 +325	75	1			0.023	
UDZ	PBAA	24	-150 +200	75	1			0.029	
UEA	PBAA	24	- 48 +10	75	1			0.043	0.054
UEB	PBAA	24	400 μ	75	1			0.040	0.048
UEC	PBAA	24	600 μ	75	1			0.042	0.044
UED	PU	14	BM(60/40)	85	1				
UEE	PU	16.5	BM(60/40)	82.5	1				
UEF	PU	19	BM(60/40)	80	1				
UEG	PU	21.5	BM(60/40)	77.5	1				
UEH	PU	24	BM(60/40)	75	1			0.780	
UEI	PU	26.5	BM(60/40)	72.5	1			1.41	
UEJ	PU	29	BM(60/40)	70	1			2.69	
UEK	PU	17	BM(60/40)	80	1	2			0.049
UEF	PU	14	BM(60/40)	80	1				0.046
UEG	PBAA	14	BM(60/40)	85	1			0.055	0.063
UEH	PBAA	16.5	BM(60/40)	82.5	1			0.053	0.053
UEI	PBAA	19	BM(60/40)	80	1			0.046	
UEJ	PBAA	21.5	BM(60/40)	77.5	1			0.040	
UEK	PBAA	24	BM(60/40)	75	1			0.023	0.027
UEL	PBAA	26.5	BM(60/40)	72.5	1			<0.022	0.017
UEM	PBAA	29	BM(60/40)	70	1			<0.022	<0.016

Table B.1. Propellant Formulations and Their Pressure Deflagration Limits (continued)

Propellant Code	Binder ¹		Ammonium Perchlorate ²		Additive, Wt%			Pressure Deflagration Limit, atm ⁶	
	Type	Wt%	Size	Wt%	Carbon Black ³	Copper Chromite ⁴	Aluminum ⁵	Without Cooling Coil	With Cooling Coil
UEZ	PBA	17	BH(60/40)	80	1	2	5	0.037	0.053
UEB	PBA	14	BH(60/40)	80	1			0.046	0.035
UEV	HTPB	14	BH(60/40)	85	1			0.033	0.033
UEW	HTPB	19	BH(60/40)	80	1			0.027	0.053
UER	HTPB	21.5	BH(60/40)	77.5	1	2	5	1.55	0.044
UEX	HTPB	17	BH(60/40)	80	1			0.694	
UEY	HTPB	14	BH(60/40)	80	1			0.057	
UES	PLMA	19	BH(60/40)	80	1			5.53	
UET	PLMA	16.5	BH(60/40)	82.5	1				
UEU	PLMA	14	BH(60/40)	85	1				
TPF 1006	FC	16	---	84					

Notes for Table B.1.

1. Binder:

FC, polyurethane binder, consists of 93.75 weight percent Estane (B. F. Goodrich 5720 x 5) and 6.25 weight percent curative from Thiokol Chemical Corp.

PBA, polybutadiene-acrylic acid copolymer binder, contained 85 weight percent polybutadiene acrylic acid obtained from Thiokol Chemical Corp. and 15 weight percent Epon 828 epoxy curative from Shell Oil Co.

HTPB, hydroxyl-terminated polybutadiene binder, was composed of 92.53 percent Polybutadiene Liquid Resin R-45HT manufactured by Atlantic Refining Co. (Lot No. 106012, OH No. 0.85 meq/100g) and 7.47 percent IPDI (isophorone diisocyanate, NCO No. 0.895 meq/100g) from Dexter Corp.

PLMA, poly(lauryl methacrylate) binder, was prepared by curing lauryl methacrylate monomer obtained from Thiokol Chemical Corp. with 0.5 percent benzoin peroxide.

FC, fluorocarbon binder, was fluoroalkyl acrylate manufactured by Thiokol Chemical Corp.

2. Ammonium perchlorate:

BH(50/50) denotes bimodal mixture of 50 percent coarse (-48 +100) and 50 percent fine (150) ammonium perchlorate. The coarse one was obtained by screening the as-received ammonium perchlorate purchased from American Potash and Chemical Corp. (No. EC-4). The fine one was the as-received ammonium perchlorate from the same company, having the particle size distribution of 50 percent under 150 and 400 and 600 ammonium perchlorate were supplied by the Naval Weapons Center. The same materials were used by Eisel (47).

3. Sterling VR carbon black was obtained from the Cabot Corp.

4. Copper chromite catalyst was obtained from Harshaw Chemical Company and contains approximately 82 percent CuO and 17 percent Cr₂O₃.

5. The aluminum designated as Grade 1-131-atomized powder (50 percent smaller than 12 microns) was obtained from the Reynolds Metals Co.

6. Those values of the pressure deflagration limit are the average of the closest extinguished and burned-out pressures.

Table B.II. Thermophysical Properties of Propellants.

Propellant Code	Density, ρ g/(cm) ³		Heat Capacity c cal/(g)(°K)	Thermal Conductivity k cal/(cm)(sec)(°K)	Thermal Diffusivity α cm ² /sec
	Measured	Calculated			
UEK	1.70	1.70	0.301	0.916×10^{-3}	1.79×10^{-3}
UEL	1.65	1.66	0.306	0.874	1.72
UEM	1.64	1.63	0.310	0.853	1.69
UEN	1.61	1.59	0.315	0.823	1.64
UEO	1.60	1.56	0.320	0.799	1.60
UEP	1.59	1.53	0.325	0.775	1.56
UEQ	1.55	1.50	0.330	0.753	1.52
UEZ	1.67	1.68	0.304	0.878	1.72
UFB	1.74	1.72	0.298	0.969	1.89
UED	1.70	1.74	0.301	0.930	1.78
UEE	1.71	1.71	0.306	0.899	1.72
UEF	1.67	1.68	0.310	0.871	1.67
UEG	1.64	1.65	0.315	0.842	1.62
UEH	--	1.62	0.320	0.815	1.57
UEI	--	1.59	0.325	0.792	1.53
UEJ	--	1.57	0.330	0.771	1.49
UFA	1.70	1.73	0.304	0.895	1.70
UFC	1.74	1.76	0.298	0.987	1.88
UEW	1.67	1.69	0.301	0.912	1.79
UEV	1.60	1.61	0.310	0.847	1.70
UER	1.57	1.57	0.315	0.816	1.65
UEX	1.68	1.66	0.304	0.872	1.73
UEY	1.66	1.71	0.298	0.965	1.89

Table B.III. Thermophysical Properties of Propellant Ingredients

Ingredients	Temperature °C	Heat Capacity cal/(g)(°K)	Density g/(cm) ³	Thermal Conductivity cal/(cm)(sec)(°K)
PBAA Binder ¹	60	0.465	0.956	0.437×10^{-3}
PU Binder ²	--	0.465	1.057	0.437×10^{-3}
HTPB Binder ²	--	0.465	0.923	0.437×10^{-3}
Ammonium Perchlorate ³	60	0.275	1.95	1.19×10^{-3}
Carbon Black ⁴	--	0.204	1.88	0.156×10^{-3}
Copper Chromite ³	--	0.146	6.15	2.17×10^{-3}
Aluminum ⁵	20	0.214	0.2699	0.50

1. The thermophysical properties of PBAA binder were taken from Keller's thesis [72].

2. The heat capacities and thermal conductivities of PU and HTPB binder were assumed to be the same as those of PBAA binder. The densities of PU and HTPB binder were obtained from the report of Steinz et al.[123].

3. The thermophysical properties of those ingredients were taken from Cheng's thesis [25].

4. The thermophysical properties of Sterling VR carbon black were assumed to be the same as those of Philblack E as given in Cheng's thesis.

5. The properties of aluminum were obtained from Kirk-Othmer Encyclopedia of Chemical Technology, Second Ed.

Vol. 1, p. 948, John Wiley and Sons, Inc. (1964).

APPENDIX C

EXPERIMENTAL APPARATUS AND CALIBRATION DATA

1. Flow and Pressure Control Components for the Combustion Chamber

The flow diagram for the combustion chamber is shown in Figure

C.1. The descriptions of the components are as follows:

<u>Component</u>	<u>Descriptions</u>
Combustion Chamber:	25 cm i.d. 44 cm height (approximately 20 liters in volume), designed and tested for maximum pressure of 200 psig, custom-made, nickel-plated.
Main Dump Tank:	1,300 liters in volume, evacuated by a type MD674 Nash Hytor Vacuum Pump in series with a No. 2-26-6 Nash Air Ejector. An absolute pressure about 0.016 atms could be maintained. The vacuum system was made by the Lang Wayne Equipment Company of Salt Lake City, Utah.
Auxiliary Dump Tank:	60 liters in volume, maximum allowable pressure 60 psig.
Main Exhaust Valve:	1-inch-port ball valve operated by Ramcon pneumatic actuator (Model P35FS

80 psi, Ramcon Division, Penwalt Corp., Elgin, Illinois).

Auxiliary Exhaust Valve: 3/8-inch needle valve operated by a pneumatic cylinder (Type A-II, Allenair Corp., Mineola, New York).

Main Orifices: 0.953, 0.238, and 0.159-cm orifices were sharp-edged ones made of graphite. The other orifices were smooth-edged stainless steel ones originally used by Schulz (refer to Table C-III).

Auxiliary Orifices: Sharp-edged graphite orifices, 0.635, 0.594, 0.475, 0.437, 0.356, 0.277, 0.198 cm in diameter, were used.

Main Exhaust Line: 1-1/2-inch pipe, approximately 4 feet long.

Auxiliary Exhaust Line: Consisted of two portions, one 3/8-inch diameter and 3 feet long and another 1-1/4-inch diameter and 7 feet long.

2. Electric Circuit for the Combustion Chamber

Figure C.2 shows the electric circuit diagram for the combustion chamber. Two control panels were used: one was located in the control room (shown on the top part of the diagram) and the other in the tunnel near the experimental apparatus. The REMOTE-LOCAL switch was designed to select one of the panels. Toggle switches and a push button switch (for nitrogen supply) were used for the hand control of tests. A pre-determined automatic sequence was generated by pushing the AUTO and

then the START push button with desired settings on timers T-1, T-2, and T-3 and on the pressure switch PS-1. After a run by automatic sequence was over, the circuit was reset by pushing the RESET push button. The RESET push button was also used to interrupt the automatic sequence during a test. Either the RESET button on the control room panel or that on the panel inside the tunnel was designed to be always ready for functioning regardless of the position of the REMOTE-LOCAL selector switch.

Automatic operation of the control circuit for the depressurization extinguishment test was used for tests in both the combustion chamber and the low-L* chamber. When the combustion chamber was used, the pressure switch was removed from the circuit because it was not needed. During tests with the smaller chamber, the timer T-1 was disconnected. The rest of the control circuit was the same for both cases.

After preparation for a run was made, an extinguishment test proceeded as follows:

- a. The electric power was introduced by the MAIN switch.
- b. The evacuated chamber was filled with nitrogen to the desired level by pushing NITROGEN ON button. When the large chamber was used, the nitrogen flow was discontinued after the chamber pressure reached the desired level, whereas it was allowed to continue when the small chamber was employed.
- c. The remote or local control of the test was determined by the REMOTE-LOCAL selector switch.

- d. The AUTO button was operated to give the following events: the magnetic switch MS-2 supplied electric power to the automatic power line and the relay R-6 was energized to close its contact R-6, which was normally open to isolate the automatic circuit from hand operating switch.
- e. The START button was pushed: the relay R-1 started the timer T-1 and energized the relay R-4 which stopped the nitrogen feeding and closed the ignition power lines (the timer T-1 was not adopted in small-chamber tests).
- f. Either when the set time on the timer T-1 was over (in combustion chamber tests) or when the system pressure reached the set pressure on the pressure switch PS-1 by the help of combustion products (in small-chamber tests), the relay R-2 was energized. The relay R-2 opened the auxiliary exhaust valve (this valve was disconnected in small-chamber tests) and started timers T-2 and T-3.
- g. When the set time on the timer T-3 was over, the oscilloscope triggering circuit was closed, if the oscilloscope was used.
- h. The timer T-2 energized the relay R-5 after the set time was over. The relay R-5 closed the auxiliary exhaust valve, simultaneously opening the main exhaust valve V-1. The relay R-5 also stopped the

power to the ignition line by opening the coil circuit of the relay R-4.

1. After a test was over, the RESET button was pushed which cut the power to the automatic circuit by de-energizing the magnet switch MS-2 and also released the relay R-2 by the help of the relays R-8 and R-2'.

3. Circuits and Components of Measuring Units

The schematic circuit diagram for the force transducer, the pressure transducer, and for photocells are given in Figures C.3, C.4, and C.5 respectively. The detailed descriptions of the key elements in those circuits and of the other instruments for data acquisition and reduction are as follows:

<u>Component or Instrument</u>	<u>Descriptions</u>
Force Transducer:	The Universal Transducing Cell Model UC3, Force Range +60 gms, Statham Instruments, Inc., Oxnard, California.
Pressure Transducer 1:	PA285TC-150-350, 0-150 psia, or
Pressure Transducer 2:	PA731TC-25-350, 0-25 psia, Statham Instruments, Inc.
Pressure Transducer 3:	Kistler Model PZ 14 quartz pickup, Kistler Instrument Corp., North Tonawanda, New York.
Photocell 1:	Type 1N2175 N-P-N Diffused Silicon Photo-Duo-Diode, Texas Instruments, Dallas, Texas.

Photocell 2:	1P40 Infrared-Sensitive Gas Photo- diode, Radio Corporation of America, Harrison, New Jersey.
24VDC Supply:	Model KR 24-.25, Universal Elec- tronics, Santa Monica, California.
Strip Chart Recorder 1:	Speedomax XL 600 Recorder, two-pen, Leeds and Northrup Co., North Wales, Pennsylvania.
Strip Chart Recorder 2:	Electronic 19 Recorder, Honeywell Inc., Denver, Colorado.
Oscilloscope:	Tektronix Model 564, Tektronix Inc., Portland, Oregon.
Oscilloscope Camera:	Tektronix Model C-2.
DC Amplifier 1:	Accudata 120, Model No. ACC-120-1, Honeywell Inc., Denver, Colorado.
DC Amplifier 2:	CRC AMPLI-VOLT, The Chemical Rubber Co., Beacon, New York.
Charge Amplifier:	Kistler S/N 166 Model 568.
Tape Recorder:	Model PI-1207, Precision Instrument, Palo Alto, California.

The force transducer was calibrated by weights and the linearity of the output with respect to the weight load was found to be excellent. Before a series of tests, an appropriate calibration factor, the output voltage per unit mass, was chosen by adjusting the input rheostat with a reference weight applied on the transducer. The zero adjustment

potentiometer was used to bring the output signal to an adequate position on the recorder. Both the input rheostat and the zero adjustment potentiometer were ten-turn Helipot precision potentiometers. The relatively low resistance of 4.7 K Ω employed in the zero adjustment potentiometer enabled to bring the output signal to zero with a load as much as 45 gm. A 24VDC power supply was replaced by a 22.5V battery when the weight signal was recorded on the oscilloscope since it produced some AC noise. The low pass filter was designed to cut off the noise in force transducer signal originated from its natural frequency about 100 Hz. The cut off frequency of the low pass filter was 22 Hz.

The circuit shown in Figure C.4 was utilized for both Statham transducers. The 12V battery was a rechargeable Cd-Ni cell. The zener diode 1N752 (zener breakdown voltage 5.6V) maintained the excitation voltage at a constant level. Pressure transducers were calibrated with a dead-weight tester. Again, the linearity between the pressure and output was good within the normal range of each unit.

Figure C.5 actually depicts two different circuits; one for a 1N2175 photodiode and the other for a 1P40 photocell.

4. Calibration of the Quick Heating Furnace

The quick heating furnace and its control circuit, as shown in Figure III.5, consist of the following major components:

<u>Component</u>	<u>Descriptions</u>
Nichrome Strip:	Tophet A Nickel Chrome, Size 1/4 x 0.0201", Ohms per foot 0.1005, Wilbur B. Driver Co., Newark, New Jersey.

Temperature Controller: Electromax C.A.T. Controller, Cat. No.
6261-2110-1-0, Range 93-1093°C,
Leeds and Northrup Co.

SCR Switch: Zero Voltage Power Pack, C12,
1144TP 1970, Leeds and Northrup Co.

Stepdown Transformer: Input 220V, 10:4 I/O ratio, Berg
Electric Co., Salt Lake City, Utah.

Thermocouples: 0.01 inch chromel and alumel type.

Calorimeter: Used for calibration:
Asymptotic Calorimeter, Model
C-1301-A-120-072, Hy-Cal Engineering,
Santa Fe Springs, California.

The performance of the temperature controller was checked by comparing the set temperature and the actual temperature of the nichrome strip which was indicated by the thermocouple output. The calibration was undertaken at two pressures, 0.85 atms and 0.01 atms. No significant effect of pressure was noted. As shown in Table C.I, the actual wall temperatures are slightly lower than the set temperatures, the offset increasing as the set temperature is increased. The offset is, however, less than ten degrees when the set temperature is less than 850°C. These calibration data related the true wall temperature to the given set temperature since the furnace set temperature was taken as the experimental variable. Also are shown the furnace heating time with and without the radiation deflector. The effect of the deflector on the heating time becomes pronounced as the

furnace set temperature is increased. When the furnace set temperature is less than 800°C, the furnace can be brought to the set temperature within a half minute.

The furnace radiation heat flux, reaching to the position where the propellant burning surface would be located, was calibrated with respect to the actual furnace wall temperature with the Hy-Cal calorimeter. An Electronic 19 recorder was used to record the thermocouple output. The calibration data are plotted in Figure C.6 along with the black body emissive power. The actual radiation flux is approximately two-thirds of the black-body flux corresponding to the measured temperature with the radiation deflector installed and only one-third of it without the radiation deflector. The spatial variation of the radiation flux was examined for three positions: 0, 1.27, and 2.22 cm above the bottom plate of the furnace. As seen from Figure C.6, the higher position receives slightly more radiation heat flux. The variation of the radiation heat flux between 1.27 cm and 2.22 cm position is noticed to be less than three percent. The propellant burning during a test usually occurred between those distances. Consequently, for the zone of interest the spatial variation of the radiation flux was concluded to be negligible.

The heating rate of propellant samples exposed to furnace heat flux was measured to standardize experimental procedures. Under the conditions for an actual depressurization extinguishment tests with furnace heating, but without the propellant burning, the temperature at the center of the sample was monitored by 0.005-inch-diameter copper-constantan thermocouples. The results are presented in

Table C.II. It is noted that almost a minute is required to heat up samples similar to those used in the extinguishment test by ten degrees when the furnace temperature is 700 to 800°C.

5. Pressure History During Depressurization Extinguishment Tests

A universal representation of the depressurization rate was needed to compare the extinguishment data from different apparatus. Although the actual measurement of the pressure history fulfils this requirement, an approximate estimation of the fractional pressure decay rate can be made by the volume and orifice size. With the assumption of an ideal nozzle, the theoretical pressure-time relationship during the blowdown of a chamber is given by the following equations:

Adiabatic blowdown

$$\frac{p}{p_o} = \left(\frac{1}{1 + \frac{\gamma - 1}{2} \frac{\beta t}{\tau}} \right)^{\frac{2\gamma}{\gamma - 1}} \quad (C-1)$$

$$\beta = \sqrt{\left(\frac{2}{\gamma + 1} \right)^{\frac{\gamma + 1}{\gamma - 1}}} \quad (C-2)$$

$$\tau = \frac{V}{A_n a_o} \quad (C-3)$$

$$a_o = \sqrt{\frac{\gamma R' T_o}{M}} \quad (C-4)$$

where p is pressure; p_o , initial pressure; γ , heat-capacity ratio; t , time; V , chamber volume; A_n , the cross-sectional area of orifice; a_o , the initial speed of sound; R' , gas constant; T_o , temperature of

gas in the chamber at start of blowdown; M, molecular weight of the gas.

Isothermal blowdown

$$\frac{p}{p_0} = e^{-\frac{\beta}{\tau} t}, \text{ or} \quad (C-5)$$

$$-\frac{d \ln p}{dt} = \frac{\beta}{\tau} \quad (C-6)$$

The pressure history during relatively slow depressurization, which condition prevails in the depressurization of the large combustion chamber for all orifice sizes, would be closely approximated by Eq. (C-6). As a first approximation, the fractional rate of depressurization could be estimated roughly by Eq. (C-6) even for the smaller chamber. Thus, the fractional rate of depressurization was calculated for both chambers with the following information:

The gas was assumed to be air at 25°C:	$\gamma = 1.403$
The volume of the larger combustion chamber:	20.12 liters
The volume of the smaller chamber:	0.98 liters
The volume of the auxiliary dump tank:	120.72 liters

The calculated results are listed in Table C.III.

The actual pressure history during depressurization from the larger chamber was measured for several orifice sizes without the burning propellant inside the chamber. It was observed that the actual pressure decay rates were bracketed by the adiabatic and the isothermal blowdown predictions. On Figure C.7, comparisons are made between the

actual pressure histories during depressurization extinguishment in the larger combustion chamber and the theoretical predictions. Except the case when the initial chamber pressure is very low, the actual pressure histories are shown to agree with the theoretical predictions reasonably well. That such a marked deviation can occur serves warning that theoretical prediction may be of chief value only in guiding the selection of the vent orifices.

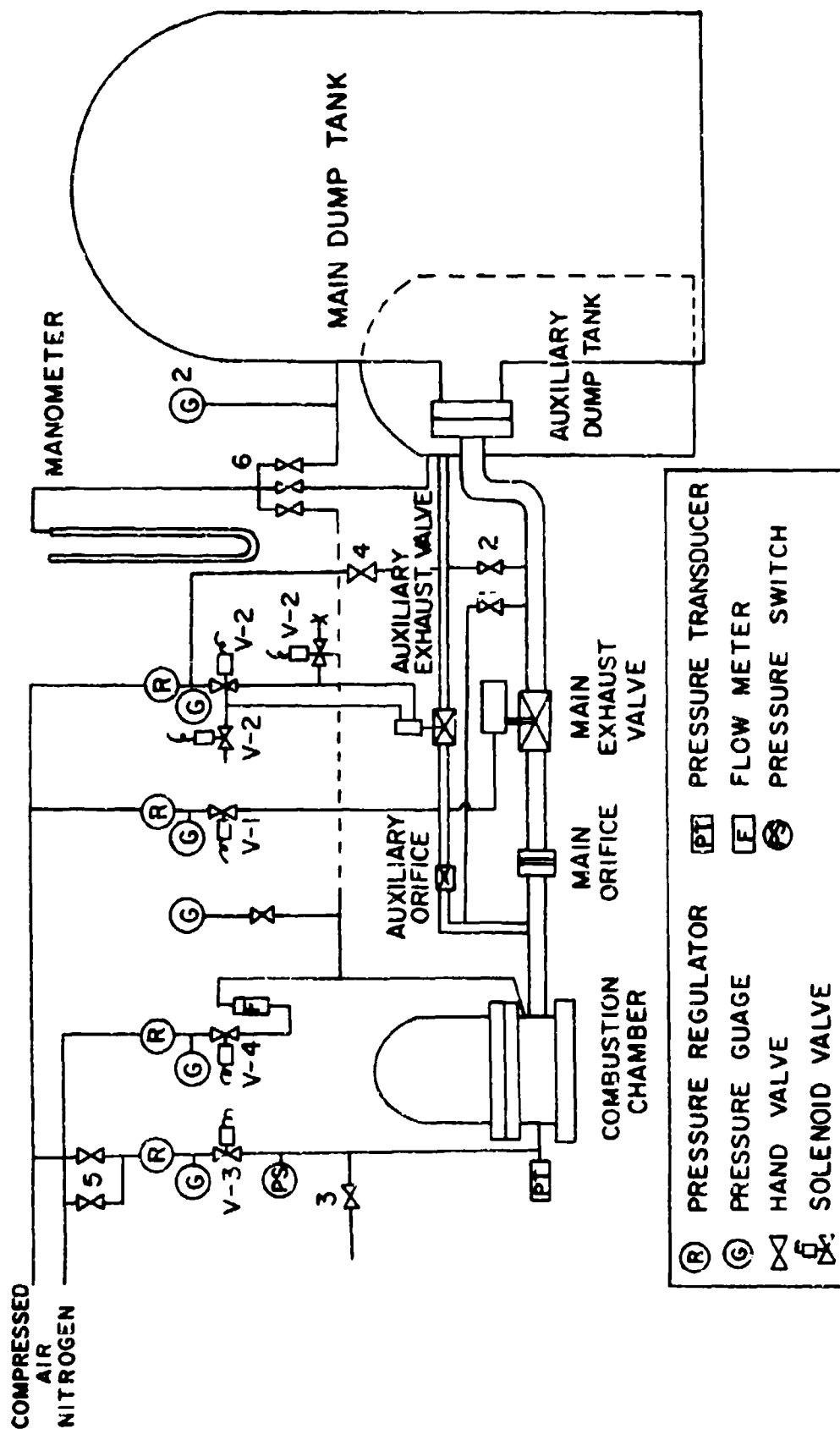


Figure C.1. Flow Diagram for the Combustion Chamber.

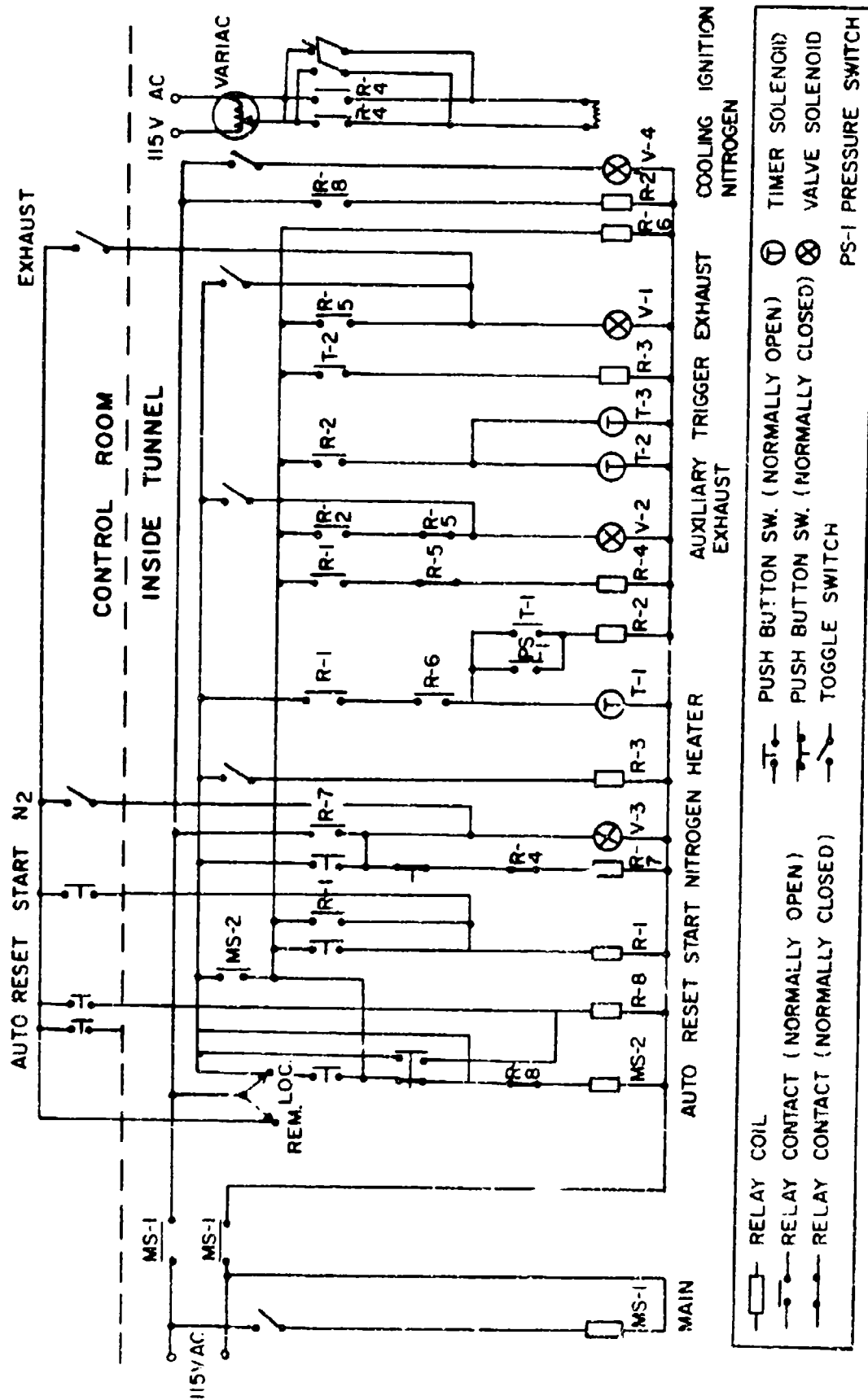


Figure C.2. Electric Circuit Diagram for the Combustion Chamber.

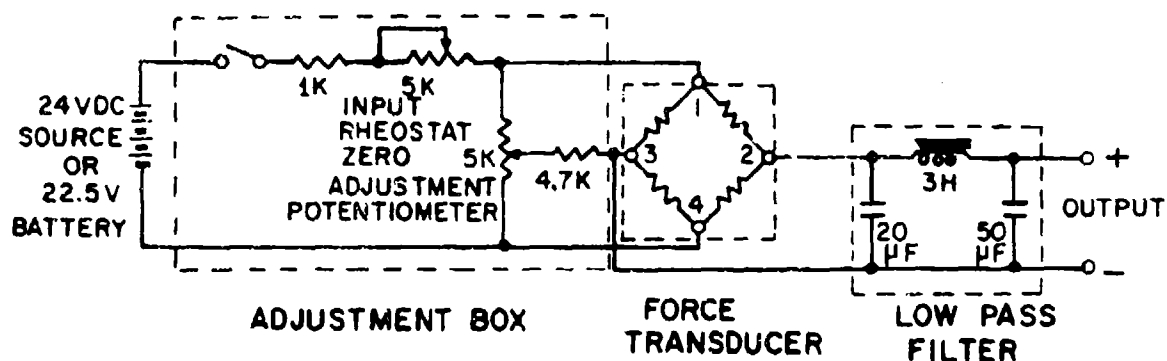


Figure C.3. Circuit Schematic Diagram for Force Transducer.

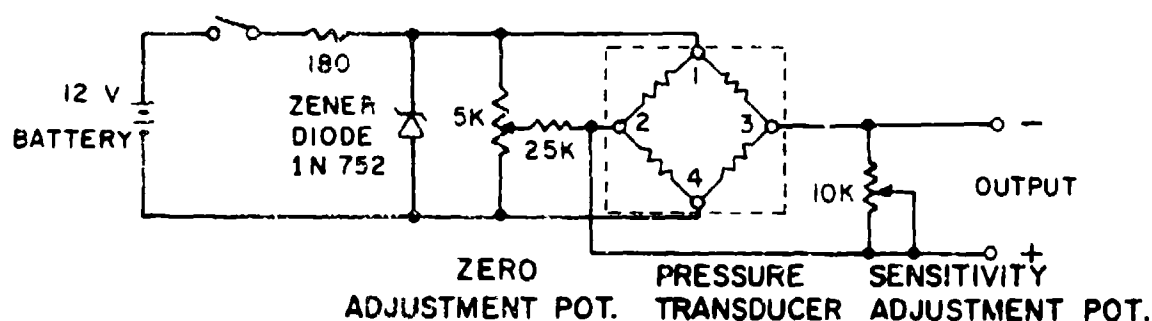


Figure C.4. Circuit Schematic Diagram for Pressure Transducer.

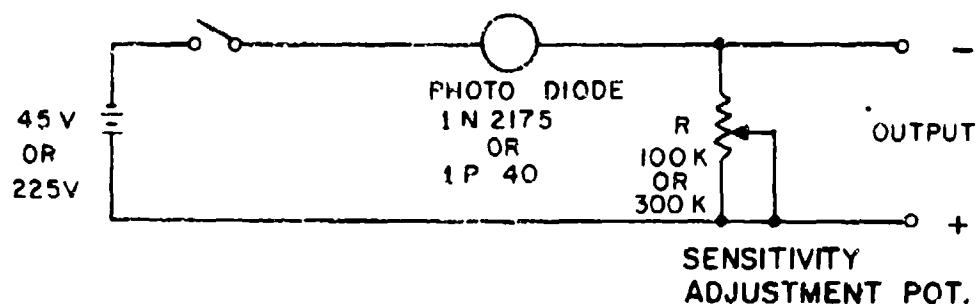


Figure C.5. Circuit Schematic Diagram for Photocells.

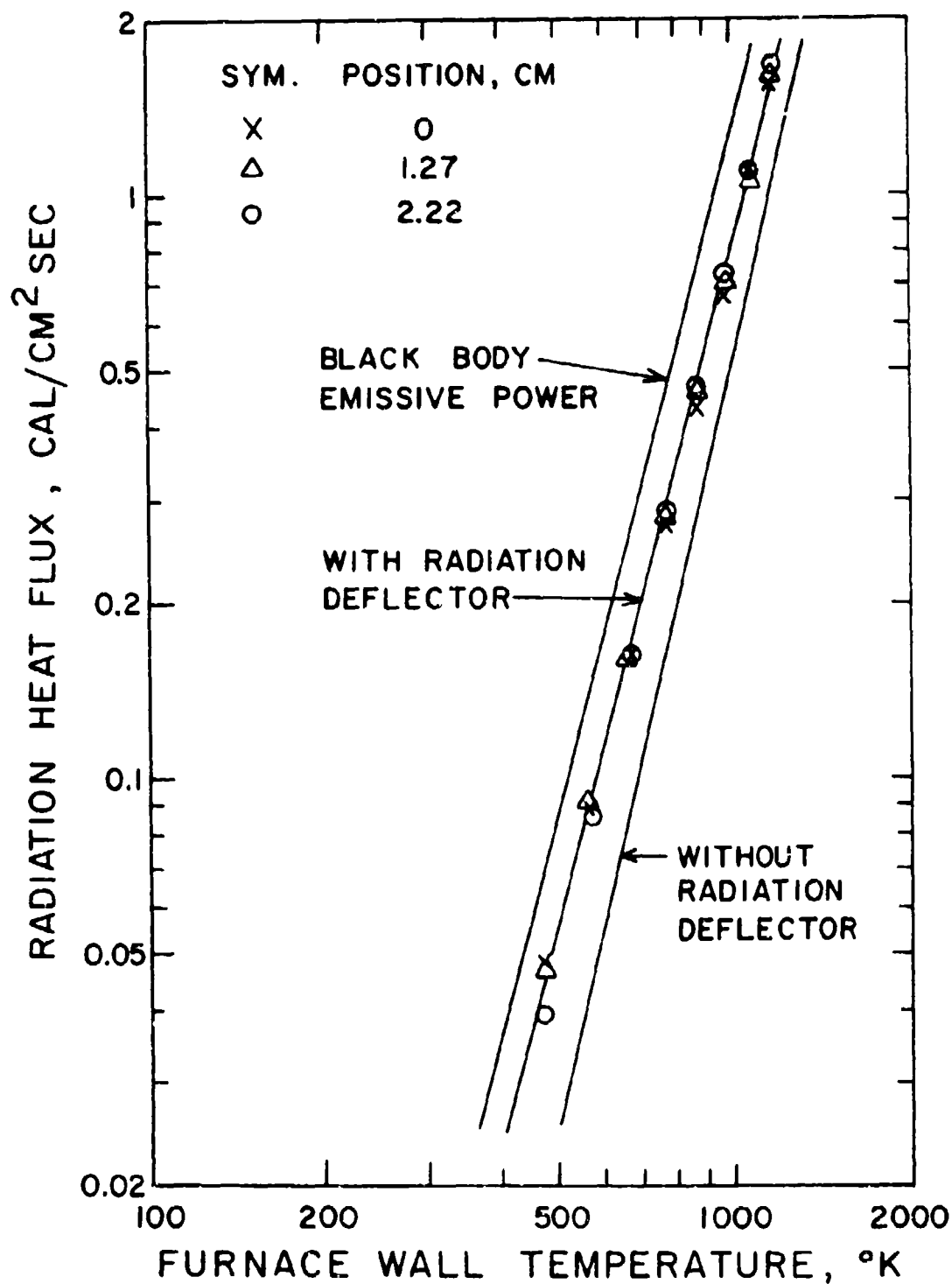


Figure C.6. Calibration Data of Furnace Heat Flux With Respect to Furnace Wall Temperature.

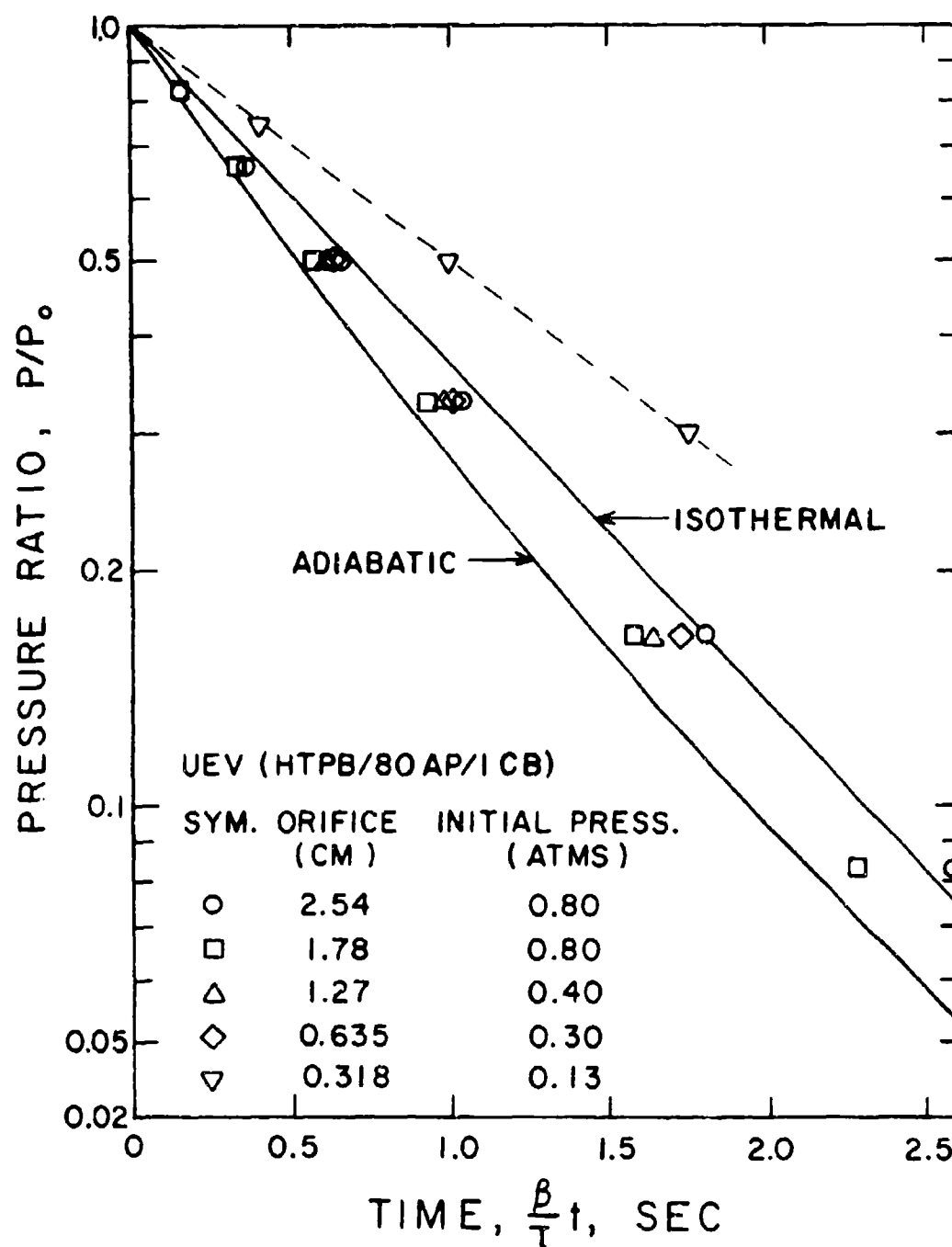


Figure C.7. Actual Pressure Histories During Depressurization Extinguishment Runs for the Combustion Chamber in Comparison With Theoretical Isothermal and Adiabatic Blow-down Curves.

Table C.I. Calibration Data of Temperature Controller for Quick Heating Furnace and Furnace Heating Times.

Controller Set Temperature °C	Actual Furnace Wall Temperature °C	Heating Time	
		Without Deflector sec	With Deflector sec
150	146	2.0	---
200	196	3.5	3.5
300	296	5.7	5.4
400	396	8.2	7.5
500	496	11.0	10.0
600	595	14.6	13.2
700	693	19.7	17.2
800	792	30.0	26.8
850	842	62.0	36.0
900	932	---	102.8

Table C.II. Heating Rates of Samples in Furnace.

Propellant: UDJ (PU/78.4 AP/2CB).

Pressure: The Combustion Chamber was Depressurized from 0.22 atms to 0.05 atms through 0.318 cm Orifice During Tests.

Sample Initial Temperature: 21°C.

No Cooling Nitrogen Was Introduced.

Sample Size		Furnace Set Temperature °C	Heating Time for Sample Center Temperature to Reach 31°C sec	Ignition Time sec
Diameter cm	Length cm			
0.95	2.22	700	24	52
1.43	0.95	750	37	--
1.43	2.54	700	56	62
1.43	2.54	750	56	--
1.43	2.54	800	50	--

Table C.III. Calculated Fractional Rates of Depressurization for Combustion Chamber and Small-L* Blow-down Chamber for Various Orifice Sizes.

Orifice Size		Fractional Rate of Depressurization Rate, sec ⁻¹		
inch	cm	Small-L* Chamber	Combustion Chamber	Combustion Chamber and Auxiliary Dump Tank
1.896	4.82	355		
1.500	3.81	223		
1.000	2.54	99.0	4.82	0.686
0.850	2.16	71.5	3.47	0.496
0.700	1.78	48.5	2.35	0.336
0.600	1.52	35.7	1.73	0.247
0.500	1.27	24.8	1.20	0.171
0.375	0.953	13.9	.675	0.0964
0.250	0.635	6.2	.300	0.0429
0.177	0.450	3.1	.150	0.0214
0.125	0.318	1.6	.0750	0.0107
0.0938	0.238		.0422	0.00603
0.0625	0.159		.0188	0.00269

APPENDIX D

INTERMITTENT BURNING OF A HIGHLY-FUELED
PU PROPELLANT UNDER FURNACE HEATING1. Background

As briefly mentioned in Chapter VI, the strands of a highly-fueled PU propellant (UDF) responded strangely when an external heat flux was imposed on the burning surface. Differing from the other propellants tested, this high P_{dl} propellant would not burn steadily at pressures below its P_{dl} , even with an external heat flux of $1.64 \text{ cal/cm}^2 \text{ sec}$. Instead, it exhibited intermittent burning with augmenting heat flux, i.e., a periodic repetition of ignition, deflagration, and extinguishment. This intermittent burning of propellant strands under relatively weak external heat flux appears to be closely related to the chuffing of rocket motors.

An extensive study on chuffing was made by Huffington [63] with cordite charges in a small vented vessel. He observed that the recession of the propellant surface during a single chuff was roughly constant more or less independent of pressure over a wide range, of chuffing frequency, and of charge design; and that the average burning rates were abnormally high during a period of chuffing. Based on those observations, he applied Frank-Kamenetsky's thermal explosion theory to explain the chuffing phenomenon, postulating that burning during

chuffing is thermally explosive in nature, being governed by a condensed-phase exothermic reaction. Clemmow and Huffington [30] extended this theory to explain oscillatory burning. Young and Angelus [138] followed a similar approach in their study of chuffing and non-acoustic instability of rocket motors fueled with modified double-base propellants. However, later investigators suggest that this approach may be erroneous, except, perhaps, for double-base propellants, because chuffing and non-acoustic instability are exhibited by many propellants for which the existence of sub-surface exothermic reactions is very questionable. Modern theories for chuffing and nonacoustic instability are based on the stability analysis of the motor considering the interaction between the combustion and mass flow through the nozzle.

However, an explanation is needed for the observation in this study that a chuffing-like phenomenon is also observed in strand burner. As the oscillatory burning of propellant strands at low pressures is due to the intrinsic instability of the combustion wave, this chuffing-like phenomenon is also thought to be a manifestation of the same inherent properties of the propellant combustion. There is, however, a fundamental difference. Oscillatory burning is continuous and self-sustained while intermittent burning needs either a finite amount of external flux to provide reignition or the persistence of local hot spots during the non-burning phase of the chuff.

2. Experiment Results

Figure D.1 shows the force transducer signals during intermittent burning at various pressures with the measured furnace temperature of

900°C. The salient periodicity is pronounced. The periodicity and the ignition and deflagration times are much influenced by the pressure. The oscillation has its greatest frequency at 0.1 atms. At higher pressures, both the ignition time and deflagration time are longer and the burning is very erratic. At very low pressure, 0.04 atms, the burning is rather smooth and slow. The jump of the force transducer signals at the initiation of burning is caused by the recoil due to the explosive mass evolution. The burning rate, being roughly indicated by the mean slope of the force transducer signal, decreases steadily as the deflagration proceeds until the extinguishment occurs. No appreciable change of mass is detected during the non-burning phase.

Visual observations during the intermittent burning at low pressures indicated that a bright flame suddenly developed all over the propellant surface and then the flame diminished in size and luminosity, until burning ceased. The extinguishment appeared to be complete, showing no sign of residual burning on the surface. A thick surface layer of modified polymer was found on the extinguished surface, which had the same appearance as those seen on the extinguished surface of the normally burning PU propellants near their low pressure deflagration limits. The thickness of the modified zone was approximately one millimeter at 0.1 atms, corresponding closely to the deflagration distance during one large cycle of the oscillatory burning of the highly-oxidized PU propellants (refer to Chapters V and VI). Again, the existence of the surface layer appears to be related to the peculiar burning nature of this highly-fueled PU propellant. Mihlfeith [87] also reported that a highly-fueled PU propellant (60% of

5 micron AP) showed periodic combustion wavelets on the burning surface when the propellant sustained combustion with intense external heat flux at atmospheric pressure.

Table D.I summarizes the data of intermittent burning of UDF propellant under furnace heating. The intermittent burning was observed to take place over a wide range of pressures when the furnace wall temperature was 900°C. The propellant would not be reignited after a chuff when lower furnace temperatures were used with higher pressure (0.5 atms or more). With a furnace wall temperature of 800°C and very low pressures (refer to Runs 20 and 21), the propellant surface regressed by successive explosions with a very short time interval. Thus, periods are shown to be unusually short.

One of the most interesting results to be noted from Table D.I is that the deflagration distance during a cycle is almost constant, about 0.6 mm, being little dependent on the pressure when the pressure is less than 0.3 atms. This result is similar to the observation made by Huffington. The burning distance during a chuff becomes greater as the pressure is increased above 0.3 atms. The dependency of burning rate on the pressure is milder than would be expected for a normal burning, as can be shown by dividing the burned distance by the burning time. The ignition time is certainly greater at higher pressures, a disagreement with the results of Yount and Angelus [138]. The total period of the intermittent burning is, accordingly, longer at a higher pressure. This tendency is again the same as Huffington's result, and opposite to

the pressure dependency of the period in continuous oscillatory burning, as shown both by Huffington and by other parts of this study.

From Figure D.1, one may notice that the average burning rate during a cycle, being the mean slope of the force transducer signal, seems to be little affected by the pressure. The observation is confirmed by Figure D.2, where the linear regression per cycle is shown to be constant over the pressure range 0.04 to 1.1 atms. This result suggests that the gross deflagration rate is almost totally determined by the rate of energy input from the external source. Thus, the energy contributed by the gas-phase flame during the intermittent burning appears to be insignificant.

Similarities appear to exist between the intermittent burning and the continuous oscillatory burning of highly-oxidized propellants at low pressures. It is instructive to compare the dimensionless frequency parameters for both cases. Computed dimensionless parameters for intermittent burning, based on the averaged burning rate, are shown in Figure D.2. Most values lie between 7 and 23 for pressures lower than 0.2 atms, bracketing values for the continuous oscillatory combustion of more highly oxidized PU propellants near their low pressure deflagration limits. Thermal capacitance of the solid phase plays a role in both cases.

In Figure D.3, the ignition period during a chuff at 0.1 atms is plotted as a function of the external heat flux in logarithmic scales. A straight line of slope -2 correlates the data, indicating that the ignition during an intermittent burning follows the prediction of the thermal ignition theory (see 72 for example).

3. Discussion of Results

a. Computation of the Net Heat of Gasification

The lack of dependence of the gross regression rate on pressure provides a means to compute the net heat of gasification. The instantaneous burning rate, r , is related to the instantaneous total feedback heat flux, f , by the energy balance at the burning surface:

$$r = \frac{f}{\rho [c(T_s - T_o) + q]} \quad (D-1)$$

With the assumption that $\rho [c(T_s - T_o) + q]$ is a constant, taking the time average for a single chuff,

$$\bar{r} = \frac{1}{\rho [c(T_s - T_o) + q]} \left(\frac{1}{\tau} \int_0^\tau f \, dt \right) \quad (D-2)$$

where \bar{r} is the averaged burning rate during a chuff and τ is the period of a chuff. Since the contribution of the energy feedback due to the gas-phase flame is insignificant during the burning period, the time averaged feedback flux can be approximated as being the external heat flux, f_r . Rearranging Eq. (D-2), we have

$$q = \frac{f_r}{\rho \bar{r}} - c(T_s - T_o). \quad (D-3)$$

With the numerical values, $f_r = 1.64 \text{ cal/cm}^2 \text{ sec}$, $\rho = 1.57 \text{ g/cm}^3$, $\bar{r} = 0.01 \text{ cm/sec}$, $c(T_s - T_o) = 100 \text{ cal/g}$, the computed q becomes 4 cal/g (endothermic). Note that with the same value of $c(T_s - T_o)$, the heat flux-augmented burning rate data give slightly negative values of q

(exothermic) for the more highly oxidized propellants (refer to Table VI.1). The result is consistent to our expectation that a more fuel-rich propellant would have a more endothermic net heat of gasification.

b. The Mechanism of Intermittent Burning

Although many features of the intermittent burning resemble those of thermal explosion, it is not likely to be explained by the thermal explosion theory alone. Rather, melting and other combustion-modifying changes of the polyurethane polymer along with temperature conditioning of the overall solid by a moderate external heat flux appear to account for the observed phenomenon.

The moderate external heat flux, which is not sufficient to help sustain the combustion wave of this propellant at the pressure level employed, heats up the solid and produces a thick thermal wave which is an effective increase in propellant temperature. The polyurethane polymer also undergoes melting and then drying changes for this pre-ignition period. The drier and warmer layer of the solid near the exposed surface eventually reaches the ignition temperature. The combustion wave generated advances to a position where the polymer melt prevails and the surface temperature is low, and stops. Another pre-heating period must transpire before the propellant is reignited. At a higher pressure the deflagration proceeds to a greater distance because a larger energy feedback from the gas-phase flame helps combustion persist at a lower propellant temperature, and therefore, a longer heating time is needed for the reignition of the extinguished propellant. The experimental results support this view.

The dominance of the condensed-phase action is the common factor for the intermittent burning of a highly-fueled PU propellant and the oscillatory burning of highly-oxidized propellants. The difference is that the oscillatory burning of highly-oxidized propellants is self-sustained due to the hotter flame and less polymer melt in the solid phase. Moreover, the oscillatory burning is inferred to be featured by the phase difference between the decomposition of the oxidizer and the binder while in intermittent burning the decompositions of the ingredients are in phase and the periodical burning nature appears purely thermal.

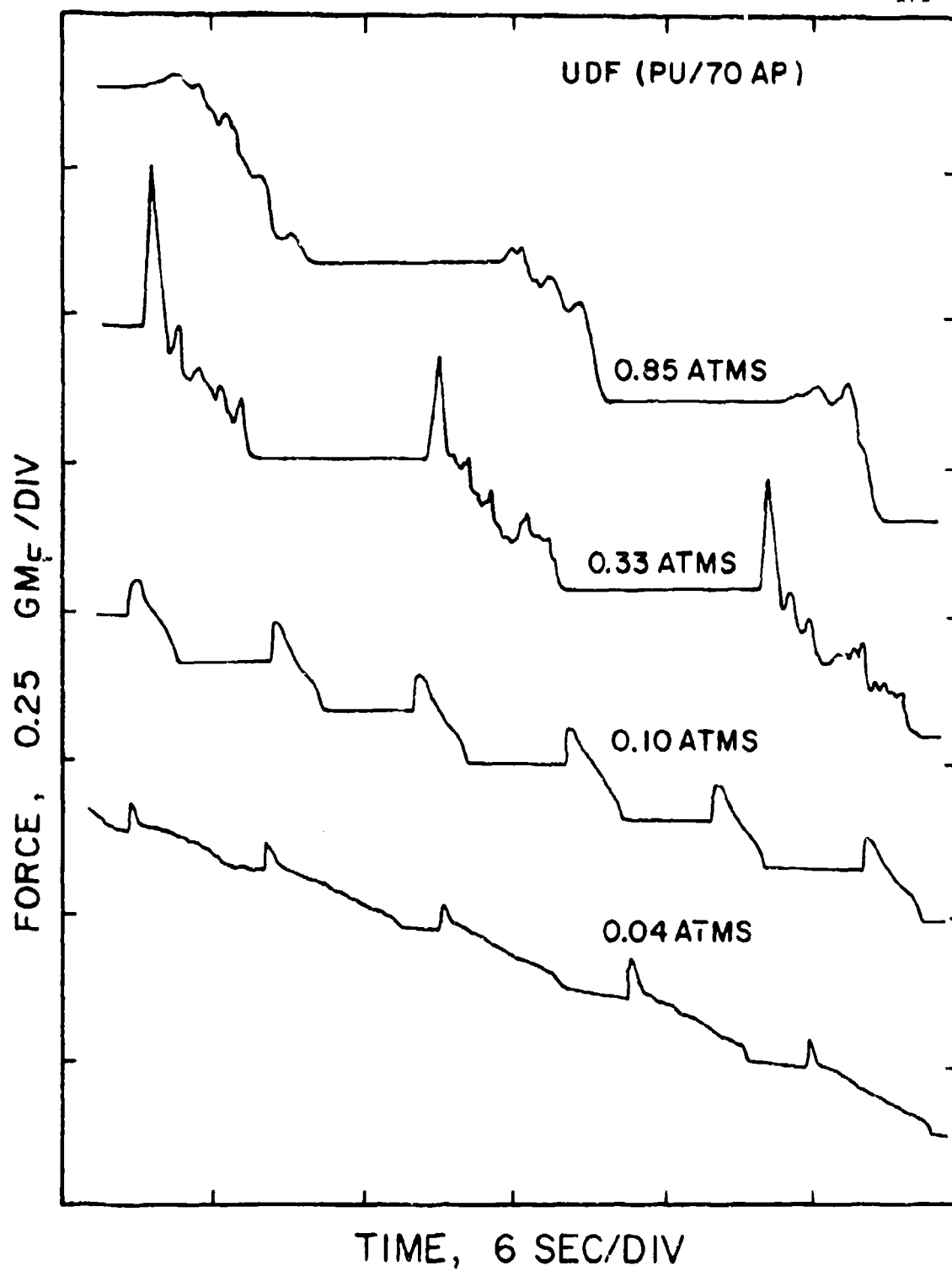


Figure D.1. Force Transducer Signals During Intermittent Burning of a Highly-fueled PU Propellant in Furnace Heated to 900°C.

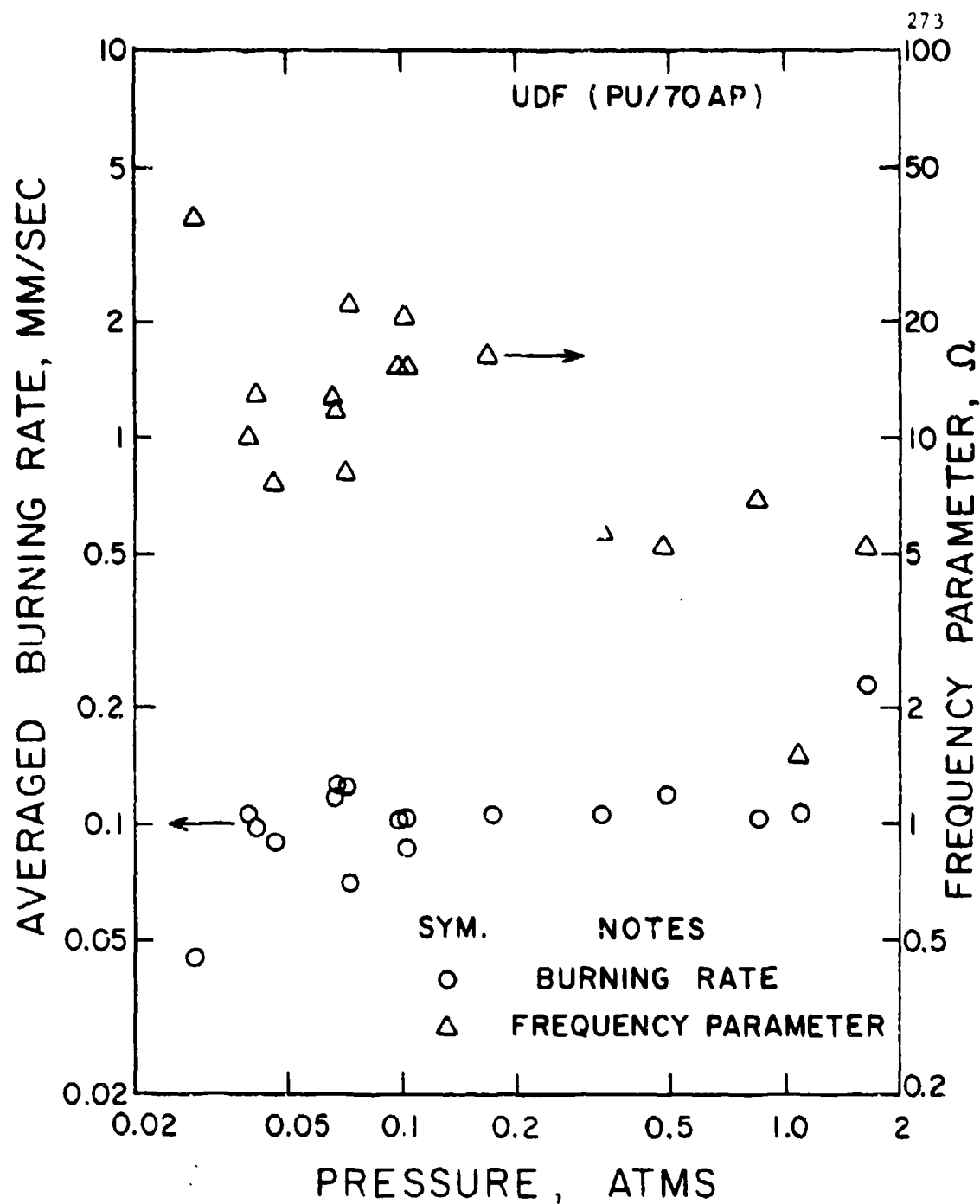


Figure D.2. Effect of Pressure on the Averaged Burning Rates and Frequency Parameters of UDF Propellant During Intermittent Burning in Furnace Heated to 900°C.

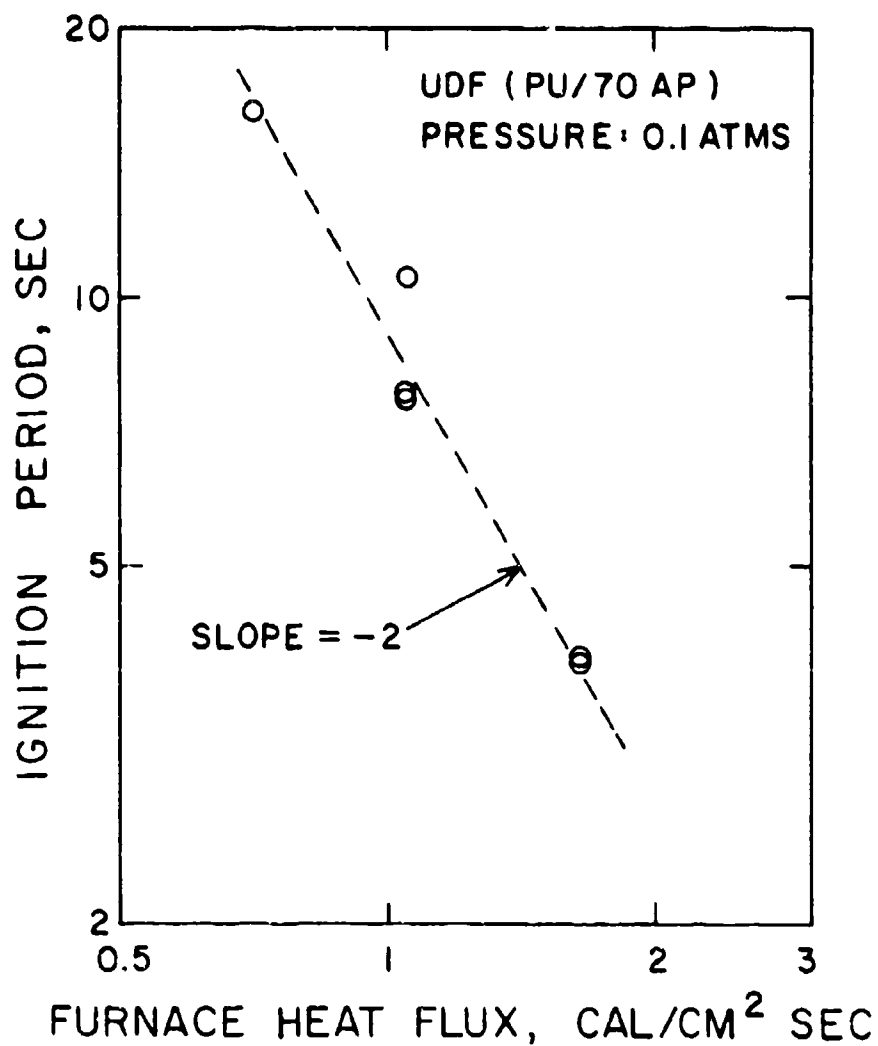


Figure D.3. Effect of Furnace Heat Flux on the Ignition Period of UDF Propellant During Intermittent Burning in Furnace.

Table D.I. Summary of Data for Intermittent Burning of UDF Propellant Under Furnace Heating

Run No.	Furnace		Pressure atms	Period, sec			Burned Distance During a Cycle mm
	Set Temp. °C	Flux cal/cm ² sec		Ignition	Burning	Total	
1110/-60	900	1.64	0.067	3.59	1.77	5.36	0.62
61	900	1.64	0.029	3.82	8.48	12.30	0.55
11110-1	900	1.64	0.068	1.80	3.00	4.80	0.62
2	900	1.64	0.100	3.96	1.92	5.88	0.60
3	900	1.64	0.102	3.90	2.10	6.00	0.52
4	900	1.64	0.104	3.95	1.88	5.83	0.60
5	900	1.64	0.040	1.56	6.54	8.10	0.86
6	900	1.64	0.042	2.32	4.78	7.10	0.70
7	900	1.64	0.047	5.84	9.16	15.0	1.38
8	900	1.64	0.074	4.86	3.60	8.46	0.59
9	900	1.64	0.072	4.51	2.63	7.14	0.90
10	900	1.64	0.172	4.31	1.11	5.42	0.56
11	900	1.64	0.334	8.23	6.33	14.60	1.54
12	900	1.64	0.495	8.39	3.94	12.33	1.48
13	900	1.64	0.845	7.74	4.08	11.82	1.23
14	900	1.64	1.66	19.8	13.2	33.0	7.62
16	900	1.64	1.09	44.0	8.4	52.4	5.64
17	800	1.06	2.89	156.0	4.8	160.8	4.17
18	700	0.71	0.107	16.1	3.25	19.35	0.86
19	800	1.06	0.100	7.74	2.28	10.02	0.68
20	800	1.06	0.042	1.06	0.32	1.38	0.12
21	800	1.06	0.070	1.29	0.36	1.65	0.07
22	800	1.06	0.167	7.81	1.56	9.37	0.51

APPENDIX E

MEASUREMENT OF THE SURFACE TEMPERATURES OF BURNING STRANDS

The low burning rates of propellants at low pressures produces thick thermal wave in the solid, which suggests a simple, direct measurement of the surface temperatures. The thermal wave thickness is of the order of one millimeter near the low-pressure deflagration limit of burning propellants. An attempt was made to measure the surface temperature with fine thermocouples.

The chromel-alumel thermocouples employed were purchased from Science Products Corp., Dover, New Jersey. The bead of the thermocouples was formed by pressing 0.005-inch thermocouple wires to give a junction 0.001 to 0.0002-inch thickness. The junction was thin and flat, and thermocouples of 0.001-inch thickness were adopted for this study.

The junction of the thermocouple was embedded in the middle of the propellant sample. A section of the sample was cut out as shown in the Figure E.1. The bead of the thermocouple was pushed into the propellant so that the flat face of the thermocouple junction was parallel to the burning surface. A small amount of Krylon acrylic solution was used to cement the pieces of the propellant together.

The time when the thermocouple bead emerged from the burning surface was determined by measurement of the electrical conductivity from the thermocouple bead to an electrode attached on one side of the

sample. The electric circuit is shown in Figure E.2. A 10 mega ohm resistor was used to isolate the conductivity measuring circuit from the thermocouple circuit.

Figure E.3 shows oscilloscope traces of the conductivity and thermocouple signals during an actual run. The photocell signal is also shown. In this test, the system pressure initially was kept at a constant level and then dropped to quench the burning after the thermocouple bead protruded from the burning surface. The point where the conductivity signal starts to fluctuate after increasing monotonically was assumed to be the moment when the thermocouple bead reaches the burning surface. This assumption was confirmed by examining the extinguished sample. In this test, the thermocouple bead projected out of the burned surface 0.3 mm, indicating that 1.2 seconds had elapsed from the moment when the bead was exposed on the burning surface until extinguishment occurred. Since the steady burning rate of this propellant at this pressure is 0.025 cm/sec, it would take 1.2 seconds for the surface to regress by 0.3 mm, which is consistent with the measured protrusion of the thermocouple. The change in the slope of the thermocouple signal shown in Figure E.1 during the rise in temperature appears to be caused by the partial quenching of the flame when the burning surface reaches the cut and glued portion of the propellant and also by the radiative heat loss from the thermocouple bead to the surroundings.

There exists, however, some uncertainty in the determination of the temperature when the thermocouple bead reaches the burning surface. As shown in Figure E.3, the point where the conductivity signal starts to fluctuate does not coincide with the time when the slope of the

thermocouple signal changes. The positioning of the thermocouple bead and the orientation of the burning surface apparently cause this uncertainty. The lower and upper bound of the surface temperature were taken at the point where the conductivity signal starts to fluctuate and at the moment when the slope of the thermocouple signal changes abruptly. The results of these preliminary runs are summarized in Table E.1. Corrections for the heat losses from the thermocouple junction by conduction through the leads and by radiation to the surroundings were not made for those temperature data. Thus, those temperatures should be taken as the minimum possible values of the real surface temperatures.

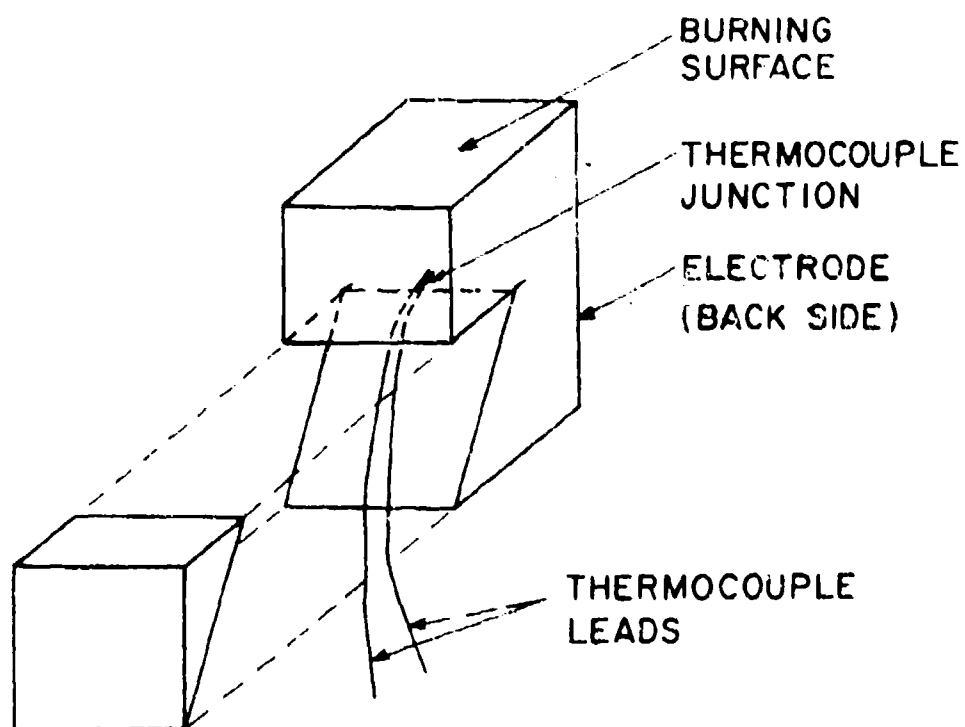


Figure E.1. Diagram Showing How the Thermocouple Junction Was Positioned in Propellant Sample.

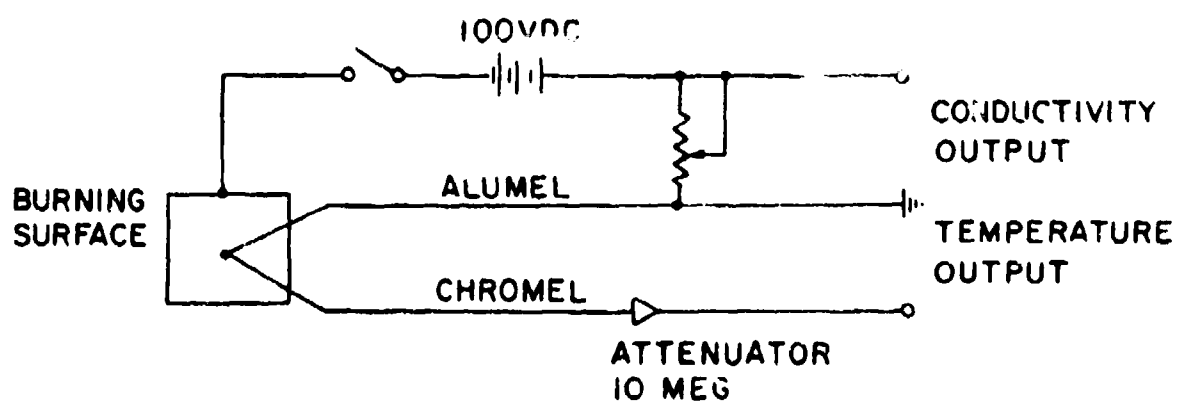


Figure E.2. Circuit Schematic Diagram for the Measurement of Burning Surface Temperatures.

APPENDIX F

ELECTRICAL PROPERTIES OF COMPOSITE PROPELLANT COMBUSTION

1. Background

During the early stage of the study on the depressurization extinguishment, difficulty was encountered with determination of the extinguishment point due to the very low luminosity of some propellant flames at low pressures. In order to overcome the difficulty, the measurement of the electric conductance across the burning propellant surface was considered as an indicator of extinguishment. Although the difficulty with the optical detection system was solved by using an improved arrangement of the photodiode, the preliminary results on the conductivity measurement across the burning surface were interesting enough to suggest some further study. The object of this program was to gain basic information on the nature of electric conductivity across the burning surface for future application of this property in characterizing the burning of composite propellants.

Yin and Hermance [137] monitored the electric conductivity across the burning surface to determine the extinguishment point during rapid depressurization. The experimental results of Bestgen and Wright [Fl] showed that the electrical conductivity through a solid propellant was strongly affected by the temperature, increasing as the temperature

was increased. This result suggests the possibility of influencing the burning rate by dissipating electric energy in the thermal wave near the surface of a burning strand. If one can introduce external energy to the surface in this manner, a significant improvement in the technique developed by Muhlfeith et al. [87] for characterizing the transient response of propellant combustion could be achieved. An alternating current with pre-assigned frequency could be introduced to the burning surface to perturb the steady burning. Muhlfeith et al. could only modify the burning rate of very cleanly burning propellants by external radiant heat flux. Aluminized propellants could not be treated.

Mayo et al. [F9] report that aluminized propellants have a much greater conductivity than non-aluminized ones, and it appeared possible to use electrical energy to perturb the burning of these systems. The modification of propellant burning rates using a strong electric field has been attempted by several investigators [F1, F9], but with little success. Bestgen and Wright [F1] observed that the regression rates of propellants were increased when the propellant temperature was enhanced by the breakdown current produced by high voltage across the propellant sample.

In the program discussed here, the electrical conductance of the burning surface was measured. The effects considered were the influence of propellant composition, electrode materials, pressure, electrode geometry, and the magnitude of the applied voltage. This investigation also included studies of the augmentation of the burning rate by electric energy and the transient response of electrical conductivity of the surface during rapid depressurization.

kept at a constant pressure during the steady-state measurement of the conductivity. Ignition was achieved by nichrome wires or pyrofuse wires. The conductivity and pressure signals were photographed on the screen of a Tektronix model 564 oscilloscope. In some cases, a Honeywell Electronic 19 recorder was used to record the conductivity signal and the pressure was read from a manometer or a pressure gauge. After burning in steady state for several seconds, the flame was quenched by rapid depressurization to permit inspection of the electrodes. The conductivity during depressurization was measured.

In many tests, the light of the flame and the weight of the sample were also monitored by a photocell and the force transducer respectively for comparison to the conductivity data.

b. Burning Rate Augmentation by High Voltage Power

A high voltage power source (maximum 5 KV) was used to introduce electrical energy to the burning surface. The preparations of samples were largely the same as (a) above. Gold foil electrode was mainly employed for these tests. In order to prevent the failure of electrodes by electrical breakdown, the electrodes were coated with thin films of a high voltage insulator (Corona Dope, G. C. Electronics). The steady-state burning rates were measured by the force transducer. The power supply was turned on when approximately half of the sample was burned, and the change in the rate of change of the weight transducer signal could be measured. The actual current and voltage during a run were read from meters.

3. Results and Discussion

a. Ohmic Nature of the Conductivity Across the Burning Surface

The current density across the burning surface was measured as a function of the applied voltage for various pressure levels and the results for 2.1 atms are shown in Figure F.3. Current densities were obtained by multiplying the ratio of the distance between electrodes to the width of an electrode to eliminate variations due to the sample geometry. A straight line passing through the origin is shown to correlate the data very well. This proportionality between current and voltage indicates an ohmic nature of the conductivity across the burning surface under the electrode geometry considered. A similar relationship was found to hold for the electrical conductivities at the other pressures.

This ohmic nature of the conductivity across the burning surface supports the contention that the current path across the burning surface is not totally through the gaseous flame. A purely gaseous conductor, being composed of uniformly ionized gases, would show a parabolic functional relationship between voltage and current [F7, F10].

b. Non-Ohmic Nature of the Conductivity Across the Burning Surface

The proportionality between voltage and current depicts only one aspect of Ohm's law. The other aspect of Ohm's law is that the resistance should be proportional to the distance between electrodes. As shown in Figure F.4, this property of Ohm's law is not well satisfied

by the resistance across the burning surface. The resistance at the pressure of 0.85 atms is proportional to the distance when the distance between electrodes is less than 0.4 cm. For the distance beyond 0.4 cm, another straight line is required to fit the data, and a discontinuity is apparent at about 0.4 cm. The conductivity data for tests at 0.067 atms which employed larger samples are also well represented by a straight line which, however, does not extend through the origin.

This non-ohmic nature of the conductivity across the burning surface indicates the complexity of the process. It appears that the conduction through the gas phase forms a large portion of the total conductivity at 0.85 atms. The sharp change of the dependency of the electric resistance on the distance between electrodes around 0.4 cm appears to be due to the space charge effect near the electrodes, and the sheath thickness of the space charge is apparently near 0.4 cm. The interaction between the gas-phase space charge and solid phase conduction may result in the observed increase of resistance before the 0.4 cm distance. When the distance is bigger than 0.4 cm, the increase of resistance with respect to distance is likely to be contributed by the solid phase since the gas-phase resistance is essentially constant. The situation is slightly different at 0.067 atms. The slope of the line correlating the resistance to distance is much steeper at 0.067 atms than at 0.85 atms when the distance between electrodes is larger than 0.4 cm. The condensed-phase conductivity could constitute a larger portion of total conductivity when the pressure is very low.

c. Separation of Conductivity Between Gas and Solid Phase

Contributions

An experiment was designed to separate the total electrical conductivity near the burning surface into the gas-phase and solid-phase contributions. The solid phase conduction was effectively eliminated by inserting a thin mica sheet in the propellant strand so that it formed a barrier parallel to the electrodes. A rubber adhesive (Rubber Adhesive 1300L, 3M Company) was used to attach the mica sheet and propellant surface together. The mica barrier was inserted only at the lower half of the propellant length so that the change of conductivity could be measured as the mica strip reached the flame front.

Data from these tests is presented in Figure F.5, as total conductance and gas conductance, as a function of the reciprocal distance between electrodes. Interestingly, the gas conductance does not vary with the distance while the solid conductance, being a dominant portion of the total conductance at this low pressure, is inversely proportional to the distance. Those results explain the strong dependency of the resistance on the distance between electrodes at 0.067 atms as seen in Figure F.4. The results also support the assumption that resistance across the gas-phase flame is concentrated around the electrodes.

d. Effect of Pressure on the Conductivity Across the Burning Surface

The total conductivities across the burning surface of several aluminized and non-aluminized propellants were measured as a function

of pressures. Figure F.6 shows some of the results. The reproducibility of the experimental data is excellent. Strangely, all propellant show a maximum conductivity at a pressure about 2 atms. In general, the total conductivity increases as the pressure is increased at pressures below 2 atms, whereas the inverse is true at higher pressures. The G and UDE propellant have almost the same conductivity above 0.2 atms. The UDE propellant conductivity at pressures below 0.2 atms is shown to increase as the system pressure is lowered. The G propellant exhibits a slow decrease of conductivity as the pressure is decreased below 0.2 atms. The conductivity of the aluminized propellant is slightly higher than those of the non-aluminized ones.

The peculiar dependency of the conductivity on the pressure required an explanation. The conductivity across the burning surface with the electrode geometry considered is influenced by many factors. The conductivity is certainly composed of both gas and solid contributions. The conductivity through the gas-phase flame is affected by the effective surface area of the electrode and the ionization potential of the electrode material and by cooling, space charges and other effects around the electrodes. Intrinsically, the gas-phase conductivity is indicative of the density of ionized particles in the gas phase so that it is very sensitive to the existence of alkali metals which could be included in the propellant sample as impurities. The heterogeneous nature of the solid phase also prohibits a simple interpretation of its electrical conductivity.

To gain some more information on the effect of various factors on the measured conductivity, the dependency of conductivity on the

electrode materials was sought. As shown in Figure F.7, the use of similar materials such as silver paint, silver leaf, and gold leaf yielded essentially the same values of conductance. However, the use of tin foil, which has a much lower melting point than the other materials, gives significantly lower conductance. Although all kinds of electrodes considered in this study apparently recede with the burning surface, the portion of electrodes which protrudes out of the burning surface appears to depend on the kind of electrode material and to have an effect on the measurement. A material which has a lower melting point could leave less protruded parts above the burning surface. The maximum conductivity around 2 atms is shown by all kinds of electrode materials. Probably, this maximum conductivity is an indication of some intrinsic nature of the propellant burning.

The peculiarity of the increased conductivity of UDE propellant for pressures lower than 0.2 atms was explained by the tests which separated the conductance into gas-phase and solid-phase contribution as shown in Figure F.8. At the very low pressures, the thermal wave in the solid phase is apparently thick enough to produce the increased conductivity. The solid phase contributes more than 90 percent of the overall conduction below 0.1 atms. As expected, the solid phase conductivity decreases as the pressure is increased and approaches a very low value at 0.5 atms. The solid-phase conductivity then tends to increase again as the pressure is further increased. This effect has not been explained. The conductivity data of the solid phase for pressures more than 0.5 atms are not, however, very reproducible. The

technique of using mica sheet is apparently not suitable at the higher pressures.

e. An Interpretation of the Maximum in the Conductivity Curves

The occurrence of the maximum in the conductivity curves around two atms is possibly explained by the thermal ionization of gaseous molecules. The alkali-metals included as impurities could be the major source of ions while the gaseous molecules of combustion products may also be dissociated to form some portion of the ions by chemi-ionization. The ion concentration due to thermal ionization can be calculated by Saha's relation [F4]:

$$\log K = \log\left(\frac{x^2}{1-x} \cdot p\right) = -\frac{U}{4.573T} + \frac{5}{2} \log T - 6.49 + \log G \quad (F-1)$$

where K is equilibrium constant for ionization; x is the fraction of the initial atoms which is ionized; p is the total pressure; U is ionization potential of the atom expressed in calories/mole; T is the absolute temperature in °K; and $G = g_+g_-/g_0$, and the g's are the statistical weights.

Equation (F-1) indicates that the ion concentration in the gas phase increases as the flame temperature is increased and as the system pressure is lowered. As mentioned in Chapter IV, the flame temperatures of composite propellants is very low at subatmospheric pressures so that the temperature effect might dominate the ionization process at low pressures. At higher pressures, however, the flame temperatures become close to adiabatic flame temperatures and do not vary significantly as the pressure is increased so that the pressure

effect may be governing. As a result, one may expect that a maximum in the conductivity would appear at some pressure above atmospheric.

f. Burning Rate Augmentation by High Voltage Power

Figure F.9 shows the conductivities across the burning surface measured when high voltages were applied. Although such measured conductivities do not change much with pressure, their magnitudes are nearly those measured by use of low voltages.

The augmentation of regression rates by the dissipated electrical energy at the burning surface was investigated for three propellants and the results for one of them is shown in Figure F.10. A detectible increase of burning rate was achieved by the dissipation of the moderate level of electric power. Some difficulty was encountered in measuring the increased burning rates. The sample had a tendency to burn faster at a position near the electrodes when the electric power was applied, which produced a wedge-shaped burning surface. Thus, the augmented burning rate was taken from the portion of weight signal immediately after the power was introduced. The other two propellants tested, UER and UEG, also showed similar augmentation of burning rates by electric power. These results suggest that electrical dissipation could be used as an alternative to the radiant energy input in the technique developed by Muhlfeith [87].

g. Transient Conductivity During Depressurization

Figure F.11 shows the oscilloscope traces of the light, conductivity, and weight signals along with the pressure signal during a slow depressurization test. In these pictures, the time when the

conductivity signal drops to zero is seen to coincide with the moment when the light luminosity disappears. The weight signal also ceases to decrease at the same instant. The numerical values of the conductivity of those runs were observed to follow the steady state values until the pressure reached a pressure slightly above the extinguishment pressure. As the extinguishment point was approached, the transient conductivity deviated from the steady state value until it dropped to zero. It appears that the conductivity during depressurization may contain some information about the burning rate response.

Another point to be noticed from these oscilloscope traces is the peculiarity of the conductivity signal of an aluminized propellant as shown in the lower figure. At pressures above 10 atms, the conductivity of the aluminized propellant is similar to that of the non-aluminized systems. However, the conductivity signal of the aluminized propellant tends to fluctuate with increasingly bigger amplitude as the pressure is lowered. The steady burning tests also showed this tendency for fluctuation of the conductivity at about the same amplitude. At subatmospheric pressures, near the limiting pressure, the fluctuation of the conductivity was observed to be so large that the momentary maximum conductivity approaches near infinite values, indicating that the surface becomes fully conductive at that moment. It appears that the agglomerated aluminum particles on the burning surface momentarily make a closed circuit before the shedding breaks the bridge. Conductivity measurement could be a useful

tool to characterize agglomeration of aluminum during the burning of aluminized propellants.

Figure F.12 shows the conductivity signal of a run made with a very slow rate of depressurization. Note the maximum in conductance at about 2 atms. The measured conductivity of this run faithfully follows the steady state value for a given pressure.

The relaxation of electric conductivity across the burning surface was followed during rapid depressurization for some propellants. As shown in Figure F.13, the conductivity signal drops very sharply near the extinction point. Figure F.14 compares the steady and transient conductivity signal during rapid depressurization. The conductivity signal is noted to deviate from the steady state value only as the extinguishment point is approached.

h. Conclusion

- (1) The measurement of the electrical conductivity across the burning surface is a useful tool to study the steady and transient propellant combustion. The extinguishment point during depressurization can easily be detected and some insight into the burning of aluminized propellants could be obtained by the conductivity measurement.
- (2) Significant amounts of power can be dissipated on the burning surface by use of high voltage. This fact could be used to advantage to improve

the experimental technique developed by
Mihlfeith for measuring response functions
by energy input to a burning surface.

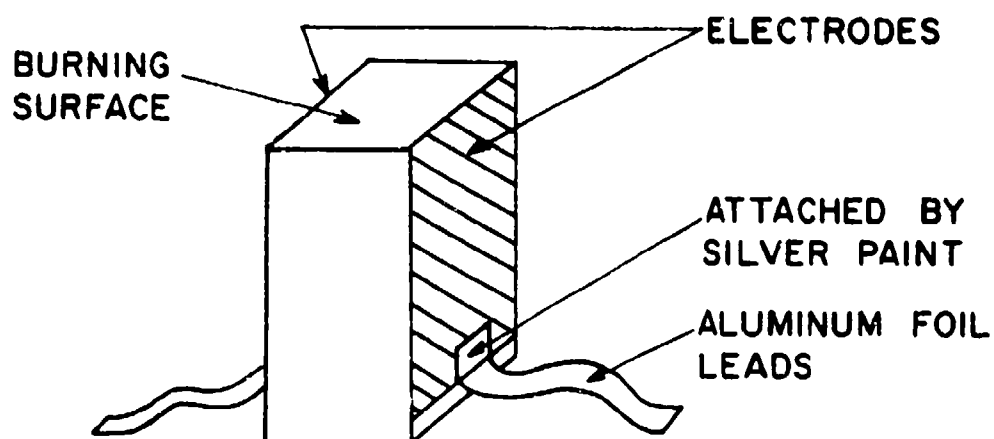


Figure F.1. Schematic Diagram of a Sample Prepared for the Measurement of Electrical Conductivity Across the Burning Surface.

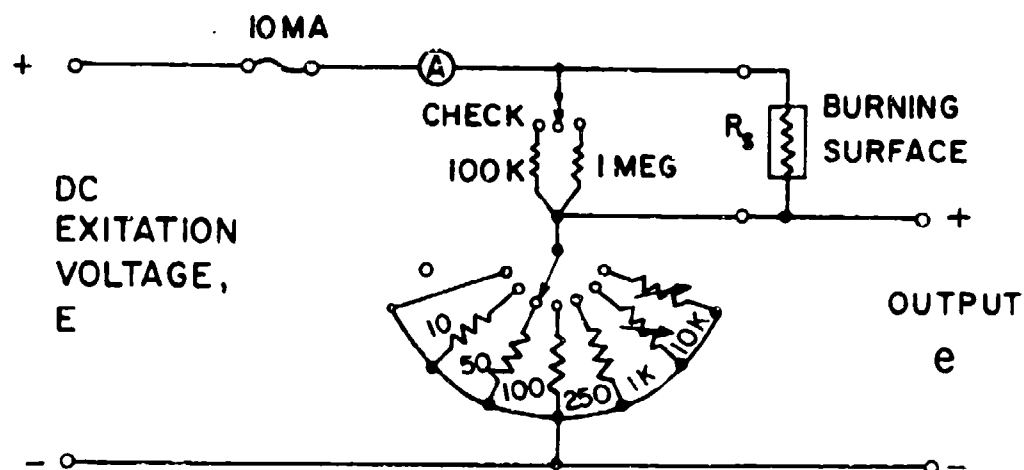


Figure F.2. Circuit Schematic Diagram of a Resistor Box for the Measurement of Electrical Conductivity.

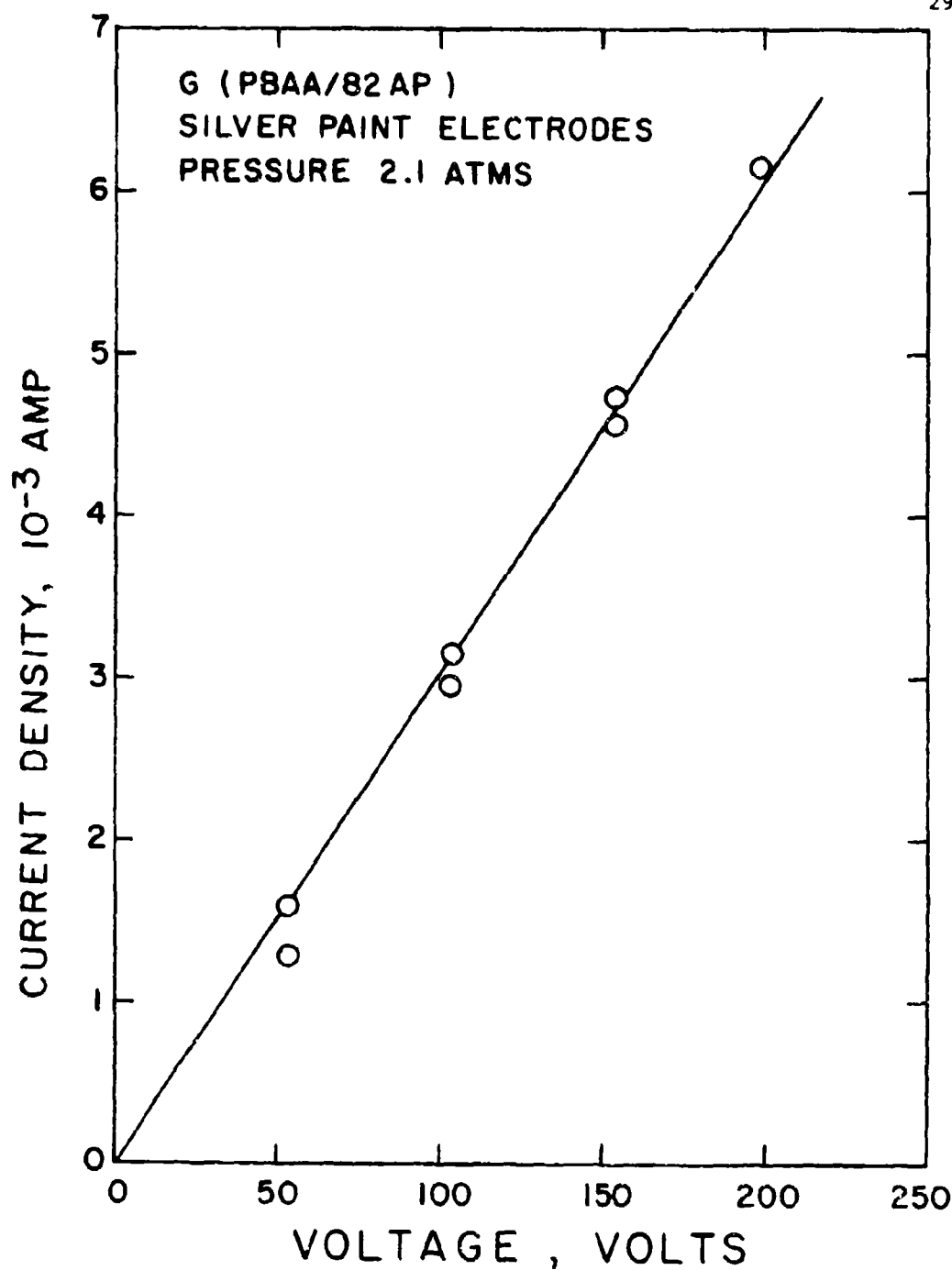


Figure F.3. The Ohmic Nature of Conductivity Across the Burning Surface. Current Densities Were Obtained by Multiplying the Ratio of Distance Between Electrodes and Electrode Width to the Measured Currents. Samples Were Approximately 0.75 cm x 0.75 cm in Cross-Section.

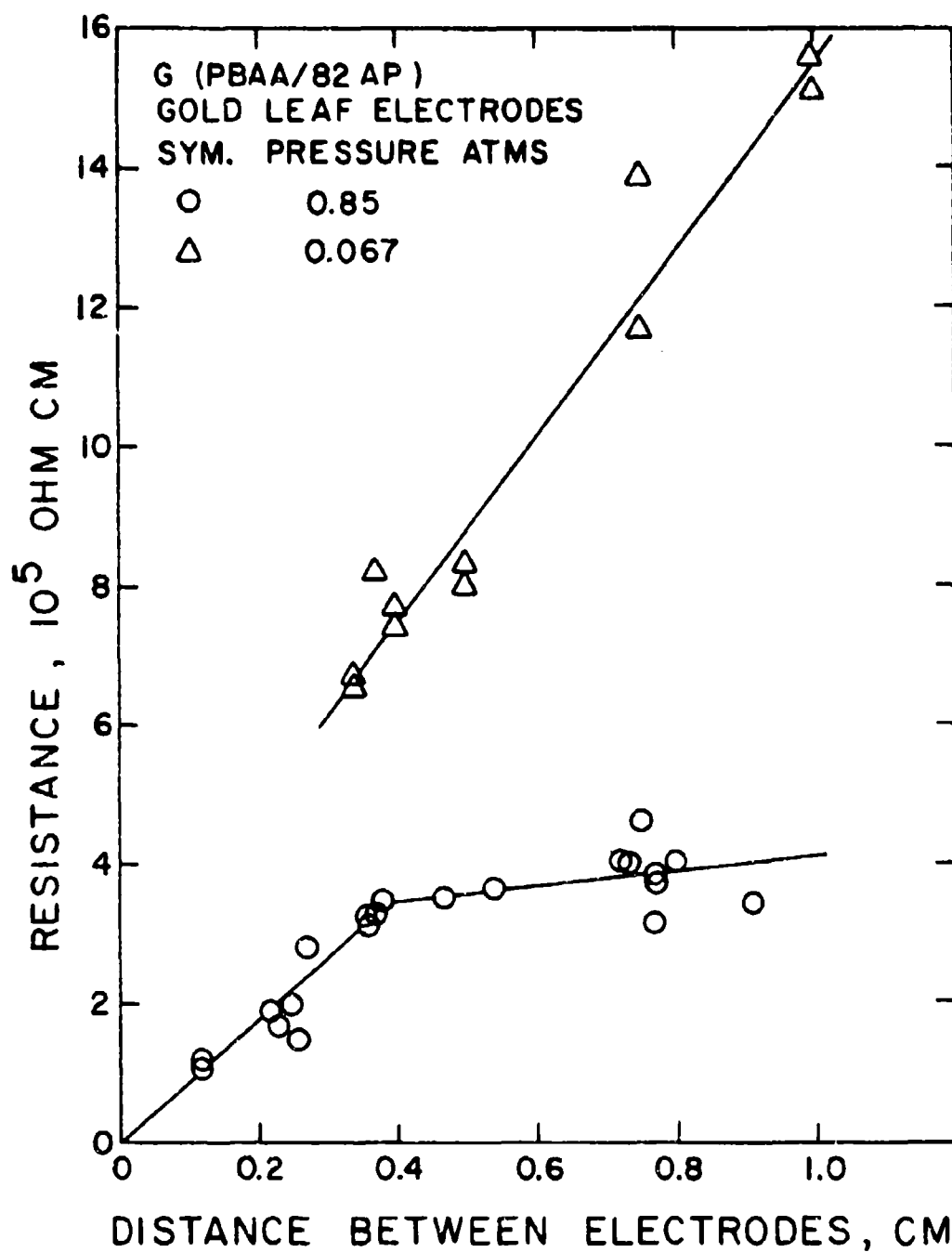


Figure F.4. Effect of Distance Between Electrodes on the Resistance Across the Burning Surface for Two Pressures. Resistances Were Obtained by Multiplying the Width of Electrodes to the Measured Values. The Width of the Electrodes Was Approximately 0.75 cm.

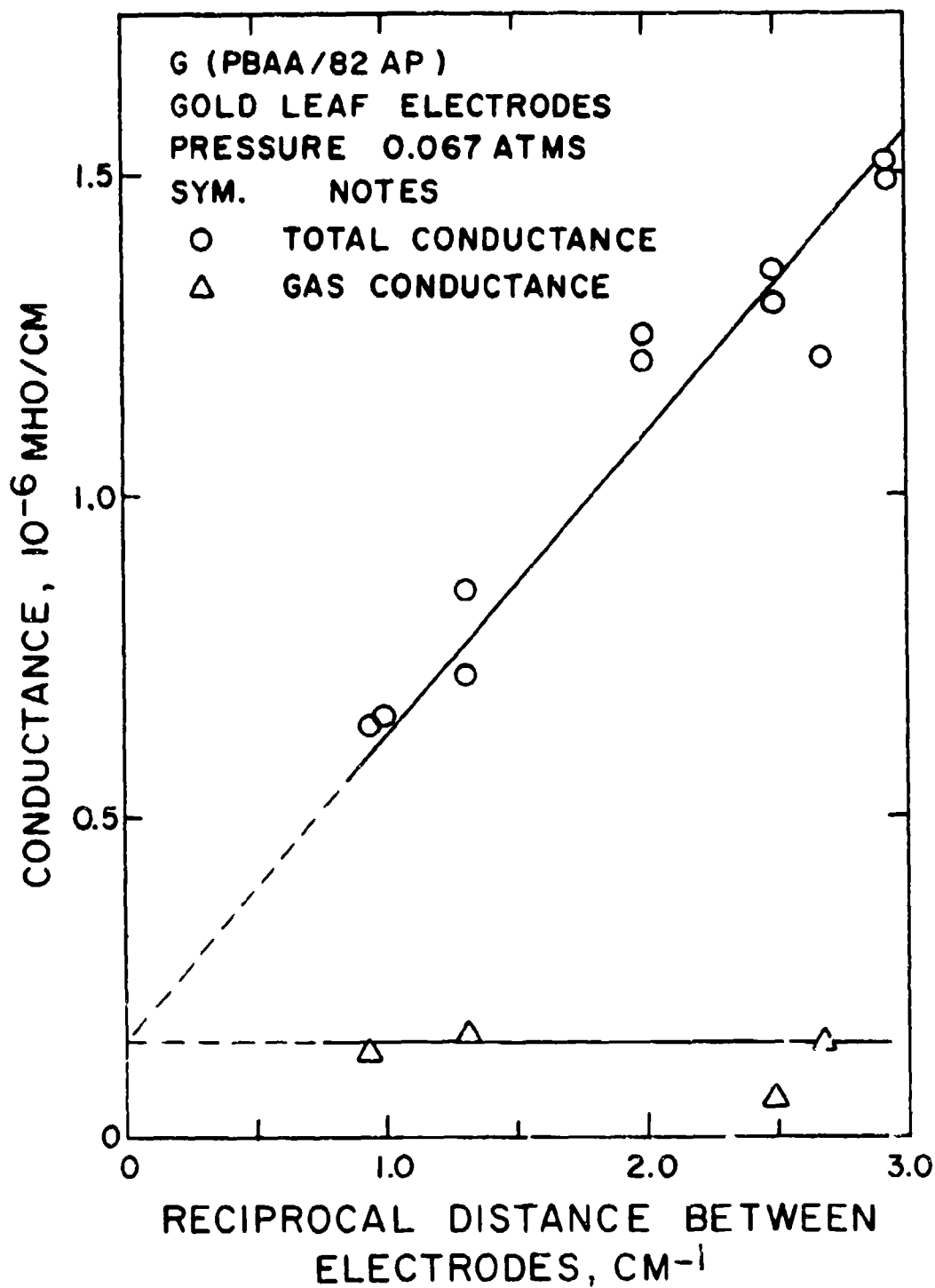


Figure F.5. Effect of Distance Between Electrodes on the Solid and Gas Conductances Across the Burning Surfaces. Conductance Data Were Obtained by Dividing the Measured Values by the Width of Electrodes. The Width of the Electrodes Was Approximately 0.75 cm.

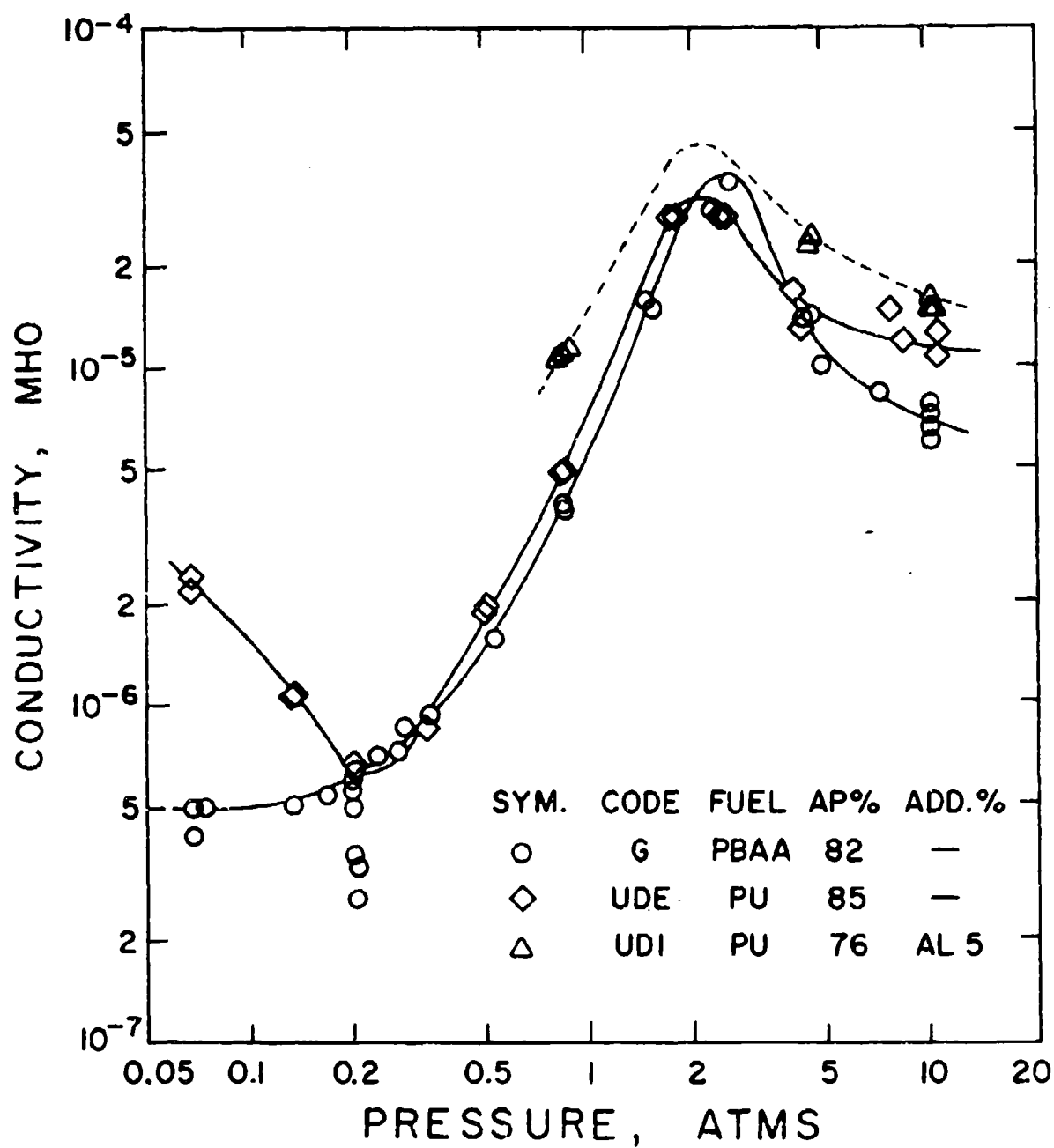


Figure F.6. Effect of Pressure on the Electrical Conductivities of Various Propellants. Silver Paint Electrodes Were Used.

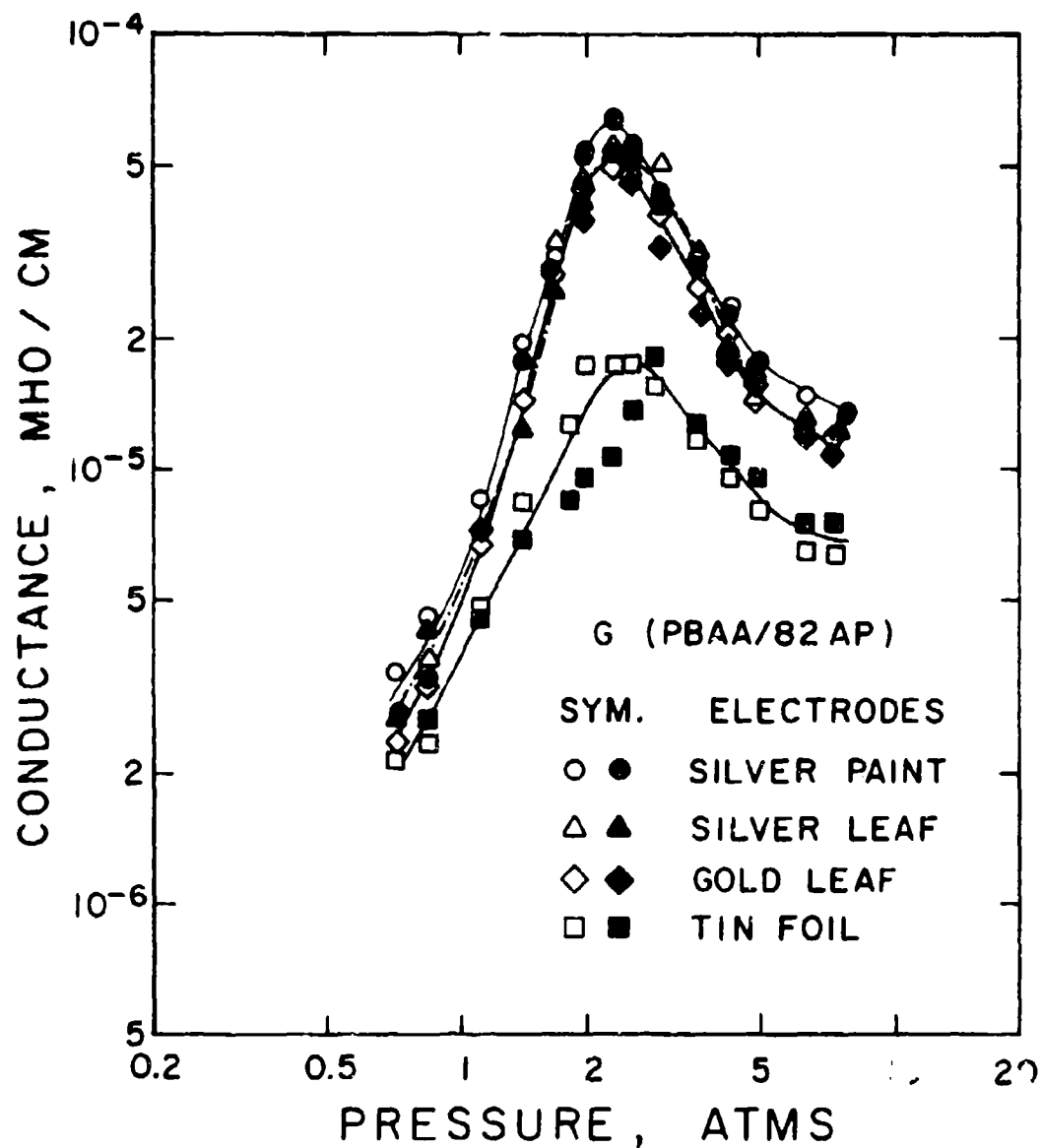


Figure F.7. Effect of Electrode Materials on the Electrical Conductance Across the Burning Surface. Samples of 0.75 cm x 0.33 cm Cross-Section Were Used. Electrodes Were Made on the 0.75-cm Sides.

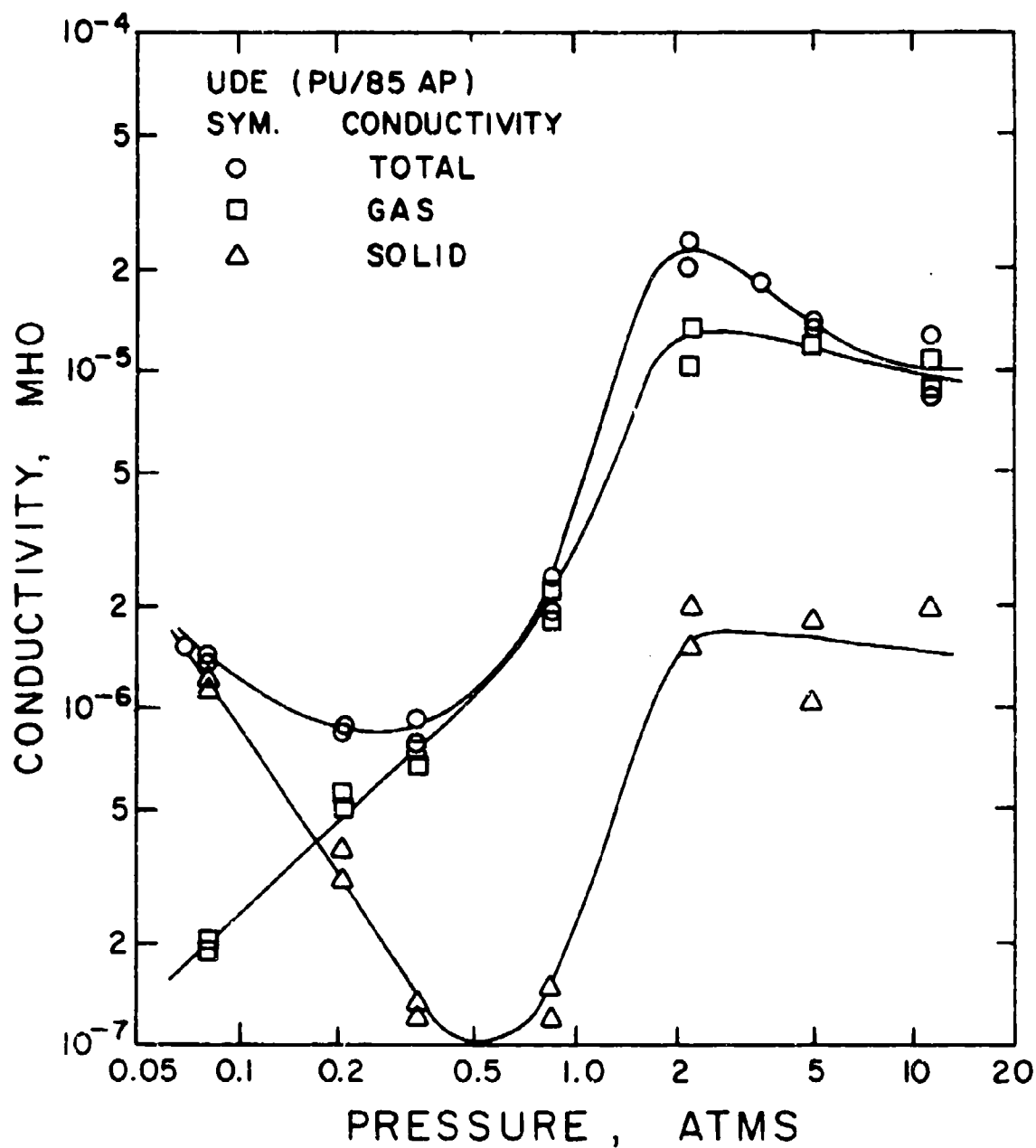


Figure F.8. Effect of Pressure on the Electrical Conductivities Through Gas and Solid Phase.

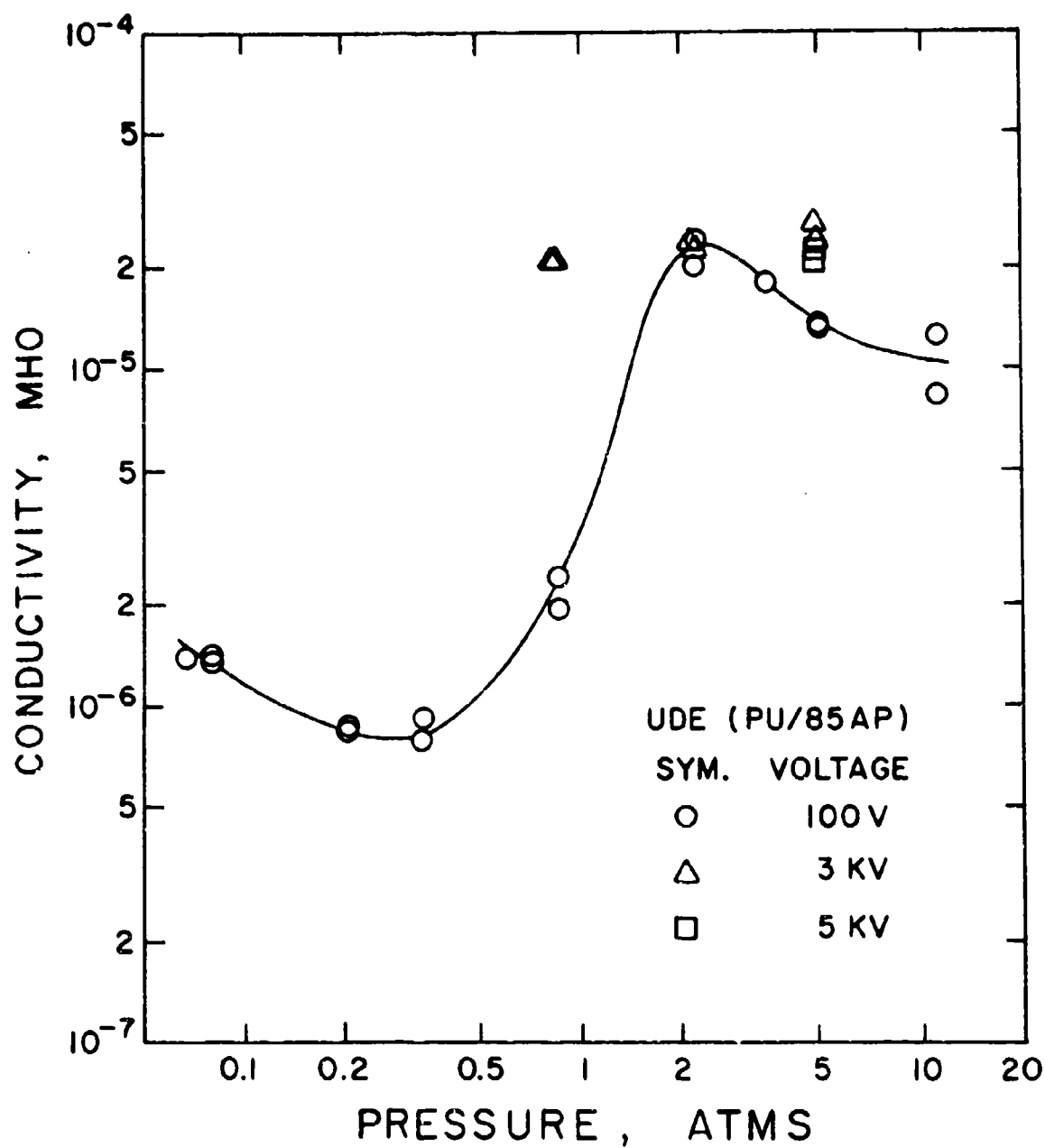


Figure F.9. Comparison of Low- and High-Voltage Conductivities for a PU Propellant. Gold Leaf Electrodes Were Used.

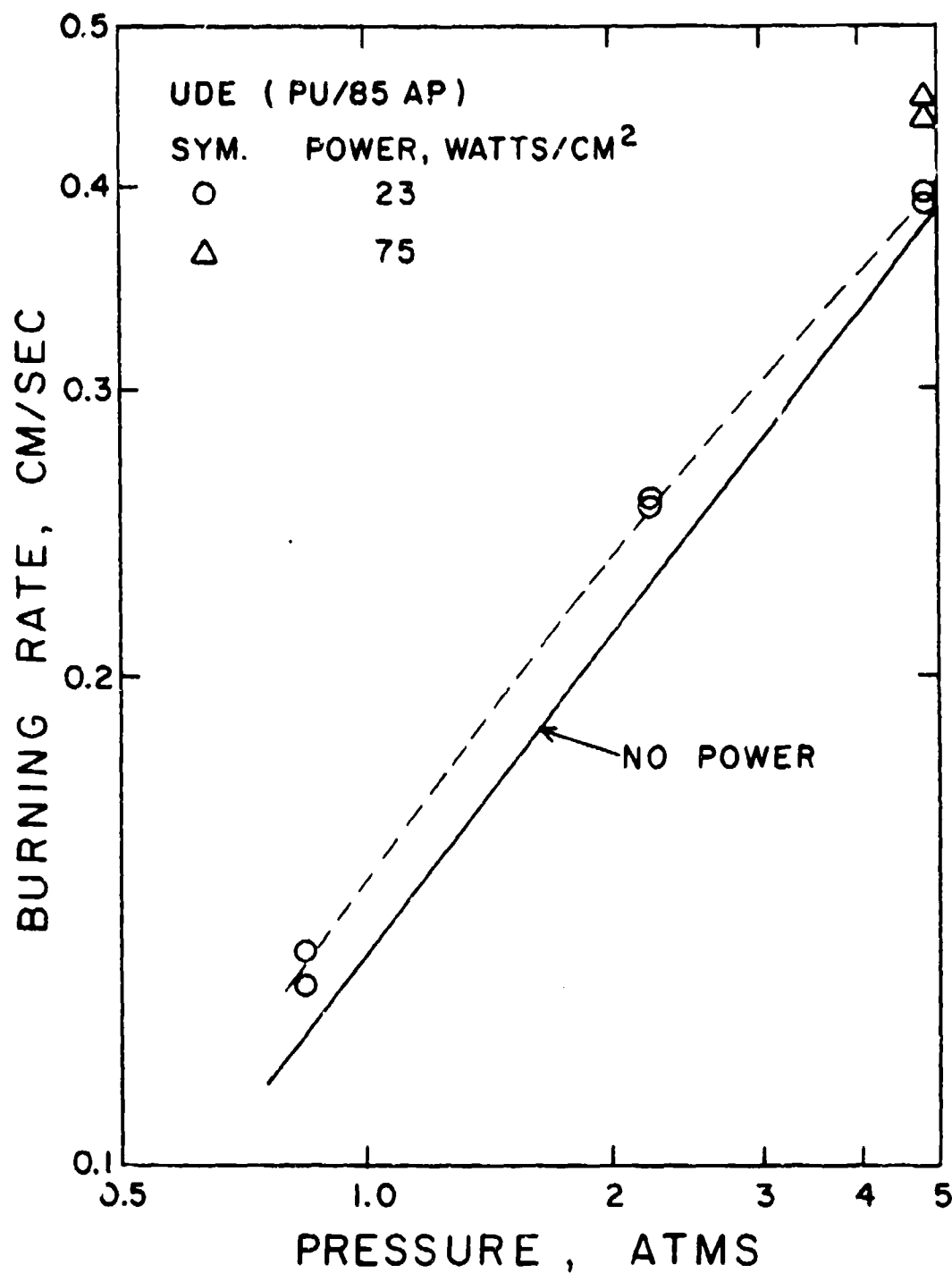
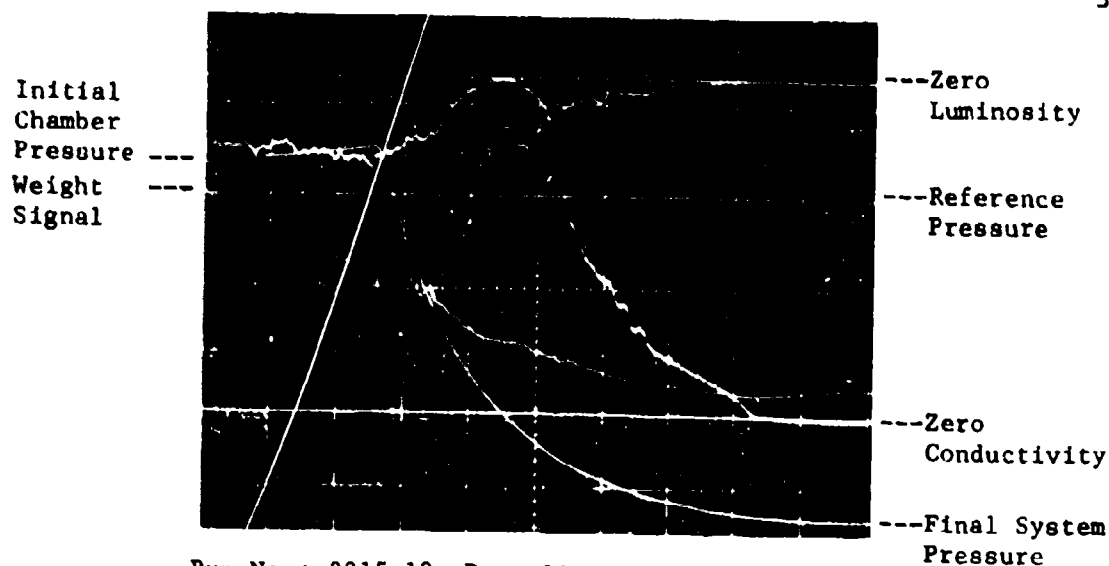
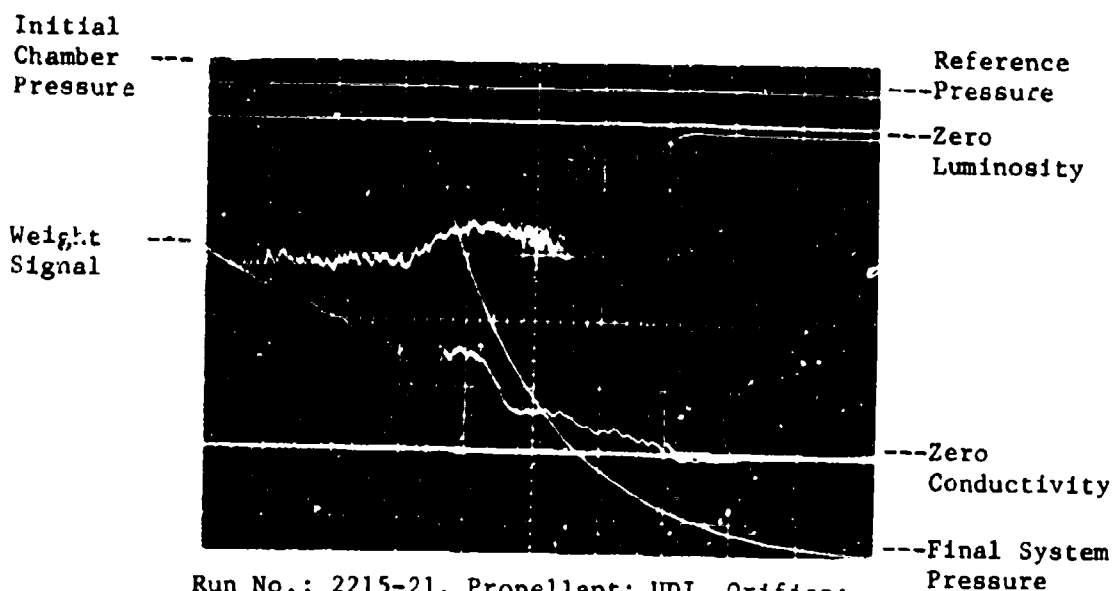


Figure F.10. Augmentation of Regression Rate of a PU Propellant by Dissipating Electric Energy on the Burning Surface.

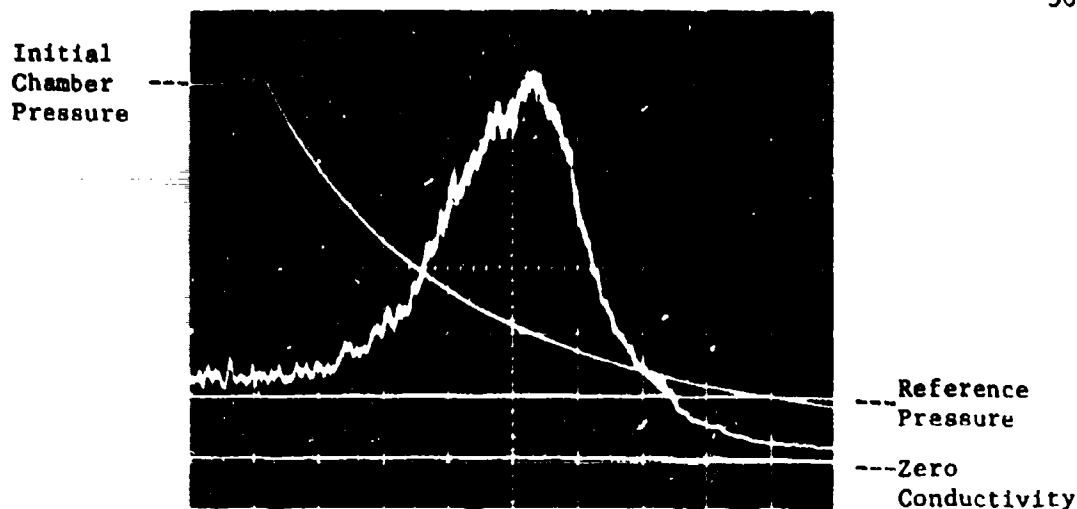


Run No.: 2215-19, Propellant: UDE, Orifice: 1.27 cm, Initial Chamber Pressure: 8.1 atms, Reference Pressure: 7.1 atms, Vertical Scale: 1.36 atms/division, Horizontal Scale: 0.5 sec/division.



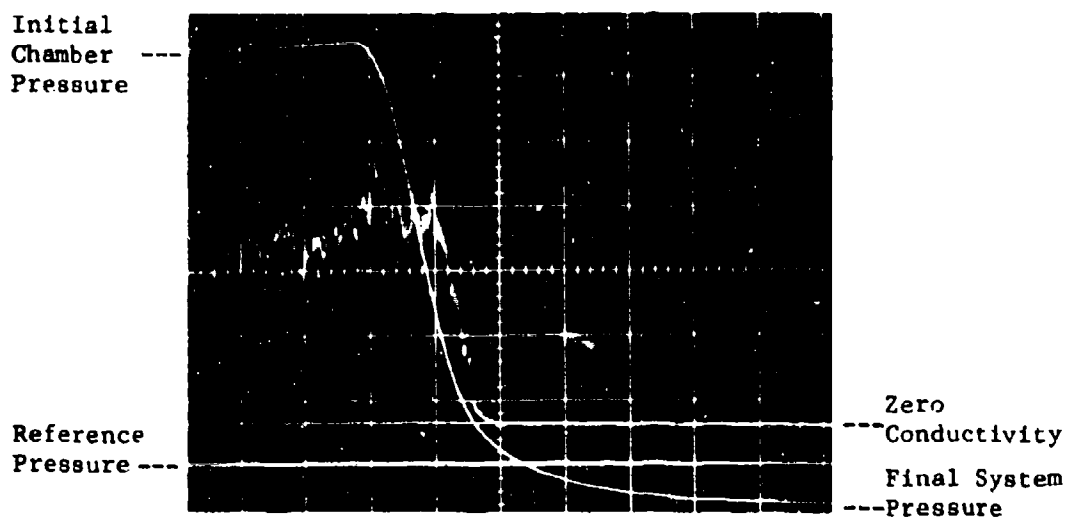
Run No.: 2215-21, Propellant: UDI, Orifice: 1.27 cm, Initial Chamber Pressure: 11 atms, Reference Pressure: 10 atms, Vertical Scale: 1.36 atms/division, Horizontal Scale: 0.5 sec/division.

Figure F.11. Oscilloscope Traces Showing Light, Conductivity Signals Near Extinguishment During Depressurization.



Run No.: 2322-2, Propellant: G, Orifice:
0.953 cm, Initial Chamber Pressure: 7.8 atms,
Reference Pressure: 0.85 atms, Vertical
Scale: Pressure, 1.36 atms/division;
Conductivity, 3.6×10^{-6} mho/division, Horizontal
Scale: 0.5 sec/division, Electrodes: Silver Paint.

Figure F.12. Typical Oscilloscope Traces of Pressure and Conductivity Signals During Slow Depressurization Using Combustion Chamber.



Run No.: 2409-4, Propellant: UDE, Orifice:
1.27 cm, Initial Chamber Pressure: 7.1 atms,
Reference Pressure: 0.85 atms, Vertical
Scale: Pressure, 1.36 atms/division; Conductivity,
 4×10^{-6} mho/division, Horizontal Scale:
50 msec/division. Result: Extinguished.

Figure F.13. Typical Oscilloscope Traces of Pressure and Conductivity Signals During Rapid Depressurization Using Small-L* Blow-down Chamber.

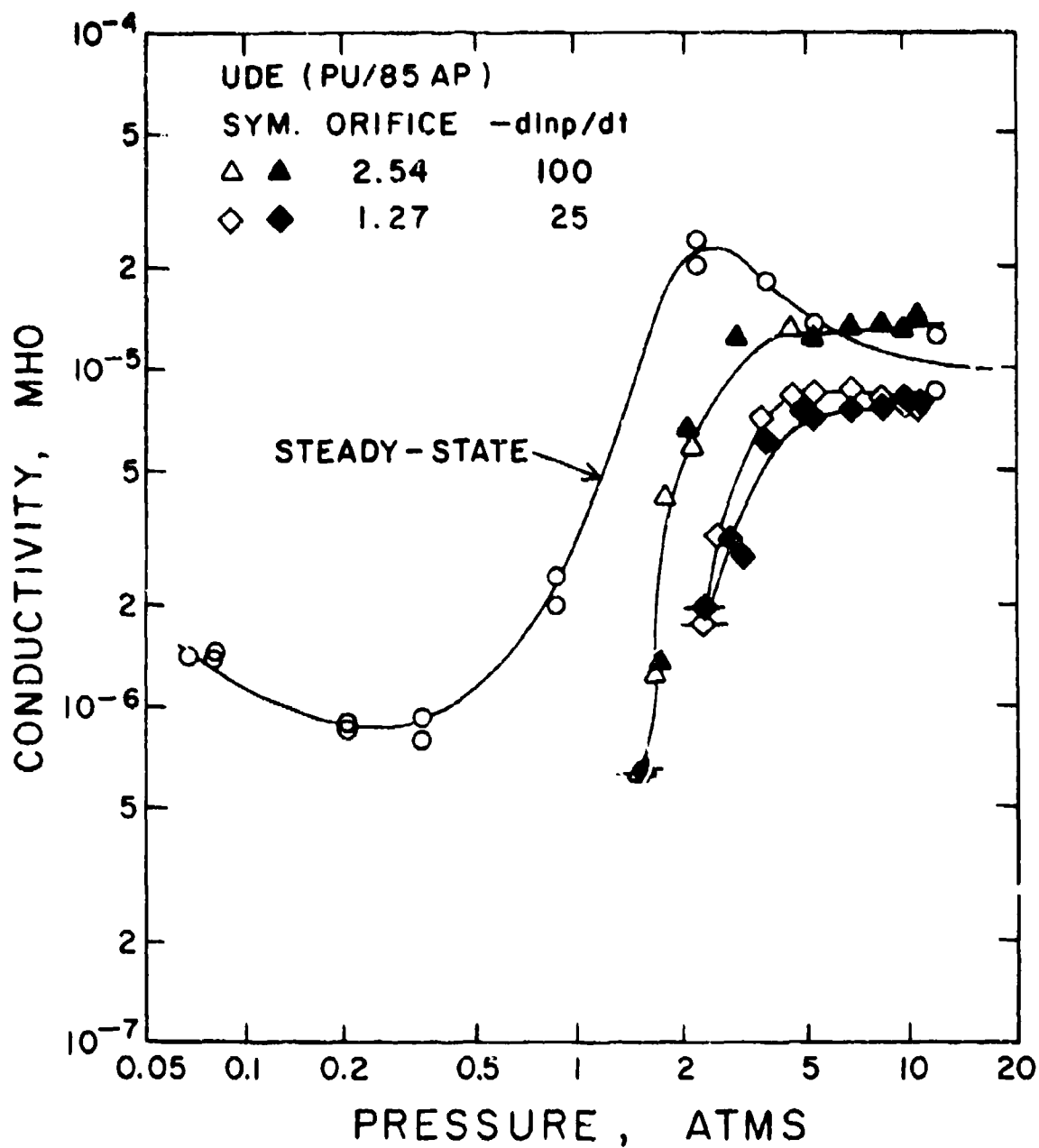


Figure F.14. Transient Conductivities During Depressurization. Gold Leaf Electrodes Were Used. Open and Filled Symbols Indicate Two Different Runs. Barred Points Indicate Extinguished Pressures.

Table F.I References for Appendix F

1. Bestgen, R. F. and Wright, H. E., "A Study of the Effects of Electric Fields on Solid Propellant Burning Rates," *AIAA Paper No. 71-174*, AIAA 9th Aerospace Sciences Meeting, New York, New York, January 25-27, 1971.
2. Bulewicz, C. M. and Padley, P. J., "A Cyclotron Resonance Study of Ionization in Low Pressure Flames," *Ninth Symposium (International) on Combustion*, p. 638, Academic Press, New York and London (1963).
3. Calcote, H. F., "Mechanism for the Formation of Ions in Flames," *Combustion and Flame*, 1, 835-401 (1957).
4. Gaydon, A. G. and Wolfhard, H. G., *Flames, Their Structure, Radiation and Temperature*, Chapter 13, London, Chapman and Hall, (1953).
5. Lawton, J. and Weinberg, F. J., *Electrical Aspects of Combustion*, Clarendon Press, Oxford (1969).
6. Maycock, J. N. and Pai Verneker, V. R., "Role of Point Defects in the Thermal Decomposition of Ammonium Perchlorate," *Proc. Roy. Soc. (London)*, A307, 303-315 (1968).
7. Thomson, J. J. and Thomson, G. F., *Conduction of Electricity through Gases*, Cambridge at the University Press p. 403 (1928).
8. Voekl, H. R., "Thermal Decomposition and Electrical Resistance of Ammonium Perchlorate under High Pressure," *ICRPG 2nd Combustion Conference*, CPIA Publication No. 105, pp. 313-317 (1966).
9. Mayo, P. J., Watermeier, L. A., and Weinberg, F. J., "Electrical Control of Solid Propellant Burning," *Proc. Roy. Soc. (London)* A284, 488-498 (1965); also Watermeier, L. A., "Optical and Electrical Properties of Solid Rocket Flames," Report BRL 1275, (March 1965).
10. Wilson, H. A., "The Electrical Conductivity of Flames," *Phil. Mag.* [6] X., 476 (1905).
11. Wise, H., "Electrical Conductivity of Solid Ammonium Perchlorate," *J. Phys. Chem.*, 71, 2843-2846 (1967).

APPENDIX G

REDUCED DATA OF EXTINGUISHMENT TESTS

Table G. I. Effect of the External Heat Flux on the Limiting Extinguishment Pressures of Various Propellants

Part 1. UEX Propellant Data

Run No. 3224	Furnace Set Temperature °C	Effective Furnace Temperature °C	Orifice cm	Cooling Nitrogen Flow Rate LPM	Initial Pressure atms	Sample Exposure Time to Furnace sec	Extinguishment Pressure atms	At Extinguishment Pressure	
								$-\frac{d \ln p}{dt}$ sec ⁻¹	Burning Rate cm/sec
1	19.3	19.3	0.953	0	0.0969	0	0.0622	0.0244	0.0125
2	19.3	19.3	0.953	0	0.107	0	0.0602	0.0207	0.0125
3	19.3	19.3	0.953	4	0.104	0	0.0615	0.00464	0.0119
4	19.3	19.3	0.953	4	0.110	0	0.0688	0.0180	0.0142
5	19.3	19.3	0.953	4	0.107	0	0.0682	0.0123	0.0129
6	200	144	0.953	4	0.0869	5	0.0688	0.0106	0.0129
7	200	144	0.953	4	0.0869	10	0.0695	0.0150	0.0139
8	200	144	0.953	4	0.0936	10.5	0.0699	0.0128	0.0141
9	300	237	0.953	4	0.0869	27	0.0615	0.0111	0.0133
10	300	237	0.953	4	0.0836	40	0.0635	0.0108	-----
11	400	319	0.953	4	0.0902	37	0.0575	0.0105	0.0121
12	400	319	0.953	4	0.0936	22	0.0635	0.00826	0.0134
13	400	319	0.953	4	0.0869	23	0.0602	0.00756	0.0110
14	500	404	0.278	4	0.0902	19	0.0582	0.0196	0.0136
15	500	404	0.278	4	0.0936	16.5	0.0595	0.0232	0.0135
16	600	487	0.278	4	0.0902	20	0.0501	0.0184	0.0125
17	600	487	0.278	4	0.0936	23	0.0515	0.0192	0.0118
18	700	577	0.278	4	0.0568	37	0.0334	0.0299	0.0116
19	700	577	0.278	4	0.0635	37	0.0321	0.0241	0.0110
20	750	619	0.278	4	0.0434	49	0.0254	0.0109	0.00946
21	750	619	0.278	4	0.0401	46	0.0261	0.00859	0.00848
22	800	672	0.450	4	0.0401	44	0.0214	0.0239	0.0108
23	800	672	0.450	4	0.0334	64	0.0207	0.0329	0.00946
24	800	672	0.450	4	0.0368	52	<0.0200	0.000	-----
25	820	692	0.450	4	0.0434	40.5	<0.0200	0.000	-----
26	850	707	0.450	4	0.0267	39	<0.0200	0.000	0.00948

¹Hand indicates that depressurization of the combustion chamber was achieved by adjusting the hand exhaust valve.

Table G. I. (Continued)
Part 2. UED Propellant Data

Run No. 3224	Furnace Set Temperature °C	Effective Furnace Temperature °C	Orifice cm	Cooling Nitrogen Flow Rate LPM	Initial Pressure atms	Sample Exposure Time to Furnace sec	Extinguishment Pressure atms	At Extinguishment Pressure	
								$-\frac{dP}{dt}$ sec ⁻¹	Burning Rate cm/sec
27	19.3	19.3	0.238(SA) ²	4	0.0802	0	0.0648	0.00460	0.00484
28	19.3	19.3	0.238(SA)	4	0.0802	0	0.0625	0.00485	0.00470
29	19.3	19.3	0.238(SA)	4	0.0802	0	0.0618	0.00483	0.00475
30	19.3	19.3	0.238(SA)	0	0.0802	0	0.0461	0.00464	0.00382
31	19.3	19.3	0.238(SA)	0	0.0802	0	0.0455	0.00461	0.00341
32	19.3	19.3	0.238(SA)	8	0.0936	0	0.0715	0.00330	0.00459
33	19.3	19.3	0.238(SA)	8	0.0936	0	0.0735	0.00442	0.00555
34	19.3	19.3	0.238(SA)	15	0.107	0	0.0719	0.00248	0.00495
35	19.3	19.3	0.238(SA)	15	0.107	0	0.0735	0.00315	0.00523
36	200	144	0.238(SA)	4	0.0802	18	0.0615	0.00485	0.00462
37	200	144	0.238(SA)	4	0.0802	18	0.0622	0.00402	0.00476
38	300	237	0.238(SA)	4	0.0802	22.5	0.0595	0.00487	0.00583
39	300	237	0.238(SA)	4	0.0802	22.5	0.0602	0.00496	0.00554
40	400	319	0.238(SA)	4	0.0802	33.5	0.0582	0.00421	0.00449
41	400	319	0.238(SA)	4	0.0802	40.0	0.0551	0.00501	0.00421
42	500	319	0.238(SA)	4	0.0802	40.0	0.0548	0.00398	0.00575
43	500	404	0.278(SA)	4	0.0648	61.5	0.0475	0.00535	0.00368
44	500	404	0.278(SA)	4	0.0662	36.0	0.0531	0.00535	0.00379
45	500	404	0.278(SA)	4	0.0658	67.5	0.0448	0.00478	0.00299
46	600	487	Hand	4	0.0525	97	0.0274	0.00796	0.00330
47	600	487	Hand	4	0.0401	44	0.0277	0.00867	0.00382
48*	600	487	Hand	4	0.0568	43	0.0424	0.0157	0.00463
48	700	577	Hand	4	0.0401	90	<0.0194	0.0000	0.00311
49	700	577	Hand	4	0.0401	65	0.0224	0.0111	0.00383
50	700	577	Hand	4	0.0401	54	0.0237	0.0162	0.00473
51	800	672	Hand	4	0.0401	84	<0.0194	0.0000	0.00416
52	800	672	Hand	4	0.0401	60	<0.0194	0.0000	0.00552

²SA indicates the conditions that the combustion chamber was connected to the auxiliary dump tank.

Table G. I. (Continued)

Part 3. UFA Propellant Data

Run No. 3224	Furnace Set Temperature °C	Effective Furnace Temperature °C	Orifice cm	Cooling Nitrogen Flow Rate LPM	Initial Pressure atms	Sample Exposure Time to Furnace sec	Extinguishment Pressure atms	At Extinguishment Pressure	
								$-\frac{dP}{dt}$ sec ⁻¹	Burning Rate cm/sec
53	19.3	19.3	0.238	4	0.0983	0	0.0485	0.0150	0.0108
54	19.3	19.3	0.238	4	0.0886	0	0.0481	0.0126	0.0110
55	200	146	0.238	4	0.0936	8.6	0.0478	0.0145	0.0117
56	200	146	0.238	4	0.0869	16.9	0.0485	0.0150	0.0115
57	300	237	0.238	4	0.0909	17.5	0.0471	0.0128	0.0121
58	300	237	0.238	4	0.0922	19.5	0.0461	0.0136	0.0107
59	400	319	0.238	4	0.0902	23.8	0.0438	0.0119	0.0106
60	400	319	0.238	4	0.0916	27.8	0.0421	0.0117	0.0102
61	500	404	0.278	4	0.0518	26	0.0398	0.0166	0.0113
62	500	404	0.278	4	0.0561	24.6	0.0394	0.0157	0.0111
63	600	487	0.318	4	0.0541	22	0.0324	0.0269	0.0116
64	600	487	0.318	4	0.0545	35	0.0301	0.0187	0.0101
65	600	487	0.318	4	0.0902	28	0.0321	0.0270	0.00905
66	700	577	Hand	4	0.0535	70	0.0204	0.00633	0.00907
67	700	577	Hand	4	0.0902	135	<0.0197	0.0000	0.00876
68	700	577	Hand	4	0.0521	70	<0.0194	0.0000	0.0106
69	700	577	Hand	4	0.0521	45	<0.0194	0.0000	0.00935

Table G. I. (Continued)
Part 4. TPF 1006 Propellant Data (in air)

Run No. 2714	Furnace Set Temperature °C	Effective Furnace Temperature °C	Orifice cm	Cooling Air Flow Rate LPM	Initial Pressure atmos	Sample Exposure Time to Furnace sec	Extinguishment Pressure atmos	At Extinguishment Pressure	
								$-\frac{d \ln p}{dt}$ sec ⁻¹	Burning Rate cm/sec
1	24	24	0.318	0	6.22	0	6.02	0.0825	no burning rate data for this propellant
2	24	24	0.318	0	6.33	0	4.80	0.0922	
3	24	24	0.318	0	6.29	0	1.94	0.0877	
4	24	24	0.318	0	6.16	0	6.09	0.0000	
5	24	24	0.318	0	6.19	0	6.16	0.0000	
6	24	24	0.318	0	6.22	0	6.02	0.0908	
7	24	24	0.318	0	6.56	0	1.73	0.0000	
8	24	24	0.318	0	6.42	0	4.59	0.0899	
9	400	319	0.318	0	6.46	0	6.46	0.0000	
10	400	319	0.318	0	6.97	6	1.26	0.0865	
11	400	319	0.318	0	6.70	14	5.61	0.0885	
12	400	319	0.318	0	6.97	27.6	1.94	0.0947	
13	500	404	0.318	0	6.84	21	6.02	0.0983	
14	500	404	0.318	0	6.50	24	0.612	0.0867	
15	500	404	0.318	0	6.19	24	0.578	0.0894	
16	600	487	0.318	0	6.16	29	0.374	0.0800	
17	600	487	0.318	0	3.61	38	0.374	0.0764	
18	700	577	0.318	0	3.71	37	0.238	0.0771	
19	700	577	0.318	0	3.50	30	0.190	0.0750	
20	800	672	0.318	0	1.97	49.5	<0.0690	0.0000	
21	800	672	0.318	0	0.205	49.0	<0.0388	0.0000	

Table G. I. (Continued)
Part 5. TFP 1006 Propellant Data (In nitrogen)

Run No. 2716	Furnace Set Temperature °C	Effective Furnace Temperature °C	Orifice cm	Cooling Nitrogen Flow Rate LPM	Initial Pressure atmos	Sample Exposure Time to Furnace sec	Extinguishment Pressure atmos	At Extinguishment Pressure	
								$\frac{d \ln p}{dt}$ sec ⁻¹	Burning Rate cm/sec
22	800	672	0.318	0	0.195	41	<0.039	0.0000	no burning rate data for this propellant
23	800	672	0.318	10	0.180	132	<0.039	0.0000	
24	800	672	1.27	10	0.282	37	0.046	0.0600	
25	700	577	0.318	0	0.565	34	0.067	0.0593	
26	700	577	0.318	0	2.84	46	0.150	0.0718	
27	700	577	0.318	0	1.90	42	0.116	0.0700	
28	700	577	0.318	0	3.57	34	0.180	0.0766	
29	700	577	0.450	15	0.986	56	0.122	0.117	
30	700	577	1.27	10	1.02	42	0.082	0.092	
31	700	577	0.318	0	2.80	40	0.16	0.0780	
32	600	487	0.318	0	3.23	47	0.32	0.0830	
33	600	487	0.318	0	5.17	30	0.33	0.0857	
34	500	404	0.318	0	5.99	27	1.33	0.103	
35	500	404	0.318	0	6.12	43	0.39	0.0828	
36	500	404	0.318	0	5.82	29	5.14	0.110	
37	400	319	0.318	0	5.82	33	1.60	0.0936	
38	400	319	0.318	0	6.12	24	0.77	0.0885	
39	400	319	0.318	0	5.99	63	0.51	0.0840	
40	400	319	0.318	0	5.61	47	0.44	0.0862	
41	24	24	0.318	0	6.02	32	5.95	0.0000	
42	24	24	0.318	0	5.71	64	2.07	0.0787	
43	24	24	1.27	0	6.09	60	2.61	0.197	

Table G. II. Data of Depressurization Extinguishment Tests Using Combustion Chamber
Part 1. UEP Propellant Data

Run No.	Orifice cm	Initial Pressure atms	Extinguishment Pressure atms	At Extinguishment Pressure				
				$-\frac{d \ln p}{dt}$ sec ⁻¹	Burning Rate, r cm/sec	Burning Rate Exponent, n	$\frac{r^2}{a}$ sec ⁻¹	$-\frac{(d \ln p)/dt}{r^2/a}$
21106-47	2.54	1.40	0.886	5.28	0.104	0.826	6.47	0.816
48	2.54	1.43	0.831	5.20	0.097	0.826	5.64	0.923
57	1.78	1.40	0.752	2.93	0.092	0.826	5.07	0.578
58	1.78	1.41	0.752	3.00	0.092	0.826	5.07	0.593
67	1.27	1.41	0.542	1.45	0.068	0.857	2.77	0.523
68	1.27	1.41	0.509	1.65	0.065	0.857	2.52	0.653
77	0.953	1.40	0.378	0.600	0.0512	0.859	1.57	0.382
78	0.953	1.40	0.396	0.629	0.0531	0.859	1.69	0.373
87	0.635	1.41	0.265	0.397	0.0362	0.917	6.786	0.506
88	0.635	1.41	0.242	0.346	0.0330	0.917	0.653	0.530
89	0.450	1.39	0.194	0.168	0.0268	0.942	0.430	0.390
90	0.450	1.38	0.164	0.146	0.0229	0.965	5.313	0.465
108	0.318	0.326	0.130	0.0618	0.0182	1.04	0.197	0.313
109	0.318	0.324	0.106	0.0628	0.0146	1.04	0.127	0.495
119	0.318	0.244	0.110	0.0636	0.0152	1.04	0.138	0.459
120	0.318	0.249	0.120	0.0602	0.0167	1.04	0.167	0.361
121	0.318	0.211	0.117	0.0639	0.0162	1.04	0.157	0.407
122	0.238	0.217	0.104	0.0250	0.0143	1.04	0.122	0.205
123	0.238	0.223	0.0912	0.0276	0.0125	1.07	0.0926	0.295
133	0.159	0.119	0.0518	0.00592	0.00642	1.22	0.0246	0.239
134	0.159	0.138	0.0508	0.00627	0.00625	1.22	0.0234	0.303
292	0.318(SA) ¹	0.100	0.0582	0.00837	0.00745	1.22	0.0332	0.252
293	0.318(SA)	0.100	0.0582	0.00837	0.00745	1.22	0.0332	0.252
294	0.238(SA)	0.0668	0.0501	0.00333	0.00620	1.22	0.0230	0.146
295	0.238(SA)	0.0668	0.0548	0.00257	0.00692	1.22	0.0287	0.0896

¹SA indicates the conditions that the combustion chamber was connected to the auxiliary dump tank.

Table G. II. (Continued)

Part 2. UFA Propellant Data

Run No.	Orifice cm	Initial Pressure atmos	Extinguishment Pressure atmos	At Extinguishment Pressure				
				$-\frac{d \ln p}{dt}$ sec ⁻¹	Burning Rate, r cm/sec	Burning Rate Exponent, n	$\frac{r^2}{a}$ sec ⁻¹	$-\frac{(d \ln p)/dt}{r^2/a}$
21106- 43	2.54	0.846	0.340	5.11	0.0620	0.883	2.25	2.26
44	2.54	0.857	0.330	5.85	0.0604	0.883	2.16	2.73
2813-212	0.450(R) ²	2.21	0.250	2.74	0.0474	0.883	1.33	2.06
216	0.450(R)	4.46	0.250	3.30	0.0474	0.883	1.33	2.48
219	0.450(R)	10.70	0.250	3.54	0.0474	0.883	1.33	2.66
21106- 41	1.27	0.334	0.154	1.13	0.0313	0.792	0.577	1.96
42	1.27	0.338	0.162	1.32	0.0327	0.792	0.629	2.10
39	0.953	0.338	0.0936	0.627	0.0312	0.845	0.264	2.38
40	0.953	0.337	0.0943	0.615	0.0213	0.845	0.267	2.31
22	0.635	0.173	0.0668	0.335	0.0157	0.947	0.145	2.31
23	0.635	0.167	0.0678	0.344	0.0161	0.947	0.153	2.25
3	0.450	0.343	0.0528	0.127	0.0124	1.009	0.0906	1.38
4	0.450	0.341	0.0495	0.123	0.0116	1.009	0.0794	1.55
37	0.450	0.167	0.0582	0.158	0.0139	1.009	0.114	1.38
38	0.450	0.170	0.0595	0.162	0.0141	1.009	0.117	1.38
117	0.318	0.0936	0.0541	0.0538	0.0127	1.009	0.0947	0.568
118	0.318	0.0668	0.0531	0.0590	0.0125	1.009	0.0915	0.642
281	0.238	0.0836	0.0508	0.0234	0.0118	1.009	0.0818	0.287
282	0.238	0.0836	0.0491	0.0234	0.0115	1.009	0.0776	0.301
285	0.238	0.110	0.0501	0.0281	0.0116	1.009	0.0794	0.354
286	0.238	0.0846	0.0501	0.0259	0.0116	1.009	0.0794	0.326
283	0.318(SA)	0.0558	0.0475	0.00667	0.0112	1.009	0.0736	0.0907
284	0.318(SA)	0.0568	0.0491	0.00662	0.0115	1.009	0.0776	0.0853

²R indicates the conditions that the small-L* blow-down chamber was employed.

Table G. II. (Continued)

Part 3. UZD Propellant Data

Run No.	Orifice cm	Initial Pressure atms	Extinguishment Pressure atms	At Extinguishment Pressure				
				$-\frac{d \ln p}{dt}$ sec ⁻¹	Burning Rate, r cm/sec	Burning Rate Exponent, n	$\frac{r^2}{a}$ sec ⁻¹	$-\frac{(d \ln p)/dt}{r^2/a}$
21106-143	2.54	1.56	0.526	5.23	0.0600	0.896	2.02	2.59
144	2.54	1.57	0.507	5.13	0.0580	0.896	1.89	2.72
145	1.78	1.55	0.413	2.77	0.0480	0.903	1.29	2.15
146	1.78	1.58	0.431	2.82	0.0500	0.903	1.41	2.01
147	1.27	1.57	0.389	1.42	0.0457	0.921	1.17	1.21
148	1.27	1.57	0.329	1.43	0.0388	0.921	0.848	1.68
149	0.953	1.57	0.234	0.696	0.0277	0.961	0.431	1.62
150	0.953	1.58	0.227	0.662	0.0272	0.961	0.415	1.60
193	0.635	0.847	0.156	0.338	0.0184	1.01	0.191	1.77
194	0.635	0.847	0.156	0.331	0.0184	1.01	0.191	1.73
195	0.635	0.847	0.156	0.331	0.0184	1.01	0.191	1.73
196	0.635	0.847	0.158	0.343	0.0187	1.01	0.196	1.74
209	0.450	0.279	0.119	0.143	0.0141	1.06	0.111	1.28
210	0.450	0.275	0.118	0.179	0.0139	1.06	0.159	1.64
223	0.318	0.283	0.0916	0.0669	0.0107	1.16	0.0640	1.04
224	0.318	0.280	0.0912	0.0656	0.0106	1.16	0.0630	1.03
236	0.238	0.212	0.0709	0.0311	0.00782	1.24	0.0344	0.904
237	0.238	0.217	0.0658	0.0322	0.00707	1.27	0.0281	1.15
238	0.238	0.216	0.0705	0.0300	0.00776	1.24	0.0338	0.887
253	0.159	0.0802	0.0572	0.00959	0.00576	1.31	0.0187	0.513
254	0.159	0.0892	0.0548	0.00890	0.00538	1.31	0.0163	0.547
265	0.318(SA)	0.0839	0.0622	0.00764	0.00660	1.31	0.0244	0.319
267	0.318(SA)	0.0822	0.0572	0.00853	0.00576	1.31	0.0187	0.456
277	0.318(SA)	0.0849	0.0535	0.00937	0.00520	1.31	0.0152	0.623
278	0.318(SA)	0.0852	0.0505	0.00927	0.00558	1.31	0.0174	0.508
279	0.318(SA)	0.0852	0.0558	0.00886	0.00520	1.31	0.0152	0.603
280	0.318(SA)	0.0872	0.0535	0.00912	0.00558	1.31	0.0174	0.220
270	0.238(SA)	0.0822	0.0558	0.00783	0.00538	1.31	0.0183	0.218
271	0.238(SA)	0.0856	0.0568	0.00400	0.00571	1.31	0.0183	0.218

Table G. II. (Continued)

Part 4. UVC Propellant Data

Run No.	Orifice cm	Initial Pressure atms	Extinguishment Pressure atms	At Extinguished Pressure				
				$-\frac{d \ln p}{dt}$ sec ⁻¹	Burning Rate, r cm/sec	Burning Rate Exponent, n	$\frac{r^2}{a}$ sec ⁻¹	$-\frac{(d \ln p)/dt}{r/a}$
21205-191	2.54	1.55	0.534	5.03	0.0618	0.927	2.04	2.48
192	2.54	1.55	0.537	5.36	0.0620	0.927	2.05	2.63
189	1.78	1.57	0.439	3.09	0.0515	0.944	1.41	2.18
190	1.78	1.55	0.429	3.12	0.0501	0.944	1.33	2.34
187	1.27	1.56	0.312	1.57	0.0366	0.955	0.712	2.20
188	1.27	1.56	0.309	1.39	0.0362	0.955	0.698	2.00
185	0.953	1.55	0.218	0.735	0.0262	0.955	0.363	2.02
186	0.953	1.57	0.220	0.727	0.0264	0.955	0.362	1.95
197	0.635	0.848	0.160	0.355	0.0193	0.965	0.198	1.80
198	0.635	0.848	0.157	0.340	0.0191	0.965	0.194	1.75
211	0.450	0.279	0.122	0.162	0.0150	0.980	0.120	1.36
212	0.450	0.279	0.119	0.163	0.0147	0.980	0.115	1.42
225	0.318	0.282	0.0882	0.0682	0.0108	1.082	0.0622	1.09
226	0.318	0.282	0.0882	0.0682	0.0108	1.082	0.0622	1.09
239	0.238	0.219	0.0645	0.0347	0.00760	1.181	0.0313	1.13
240	0.238	0.216	0.0678	0.0330	0.00810	1.181	0.0349	0.948
255	0.159	0.0919	0.0582	0.00839	0.00670	1.211	0.0239	0.352
256	0.159	0.0826	0.0548	0.00914	0.00622	1.211	0.0206	0.445
263	0.318 (SA)	0.0866	0.0548	0.00878	0.00622	1.211	0.0206	0.427
259	0.318 (SA)	0.0869	0.0558	0.00868	0.00640	1.211	0.0217	0.399
275	0.318 (SA)	0.0846	0.0478	0.00937	0.00522	1.211	0.0145	0.647
276	0.318 (SA)	0.0869	0.0478	0.0101	0.00522	1.211	0.0145	0.698
272	0.238 (SA)	0.0866	0.0465	0.00345				
273	0.238 (SA)	0.0832	0.0508	0.00342				
274	0.238 (SA)	0.0886	0.0528	0.00303				
					0.00565	1.211	0.0169	0.334
					0.00598	1.211	0.0190	0.160

Table G. II. (Continued)

Part 5. UEV Propellant Data

Run No.	Orifice cm	Initial Pressure atmos	Extinguishment Pressure atmos	At Extinguished Pressure				
				$-\frac{d \ln p}{dt}$ sec ⁻¹	Burning Rate, r cm/sec	Burning Rate Exponent, n	$\frac{r^2}{a}$ sec ⁻¹	$-\frac{(d \ln p)/dt}{r^2/a}$
21106- 49	2.54	0.846	0.279	4.93	0.0497	0.771	1.45	3.40
50	2.54	0.846	0.322	4.79	0.0555	0.771	1.31	2.65
59	1.78	0.849	0.243	2.75	0.0445	0.771	1.16	2.37
60	1.78	0.849	0.243	2.75	0.0445	0.771	1.16	2.37
69	1.27	0.836	0.173	1.37	0.0347	0.795	0.689	1.99
70	1.27	0.839	0.172	1.25	0.0341	0.795	0.683	1.83
79	0.953	0.846	0.101	0.405	0.0218	0.839	0.280	1.45
80	0.953	0.856	0.112	0.598	0.0238	0.839	0.333	1.80
91	0.635	0.325	0.0719	0.302	0.0162	0.938	0.154	1.96
92	0.635	0.326	0.0685	0.306	0.0156	0.908	0.143	2.14
100	0.450	0.157	0.0515	0.141	0.0118	0.934	0.0817	1.73
101	0.450	0.202	0.0585	0.137	0.0134	0.934	0.105	1.30
110	0.318	0.138	0.0424	0.0484	0.0975	0.949	0.0559	0.865
111	0.318	0.157	0.0408	0.0500	0.0942	0.949	0.0523	0.958
124	0.238	0.109	0.0307	0.0667				
125	0.232	0.0836	0.0344	0.0155	0.0800	0.949	0.0376	0.411
126	0.238	0.0822	0.0364	0.0137	0.0845	0.949	0.0419	0.327
138	0.238(SA)	0.0381	0.0311	0.006				
289	0.318(SA)	0.0515	0.0328	0.0436	0.0764	0.949	0.0343	0.127
290	0.318(SA)	0.0836	0.0304	0.0461				
291	0.318(SA)	0.0468	0.0294	0.0401				

Table G. II. (Continued)

Part 6. VEX Propellant Data

Run No.	Orifice cm	Initial Pressure atms	Extinguishment Pressure atms	At Extinguishment Pressure					
				$-\frac{d \ln p}{dt}$ sec ⁻¹	Burning Rate, r cm/sec	Burning Rate Exponent, n	$\frac{r^2}{a}$ sec ⁻¹	$-\frac{(d \ln p)/dt}{r/a}$	
21106-	51	2.54	0.858	0.170	5.12	0.0640	0.627	2.34	2.16
	52	2.54	0.863	0.170	5.00	0.0640	0.627	2.34	2.11
	61	1.78	0.847	0.115	2.91	0.0500	0.627	1.43	2.01
	62	1.78	0.847	0.122	2.74	0.0520	0.627	1.55	1.76
	71	1.27	0.836	0.0852	1.38	0.0402	0.757	0.925	1.48
	72	1.27	0.846	0.0819	1.36	0.0392	0.788	0.880	1.54
	81	0.953	0.839	0.0675	0.687	0.0334	0.848	0.041	1.07
	82	0.953	0.852	0.0648	0.663	0.0322	0.874	0.594	1.12
	93	0.635	0.337	0.0558	0.313	0.0278	0.935	0.442	0.709
	94	0.635	0.337	0.0572	0.344	0.0283	0.935	0.458	0.744
	102	0.450	0.178	0.0541	0.150	0.0270	0.935	0.416	0.357
	103	0.450	0.167	0.0535	0.149	0.0265	0.935	0.401	0.368
	112	0.318	0.166	0.0508	0.0467				
	113	0.318	0.166	0.0528	0.0538	0.0262	0.935	0.392	0.136
	127	0.238	0.114	0.0518	0.0224				
	128	0.318	0.112	0.0501	0.0284				
	129	0.318	0.117	0.0535	0.0291	0.0265	0.935	0.401	0.0717
287	0.318(SA)	0.0852	0.0515	0.00504					
288	0.318(SA)	0.0635	0.0498	0.00566					

Table G. II. (Continued)

Part 7. UFM Propellant Data

Run No.	Orifice cm	Initial Pressure; atms	Extinguishment Pressure atms	At Extinguishment Pressure				
				$-\frac{d \ln p}{dt}$ sec ⁻¹	Burning Rate, r cm/sec	Burning Rate Exponent, n	$\frac{r^2}{a}$ sec ⁻¹	$-\frac{(d \ln p)/dt}{r^2/a}$
21106-169	2.54	0.836	0.237	5.35	0.0470	0.826	1.24	4.32
170	2.54	0.836	0.290	5.11	0.0474	0.826	1.26	4.07
163	1.78	0.836	0.253	2.76	0.0422	0.826	0.993	2.84
164	1.78	0.836	0.251	2.59	0.0419	0.826	0.983	2.63
157	1.27	0.842	0.190	1.49	0.0331	0.851	0.615	2.42
158	1.27	0.842	0.190	1.51	0.0331	0.851	0.615	2.45
151	0.953	0.842	0.134	0.670	0.0243	0.878	0.328	2.03
152	0.953	0.842	0.139	0.580	0.0251	0.878	0.352	1.93
201	0.635	0.535	0.106	0.352	0.0200	0.894	0.223	1.58
202	0.635	0.531	0.0986	0.363	0.0187	0.894	0.196	1.86
213	0.450	0.286	0.0819	0.153	0.0157	0.909	0.138	1.12
214	0.450	0.281	0.0839	0.167	0.0162	0.909	0.147	1.14
215	0.450	0.282	0.0795	0.172	0.0153	0.909	0.131	1.31
227	0.318	0.282	0.0588	0.0597	0.0117	0.965	0.0765	0.734
228	0.318	0.282	0.0545	0.0650	0.0108	0.965	0.0554	0.994
242	0.238	0.161	0.0458	0.0226	0.0093	0.965	0.0484	0.468
243	0.238	0.144	0.0428	0.0226				
244	0.238	0.174	0.0458	0.0263				
258	0.318(SA)	0.0725	0.0434	0.0723				
259	0.318(SA)	0.0719	0.0424	0.00677				

Table G. II. (Continued)

Part 8. UEG Propellant Data

Run No.	Orifice cm	Initial Pressure atms	Extinguishment Pressure atms	At Extinguishment Pressure				
				$-\frac{d \ln p}{dt}$ sec ⁻¹	Burning Rate, r cm/sec	Burning Rate Exponent, n	$\frac{r^2}{a}$ sec ⁻¹	$-\frac{(d \ln p)/dt}{r^2/a}$
21106-171	2.54	0.836	0.271	5.28	0.0479	0.771	1.21	4.34
172	2.54	0.836	0.287	4.79	0.0502	0.771	1.34	3.61
165	1.78	0.836	0.251	2.81	0.0451	0.771	1.07	2.61
166	1.78	0.836	0.254	2.82	0.0454	0.771	1.09	2.58
159	1.27	0.842	0.179	1.52	0.0350	0.795	0.651	2.33
160	1.27	0.842	0.178	1.50	0.0348	0.795	0.641	2.34
153	0.953	0.842	0.126	0.544	0.0267	0.821	0.377	1.44
154	0.953	0.842	0.126	0.576	0.0267	0.821	0.377	1.52
203	0.635	0.535	0.0912	0.344	0.0198	0.932	0.207	1.67
204	0.635	0.535	0.0936	0.379	0.0204	0.932	0.220	1.72
216	0.450	0.281	0.0815	0.168	0.0180	0.951	0.171	0.983
217	0.450	0.282	0.0688	0.162	0.0153	1.010	0.124	1.31
218	0.450	0.281	0.0719	0.163	0.0160	0.993	0.136	1.21
229	0.318	0.232	0.0515	0.0669	0.0111	1.166	0.0651	1.07
230	0.318	0.283	0.0518	0.0684	0.0112	1.166	0.0661	1.08
245	0.238	0.176	0.0394	0.0254				
246	0.238	0.174	0.0374	0.0232				
247	0.238	0.145	0.0408	0.0221				
260	0.318(SA)	0.0692	0.0394	0.90711				
261	0.318(SA)	0.0722	0.0381	0.97649				

Table G. II. (Continued)

Part 9. UEN Propellant Data

Run No.	Orifice cm	Initial Pressure atms	Extinguishment Pressure atms	At Extinguishment Pressure				
				$-\frac{d \ln p}{dt}$ sec ⁻¹	Burning Rate, r cm/sec	Burning Rate Exponent, n	$\frac{r^2}{a}$ sec ⁻¹	$-\frac{(d \ln p)/dt}{r^2/a}$
21106-	53	0.839	0.201	4.68	0.0558	0.681	1.84	2.56
	54	0.846	0.201	5.39	0.0558	0.681	1.84	2.32
	63	0.849	0.134	2.59	0.0430	0.681	1.09	2.36
	64	0.849	0.134	2.70	0.0430	0.681	1.09	2.48
	73	0.846	0.0926	1.54	0.0327	0.769	0.634	2.42
	74	0.849	0.0926	1.46	0.0327	0.769	0.634	2.31
	83	0.842	0.0722	0.660	0.0267	0.816	0.422	1.57
	84	0.842	0.0722	0.698	0.0267	0.816	0.422	1.66
	95	0.322	0.0578	0.299	0.0720	0.906	0.287	1.04
	96	0.333	0.0585	0.313	0.0722	0.906	0.292	1.08
	104	0.168	0.0518	0.142	0.0202	0.906	0.241	0.588
	105	0.165	0.0525	0.157	0.0204	0.906	0.246	0.637
	114	0.201	0.0528	0.0513	0.0205	0.906	0.249	0.207
	115	0.107	0.0488	0.0556				
131	0.217	0.0501	0.0446					
132	0.262	0.0511	0.0333					

Table G. II. (Continued)

Part 10. UZ Propellant Data

Run No.	Orifice cm	Initial Pressure atms	Extinguishment Pressure atms	At Extinguishment Pressure				
				$-\frac{d \ln p}{dt}$ sec ⁻¹	Burning Rate, r cm/sec	Burning Rate Exponent, n	$\frac{r^2}{a}$ sec ⁻¹	$-\frac{(d \ln p)/dt}{r^2/a}$
21106- 55	2.54	0.856	0.0729	4.87	0.098	0.506	5.58	0.873
56	2.54	0.846	0.0548	4.85	0.0835	0.570	4.06	1.20
65	1.78	0.859	0.0424	2.75	0.0703	0.676	2.87	0.749
66	1.78	0.856	0.0424	3.40	0.0703	0.676	2.87	1.18
75	1.27	0.852	0.0368	1.21	0.0650	0.676	2.46	0.492
76	1.27	0.846	0.0368	1.28				
85	0.953	0.847	0.0297	0.568				
86	0.953	0.846	0.0297	0.727				
97	0.635	0.212	0.041	0.338	0.0724	0.676	3.04	0.111
98	0.635	0.208	0.0267	0.246				
99	0.635	0.199	0.0314	0.317				
106	0.450	0.109	0.0247	0.122				
107	0.450	0.110	0.0274	0.105				
116	0.318	0.0428	0.0241	0.714				

Table G. II. (Continued)
Part II. UEX Propellant Data

Run No.	Orifice cm	Initial Pressure atmos	Extinguishment Pressure atmos	At Extinguishment Pressure				
				$-\frac{d \ln p}{dt}$ sec ⁻¹	Burning Rate, r cm/sec	Burning Rate Exponent, n	$\frac{r^2}{a}$ sec ⁻¹	$-\frac{(d \ln p)/dt}{r^2/a}$
21106-173	2.54	0.836	0.220	5.26	0.0515	0.777	1.48	3.55
174	2.54	0.836	0.217	5.17	0.0517	0.777	1.44	3.59
167	1.78	0.836	0.194	3.10	0.0468	0.777	1.22	2.54
168	1.78	0.836	0.196	3.11	0.0470	0.777	1.23	2.51
161	1.27	0.836	0.142	1.41	0.0360	0.822	0.727	1.94
162	1.27	0.836	0.140	1.36	0.0357	0.822	0.709	1.92
155	0.953	0.842	0.116	0.671	0.0302	0.854	0.509	1.31
156	0.953	0.842	0.116	0.694	0.0302	0.854	0.510	1.36
183	0.953	0.838	0.112	0.678	0.0292	0.854	0.476	1.42
184	0.953	0.838	0.109	0.663	0.0287	0.854	0.460	1.44
205	0.635	0.508	0.046	0.375	0.0252	0.890	0.355	1.06
206	0.635	0.535	0.0986	0.346	0.0261	0.886	0.381	0.909
219	0.450	0.285	0.0876	0.172	0.0233	0.900	0.303	0.566
220	0.450	0.285	0.0829	0.181	0.0223	0.919	0.277	0.651
231	0.318	0.286	0.0578	0.0699	0.0186	1.022	0.194	0.325
232	0.318	0.286	0.0685	0.0629	0.0174	1.022	0.169	0.147
243	0.238	0.142	0.0645	0.0249				
249	0.238	0.143	0.0568	0.0276				
250	0.238	0.143	0.0561	0.0268				
262	0.318(SA)	0.0699	0.0551	0.00642				
263	0.318(SA)	0.0862	0.0558	0.00704				

Table G. II. (Continued)

Part 12. UPB Propellant Data

Run No.	Orifice cm	Initial Pressure atms	Extinguishment Pressure atms	At Extinguishment Pressure				
				$-\frac{d \ln p}{dt}$ sec ⁻¹	Burning Rate, r cm/sec	Burning Rate Exponent, n	$\frac{r^2}{a}$ sec ⁻¹	$-\frac{(d \ln p)/dt}{r^2/a}$
21106-175	2.54	0.837	0.207	5.10	0.0543	0.698	1.56	3.26
176	2.54	0.837	0.209	5.41	0.0549	0.698	1.59	3.39
177	1.78	0.837	0.175	2.62	0.0488	0.704	1.25	2.09
178	1.78	0.837	0.167	2.82	0.0470	0.704	1.17	2.42
179	1.27	0.837	0.118	1.27	0.0367	0.732	0.714	1.78
180	1.27	0.837	0.127	1.17	0.0387	0.718	0.793	1.47
181	0.953	0.837	0.0922	0.652	0.0273	0.805	0.394	1.66
182	0.953	0.837	0.0836	0.651	0.0277	0.805	0.406	1.61
207	0.635	0.528	0.0702	0.305	0.0238	0.834	0.299	1.02
208	0.635	0.535	0.0682	0.328	0.0232	0.845	0.284	1.15
221	0.450	0.287	0.0565	0.172	0.0196	0.933	0.204	0.845
222	0.450	0.287	0.0548	0.152	0.0191	0.933	0.193	0.789
233	0.318	0.287	0.0424	0.0717				
234	0.318	0.287	0.0505	0.0695				
235	0.318	0.290	0.0478	0.0650				
251	0.238	0.112	0.0475	0.0236				
252	0.238	0.114	0.0481	0.0236				
264	0.318(SA)	0.0709	0.0485	0.00662				
265	0.318(SA)	0.0702	0.0481	0.00638				